MIT-EL 92-001

Molecular Simulation of Gas Hydrates

Final Report

to

Norsk Hydro

by

Kevin Sparks
Jefferson Tester

Energy Laboratory
and
Chemical Engineering Department
Massachusetts Institute of Technology
77 Massachusetts Avenue, Room E40-455
Cambridge, Massachusetts 02139-4307

May, 1992

Table of Contents

1. MOTIVATION AND PROJECT SCOPE

Water clathrates, often referred to as gas hydrates, are crystalline solids composed of an open network of host water molecules arranged in such a way that they create large void cavities or cages capable of entrapping a number of different low molecular weight guest molecules. The term clathrate was derived from the Latin word clathratus meaning to be enclosed or protected by cross bars of a grating. Powell first used the word in 1948 to describe the peculiar cage-like characteristic of these compounds.

Gas hydrates were first identified to be the cause of plugged gas transmission lines by Hammerschmidt in 1934. Since the formation of solid compounds in a natural gas process stream can also impede heat transfer and erode blades on turbine expanders, many of the studies involving hydrates during the last 50 years have been directed toward their prevention. In fact, the work of Deaton and Frost in 1946, resulted in the development of regulations limiting the water content of natural gas.

Natural deposits of methane gas hydrates were first discovered in the Soviet Union in the early 1960's. They have since been reported in porous sediments in arctic regions and below the sea floor. It appears that favorable conditions for gas hydrate formation exist in about 25% of the earth's land mass. Pressure and temperature conditions in the ocean are such that hydrates could easily exist in about 90% of the ocean floor sediments. Recent estimates indicate that the amount of natural gas trapped in these *in situ* hydrate clathrates may be as much as 10^{28} standard m^3 (Holder et al., 1980). With current annual world energy use equivalent to nearly 10^{23} standard m^3 of natural gas, these naturally occurring gas hydrate deposits have the potential of providing a clean energy source for nearly 10000 years (Barraclough, 1980)

The water clathrate structure is a polymeric three-dimensional crystalline lattice connected by nearly tetrahedral hydrogen bonds. Although clathrate hydrates are known to form several different types of structures, including a recently reported hexagonal form (Ripmeester et al., 1987), they generally crystallize in one of two cubic structures. The unit cell of a structure I water clathrate is cubic with space group *Pm3n* and a lattice constant of 12 Å at 248 K. For every 46 water molecules, there are 2 pentagonal dodecahedral cavities and 6 tetrakaidecahedral cavities. The unit cell of a structure II water clathrate is cubic with space group *Fd3m* and a lattice constant of 17 Å at 253 K. For every 136 water molecules, there are 16 pentagonal dodecahedral cavities and 8 hexakaidecahedral cavities. (See Chapter 4 for details)

The key characteristic of these unique compounds is that the host structure is thermodynamically unstable unless a number of the voids or cavities are filled by guest molecules. It is the relatively weak van der Waals interactions between the host water molecules and the entrapped guest molecules that ultimately stabilizes the compound. The diameters of the voids formed by the lattice are such that the attractive intermolecular forces between the host water molecules are strong enough to collapse the hydrogen-bonded host structure. Water clathrates are generally regarded as nonstoichiometric compounds since all available cages within the lattice structure need not be occupied in a stable equilibrium situation.

The macroscopic properties of gas hydrates are determined to a large degree by the molecular structure of the host lattice and the nature of the interaction between the host and guest molecules. The complete characterization of these intramolecular and intermolecular interactions is essential if one is to accurately predict the thermodynamic, kinetic, and transport properties of clathrates. To date, however, the models used to evaluate the configurational properties of clathrates have, for the most part, utilized a spherically symmetric Lennard-Jones Devonshire cell theory approach first proposed by van der Waals and Platteeuw in 1959. Their model neglected the asymmetries within the

clathrate structure. These asymmetries arise from the structure of the guest molecule as well as from the geometry of the host lattice cages that contain the guest molecules. For example, the behavior of a linear guest such as carbon dioxide would be expected to be different from that of a spherically symmetric guests such as argon or methane. Large discrepancies could result if branched guests such as isobutane or cyclopropane were treated as being spherically symmetric.

Previous researchers have found it necessary to adjust the various intermolecular interaction parameters in order to adequately fit experimental hydrate equilibria data. They also generally specify *a priori* whether or not a compound can actually from a hydrate, and if so, specify the clathrate structure and what cavity types can be occupied.

Anderson and Prausnitz (1986) recently claimed that most of the disagreement between experimental and their correlations is inherently due to the symmetry assumption of the van der Waals and Platteeuw hydrate model. The inadequacies of the spherical cell model have been under scrutiny for some time, yet it is still the theory of choice for many investigators.

Research carried out in out laboratory at MIT has extended the van der Waals and Platteeuw theory and reevaluated its underlying assumptions. The use of deterministic molecular simulations have allowed us to accurately account for the asymmetries which arise from the guest-host interactions.

We have improved the existing van der Waals-Platteeuw model by a fundamental reformulation to reestablish the physical significance of the potential parameters that are used to characterize intermolecular forces between the guest and host molecules. This is an important requirement, since the model has previously been used with non-unique potential parameters regressed from experimental hydrate phase equilibrium data.

Overall, this work involves a rigorous molecular level treatment of water clathrate systems. The results of our deterministic molecular simulations provide new fundamental insight into the interpretation of intermolecular forces responsible for the stabilization of these rather unique compounds. Aside from these fundamental contributions, the methodologies and predictive capabilities of our work can be used for accurate specification of phase equilibria in complex systems. Specifically, this work is applicable to problems dealing with the formation and stability of *in situ* natural gas hydrates, as well as problems in the production, pipeline transmission, and storage of natural gas.

2. INTRODUCTION AND BACKGROUND

2.1 General Clathrate Properties

Water clathrates, often referred to as gas hydrates, are crystalline solids composed of an open network of host water molecules arranged in such a way that they create large void cavities or cages capable of entrapping a number of different low molecular weight guest molecules. The term clathrate was derived from the Latin word clathratus meaning to be enclosed or protected by cross bars of a grating. Powell first used the word in 1948 to describe the peculiar cage-like characteristic of these compounds.

Water clathrates were first discovered in 1810, by Sir Humphrey Davy, an English chemist, who observed a yellow precipitate while passing chlorine gas through water at temperatures near 0 °C. He identified this solid compound as a hydrate of chlorine.

Gas hydrates were found to be the cause of plugged gas transmission lines by Hammerschmidt in 1934. Since the formation of solid compounds in a natural gas process stream can also impede heat transfer and erode blades on turbine expanders, many of the studies involving hydrates during the last 50 years have been directed toward their prevention. In fact, the work of Deaton and Frost in 1946, resulted in the development of regulations limiting the water content of natural gas.

Water clathrates have been proposed and used in a number of separation processes. Specifically, they have been used successfully in the desalination of seawater (Barduhn et al., 1962) and in the separation of light gases. The transportation and storage of natural gas in the form of solid gas hydrates has also been suggested (Miller et al., 1945). Hydrates have also been considered as a possible solution to the global CO_2 problem.

The deep sea injection of carbon dioxide from large concentrated sources, could provide a mechanism for CO_2 storage, as a solid clathrate.

For fundamental chemistry studies, the long term stabilization of reactive small molecules is normally very difficult to achieve except at low temperatures. It has been suggested that clathrates offer one possible solution to this problem (Goldberg, 1963). Once stabilized within the clathrate cage, free radicals and other small reactive molecules can be studied using spectroscopic, dielectric, and NMR techniques (Davidson, 1971; Davidson et al., 1977; Davidson et al., 1984; Matsuo, 1984).

2.2 Natural Gas Hydrates

Natural deposits of methane gas hydrates were first discovered in the Soviet Union in the early 1960's. They have since been reported in porous sediments in arctic regions and below the sea floor as shown in Figure 2.1. It appears that favorable conditions for gas hydrate formation exist in about 25% of the earth's land mass. Pressure and temperature conditions in the ocean are such that hydrates could easily exist in about 90% of the ocean floor sediments. Recent estimates indicate that the amount of natural gas trapped in these *in situ* hydrate clathrates may be as much as 10^{28} standard m^3 (Holder et al., 1980). With current annual world energy use equivalent to nearly 10^{23} standard m^3 of natural gas, these naturally occurring gas hydrate deposits have the potential of providing a clean energy source for nearly 10000 years (Barraclough, 1980)

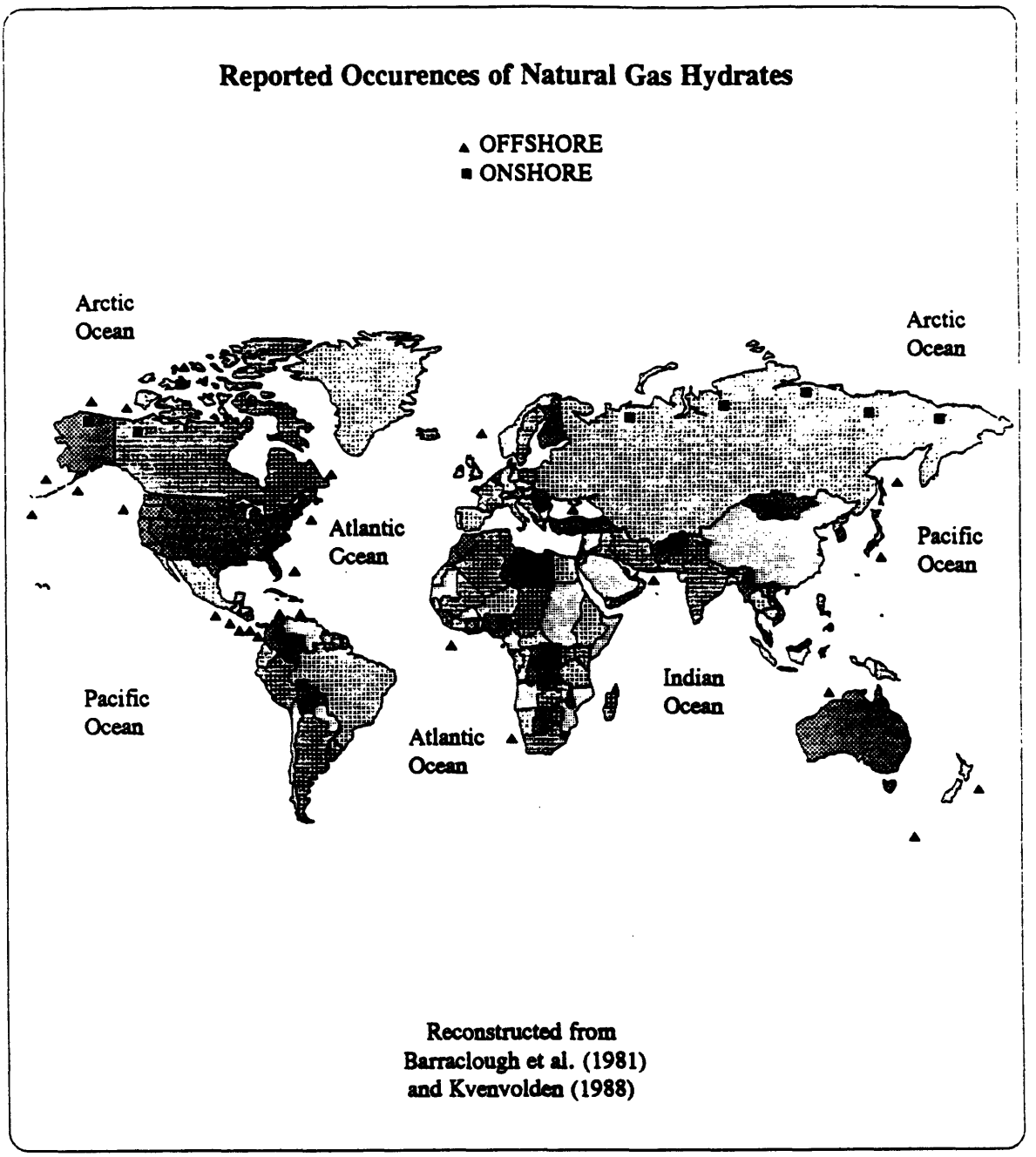

Figure 2.1 Reported Occurrences of Natural Gas Hydrates

2.3 General Observations

The water clathrate structure is a polymeric three-dimensional crystalline lattice connected by nearly tetrahedral hydrogen bonds. Although clathrate hydrates are known to form several different types of structures, including a recently reported hexagonal form (Ripmeester et al., 1987), they generally crystallize in one of two cubic structures. The unit cell of a structure I water clathrate is cubic with space group *Pm3n* and a lattice constant of 12 Å. For every 46 water molecules, there are 2 pentagonal dodecahedral cavities and 6 tetrakaidecahedral cavities. The unit cell of a structure II water clathrate is cubic with space group *Fd3m* and a lattice constant of 17 Å. For every 136 water molecules, there are 16 pentagonal dodecahedral cavities and 8 hexakaidecahedral cavities. The polyhedra of these two distinct structures are shown in Figure 2.2. The unit cells for each of the structure types are shown in Figures 2.3 and 2.4. A detailed description of structural characteristics of the two water clathrate types is given in Chapter 4.

Clathrate networks consisting of hydrogen-bonded host water molecules are in fact unstable by themselves unless a number of the voids or cavities are filled by guest molecules. It is the interaction of these enclathrated guest molecules with the host lattice that ensures the stabilization of the host lattice structure. The diameters of the voids formed by the lattice are such that the attractive intermolecular forces between the host water molecules are strong enough to collapse the hydrogen-bonded host structure. It is the relatively weak van der Waals interactions between the host water molecules and the entrapped guest molecules that ultimately stabilizes the compound. Several of the larger hydrate forming compounds, although capable of stabilizing the larger cavities within the overall clathrate structure, require the presence of a second hydrate forming component, often regarded as a *hilfgas* (help-gas), to complete the stabilization of the structure. Water clathrates are

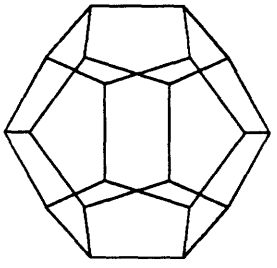

Pentagonal Dodecahedron

(12 sided)

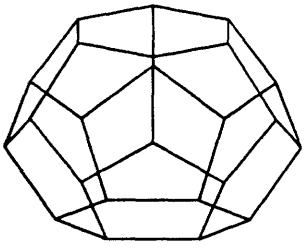

Tetrakaidecahedron

(14 sided)

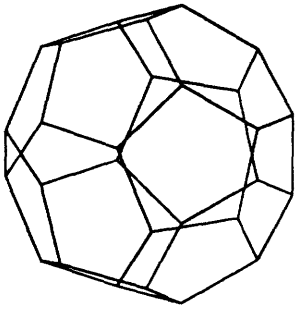

Hexakaidecahedron

(16 sided)

Figure 2.2 Water Clathrate Polydedra

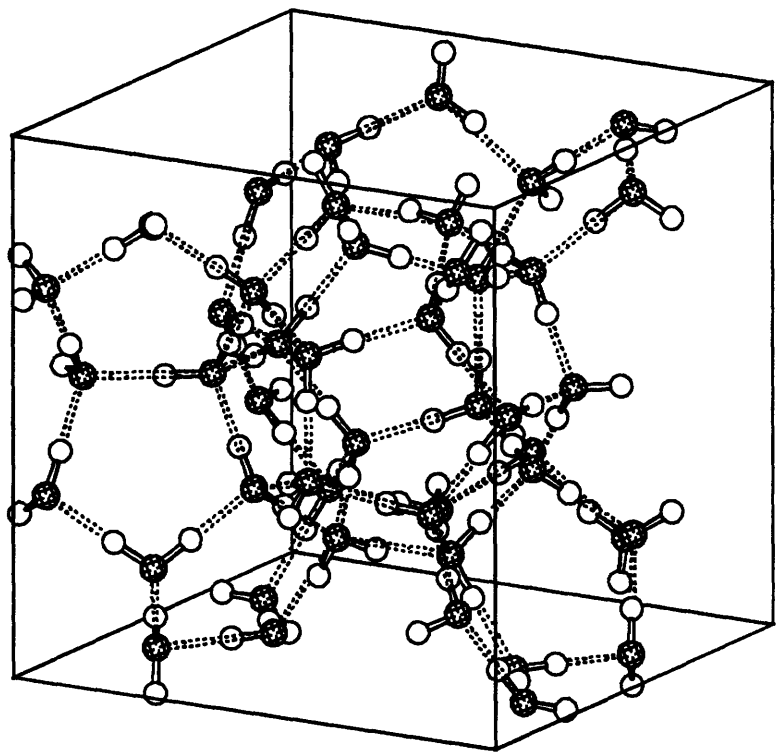

Figure 2.3 Structure I Water Clathrate Unit Cell

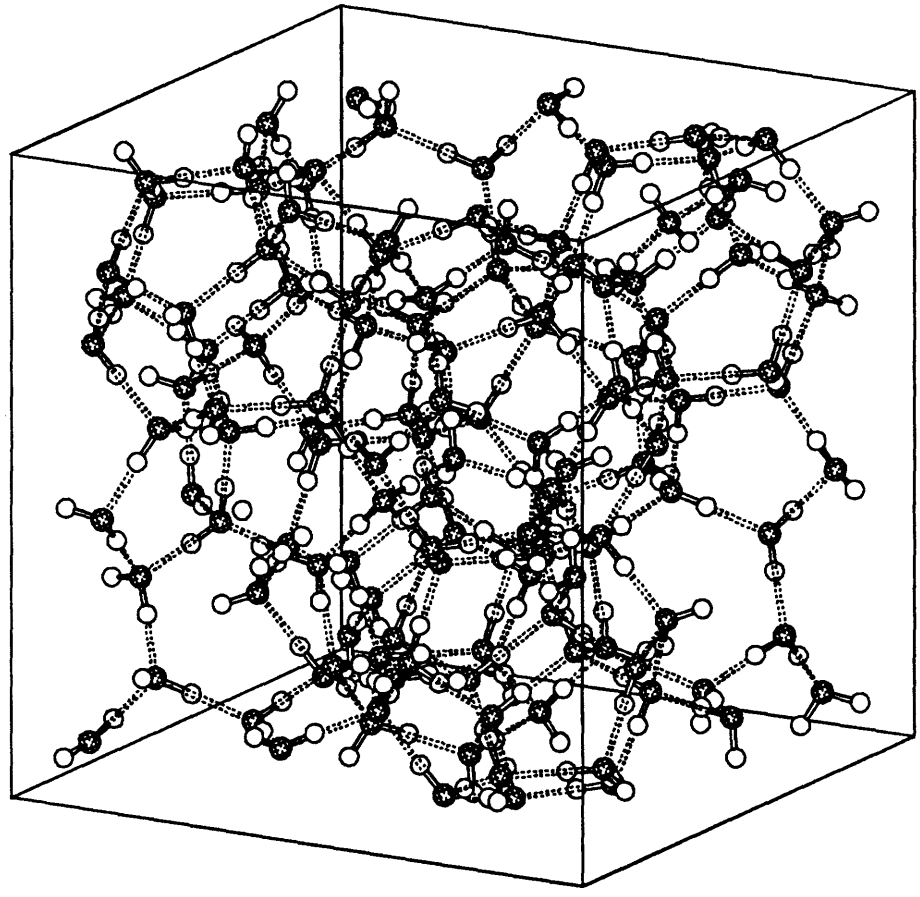

Figure 2.4 Structure II Water Clathrate Unit Cell

generally regarded as nonstoichiometric compounds since all available cages within the lattice structure need not be occupied to ensure stability.

A pure gas water clathrate can be treated thermodynamically as a two-component system consisting of water and a particular guest component. Multicomponent gas hydrates can be treated in a similar fashion if the composition of the gas phase is fixed. When three equilibrium phases are present, the system will be monovariant, and fixing the temperature should specify the pressure. These equilibrium vapor pressures are commonly measured as a function of temperature for various three-phase, monovariant systems. For example, when either ice or liquid water, solid gas hydrate, and vapor are present in equilibrium, the measured pressure is referred to as the dissociation pressure. A phase diagram for water and various natural gas components is shown in Figure 2.5. It should be noted that the dashed vertical line representing the ice-line is incorrectly drawn at the higher pressures. The line should strictly curve to the left at the higher pressures.

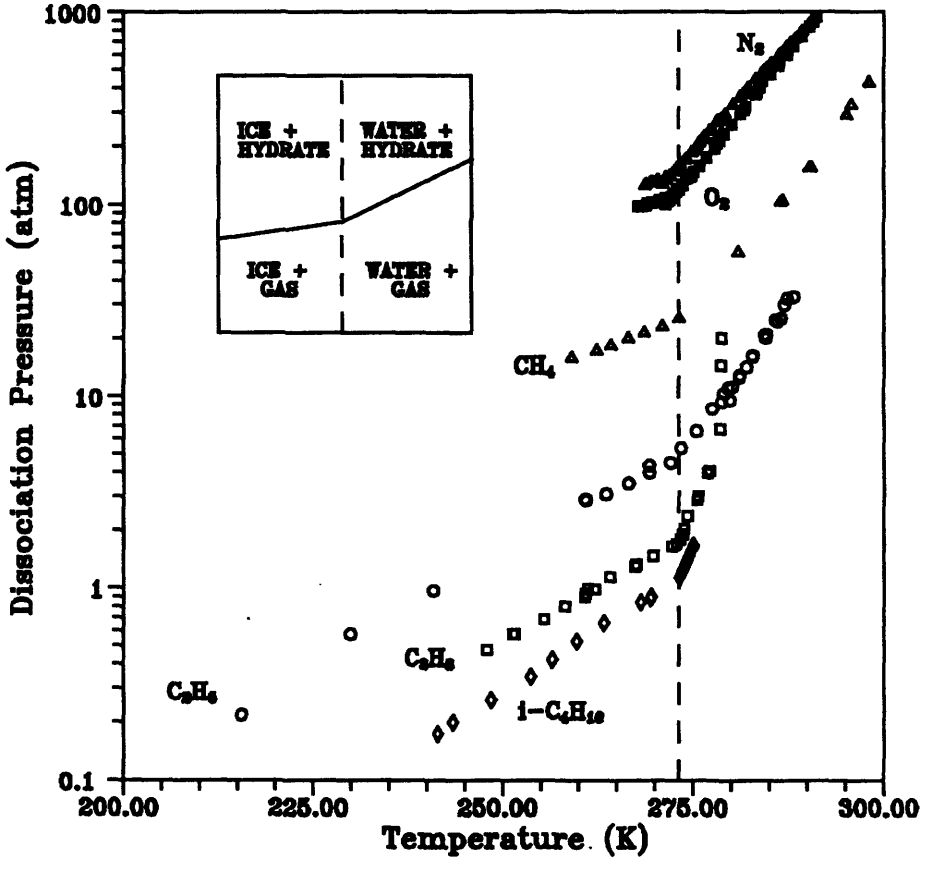

Figure 2.5 Phase Diagram for Water and Various Natural Gas Components

2.4 Overview of Previous Theoretical Work

In 1959, van der Waals and Platteeuw proposed that the thermodynamic properties of clathrates could be derived from a simple model corresponding to the three-dimensional generalization of ideal localized adsorption. The model assumes the empty host lattice to be thermodynamically unstable. The difference between μ_w^β, the chemical potential of H_2O in the unstable empty lattice, and μ_w^H, the chemical potential of H_2O in the occupied lattice, is given by

$$\Delta \mu_w^H \equiv \mu_w^H - \mu_w^\beta = -kT \sum_i \nu_i \ln\left(1 + \sum_J C_{Ji} f_J\right) \tag{2.1}$$

where k is Boltzmann's constant, T is the absolute temperature, and ν_i is defined as the number of type i cavities per water molecule in the host lattice, f_J is the fugacity of guest component J, and C_{Ji} is the Langmuir constant for a type J guest component encaged within a type i cavity and is defined by

$$C_{Ji} \equiv \frac{Z_{Ji}}{kT} \tag{2.2}$$

where the "free volume" or configurational integral, Z_{Ji}, is given by

$$Z_{Ji} = \frac{1}{8\pi^2} \int_V e^{-U(r,\theta,\phi,\alpha,\beta,\gamma)/kT} r^2 \sin\theta \, d\theta \, d\phi \, dr \, d\alpha \sin\beta \, d\beta \, d\gamma \tag{2.3}$$

where U is the total interaction potential between the guest molecule and all host molecules defined in spherical coordinates r, θ, and ϕ and Euler orientation angles α, β, and γ for the guest molecule. Unfortunately, the asymmetries of the host lattice cavities and of the guest molecule itself makes analytical integration intractable. Generally, a Lennard-Jones and Devonshire liquid cell theory approach has been adopted for the quantitative evaluation of the configurational partition function of the guest "solute"

The Kihara potential is represented by

$$U(r) = \infty \qquad r \leq 2a$$

$$U(r) = 4\varepsilon\left(\left(\frac{(\sigma - 2a)}{(r - 2a)}\right)^{12} - \left(\frac{(\sigma - 2a)}{(r - 2a)}\right)^{6}\right) \qquad r > 2a \tag{2.8}$$

where $2a$ is the molecular hard core diameter, σ is the collision diameter, and ε is the characteristic energy. They also attempted to account for the general shape of the guest molecule by considering two cases, specifically a molecule with a thin rod core such as N_2 or C_2H_6, and a molecule with a spherical core such as CH_4 or Ar. The host molecules were modeled as point molecules having no hard core diameter.

Nagata and Kobayashi (1966) extended the method to the prediction of dissociation pressures of mixed gas hydrates from data for hydrates of pure gases with water. They used the Kihara potential for spherical and rodlike molecules to describe the interaction between the encaged guest and the host lattice.

Parrish and Prausnitz (1972) later extended the use of the van der Waals and Platteeuw hydrate model to the prediction of the dissociation pressures of gas hydrates formed by gas mixtures both above and below the ice point. They also chose to use the Kihara potential with a spherical core to model the gas-water interaction in the clathrate cavity.

Recently, John and Holder (1985) examined the validity of the spherical cell approximation. Using the Kihara potential in all of their calculations, they proposed several modifications to original van der Waals and Platteeuw treatment:

molecule within the host lattice cavity. It is generally assumed that the host water molecules are uniformly distributed on a spherical surface corresponding to an average cavity radius. This spherical cell model simplifies the integration of Equation (2.3) considerably.

$$Z_{J_i} = 4\pi \int e^{-U(r)/kT} r^2 dr \tag{2.4}$$

Van der Waals and Platteeuw used a Lennard-Jones (6-12) potential in the development of the spherically symmetric cell potential model

$$U(r) = 4\varepsilon\left(\left(\frac{\sigma}{r}\right)^{12} - \left(\frac{\sigma}{r}\right)^{6}\right) \tag{2.6}$$

where r is the usual distance between molecular centers, σ is the collision diameter, and ε is the characteristic energy. The actual Lennard-Jones parameters for the guest-host interactions were determined using the Berthelot geometric mean approximation for ε, and the hard sphere approximation for σ.

$$\varepsilon = \left(\varepsilon_{guest}\,\varepsilon_{host}\right)^{1/2}$$

$$\sigma = \frac{(\sigma_{guest} + \sigma_{host})}{2} \tag{2.7}$$

The discrepancy between theory and experiment later directed McKoy and Sinanoglu (1963) to study the Lennard-Jones (6-12), (7-28), and Kihara potentials in the spherical cell model.

- The choice of cell size used in the model (John and Holder, 1981).

- The addition of terms to account for the contribution of second and subsequent water shells to the potential energy of the guest-host interactions (John and Holder, 1982).

- The addition of an empirical corresponding states correlation to correct the results of the smoothed Lennard-Jones Devonshire model (John and Holder, 1985a, b).

These modifications attempted to remove the inadequacies of the spherical cell approximation but unfortunately to some extent tend to cloud the significance of the van der Waals and Platteeuw physical model. Although John and Holder maintain that their potential parameters are consistent with those observed for viral coefficient data, the have effectively introduced new empirically fitted parameters such as the cell radius into the model.

Almost without exception, the interaction potential parameters used in these lattice models are determined *ad hoc* by fitting experimental phase equilibrium data such as along various univariant, three-phase dissociation pressure curves (Parrish and Prausnitz, 1972; Nagata and Kobayashi, 1966). The parameters obtained in this manner are not uniquely defined. Often, agreement between intermolecular parameters obtained from fitting hydrate dissociation pressure data and from gas-phase second virial coefficient or viscosity measurements is poor (Tse and Davidson, 1982).

Since the macroscopic properties of water clathrates are determined to a large degree by the molecular structure of the host lattice and the nature of the interaction between the host and guest molecules, the complete characterization of these

intramolecular and intermolecular interactions is essential if we are to accurately predict the thermodynamic properties of clathrate compounds. To date, however, the models used to evaluate the configurational properties of these gas hydrates have for the most part utilized the spherically-symmetric Lennard-Jones Devonshire cell theory approach and have therefore neglected the asymmetries within the clathrate structure. These asymmetries arise from the structure of the guest molecules as well as from the geometry of the host lattice cages that contain the guest molecules. For example, a linear guest such as CO_2 would be expected to behave differently from that of spherically symmetric guests such as Ar or CH_4. Large discrepancies could result if branched guests such as i-C_4H_{10} or cyclopropane were treated as being spherically symmetric. In fact, Anderson and Prausnitz (1986) recently claimed that most of the disagreement between experiment and theory is inherently due to symmetry assumption of the van der Waals and Platteeuw clathrate model. The inadequacies of the spherical cell model have been under scrutiny for some time, yet it is still the theory of choice for many investigators.

The work presented here therefore represents an extensive evaluation of the van der Waals and Platteeuw theory and its underlying assumptions. Given the crystallographic data of the two water clathrate structures we were able to accurately account for the asymmetries which arise from the guest-host interactions while maintaining the physical significance of the potential parameters that are used to characterize the intermolecular forces between guest and host molecules. This we considered an important requirement, especially since the spherical cell model uses non-unique potential parameters regressed from experimental dissociation pressure data. Molecular dynamics simulations also were used to study the motion of guests within the host lattice cavities. Additionally, this enabled us to quantitatively estimate the lattice distortions associated with the large more asymmetric guest molecules.

3. PROJECT OBJECTIVES AND APPROACH

The objective of this work was to develop a comprehensive physical and quantitative description of the configurational characteristics of water clathrates using molecular simulation methods. Our approach was as follows:

1) Perform a rigorous review of the van der Waals and Platteeuw (1959) clathrate model.

2) Implement an accurate and reliable multi-dimensional integration algorithm for the computation of the configurational partition function while accurately accounting for the structural characteristics and asymmetries of the rigid host lattice and the entrapped guest molecule.

3) Critically review the current state of intermolecular potential functions, particularly those indicative of the hydrophobic type interactions associated with the modeling of the guest-host intermolecular interaction potential.

4) Examine the contribution subsequent water shells have on the total potential energy of the guest-host interaction.

5) Examine the effect of the inclusion of guest-guest interactions on the total guest potential energy.

6) Estimate site-site potential parameters for the intermolecular interactions between water and the key groups ($-CH_2-$ and $-CH_3-$) for hydrocarbon guest molecules. Experimental data for model hydrate systems where only one cavity type of a Structure I clathrate will be used to obtain these parameters.

7) Use molecular dynamics simulation methods to investigate the lattice distortion issues associated with the formulation of the van der Waals and Platteeuw model.

8) Evaluate the feasibility of using molecular dynamics methods to investigate the molecular clustering and nucleation phenomena associated with solid hydrate formation.

4. WATER CLATHRATE STRUCTURES

4.1 Crystallographic Studies

A number of articles have discussed the structural aspects of water clathrates as determined by a variety of x-ray diffraction techniques (von Stackelberg and Müller, 1951; Claussen, 1951; Pauling and Marsh, 1952; von Stackelberg and Müller, 1954; Jeffrey, 1962; McMullan and Jeffrey, 1965; Mak and McMullan, 1965; Jeffrey, 1984; Tse et al., 1986).

Neutron scattering techniques have also been used to further refine the crystalline structural database of the water clathrates (Hollander and Jeffrey, 1977; Chiari and Ferraris, 1982; Tse et al., 1986). Hollander and Jeffrey (1977) performed a neutron diffraction study of the crystal structure of ethylene oxide deuterohydrate providing more precise data relating the hydrogen bonding characteristics in the water clathrate.

Water clathrates generally crystallize in one of two cubic structures. The unit cell of a structure I hydrate is cubic with space group *Pm3n* and a lattice constant of 12.03±0.01 Å at 248 K. For every 46 water molecules, there are 2 pentagonal dodecahedral cavities and 6 tetrakaidecahedral cavities. The unit cell of a structure II hydrate is cubic with space group *Fd3m* and a lattice constant of 17.31±0.01 Å at 253 K. For every 136 water molecules, there are 16 pentagonal dodecahedral cavities and 8 hexakaidecahedral cavities.

The pentagonal dodecahedral cavity, common to both structures, is the simplest of the three cavity types. It has 12 regular pentagonal faces (F), 20 vertices (V), and 30 edges (E). The oxygens occupy the vertices while it is thought that the hydrogens lie on

the edges of the polyhedra. Euler's theory relating to convex polyhedra provides a simple means of relating the number of faces and vertices to the number of edges:

$$12F + 20V = 30E + 2 \tag{4.1}$$

The tetrakaidecahedral cavity has 2 hexagonal and 12 pentagonal faces, 24 vertices, and 36 edges:

$$14F + 24V = 36E + 2 \tag{4.2}$$

The hexakaidecahedral cavity has 4 hexagonal and 12 pentagonal faces, 28 vertices, and 42 edges:

$$16F + 28V = 42E + 2 \tag{4.3}$$

The polyhedra of these two distinct structures are shown in Figures 4.1 and 4.2. The lattice characteristics of the two structures are given in Table 4.1.

In some cases, determining a particular clathrate structure can be difficult experimentally, and some ambiguities in interpretation may exist. For example, until recently it was believed that the small molecules, specifically those smaller than propane, preferentially form structure I water clathrates. Measurements have since shown that Ar, Kr, N_2, and O_2 form Structure II hydrates (Davidson et al., 1984; Tse et al., 1986). The van der Waals radius and ideal stoichiometric composition of several of the more common hydrate formers are shown in Table 4.2. Tabulated Lennard-Jones parameters were used to estimate the van der Waals radii of the different water clathrate forming compounds (Reid et al., 1987).

pentagonal dodecahedron
(12 sided)

tetrakaidecahedron
(14 sided)

Figure 4.1 Structure I - Water Clathrate Polyhedra

pentagonal dodecahedron
(12 sided)

hexakaidecahedron
(16 sided)

Figure 4.2 Structure II - Water Clathrate Polyhedra

	Structure I	*Structure II*
Water molecules per unit cell	46	136
Cavities per unit cell		
Small	2	16
Large	6	8
Average Cavity Radius		
Small	3.905 Å	3.902 Å
Large	4.326 Å	4.682 Å
Space Group	*Pm3n*	*Fd3m*
Lattice Constant	12.03±0.01 Å	17.31±0.01 Å
Typical Guest Compounds	Methane Ethane Ethylene CO_2 Xenon * Cyclopropane H_2S	Argon Krypton Nitrogen Oxygen Propane * Cyclopropane i-Butane
Ideal Composition	$M_1 \cdot 3M_2 \cdot 23H_2O$	$2M_1 \cdot M_2 \cdot 17H_2O$

M_1 - molecules occupying small cavities

M_2 - molecules occupying large cavities

* Forms Both Types

Table 4.1 Structure I and Structure II Hydrate Lattice Properties

Structure I Water Clathrates	van der Waals Radius (Å)	Ideal Chemical Formula
Methane	2.019	$4CH_4 \cdot 23H_2O$
Ethane	2.494	$3C_2H_6 \cdot 23H_2O$
Ethylene	2.337	$4C_2H_4 \cdot 23H_2O$
Carbon Dioxide	2.212	$4CO_2 \cdot 23H_2O$
Xenon	2.272	$4Xe \cdot 23H_2O$
Cyclopropane	2.698	$3C_3H_6 \cdot 23H_2O$
Hydrogen Sulfide	2.034	$4H_2S \cdot 23H_2O$

Structure II Water Clathrates	van der Waals Radius (Å)	Ideal Chemical Formula
Argon	1.988	$3Ar \cdot 17H_2O$
Krypton	2.052	$3Kr \cdot 17H_2O$
Nitrogen	2.132	$3N_2 \cdot 17H_2O$
Oxygen	1.946	$3O_2 \cdot 17H_2O$
Propane	2.873	$C_3H_8 \cdot 17H_2O$
Cyclopropane	2.698	$C_3H_6 \cdot 17H_2O$
i-butane	2.962	$C_4H_{10} \cdot 17H_2O$

$$\textit{van der Waals radius} \approx 2^{-5/6}\sigma$$

Table 4.2 Ideal Water Clathrate Composition

The Structure I and II oxygen fractional position generating functions and a summary of the fractional positional parameters are given in Tables 4.3 and 4.4. The parameters include those reported by Pauling and Marsh (1952), Stackelburg and Müller (1954), McMullan and Jeffrey (1965), Mak and McMullan (1965), and Hollander and Jeffrey (1977). The fractional locations of the various polyhedra are given in Tables 4.5 and 4.6. Further discussion regarding the nomenclature and usage of these functions is omitted here, instead the reader is directed to the classic reference by Hahn (1988).

For the purpose of this work, the fractional positional parameters reported by McMullan and Jeffrey (1965) and Mak and McMullan (1965) were chosen to best represent the oxygen positions within the Structure I and II water clathrates. The parameters determined by Hollander and Jeffrey (1977) were excluded since they were derived from measurements on a deuterohydrate.

Tse et al. (1987) measured the lattice constant for the structure I water clathrate of ethylene oxide from 18 to 260 K. They fit the experimental lattice constant, *a(T)*, to a quadratic polynomial in temperature, given by:

$$a(T)\,(\text{Å}) = 11.835 + 2.2173\times10^{-5}\,T\,(K^{-1}) + 2.2415\times10^{-6}\,T^{2}\,(K^{-2}) \qquad (4.4)$$

Their results compared favorably with those reported by McIntyre and Petersen (1967). Tse found over the temperature range from 20 to 250 K, the lattice constant increased by 0.13 Å or about 1.1%. This slight temperature dependence we therefore chose to omit. Instead choosing to hold the lattice constants to fixed values, specifically, 12.03 Å for the structure I water clathrate as reported by McMullan and Jeffrey (1965) and 17.31 Å for the structure II water clathrate as reported by Mak and McMullan (1965).

The resulting fractional Miller indices coordinates of the host water molecules in the first shell of the different polyhedra are given in Tables 4.7, 4.8, 4.9, and 4.10. The hydrogen bonding characteristics resulting from a statistical analysis of the oxygen

positions are tabulated for both structures in Table 4.11. Figures 4.3 and 4.4 graphically illustrate the resulting hydrogen bond length distributions and hydrogen bond angle distributions.

Set = (k) Multiplicity = 24		
x	*y*	*z*
0	y	z
0	- y	z
0	y	- z
0	- y	- z
z	0	y
z	0	- y
- z	0	y
- z	0	- y
y	z	0
- y	z	0
y	- z	0
- y	- z	0
½ + x	½	½ - z
½ - y	½	½ - z
½ + y	½	½ + z
½ - y	½	½ + z
½	½ + z	½ - y
½	½ + z	½ + y
½	½ - z	½ - y
½	½ - z	½ + y
½ + z	½ + y	½
½ + z	½ - y	½
½ - z	½ + y	½
½ - z	½ - y	½

Set = (i) Multiplicity = 16		
x	*y*	*z*
x	x	x
- x	- x	x
- x	x	- x
x	- x	- x
½ + x	½ + x	½ - x
½ - x	½ - x	½ - x
½ + x	½ - x	½ + x
½ - x	½ + x	½ + x
- x	- x	- x
x	x	- x
x	- x	x
- x	x	x
½ - x	½ - x	½ + x
½ + x	½ + x	½ + x
½ - x	½ + x	½ - x
½ - x	½ + x	½ - x

Pauling and Marsh (1952) y(k) = 0.310 z(k) = 0.116
Stackelburg and Muller (1954) y(k) = 0.307 z(k) = 0.117
McMullan and Jeffrey (1965) y(k) = 0.30710 z(k) = 0.11819
Hollander and Jeffrey (1977) y(k) = 0.30822 z(k) = 0.11732 * deuterohydrate

Set = (c) Multiplicity = 6		
x	*y*	*z*
¼	0	½
¾	0	½
½	¼	0
½	¾	0
0	½	¼
0	½	¾

Origin		
0	0	0

Pauling and Marsh (1952) x(i) = 0.183
Stackelburg and Muller (1954) x(i) = 0.190
McMullan and Jeffrey (1965) x(i) = 0.18362
Hollander and Jeffrey (1977) x(i) = 0.18375 * deuterohydrate

Table 4.3 Structure I - Oxygen Fractional Position Generating Functions

Set = (g) Multiplicity = 96		
x	*y*	*z*
x	x	z
- x	½ - x	½ + z
½ - x	½ + x	- z
½ + x	- x	½ - z
z	x	x
½ - z	- x	½ - x
- z	½ - x	½ + x
½ - z	½ + x	- x
x	z	x
½ - x	½ + z	- x
½ + x	- z	½ - x
- x	½ - z	½ + x
¾ + x	¼ + x	¾ - z
¼ - x	¼ - x	¼ - z
¼ + x	¾ - x	¾ + z
¾ - x	¾ + x	¼ + z
¾ + x	¼ + z	¾ - x
¾ - x	¾ + z	¼ + x
¼ - x	¼ + z	¼ - x
¼ + x	¾ - z	¾ + x
¾ + z	¼ + x	¾ - x
¼ + z	¾ - x	¾ + x
¾ - z	¾ + x	¼ + x
¼ - z	¼ - x	¼ - x

Set = (e) Multiplicity = 32		
x	*y*	*z*
x	x	x
- x	½ - x	½ + x
½ - x	½ + x	- x
½ + x	- x	½ - x
¾ - x	¼ + x	¾ - x
¼ - x	¼ - x	¼ - x
¼ + x	¾ - x	¾ + x
¾ - x	¾ + x	¼ + x

Stackelburg and Muller (1954) x(g) = - 0.057 z(g) = - 0.242
Mak and McMullan (1965) x(g) = - 0.05744 z(g) = - 0.24487

Set = (a) Multiplicity = 8		
x	*y*	*z*
0	0	0
¾	¼	¾

Origin		
- 1/8	- 1/8	- 1/8

Generating Translations		
0	0	0
0	½	½
½	0	½
½	½	0

Stackelburg and Muller (1954) x(e) = - 0.093
Mak and McMullan (1965) x(e) = - 0.09228

Table 4.4 Structure II - Oxygen Fractional Position Generating Functions

Pentagonal Dodecahedron

Set = (a) Multiplicity = 2			
	x	*y*	*z*
1	0.00	0.00	0.00
2	0.50	0.50	0.50

Tetrakaidecahedron

Set = (d) Multiplicity = 6			
	x	*y*	*z*
1	0.25	0.50	0.00
2	0.00	0.25	0.50
3	0.50	0.00	0.25
4	0.75	0.50	0.00
5	0.00	0.75	0.50
6	0.50	0.00	0.75

Table 4.5 Structure I - Water Clathrate Cell Fractional Locations

Pentagonal Dodecahedron

Set = (c) Multiplicity = 16			
	x	*y*	*z*
1	0.25	0.25	0.25
2	0.00	0.50	0.75
3	0.50	0.75	0.00
4	0.75	0.00	0.50
5	0.25	0.75	0.75
6	0.00	0.00	0.25
7	0.50	0.25	0.50
8	0.75	0.50	0.00
9	0.75	0.25	0.75
10	0.50	0.50	0.00
11	0.00	0.75	0.50
12	0.25	0.00	0.00
13	0.75	0.75	0.25
14	0.50	0.00	0.75
15	0.00	0.25	0.00
16	0.25	0.50	0.50

Hexakaidecahedron

Set = (b) Multiplicity = 8			
	x	*y*	*z*
1	0.625	0.625	0.625
2	0.375	0.875	0.375
3	0.625	0.125	0.125
4	0.375	0.375	0.875
5	0.125	0.625	0.125
6	0.875	0.875	0.875
7	0.125	0.125	0.625
8	0.875	0.375	0.375

Table 4.6 Structure II - Water Clathrate Cell Fractional Locations

Fractional Miller Indices Coordinates of the Host Water Molecules (Oxygen Atoms) in the First Shell of the Structure I Pentagonal Dodecahedron Centered at (0,0,0) with a Lattice Constant of 12.03 Å				
Host Number	*x*	*y*	*z*	*Distance from Cell Center Å*
1	0.1836	0.1836	0.1836	3.8256
2	-0.1836	-0.1836	0.1836	3.8256
3	-0.1836	0.1836	-0.1836	3.8256
4	0.1836	-0.1836	-0.1836	3.8256
5	0.1836	-0.1836	0.1836	3.8256
6	-0.1836	0.1836	0.1836	3.8256
7	0.1836	0.1836	-0.1836	3.8256
8	-0.1836	-0.1836	-0.1836	3.8256
9	-0.1182	0.0000	-0.3071	3.9586
10	0.1182	0.0000	0.3071	3.9586
11	0.3071	0.1182	0.0000	3.9586
12	0.0000	-0.3071	0.1182	3.9586
13	-0.3071	-0.1182	0.0000	3.9586
14	0.1182	0.0000	-0.3071	3.9586
15	-0.1182	0.0000	0.3071	3.9586
16	0.0000	0.3071	0.1182	3.9586
17	0.3071	-0.1182	0.0000	3.9586
18	0.0000	-0.3071	-0.1182	3.9586
19	-0.3071	0.1182	0.0000	3.9586
20	0.0000	0.3071	-0.1182	3.9586

* Lattice parameters taken from McMullan and Jeffrey (1965)

Table 4.7 Structure I - Dodecahedron Oxygen Coordinates

Fractional Miller Indices Coordinates of the Host Water Molecules (Oxygen Atoms) in the First Shell of The Structure I Tetrakaidecahedron Centered at (0,0,0) with a Lattice Constant of 12.03 Å				
Host Number	*x*	*y*	*z*	*Distance from Cell Center Å*
1	0.1182	-0.2500	0.1929	4.0561
2	0.1929	0.2500	-0.1182	4.0561
3	-0.1182	-0.2500	-0.1929	4.0561
4	-0.1929	0.2500	-0.1182	4.0561
5	0.1182	-0.2500	-0.1929	4.0561
6	-0.1929	0.2500	0.1182	4.0561
7	-0.1182	-0.2500	0.1929	4.0561
8	0.1929	0.2500	0.1182	4.0561
9	0.0000	0.2500	0.2500	4.2532
10	0.0000	0.2500	-0.2500	4.2532
11	-0.2500	-0.2500	0.0000	4.2532
12	0.2500	-0.2500	0.0000	4.2532
13	0.1836	-0.0664	-0.3164	4.4726
14	-0.3164	0.0664	-0.1836	4.4726
15	0.1836	-0.0664	0.3164	4.4726
16	0.3164	0.0664	0.1836	4.4726
17	-0.1836	-0.0664	-0.3164	4.4726
18	-0.3164	0.0664	0.1836	4.4726
19	0.3164	0.0664	-0.1836	4.4726
20	-0.1836	-0.0664	0.3164	4.4726
21	-0.3818	-0.0571	0.0000	4.6441
22	0.0000	0.0571	-0.3818	4.6441
23	0.0000	0.0571	0.3818	4.6441
24	0.3818	-0.0571	0.0000	4.6441

* Lattice parameters taken from McMullan and Jeffrey (1965)

Table 4.8 Structure I - Tetrakaidecahedron Oxygen Coordinates

Fractional Miller Indices Coordinates of the Host Water Molecules (Oxygen Atoms) in the First Shell of the Structure II Pentagonal Dodecahedron Centered at (0,0,0) with a Lattice Constant of 17.31 Å				
Host Number	*x*	*y*	*z*	*Distance from Cell Center Å*
1	-0.1250	-0.1250	-0.1250	3.7477
2	0.1250	0.1250	0.1250	3.7477
3	0.0327	0.2173	0.0327	3.8457
4	0.0327	0.0327	0.2173	3.8457
5	0.2173	0.0327	0.0327	3.8457
6	-0.0327	-0.0327	-0.2173	3.8457
7	-0.2173	-0.0327	-0.0327	3.8457
8	-0.0327	-0.2173	-0.0327	3.8457
9	0.1824	-0.1199	0.0676	3.9555
10	-0.1824	-0.0676	0.1199	3.9555
11	-0.1824	0.1199	-0.0676	3.9555
12	-0.1199	0.0676	0.1824	3.9555
13	-0.0676	0.1199	-0.1824	3.9555
14	0.0676	-0.1199	0.1824	3.9555
15	-0.1199	0.1824	0.0676	3.9555
16	0.0676	0.1824	-0.1199	3.9555
17	0.1824	0.0676	-0.1199	3.9555
18	-0.0676	-0.1824	0.1199	3.9555
19	0.1199	-0.0676	-0.1824	3.9555
20	0.1199	-0.1824	-0.0676	3.9555

* Lattice parameters taken from Mak and McMullan (1965)

Table 4.9 Structure II - Dodecahedron Oxygen Coordinates

Fractional Miller Indices Coordinates of the Host Water Molecules (Oxygen Atoms) in the First Shell of the Structure II Hexakaidecahedron Centered at (0,0,0) with a Lattice Constant of 17.31 Å				
Host Number	*x*	*y*	*z*	*Distance from Cell Center Å*
1	-0.0574	0.0574	-0.2551	4.6340
2	0.0574	-0.0574	-0.2551	4.6340
3	0.2551	0.0574	0.0574	4.6340
4	-0.0574	0.2551	-0.0574	4.6340
5	0.0574	-0.2551	-0.0574	4.6340
6	-0.0574	-0.0574	0.2551	4.6340
7	-0.0574	-0.2551	0.0574	4.6340
8	0.2551	-0.0574	-0.0574	4.6340
9	-0.2551	-0.0574	0.0574	4.6340
10	0.0574	0.0574	0.2551	4.6340
11	-0.2551	0.0574	-0.0574	4.6340
12	0.0574	0.2551	0.0574	4.6340
13	-0.1926	-0.1926	-0.0051	4.7157
14	-0.1926	0.1926	0.0051	4.7157
15	-0.0051	0.1926	0.1926	4.7157
16	-0.1926	-0.0051	-0.1926	4.7157
17	0.0051	-0.1926	0.1926	4.7157
18	0.1926	0.1926	-0.0051	4.7157
19	0.1926	0.0051	-0.1926	4.7157
20	-0.0051	-0.1926	-0.1926	4.7157
21	0.0051	0.1926	-0.1926	4.7157
22	0.1926	-0.0051	0.1926	4.7157
23	-0.1926	0.0051	0.1926	4.7157
24	0.1926	-0.1926	0.0051	4.7157
25	0.1577	-0.1577	0.1577	4.7281
26	0.1577	0.1577	-0.1577	4.7281
27	-0.1577	-0.1577	-0.1577	4.7281
28	-0.1577	0.1577	0.1577	4.7281

* Lattice parameters taken from Mak and McMullan (1965)

Table 4.10 Structure II - Hexakaidecahedron Oxygen Coordinates

Structure I Hydrogen Bonded O-O Distance	
O-O Distance	*Fraction*
2.767 Å	0.087
2.779 Å	0.522
2.815 Å	0.261
2.839 Å	0.130
Average Distance = 2.795 Å	

Structure II Hydrogen Bonded O-O Distance	
O-O Distance	*Fraction*
2.768 Å	0.118
2.777 Å	0.353
2.796 Å	0.353
2.809 Å	0.176
Average Distance = 2.788 Å	

Structure I Hydrogen Bonded O-O-O Angle	
O-O-O Angle	*Fraction*
105.45°	0.087
106.38°	0.174
106.47°	0.174
108.30°	0.174
108.56°	0.087
110.61°	0.174
111.31°	0.043
124.34°	0.087
Average Angle = 109.35°	

Structure II Hydrogen Bonded O-O-O Angle	
O-O-O Angle	*Fraction*
105.68°	0.235
107.34°	0.118
107.92°	0.118
108.56°	0.235
109.47°	0.058
111.51°	0.118
119.87°	0.118
Average Angle = 109.39°	

Table 4.11 Water Clathrate Hydrogen Bond Characteristics

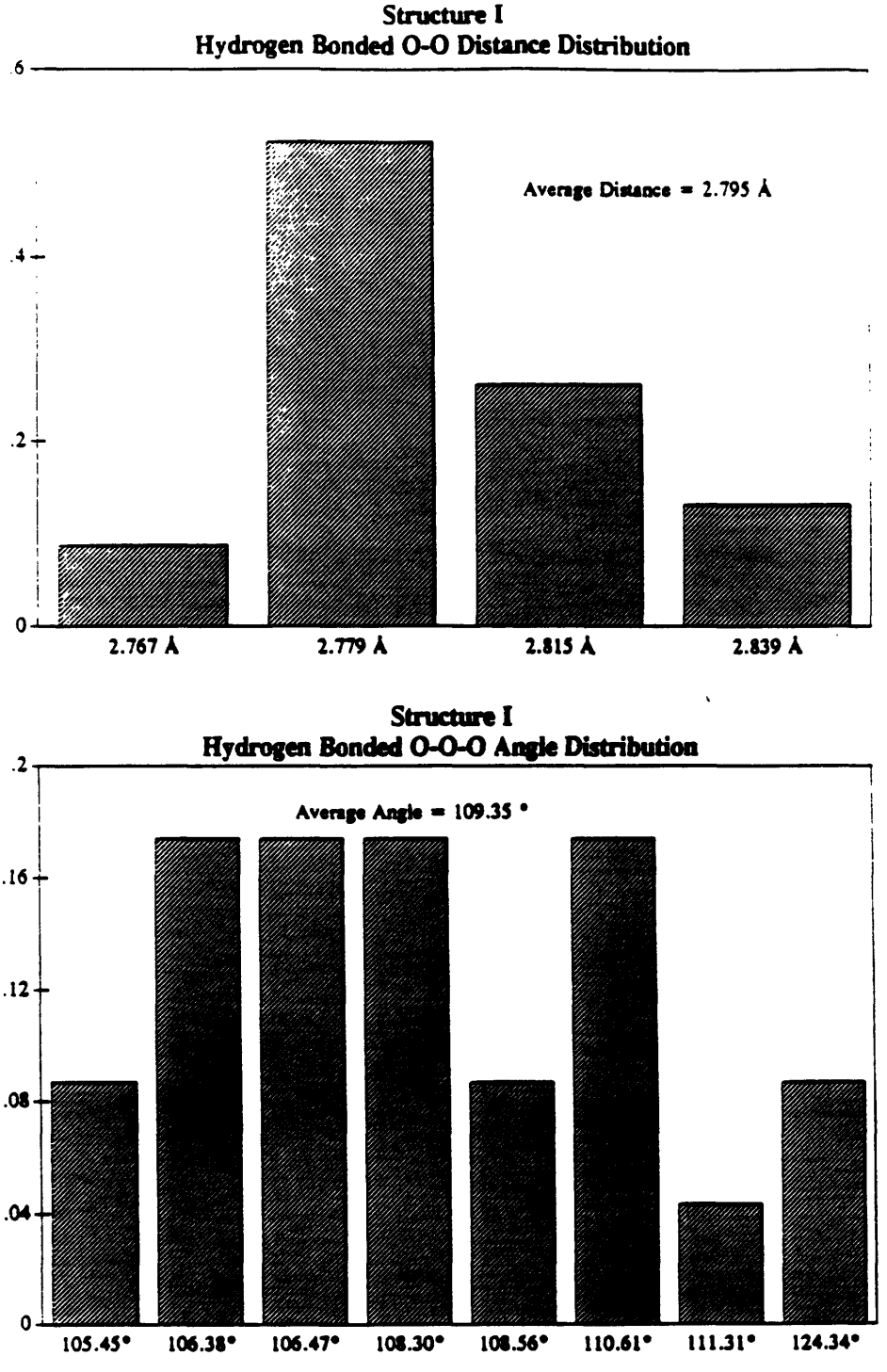

Figure 4.3 Structure I - Hydrogen Bond Characteristics

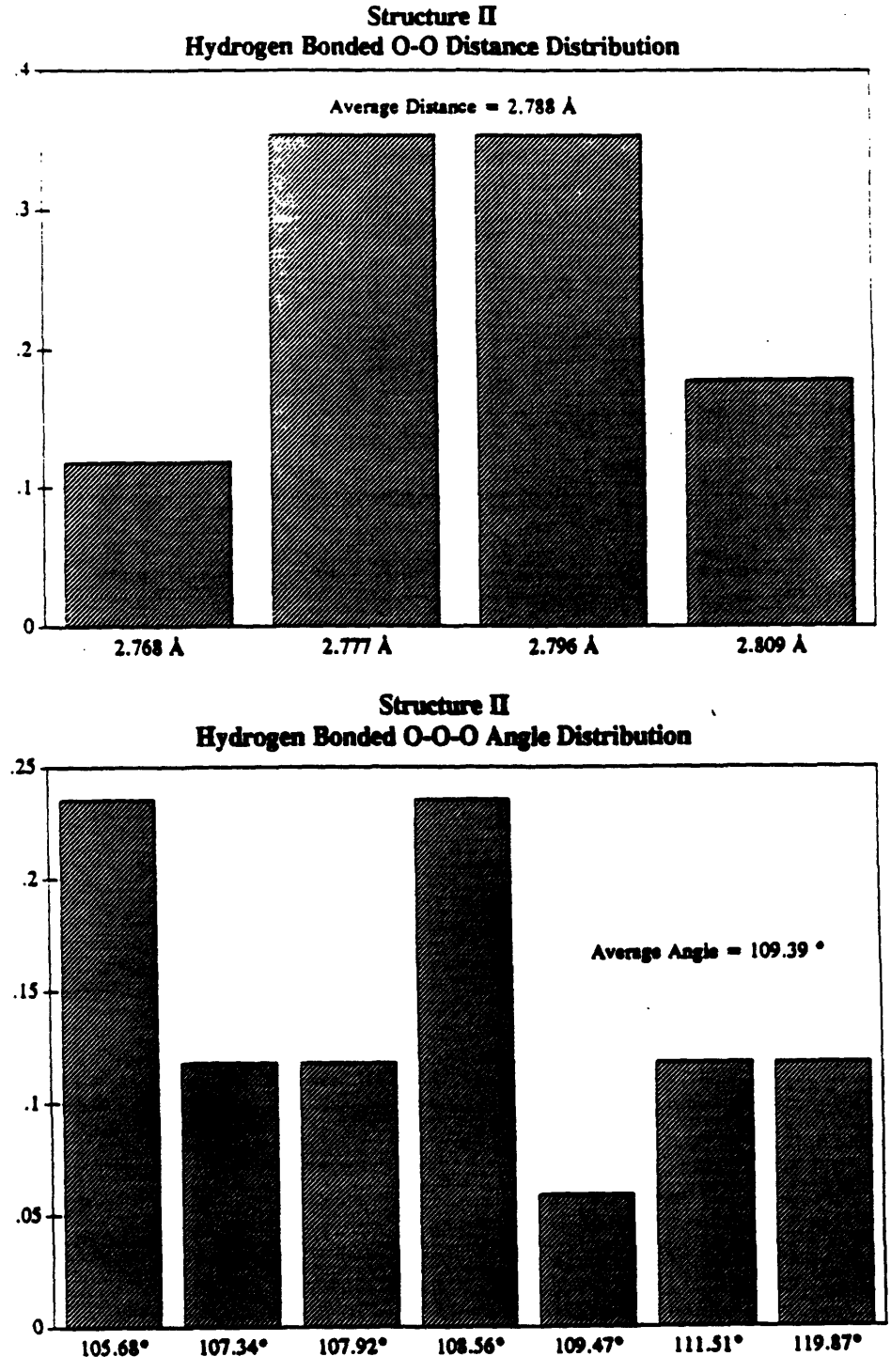

Figure 4.4 Structure II - Hydrogen Bond Characteristics

4.2 Proton Placement

A knowledge of the water clathrate proton distribution is important in understanding the configurational characteristics of the guest-host intermolecular interactions. Unfortunately, it is extremely difficult to resolve the proton positions directly from diffraction type studies. Since the water molecule protons are, however, generally assumed to lie on the edges of the various polyhedra, with the oxygen atoms located at their vertices, half-atom positions are generally reported along with the refined oxygen positions (McMullan and Jeffrey, 1965; Mak and McMullan, 1965; Hollander and Jeffrey,1977).

Although a knowledge of the proton half-atom positions is useful, it is usually necessary to require a more explicit proton location assignment. This can be difficult since the water molecule protons in the water clathrate structures are rotationally disordered. They must, however, conform to the rules developed by Bernal and Fowler (1933) as cited in their remarkable study of the structural nature of water. These rules, conveniently condensed by Rahman and Stillinger (1972), are outlined below:

Bernal-Fowler Rules

(i) Water clathrate host lattice consists of intact (non-dissociated) water molecules.

(ii) The oxygens form the host lattice with very nearly tetrahedral coordination.

(iii) Each hydrogen bond between two neighboring oxygens is made up of a single proton covalently bonded to one of the oxygens and hydrogen bonded to the other.

(iv) All proton configurations satisfying conditions (i), (ii), and (iii) are equally probable.

Another constraint we must consider in the proton location assignment is that of the net dipole moment of the entire water clathrate structure.

$$\sum_{i=1}^{N} \vec{\mu}_i = 0 \tag{4.5}$$

Keeping these requirements in mind, an algorithm was constructed to randomly assign the protons to their respective positions. Nearly half a million configurations, each conforming to the Bernal-Fowler "rules", were generated for each water clathrate structure and desired H_2O molecule geometry. The experimental geometry of the H_2O monomer [r(OH) = 0.9572 Å, $\angle$HOH = 104.52°] was chosen as was the geometry corresponding to the Simple Point Charge (SPC) model [r(OH) = 1.0 Å, $\angle$HOH = 109.47°] as proposed by Berendson et al. (1981). The SPC model, further discussed in a later chapter, was selected because of its prior use in molecular simulation studies of water clathrates and ices (Tse and Klein, 1983; Tse and Klein, 1983; Tse, Klein, and McDonald, 1983; Tse, Klein, and McDonald, 1984; Tse and Klein, 1987; Marchi and Mountain, 1987; Basu and Mountain, 1988; Rodger, 1989). The resulting configuration with the lowest net dipole moment was then selected as a valid proton assignment.

The program SCHAKAL (Keller, 1988) was used to generate the following illustrations of the two water clathrate structures. The positions of the various polyhedra within the host lattices are depicted in Figures 4.5 and 4.6. The cavities are represented

as spheres with diameters half that of the average diameter of the actual cavities. The smaller cavities representing the pentagonal dodecahedral cavities and the larger cavities representing either the tetrakaidecahedral cavities or the hexakaidecahedral cavities. A ball and stick representation of the unit cell of the structure I water clathrate is shown in Figure 4.7. A depiction of the hydrogen bonds between neighboring oxygens (dashed-lines) is presented for the structure I unit cell in Figure 4.8. Two space filling views of the structure I unit cell are shown in Figures 4.9 and 4.10. A ball and stick representation of the unit cell of the structure II water clathrate is shown in Figure 4.11. A depiction of the hydrogen bonds between neighboring oxygens (dashed-lines) is presented for the structure I unit cell in Figure 4.12. Two space filling views of the structure I unit cell are shown in Figures 4.13 and 4.14. A ball and stick representation of the structure I pentagonal dodecahedral cavity is shown in Figure 4.15. A depiction of its hydrogen bonds is presented in Figure 4.16 while a full space filling view is shown in Figures 4.17. A ball and stick representation of the structure I tetrakaidecahedral cavity is shown in Figure 4.18. A depiction of its hydrogen bonds is presented in Figure 4.19 while a full space filling view is shown in Figures 4.20. A ball and stick representation of the structure II pentagonal dodecahedral cavity is shown in Figure 4.21. A depiction of its hydrogen bonds is presented in Figure 4.22 while a full space filling view is shown in Figures 4.23. A ball and stick representation of the structure II hexakaidecahedral cavity is shown in Figure 4.24. A depiction of its hydrogen bonds is presented in Figure 4.25 while a full space filling view is shown in Figures 4.26.

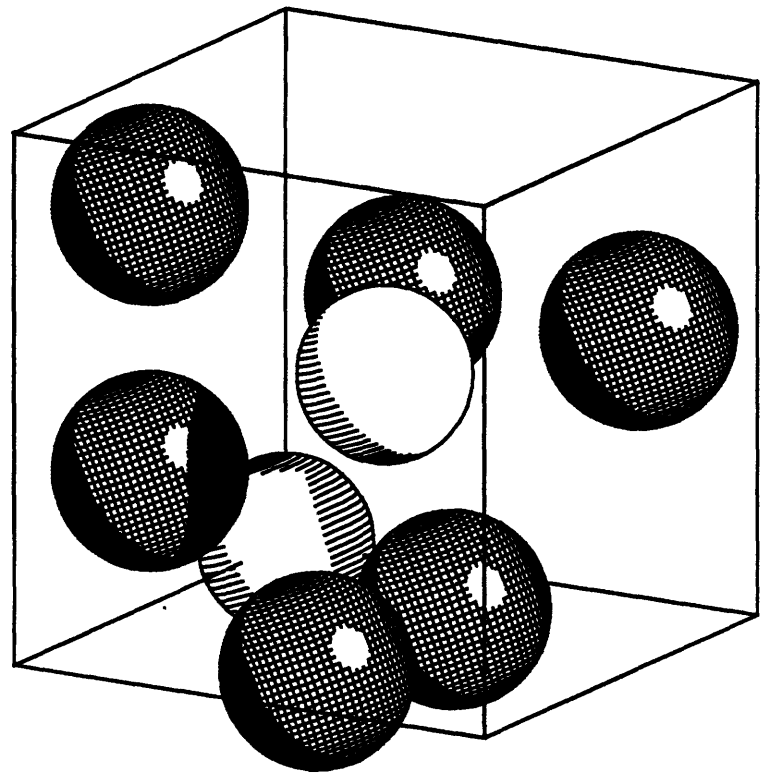

Figure 4.5 Structure I Water Clathrate Cavity Positions

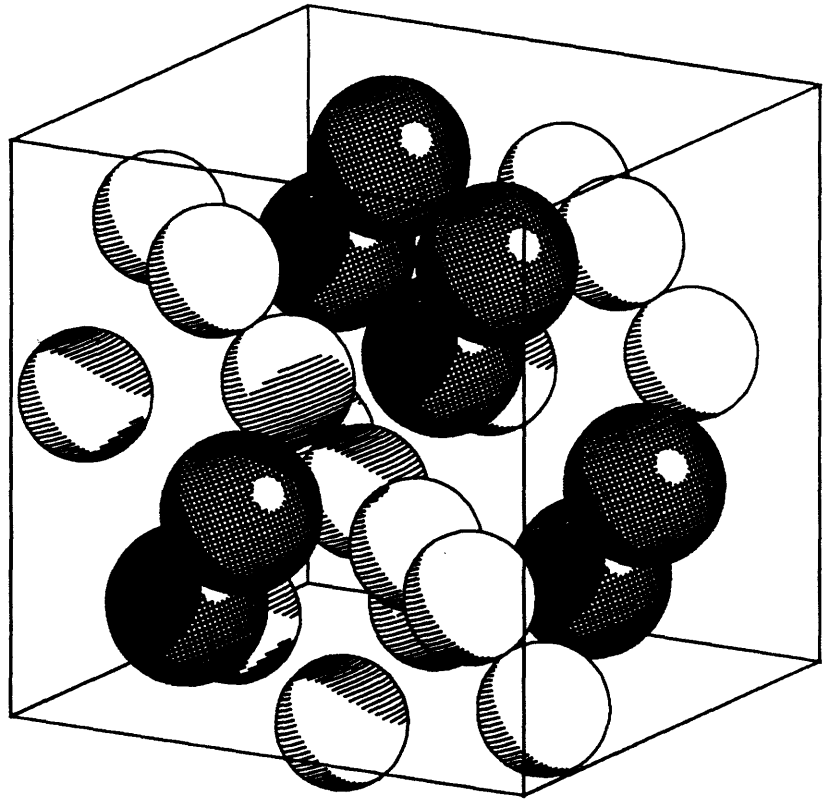

Figure 4.6 **Structure II Water Clathrate Cavity Positions**

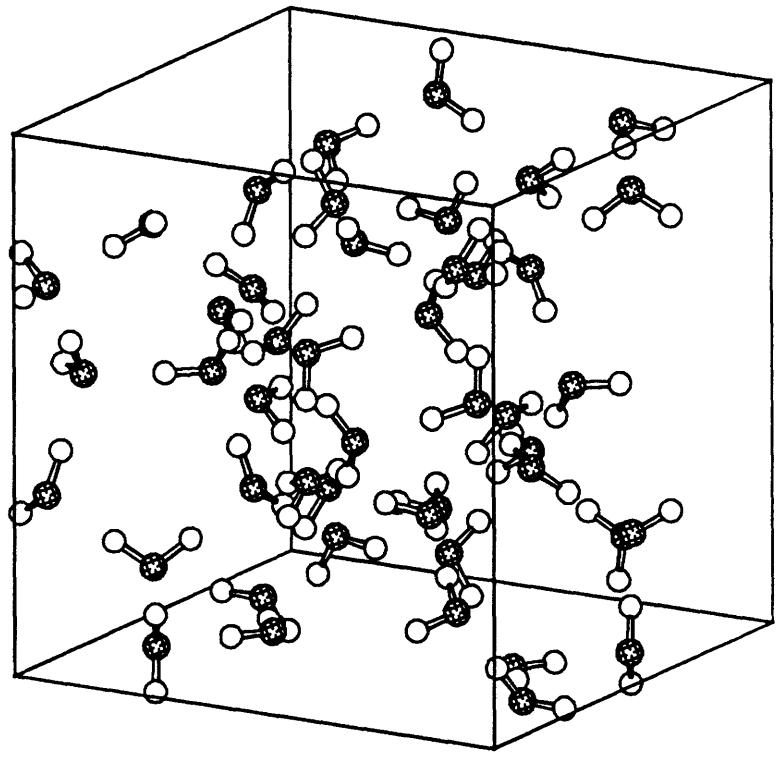

Figure 4.7 Ball and Stick Representation of the Structure I Unit Cell

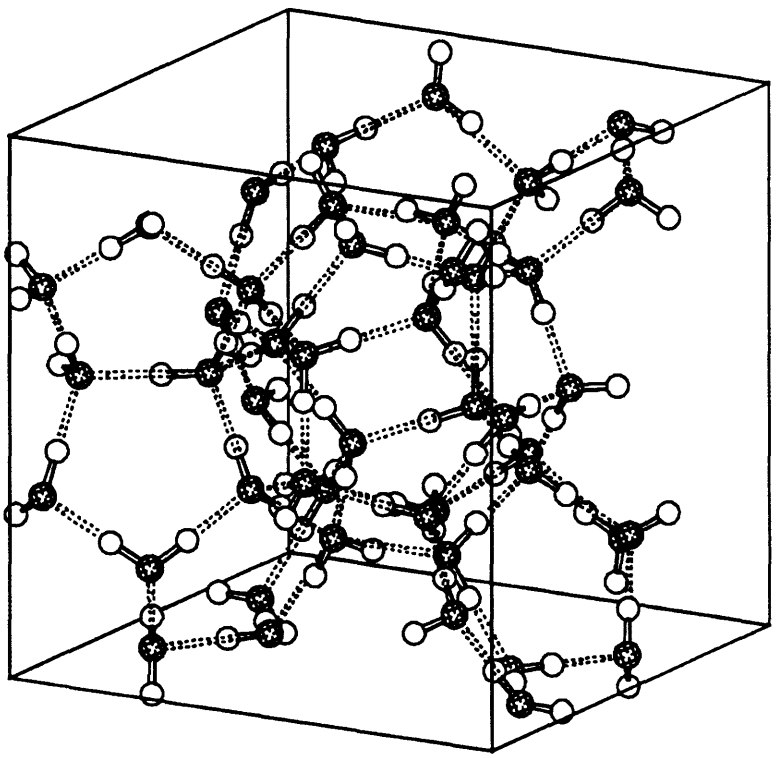

Figure 4.8 Hydrogen Bond Depiction of the Structure I Unit Cell

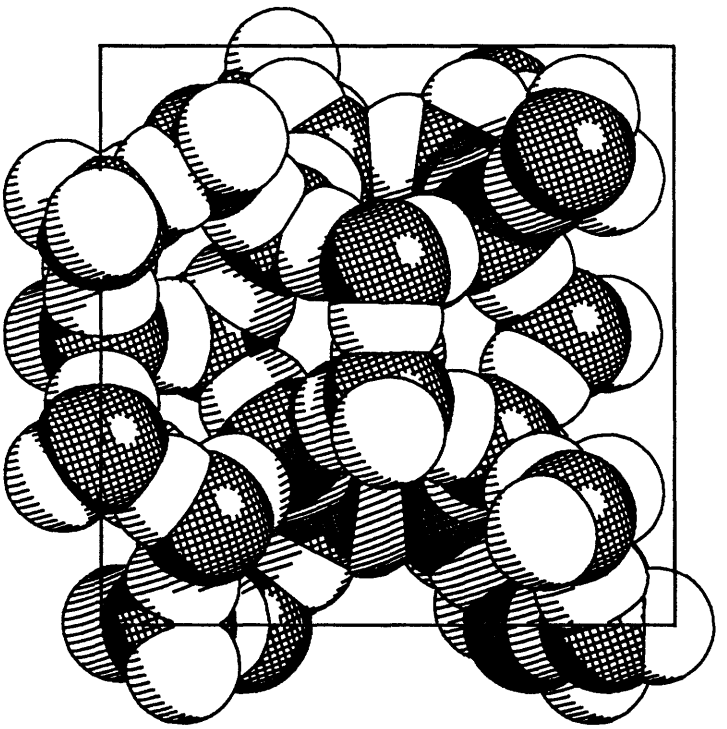

Figure 4.9 **Space Filling Representation of the Structure I Unit Cell**

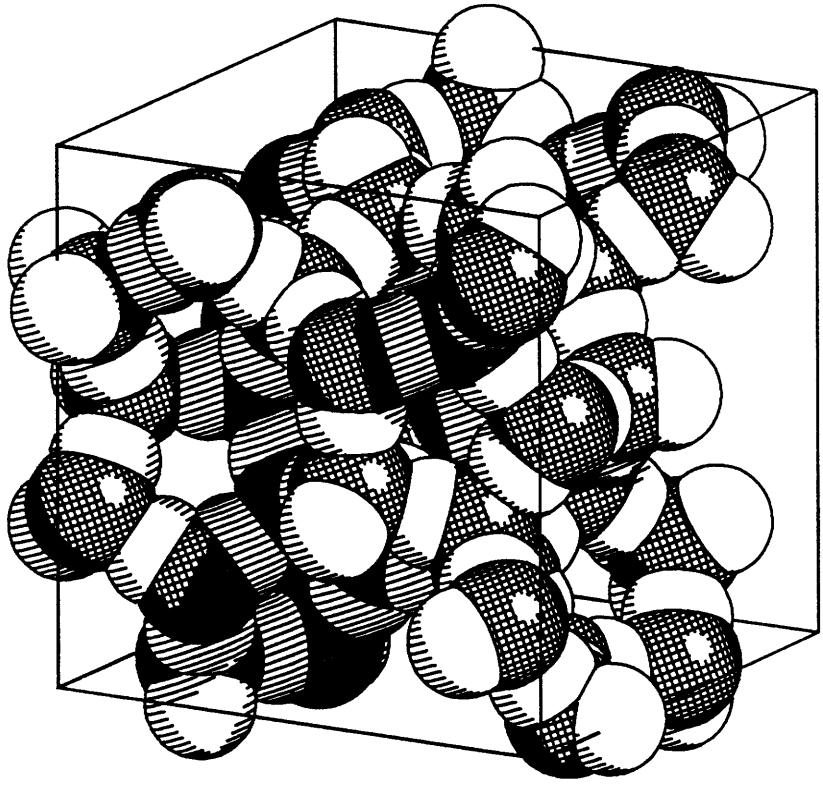

Figure 4.10 **Space Filling Representation of the Structure I Unit Cell**

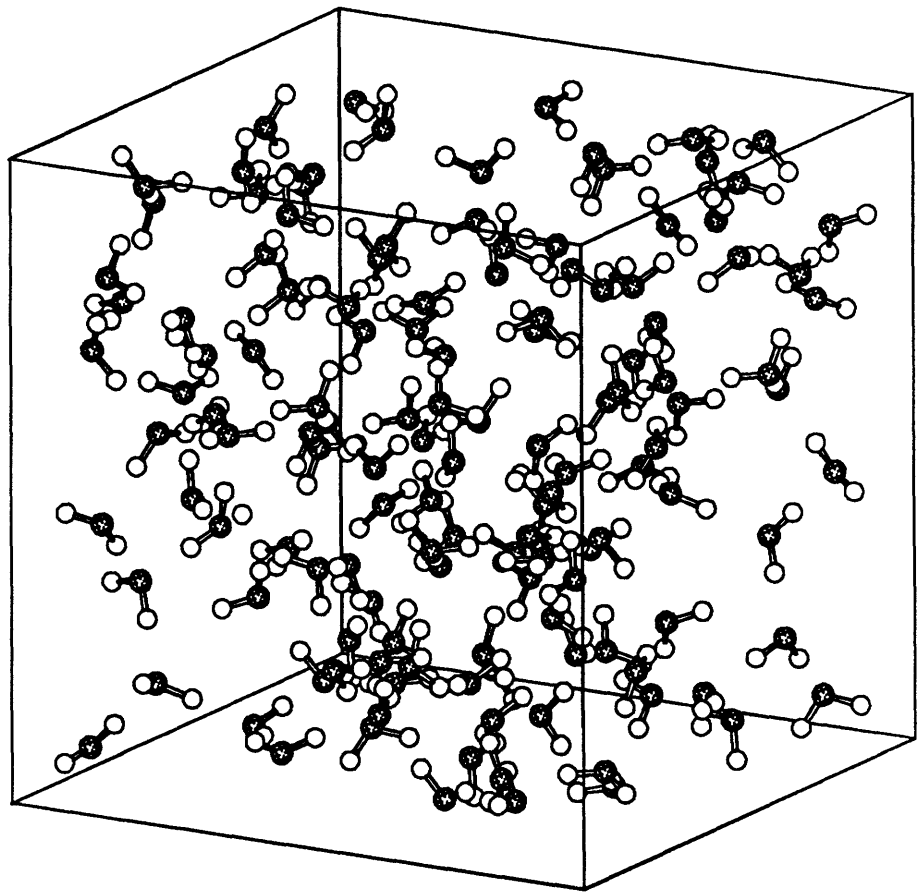

Figure 4.11 **Ball and Stick Representation of the Structure II Unit Cell**

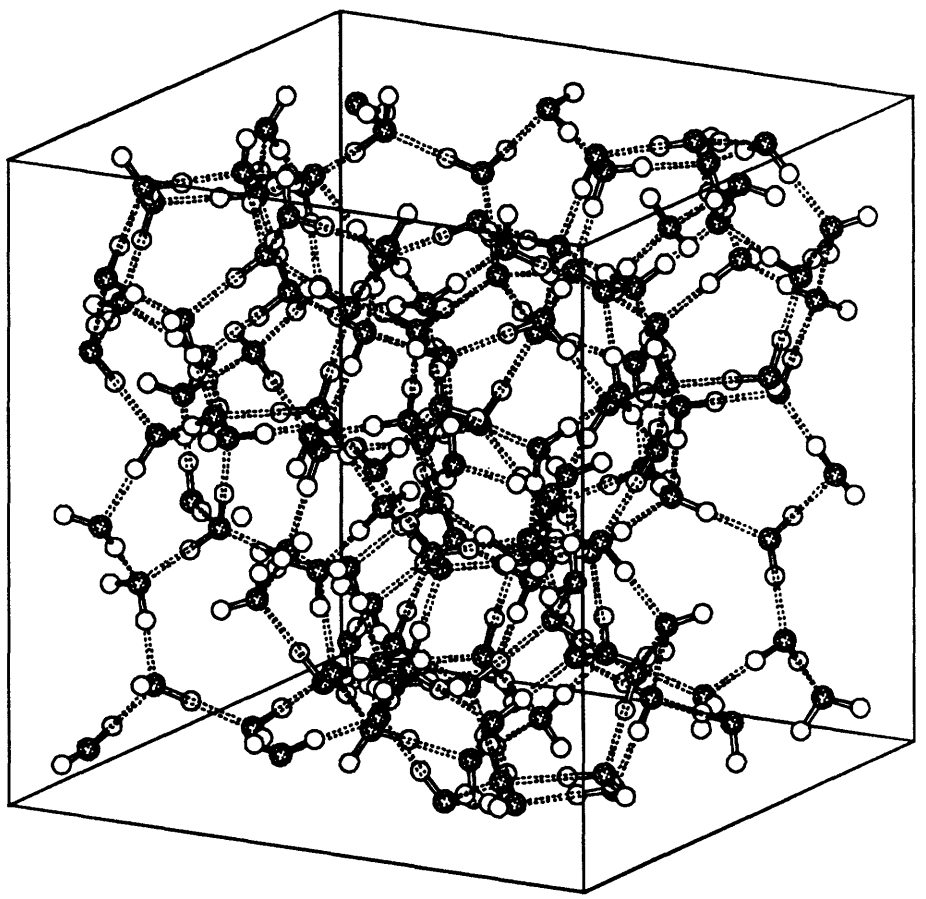

Figure 4.12 **Hydrogen Bond Depiction of the Structure II Unit Cell**

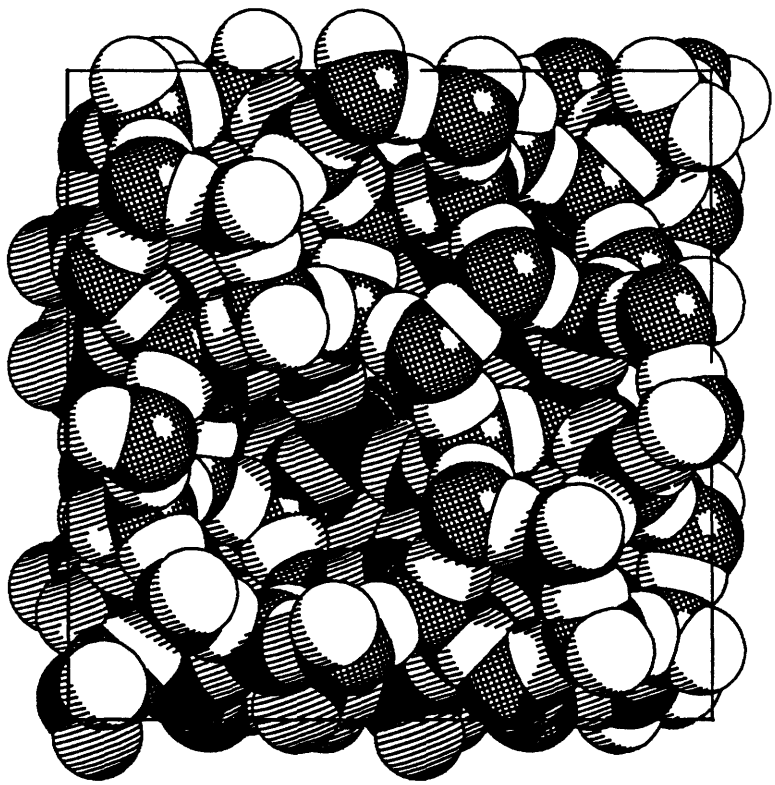

Figure 4.13 **Space Filling Representation of the Structure II Unit Cell**

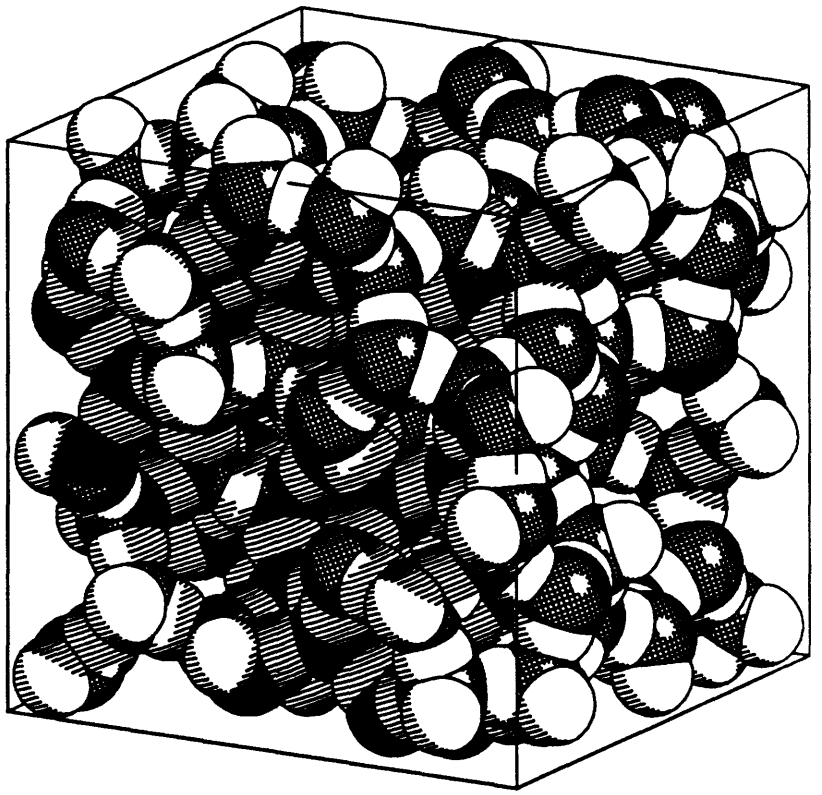

Figure 4.14 **Space Filling Representation of the Structure II Unit Cell**

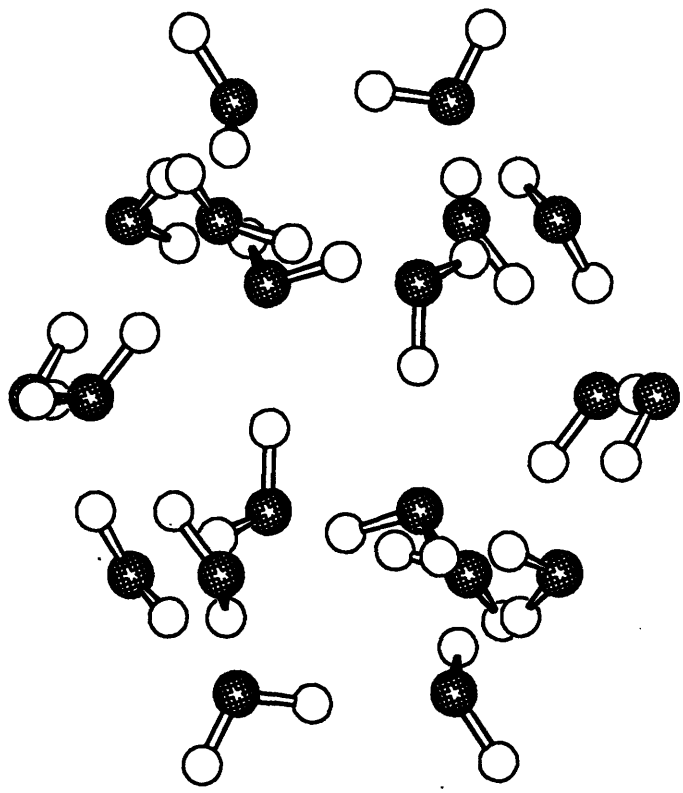

Figure 4.15 **Ball and Stick Representation of the Structure I Dodecahedron**

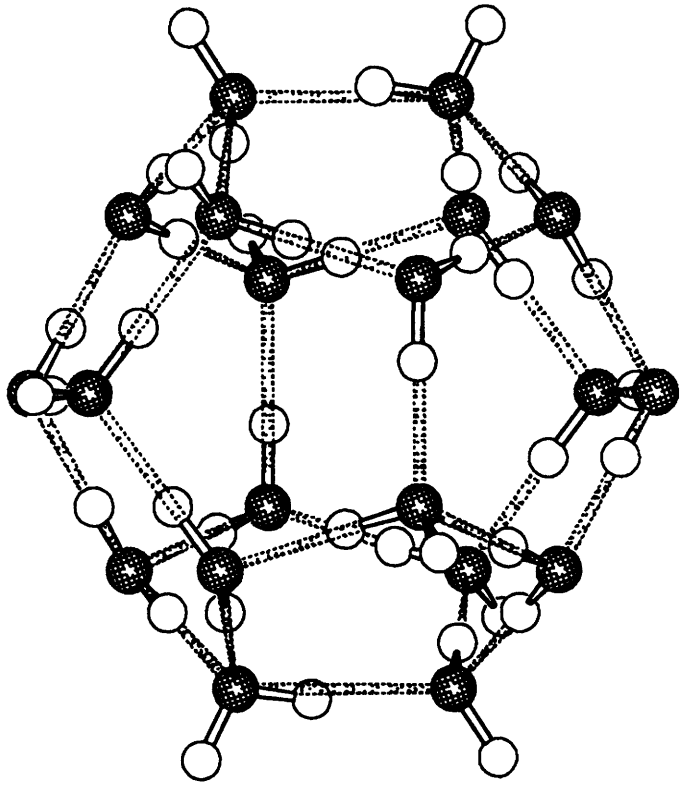

Figure 4.16 **Hydrogen Bond Depiction of the Structure I Dodecahedron**

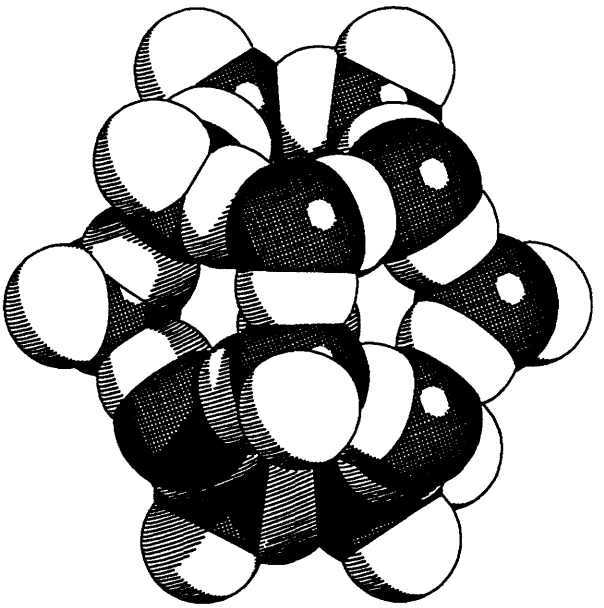

Figure 4.17 **Space Filling Representation of the Structure I** Dodecahedron

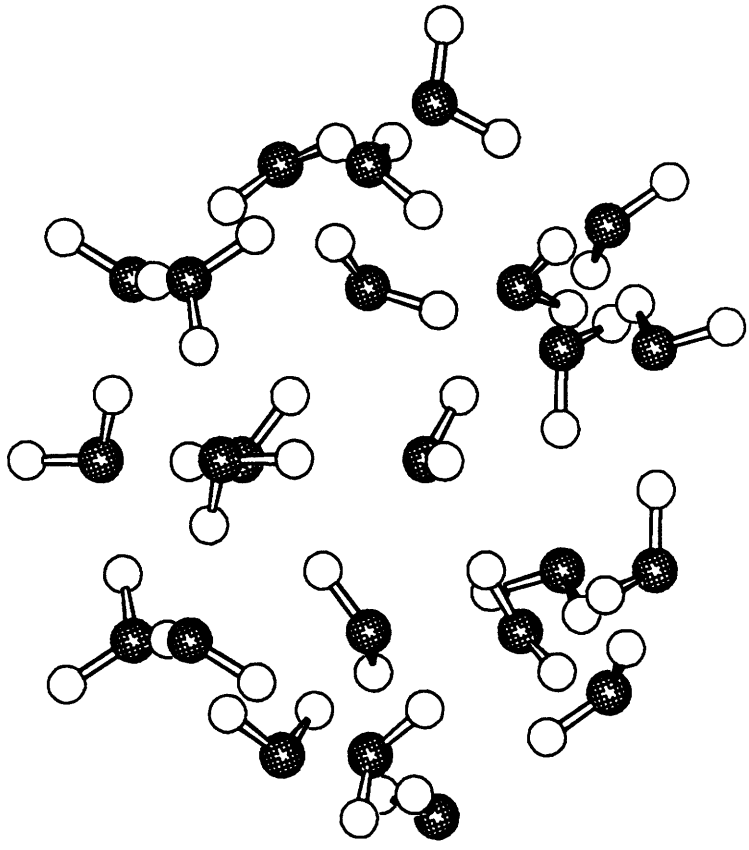

Figure 4.18 **Ball and Stick Representation of the Structure I Tetrakaidecahedron**

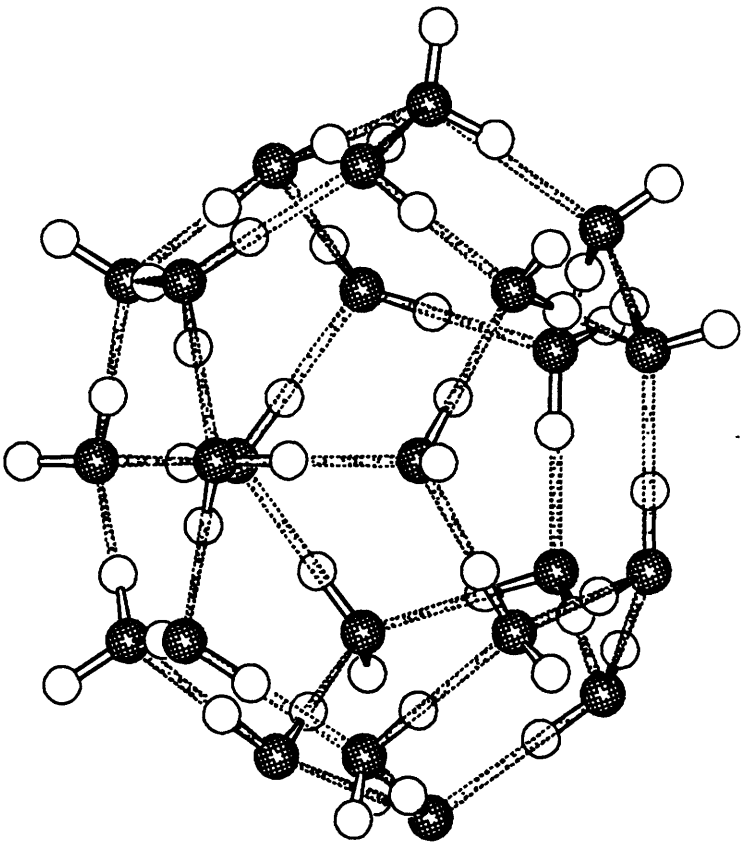

Figure 4.19 Hydrogen Bond Depiction of the Structure I Tetrakaidecahedron

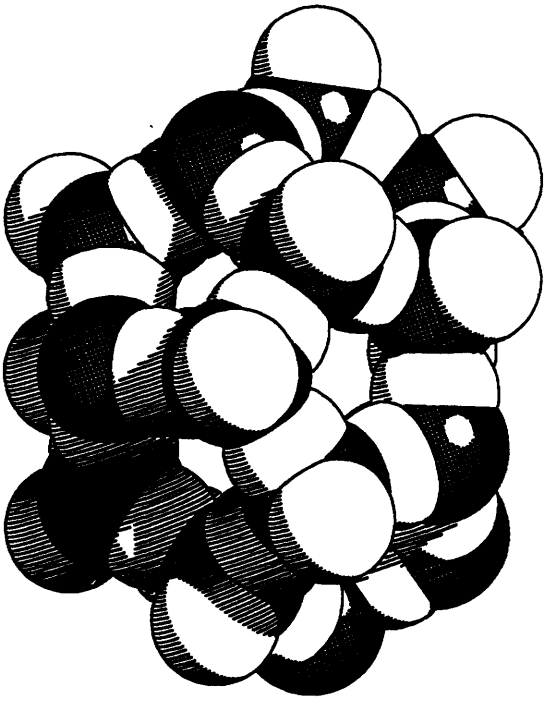

Figure 4.20 **Space Filling Representation of the Structure I** Tetrakaidecahedron

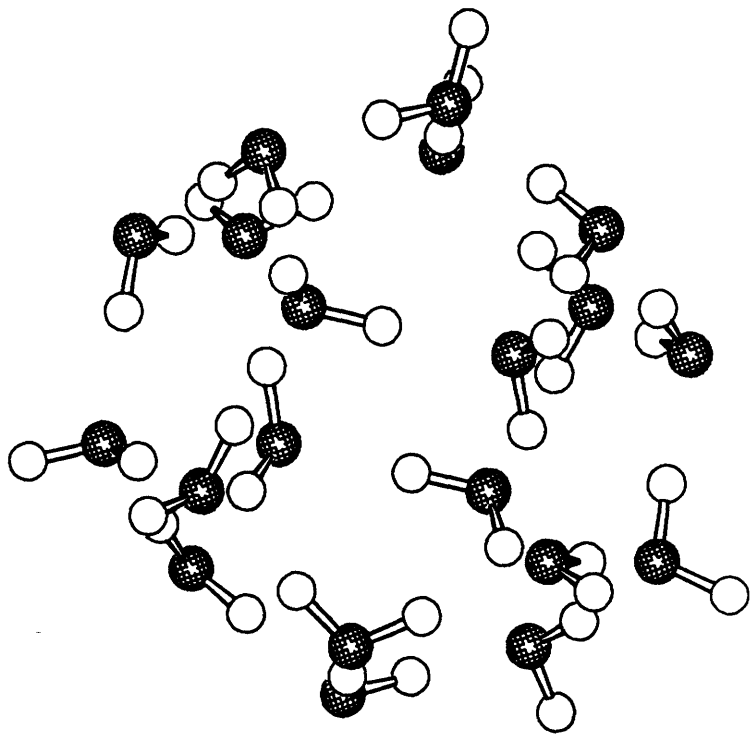

Figure 4.21 **Ball and Stick Representation of the Structure II Dodecahedron**

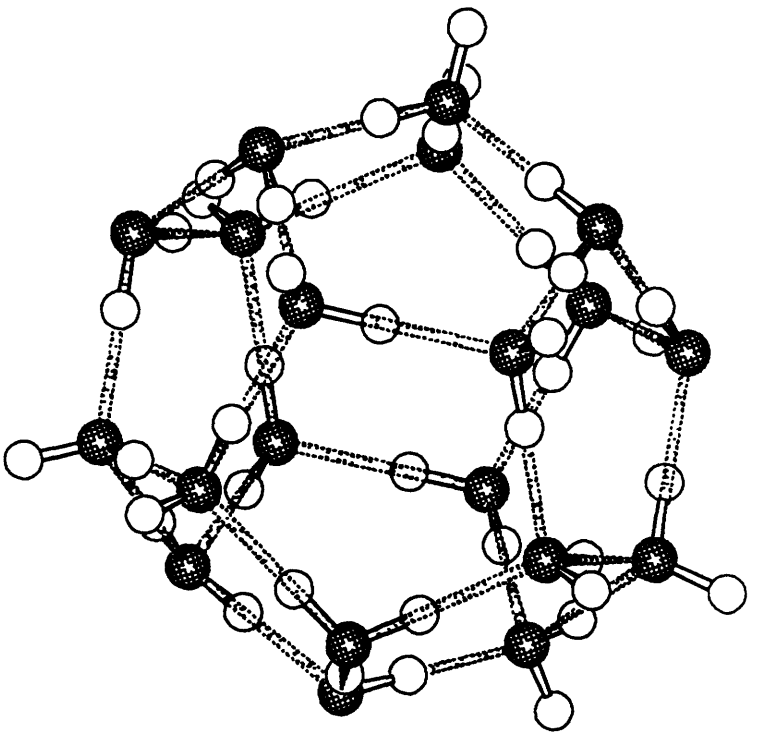

Figure 4.22 **Hydrogen Bond Depiction of the Structure II Dodecahedron**

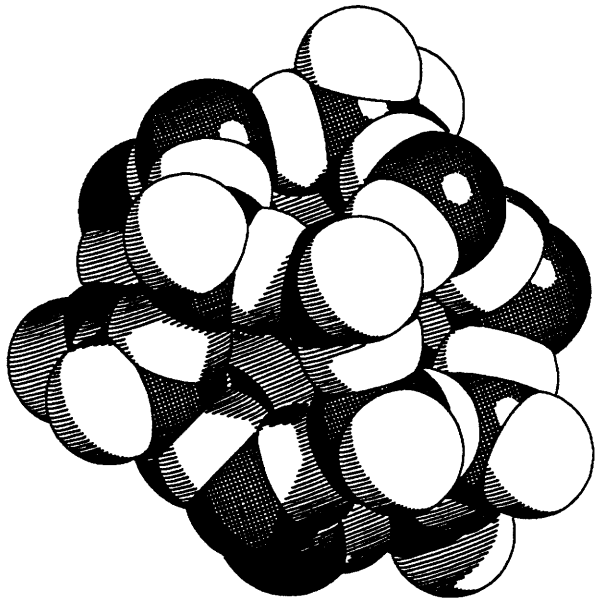

Figure 4.23 **Space Filling Representation of the Structure II** Dodecahedron

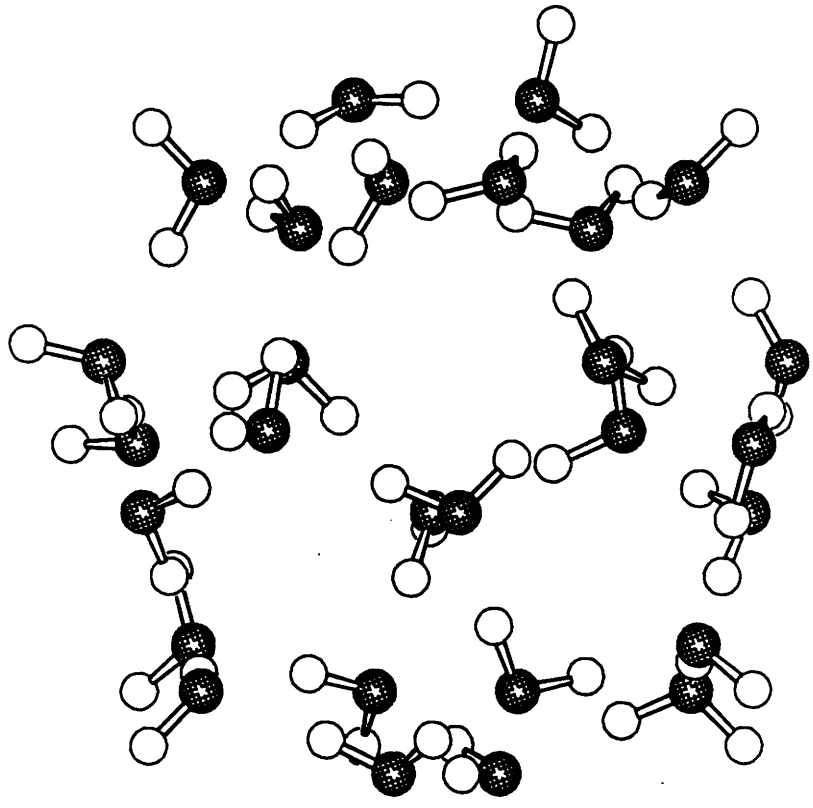

Figure 4.24 **Ball and Stick Representation of the Structure II** Hexakaidecahedron

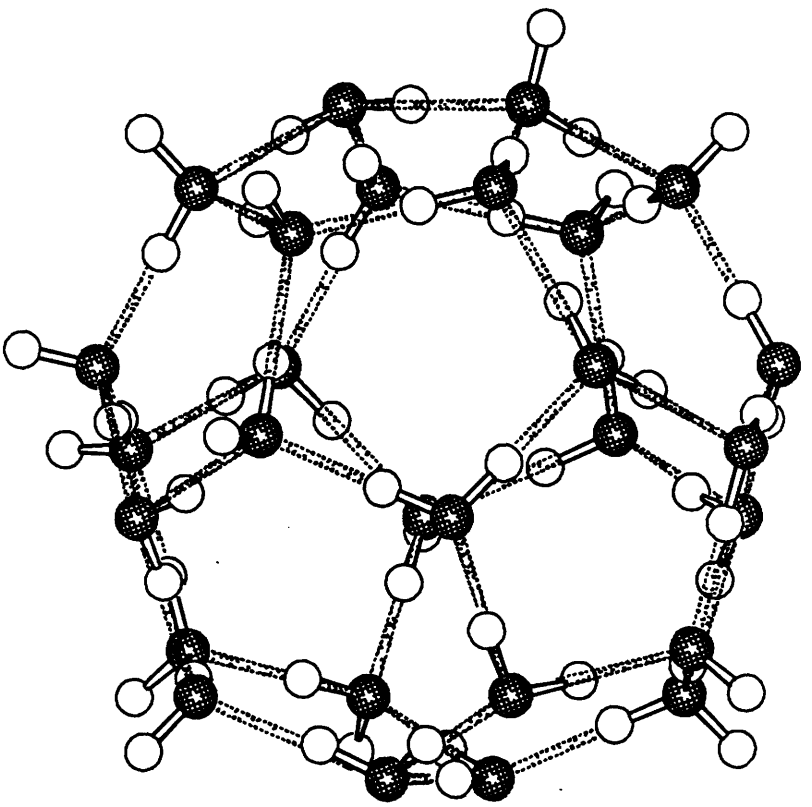

Figure 4.25 **Hydrogen Bond Depiction of the Structure II** Hexakaidecahedron

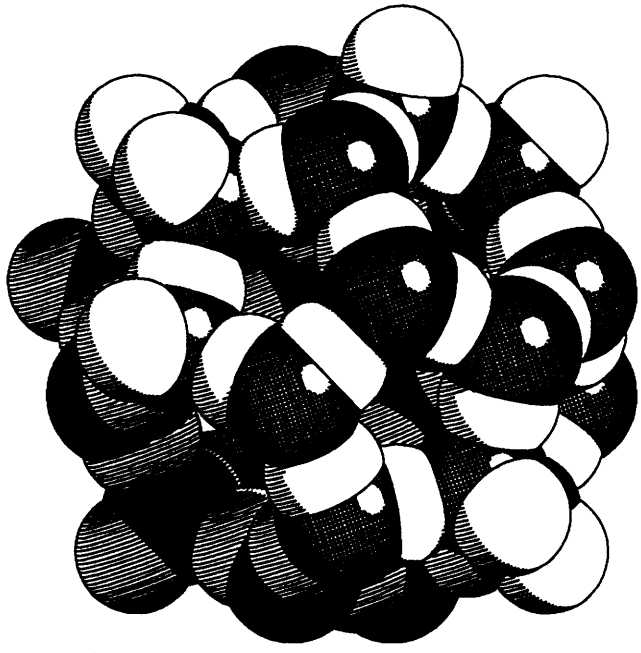

Figure 4.26 **Space Filling Representation of the Structure II** Hexakaidecahedron

5. STATISTICAL MECHANICAL THEORY OF CLATHRATES

5.1 Rigorous Review of van der Waals and Platteeuw Model

In 1959, van der Waals and Platteeuw proposed that the thermodynamic properties of clathrates could be derived from a simple model corresponding to the three-dimensional generalization of ideal localized adsorption. The formulation of their model is based on several important assumptions:

1) *Neglect cage distortions:*
The contribution of the host molecules to the total free energy is independent of the mode of occupation of the cavities.

2) *Single molecule occupation of cages:*
The guest molecules are localized in the cavities, and a host cavity can never hold more than one guest molecule.

3) *Neglect guest-guest interactions:*
Interactions between neighboring guest molecules are ignored.

4) *Classical statistics are valid:*
The temperatures of interest are such that Boltzmann statistics are applicable.

If we assume the contribution the host water molecules have on the total free energy of the clathrate structure is independent of the mode of occupation of the cavities (assumption (1)) then we can write that the total free energy as simply the

sum of the free energy of all of the encaged guest molecules and the free energy of the empty host lattice.

$$A(N,V,T) = A^{\beta} + A^{M} \tag{5.1}$$

where $A(N,V,T)$ is the total Helmholtz free energy defined for a system containing N molecules with a volume V and at a temperature T. A^{β} is the Helmholtz free energy of the empty host lattice and A^{M} is the Helmholtz free energy of the "encaged" solute or guest molecules.

Statistical mechanics provides the following relationship:

$$A(N,V,T) = -kT \ln Q(N,V,T) \tag{5.2}$$

where $Q(N,V,T)$ is the canonical partition function of the entire clathrate phase including guest and host contributions.

If we combine Equations (5.1) and (5.2), then

$$Q(N,V,T) = e^{-A^{\beta}/kT} e^{-A^{M}/kT} = e^{-A^{\beta}/kT} Q^{M} \tag{5.3}$$

where Q^{M}, the canonical partition function of the encaged guest molecules, is expressed as

$$Q^{M} = \prod_{i} \Omega_{i} \prod_{J} q_{Ji}^{N_{Ji}} \tag{5.4}$$

and Ω_i is a combinatorial factor describing the number of distinct ways in which N_{Ai}, N_{Bi}, ..., N_{Mi} solute molecules can be distributed over $\nu_i N_w$ cavities of type i. ν_i is defined as the number of type i cavities per water molecule in the host lattice, N_w is the total number of water molecules, and q_{Ji} is the molecular partition function of a type J solute molecule (A, B, ..., M) when encaged in a type i cavity.

If we now assume single molecule occupation of the cavities at most (assumption 2), the combinatorial factor can be expressed as

$$\Omega_i = \frac{(\nu_i N_w)!}{(\nu_i N_w - \sum_J N_{Ji})! \prod_J N_{Ji}!} \tag{5.5}$$

Combining Equations (5.3), (5.4), and (5.5) yields the following expression

$$Q = e^{-A^\beta/kT} \prod_i \left(\frac{(\nu_i N_w)!}{(\nu_i N_w - \sum_J N_{Ji})! \prod_J N_{Ji}!} \prod_J q_{Ji}^{N_{Ji}} \right) \tag{5.6}$$

The absolute activity, λ_J, of component J, is defined by

$$\mu_J \equiv kT \ln \lambda_J \tag{5.7}$$

where μ_J is the chemical potential of species J. If we multiply Equation (5.6) by the product

$$\lambda_A^{N_{A1}} \lambda_A^{N_{A2}} \ldots \lambda_B^{N_{B1}} \ldots \lambda_M^{N_{Mn}} = \prod_i \prod_J \lambda_J^{N_{Ji}} \tag{5.8}$$

while summing over all possible values of N_{Ji}, we obtain the following function

$$\Xi = e^{-A^\beta/kT} \sum_{N_{Ji}} \prod_i \left(\frac{(\nu_i N_w)!}{(\nu_i N_w - \sum_J N_{Ji})! \prod_J N_{Ji}!} \prod_J q_{Ji}^{N_{Ji}} \lambda_J^{N_{Ji}} \right) \tag{5.9}$$

Equation (5.9) can be further simplified through the use of the multinomial expansion

$$\left(1 + \sum_J q_{Ji}\lambda_J\right)^{\nu_i N_w} = \sum_{N_{Ji}} \left(\frac{(\nu_i N_w)!}{(\nu_i N_w - \sum_J N_{Ji})! \prod_J N_{Ji}!} \prod_J q_{Ji}^{N_{Ji}} \lambda_J^{N_{Ji}} \right) \tag{5.10}$$

to the following expression

$$\Xi = e^{-A^\beta/kT} \prod_i \left(1 + \sum_J q_{Ji}\lambda_J \right)^{\nu_i N_w} \tag{5.11}$$

By definition, f_J, the fugacity of component J is related to the chemical potential by

$$\mu_J = kT \ln f_J + \mu_J^0(T) \tag{5.12}$$

where the pressure independent ideal gas function, μ_J^0, is given by

$$\mu_J^0(T) = -kT \ln\left(q_{J,t} q_{J,v} q_{J,r}\right) \tag{5.13}$$

where $q_{J,t}$ is the ideal gas individual translational partition function of a molecule of type J, $q_{J,v}$ is the individual ideal gas vibrational partition function, and $q_{J,r}$ is the individual ideal gas rotational partition function. We can therefore express the absolute activity of component J as

$$\lambda_J = \frac{1}{kT}\left(\frac{f_J}{q_{J,t} q_{J,v} q_{J,r}}\right) \tag{5.14}$$

The molecular partition function of a type J molecule when encaged in a type i cavity can be expressed as

$$q_{Ji} \equiv q_{J,t}\, q_{J,v}\, q_{J,r}\, Z_{Ji} \tag{5.15}$$

where Z_{Ji} is the configurational integral of a single guest molecule of type J in a cavity of type i. Combining Equations (5.11), (5.13), and (5.14) results in

$$\Xi = e^{-A^{\beta}/kT} \prod_i \left(1 + \sum_J \frac{Z_{Ji}}{kT} f_J \right)^{\nu_i N_w} \tag{5.16}$$

If we define the "Langmuir Constant", C_{Ji}, as

$$C_{Ji} \equiv \frac{Z_{Ji}}{kT} \tag{5.17}$$

then

$$\Xi = e^{-A^{\beta}/kT} \prod_i \left(1 + \sum_J C_{Ji} f_J \right)^{\nu_i N_w} \tag{5.18}$$

C_{Ji} accounts for the guest-host intermolecular interaction and can be related to the "free volume" or configurational partition function by the following 6-dimensional integral over the system volume V.

$$C_{Ji} = \frac{(kT)^{-1}}{8\pi^2} \int_V e^{-U(r,\theta,\phi,\alpha,\beta,\gamma)/kT} r^2 \sin\theta \, d\theta \, d\phi \, dr \, d\alpha \sin\beta \, d\beta \, d\gamma \tag{5.19}$$

where U is the total intermolecular interaction potential between the guest molecule and all host molecules defined in spherical coordinates r, θ, and ϕ and Euler orientation angles α, β, and γ for the guest molecule. Evaluation methods for C_{Ji} are described in Chapter 6.

Equation (5.17) is a grand canonical partition function with respect to the encaged guest molecules [superscript *M*], but an ordinary canonical partition function with respect to the host lattice [superscript H]. We can therefore write

$$\Xi = Q^H \Xi^M \tag{5.20}$$

Statistical mechanics gives us the needed link with thermodynamics by the relations (McQuarrie, 1976):

$$dA^H = -d(kT \ln Q^H) = -S^H dT - P dV^H + \mu_w^H dN_w \tag{5.21}$$

$$d(pV^M) = d(kT \ln \Xi^M) = S^M dT + P dV^M + \sum_J N_w d\mu_J \tag{5.22}$$

Subtracting Equation (5.21) from Equation (5.22) yields

$$d(kT \ln \Xi) = S dT + P dV + \sum_J N_J d\mu_J - \mu_w^H dN_w \tag{5.23}$$

The chemical potential of the water in hydrate phase follows immediately from Equation (5.23)

$$\frac{\mu_w^H}{kT} = -\left(\frac{\partial \ln \Xi}{\partial N_w}\right)_{T,V,\mu_J} \tag{5.24}$$

Applying Equation (5.24) to Equation (5.18) yields

$$\frac{\mu_w^H}{kT} = \frac{1}{kT}\left(\frac{\partial A^\beta}{\partial N_w}\right) - \sum_i \nu_i \ln\left(1 + \sum_J C_{Ji} f_J\right) \tag{5.25}$$

or simply

$$\frac{\mu_w^H}{kT} = \frac{\mu_w^\beta}{kT} - \sum_i \nu_i \ln\left(1 + \sum_J C_{Ji} f_J\right) \tag{5.26}$$

where

$$\left(\frac{\partial A^\beta}{\partial N_w}\right)_{T,V} \equiv \mu_w^\beta \tag{5.27}$$

μ_w^β being the chemical potential of the host water molecules in the hypothetical empty lattice.

The composition of the clathrate follows similarly from Equation (5.23)

$$N_k = \left(\frac{\partial \ln \Xi}{\partial \mu_k}\right)_{T,V,N_w,\mu_{J[J\neq k]}} \tag{5.28}$$

which can be equivalently rewritten as either

$$N_k = \lambda_k \left(\frac{\partial \ln \Xi}{\partial \lambda_k}\right)_{T,V,N_w,\lambda_{J[J\neq k]}} \tag{5.29}$$

or

$$N_k = f_k \left(\frac{\partial \ln \Xi}{\partial f_k}\right)_{T,V,N_w,f_{J[J\neq k]}} \tag{5.30}$$

Thus the composition of the water clathrate is given by

$$N_k = f_k \left(\frac{\partial \ln \Xi}{\partial f_k} \right)_{T,V,N_w,f_{J(J \neq k)}} = \sum_i \frac{\nu_i N_w C_{ki} f_k}{(1 + \sum_J C_{Ji} f_J)} \tag{5.31}$$

The composition of a type i cavity being

$$N_{ki} = \frac{\nu_i N_w C_{ki} f_k}{(1 + \sum_J C_{Ji} f_J)} \tag{5.32}$$

Dividing N_{ki} by the total number of cavities of type i, $\nu_i N_w$, yields the following result

$$y_{ki} = \frac{N_{ki}}{\nu_i N_w} = \frac{C_{ki} f_k}{(1 + \sum_J C_{Ji} f_J)} \tag{5.33}$$

where y_{ki} is the probability of finding a guest molecule of type k in a type i cavity.

Now, if we reexamine Equation (5.26), rewritten here for convenience

$$\frac{\Delta\mu_w^{\beta-H}}{kT} \equiv \frac{\mu_w^{\beta}}{kT} - \frac{\mu_w^{H}}{kT} = \sum_i \nu_i \ln\left(1 + \sum_J C_{Ji} f_J\right) \tag{5.34}$$

it is evident that the equation can be equivalently expressed as

$$\frac{\Delta\mu_w^{\beta-H}}{kT} = -\sum_i \nu_i \ln\left(\frac{1}{1 + \sum_J C_{Ji} f_J}\right) \tag{5.35}$$

and if we simply add and subtract the simple summation involving the Langmuir constant and the guest component fugacity to the numerator of Equation (5.34) we get

$$\frac{\Delta\mu_w^{\beta-H}}{kT} = -\sum_i \nu_i \ln\left(\frac{1 + \sum_J C_{Ji} f_J - \sum_J C_{Ji} f_J}{1 + \sum_J C_{Ji} f_J}\right) \tag{5.36}$$

which can be further simplified to

$$\frac{\Delta\mu_w^{\beta-H}}{kT} = -\sum_i \nu_i \ln\left(1 - \sum_J \frac{C_{Ji} f_J}{1 + \sum_J C_{Ji} f_J}\right) \tag{5.37}$$

or equivalently

$$\frac{\Delta\mu_w^{\beta-H}}{kT} = -\sum_i \nu_i \ln\left(1 - \sum_J y_{Ji}\right) \tag{5.38}$$

where now the chemical potential difference, $\Delta\mu_w^{\beta-H}$, is simply related to the composition of the hydrate in terms of the fractional cavity occupation probabilities, y_{Ji}.

5.2 Phase Equilibria

A pure gas hydrate can be treated thermodynamically as a two-component system consisting of water and a particular guest component. When three equilibrium phases are present, the system will be monovariant, and fixing the temperature should specify the pressure. The equilibrium vapor pressure, often referred to as the dissociation pressure, is commonly measured as a function of temperature for various three-phase, monovariant systems. Multicomponent water clathrates gas hydrates are generally treated in a similar fashion by fixing the gas phase composition.

Equilibrium requires that the chemical potential of water in hydrate phase must be equal to the chemical potential of water in either the solid ice phase, or the liquid aqueous phase, depending on whether the temperature is above or below the ice point. If we assume that there is no significant freezing point depression associated with the solubilization of the guest components in the liquid water, then this can be written approximately as:

(T < 273.15 K)

$$\begin{aligned} \mu_w^H &= \mu_w^\alpha \\ \mu_w^\beta - \mu_w^H &= \mu_w^\beta - \mu_w^\alpha \\ \Delta\mu_w^{\beta\text{-}H} &= \Delta\mu_w^{\beta\text{-}\alpha} \end{aligned} \tag{5.39}$$

(T > 273.15 K)

$$\begin{aligned} \mu_w^H &= \mu_w^L \\ \mu_w^\beta - \mu_w^H &= \mu_w^\beta - \mu_w^L \\ \Delta\mu_w^{\beta\text{-}H} &= \Delta\mu_w^{\beta\text{-}L} \end{aligned} \tag{5.40}$$

where μ_w^H is the chemical potential of water in the hydrate phase, μ_w^α is the chemical potential of water in the solid ice phase (assumed to be pure), μ_w^L is the chemical potential of water in the liquid aqueous phase, and μ_w^β is the chemical potential of the hypothetical empty hydrate phase.

Thermodynamically, we know the total differential of the quantity μ/T as a simple function of temperature and pressure can be written as

$$d(\mu/T) = \left(\frac{\partial(\mu/T)}{\partial T}\right)_{P,x} dT + \left(\frac{\partial(\mu/T)}{\partial P}\right)_{T,x} dP \quad , \tag{5.41}$$

where the temperature derivative is given by the familiar Gibbs-Helmholtz relationship:

$$\left(\frac{\partial(\mu/T)}{\partial T}\right)_{P,x} = -\frac{\Delta H}{T^2} \tag{5.42}$$

and

$$\left(\frac{\partial(\mu/T)}{\partial P}\right)_{T,x} = \frac{\Delta V}{T} \tag{5.43}$$

Thus the expression for the total differential, rewritten as

$$d(\mu/T) = \frac{\Delta H}{T^2} dT + \frac{\Delta V}{T} dP \quad , \tag{5.44}$$

gives us the additional equation needed to model the equilibrium properties of water clathrates.

Following the convention proposed by Holder et al. (1980), the chemical potential difference between water in the hypothetical empty clathrate phase (β) and water in either the pure ice phase (α) or aqueous liquid phase (L) can be expressed as:

$$\frac{\Delta\mu_w^{\beta\text{-}L,\alpha}(T,P)}{kT} = \frac{\Delta\mu_w^{\beta\text{-}L,\alpha}(T_0,0)}{kT_0} - \int_{T_0}^{T}\left(\frac{\Delta H_w^{\beta\text{-}L,\alpha}}{kT^2}\right)_P dT$$

$$+ \int_0^P \left(\frac{\Delta V_w^{\beta\text{-}L,\alpha}}{kT}\right)_T dP - \ln a_w^L \qquad (5.45)$$

where $\Delta\mu_w^{\beta\text{-}L}(T_0,0)$ is the reference chemical potential difference at the reference temperature, T_0, and zero pressure. The temperature dependence of the enthalpy difference is given by

$$\Delta H_w^{\beta\text{-}L,\alpha} = \Delta H_w^{\beta\text{-}L,\alpha}(T_0) + \int_{T_0}^{T} \Delta C_p^{\beta\text{-}L,\alpha}\, dT \qquad (5.46)$$

where the heat capacity difference is approximated by

$$\Delta C_{p_w}^{\beta\text{-}L,\alpha} = \Delta C_{p_w}^{\beta\text{-}L,\alpha}(T_0) + b^{\beta\text{-}L,\alpha}(T - T_0) \qquad (5.47)$$

The volume difference in Equation (5.44) is assumed to be constant. The additional term involving the activity of water, a_w^L, is a correction for the chemical potential difference from that in pure liquid water to that in the water-rich aqueous phase. The reference temperature, T_0, is usually taken to be 273.15 K.

Equations (5.45), (5.46), and (5.47) combined with the statistical mechanically derived expressions for the chemical potential difference, rewritten here for convenience

$$\frac{\Delta\mu_w^{\beta-H}}{kT} = \sum_i \nu_i \ln\left(1 + \sum_J C_{Ji} f_J\right) \tag{5.48}$$

$$\frac{\Delta\mu_w^{\beta-H}}{kT} = -\sum_i \nu_i \ln\left(1 - \sum_J y_{Ji}\right) \tag{5.49}$$

provide the necessary relationships needed to perform phase equilibrium calculations.

For example for a single guest component J structure I water clathrate, the chemical potential difference can be written as

$$\frac{\Delta\mu_w^{\beta-H}}{kT} = -\frac{1}{23}\ln\left(1 - y_{J,1}\right) - \frac{3}{23}\ln\left(1 - y_{J,2}\right) \tag{5.50}$$

Therefore if we were able to accurately measure the composition of a water clathrate as a function of both temperature and pressure, then we could easily correlate the chemical potential difference through the use of Equations (5.45), (5.46), and (5.47). This however, would require that the fractional occupation of both cavity types be known, and unfortunately, this is practically impossible to do from a simple overall compositional measurement. However, there exists several clathrate systems in which only the larger of the cavities is actually filled by the guest component. In such a case as this, $y_{J,1}$ would equal zero, thus reducing Equation (5.50) to

$$\frac{\Delta\mu_w^{\beta-H}}{kT} = -\frac{3}{23}\ln\left(1 - y_{J,2}\right) \tag{5.51}$$

where now the fractional occupation probability of the tetrakaidehedral cavities is simply related to the overall composition of the hydrate by the expression

$$y_{J,2} = \frac{x_J}{(6/(6+46))} \tag{5.52}$$

where x_J is the measured mole fraction of the guest component in the water clathrate. The denominator represents the ideal composition with completely filled cavities.

This simple compositional relationship provides a simple means for the determination of the thermodynamic reference properties of structure I water clathrate systems. The currently accepted parameters are those derived from the reanalysis (Holder et al., 1984) of the meticulous compositional measurements of the structure I cyclopropane water clathrate system (Dharmawardhana et al., 1980, 1981). These parameters are given in Table 5.1.

The thermodynamic reference properties of the structure II water clathrate system are not given here since insufficient compositional data has been taken for a proper correlational analysis. The use of the Langmuir constant form of the chemical potential difference expression ((Equation (5.48)) along with the simplistic treatment of the Langmuir constant evaluation places great uncertainty on the currently published parameters.

Thermodynamic Reference Properties Structure I - Water Clathrate	
Chemical Potential Difference (T_o, P_o) [1,2]	
$\Delta\mu_w^{\beta-\alpha}$	1299.4 J mol^{-1}
Enthalpy Difference (T_o, P_o) [1,2]	
$\Delta H_w^{\beta-\alpha}$	1861.0 J mol^{-1}
Heat of Fusion (T_o, P_o)	
$\Delta H_w^{L-\alpha}$	6009.5 J mol^{-1}
Volume Differences [3]	
$\Delta v_w^{\beta-\alpha}$	3.0×10^{-6} m^3 mol^{-1}
$\Delta v_w^{L-\alpha}$	-1.634×10^{-6} m^3 mol^{-1}
Heat Capacity Differences [4]	
($T > T_o$)	
$\Delta C_p^{\beta-L}$	-37.32 J mol^{-1} K^{-1}
$b^{\beta-L}$	0.179 J mol^{-1} K^{-2}
($T < T_o$)	
$\Delta C_p^{\beta-\alpha}$	0.565 J mol^{-1} K^{-1}
$b^{\beta-\alpha}$	0.002 J mol^{-1} K^{-2}
[1] *Holder, Malekar, and Sloan (1984)* [2] *Dharmawardhana, Parrish, and Sloan (1980, 1981)* [3] *van Stackelberg and Müller (1954)* [4] *Holder, Corbin, and Papadopoulos (1980)* T_o = 273.15 K P_o = 0 atm	

Table 5.1 Thermodynamic Reference Properties - Structure I Water Clathrate

6. CONFIGURATIONAL PARTITION FUNCTION

Having derived an equation in Section 5.1 (see Equation (5.24)) for the chemical potential difference between water in the hydrate phase and water in the hypothetical empty hydrate. We must find a way to calculate the guest-host configurational partition function. Specifically, if the guest molecule is modeled as a multi-site rigid body, then the six orientational degrees of freedom associated with the guest within a clathrate cavity must be considered directly in the evaluation of the configurational partition function over the system volume V

$$Z_{Ji} = \frac{1}{8\pi^2} \int_V e^{-U(r,\theta,\phi,\alpha,\beta,\gamma)/kT} r^2 \sin\theta \, d\theta \, d\phi \, dr \, d\alpha \sin\beta \, d\beta \, d\gamma \tag{6.1}$$

where U is the total interaction potential between the guest molecule and all of the host water molecules. The position and orientation of the guest is given by the spherical coordinates r, θ, and ϕ, defined in terms of the center of a given cavity, and the Euler angles α, β, and γ. The factor of $8\pi^2$ simply being a normalization constant. The Euler angles are shown illustrated in Figure 6.1.

The transformation from the body-fixed cartesian coordinate system of a multi-site guest molecule can be transformed into the space-fixed cartesian coordinate system, defined in terms of the center of a given clathrate cavity, via the rotational transformation

$$x' = Ax \tag{6.2}$$

where A, the rotational transformation matrix, defined as merely the product of three rotational matrices

$$A = BCD \tag{6.3}$$

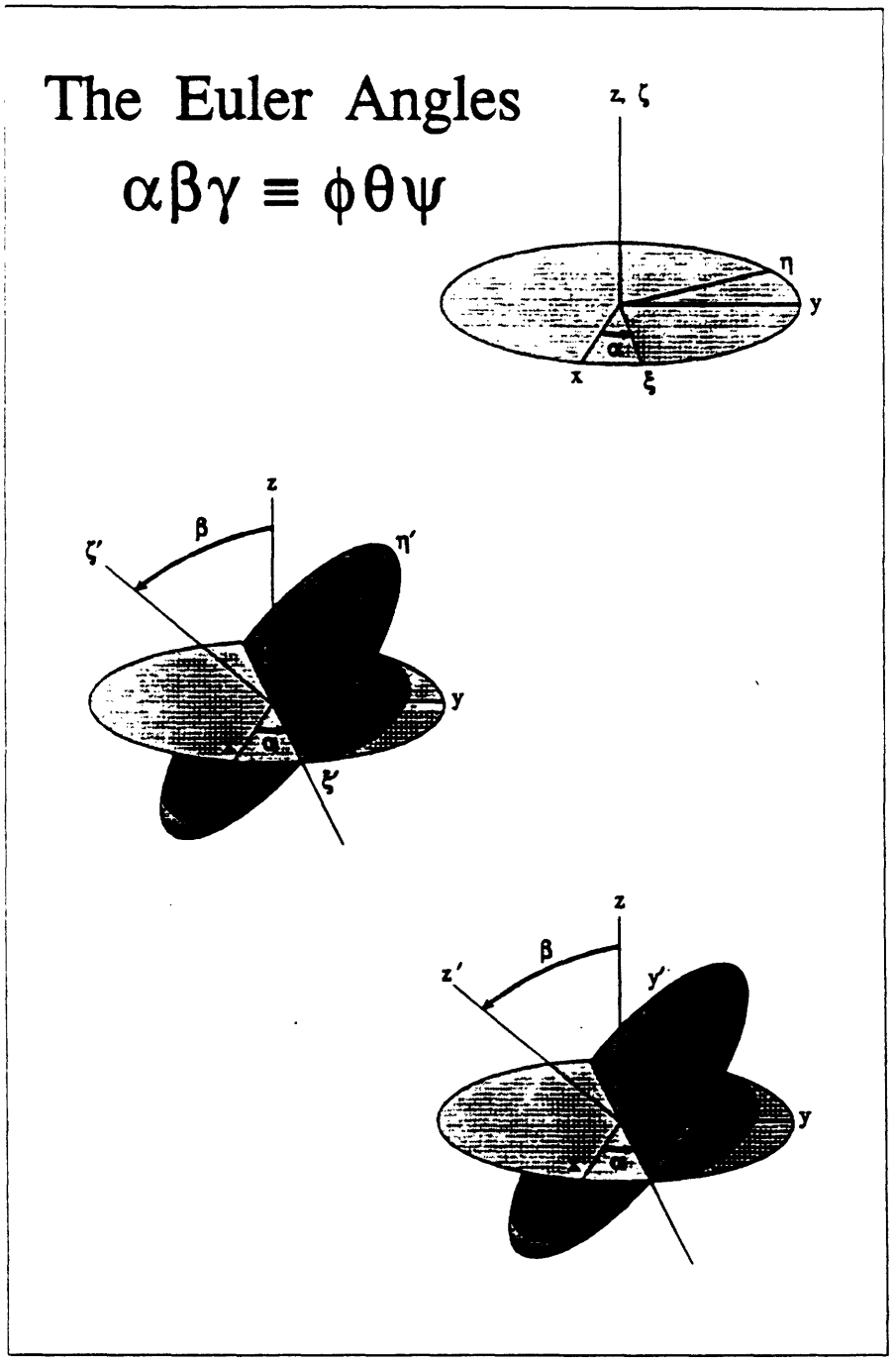

Figure 6.1 The Euler Angles (Goldstein, 1982)

is given by

$$\boldsymbol{A}=\begin{pmatrix} \cos\gamma\cos\alpha-\cos\beta\sin\alpha\sin\gamma & \cos\gamma\sin\alpha+\cos\beta\cos\alpha\sin\gamma & \sin\gamma\sin\beta \\ -\sin\gamma\cos\alpha-\cos\beta\sin\alpha\cos\gamma & -\sin\gamma\sin\alpha+\cos\beta\cos\alpha\cos\gamma & \cos\gamma\sin\beta \\ \sin\beta\sin\alpha & -\sin\beta\cos\alpha & \cos\beta \end{pmatrix} \tag{6.4}$$

Specifically, in terms of Figure 6.1, the transformation $\boldsymbol{D}$ corresponds to a rotation about the z axis

$$\boldsymbol{D}=\begin{pmatrix} \cos\alpha & \sin\alpha & 0 \\ -\sin\alpha & \cos\alpha & 0 \\ 0 & 0 & 1 \end{pmatrix} \tag{6.5}$$

the transformation $\boldsymbol{C}$ is a rotation about the ξ axis

$$\boldsymbol{C}=\begin{pmatrix} 1 & 0 & 0 \\ 0 & \cos\beta & \sin\beta \\ 0 & -\sin\beta & \cos\beta \end{pmatrix} \tag{6.6}$$

and finally the transformation $\boldsymbol{B}$ is a rotation about the ζ axis

$$\boldsymbol{B}=\begin{pmatrix} \cos\gamma & \sin\gamma & 0 \\ -\sin\gamma & \cos\gamma & 0 \\ 0 & 0 & 1 \end{pmatrix} \tag{6.7}$$

6.1 Previous Methods

6.1.1 Lennard-Jones Devonshire (LJD) Approximation

The asymmetries of the host lattice cavities and of the guest molecule itself makes analytical evaluation of the six-dimensional integral of Equation (5.18) intractable. Therefore a Lennard-Jones and Devonshire liquid cell theory approach is often adopted for the quantitative evaluation of the configurational partition function of the guest "solute" molecule within the host lattice cavity. The host water molecules are assumed to be uniformly distributed on a spherical surface corresponding to an average cavity radius. The guest molecule is also usually assumed to be spherically symmetric. This LJD spherical cell approach simplifies the integration considerably to a one-dimensional integral in r:

$$C_{Ji} = \frac{4\pi}{kT} \int e^{-W(r)/kT} r^2 \, dr \tag{6.8}$$

where the spherically symmetric cell potential, $W(r)$ is determined from

$$W(r) = \frac{1}{4\pi} \int_0^{2\pi} \int_0^{\pi} U(r,\theta,\phi) \sin\theta \, d\theta \, d\phi \tag{6.9}$$

The actual choice of the guest-host intermolecular interaction potential is a point of great concern and is therefore discussed extensively in Section 7.1.

6.1.2 Monte Carlo Simulation Techniques

In an earlier attempt to resolve the problems inherent to the spherical cell approximation, Tester et al. (1972) accounted for the asymmetries of the host lattice by using a Metropolis sampling Monte Carlo procedure (Metropolis et al., 1953) in the prediction of the equilibrium dissociation pressures for a variety of different water clathrates. A stochastic Monte Carlo (MC) approach of statistically sampling the states available to the guest molecule inside the host water cage was used to estimate the configurational partition function.

$$Z_{Ji} = \int_V e^{-U/kT}\, dV \tag{6.10}$$

The value of the configurational integral was approximated using the mean value theorem of integral calculus as

$$Z_{Ji} \equiv \langle e^{-U/kT} \rangle V_{Ji} \approx e^{-\langle U/kT \rangle} V_{Ji} \tag{6.11}$$

where $\langle\, U/kT \,\rangle$ was a Metropolis-averaged characteristic potential energy between the guest J and the host molecules associated with a type i cell, and V_{Ji} is the effective "free volume" available to the guest molecule within the clathrate cage.

Using the Berthelot geometric mean approximation for ε, and the hard sphere approximation for σ, the Lennard-Jones parameters for the host water molecules were adjusted to constrain the predicted dissociation pressure to match the experimental dissociation pressure of the argon-water clathrate at 0 °C. These "adjusted" parameters were then used to predict the dissociation pressures of other gas hydrate systems. These early calculations by Tester et al. (1972) were performed with the assumption that argon preferentially formed a Structure I hydrate, later crystallographic data indicated that argon instead forms a Structure II hydrate (Davidson et al., 1984). Nonetheless, although the

numerical values are obviously incorrect for a pure argon hydrate, the methodology was still a pioneering step in the modeling of the configurational characteristics of water clathrates.

In a separate study, Tse and Davidson (1982) also compared the spherical cell model with the Monte Carlo approach. They found the two models predict similar dissociation pressures for a number of the smaller hydrate guest molecules such as *Ar* and *Kr*. However, both models tend to inadequately predict thermodynamic properties for the larger less symmetric hydrate formers such as CH_4 and CF_4 when the simplistic 2-parameter, Lennard-Jones (6-12) interaction potential is used to describe the guest-host interactions. With these results they went on to construct a more theoretically realistic exp-6-8-10 potential model

$$U(r) = Ae^{-br} - \frac{C_6}{r^6} - \frac{C_8}{r^8} - \frac{C_{10}}{r^{10}} \qquad (6.12)$$

hoping to better model the higher-order dispersive interactions (dipole-quadrupole, quadrupole-quadrupole). Using the discrete Monte Carlo integration scheme (Tester et al., 1972) Tse and Davidson found the results to be very promising. Unfortunately, the poor quality of the experimental values of the exp-6-8-10 potential parameters limited the evaluation of their model.

A major problem associated with using a Metropolis type method, succinctly stated by Stroud et al. (1976), is that the method was really only designed to offer a simple method of estimating the ratio of two partition functions, such as those associated with an average property. For example, the average potential energy, expressed by

$$\langle U \rangle = \frac{\int\int \ldots \int U\, e^{-U/kT}\, dx_1 dx_2 \ldots dx_N}{\int\int \ldots \int e^{-U/kT}\, dx_1 dx_2 \ldots dx_N} \tag{6.13}$$

where $\langle U \rangle$ is the ensemble average of the potential energy. Although the sampling algorithm proposed by Metropolis et al. (1953) easily can be used to estimate the ensemble average of the potential energy, $\langle U \rangle$, it unfortunately, tells you nothing about the individual components of Equation (6.13), specifically the magnitude of either the numerator or the denominator. One should note, of course, that the modeling of water clathrates with the van der Waals-Platteeuw formulation requires only the evaluation of the configurational integral, or simply the denominator of Equation (6.13).

Another problem of using a Metropolis sampling procedure for clathrate modeling involves the determination of the "free volume" available to the guest molecules within the various cavities. Since the configurational volume associated with Metropolis sampling does not correspond to the "free volume" of the guest, this volume can only be estimated in terms of the region in which moves are "accepted". Under these conditions, the free volume is virtually impossible to calculate with sufficient accuracy, thus making the Metropolis sampling scheme and Equation (6.11) rather impractical to use in the evaluation of the configurational partition function.

6.1.3 Molecular Dynamics Techniques

Molecular Dynamics (MD) simulations on the Structure I water clathrates of methane, tetrafluoromethane, cyclopropane, ethylene oxide, and xenon have been carried out by Tse, Klein, and McDonald (1983a, b, 1984). Their primary objective was to investigate the phonon-scattering mechanism possibly responsible for the anomalous behavior of the thermal conductivity with respect to that of ice.

Tse, McKinnon, and Marchi (1987) have used constant pressure molecular dynamics calculations to simulate the thermal expansion of ice and the structure I hydrate. Marchi and Mountain (1987) performed similar calculations for the structure II hydrate.

Basu and Mountain (1988) have even used the dynamical properties derived from molecular dynamics calculations to evaluate the performance of rigid cell models, inherent to the evaluation of the configurational partition function, in the modeling of guest molecule dynamics.

The inadequacies of the LJD spherical cell approximation compelled Holder and Hwang (1987) to also try to account for the asymmetries associated with the host lattice. However, they chose to use MD rather than MC as a method for calculating the guest-host configurational partition function. In using the molecular dynamics method, they followed the trajectory of the guest within an assumed rigid water clathrate cavity using the Kihara potential to model the intermolecular interactions between the guest and the host water molecules. The time-averaged potential energy and an estimate of the "free volume" derived from the resulting trajectories of the guest molecule were then utilized via the mean value theorem (Equation (6.12)) to estimate the value of the configurational integral. However, in comparing their results with their earlier work (John and Holder, 1985) they found considerable differences between the Langmuir constants determined

via the MD method and those determined directly by a full three-dimensional integration. They concluded improperly that the three-dimensional integrations were incapable of capturing the orientational localizations, and as such gave incorrect higher values for the corresponding configurational integrations. These issues will be discussed further in Section 8.3.

6.2 Configurational Integral Evaluation

We explored several methods to evaluate the guest-host configurational partition function. Initially, the Metropolis Monte Carlo sampling technique described earlier was implemented. However, due to the uncertainties of the "free volume" estimates, this method was quickly abandoned. This method did, however, provide an accurate estimate of the ensemble averaged guest-host potential energy as defined by Equation (6.10). Therefore, the results of the Metropolis MC simulation could be used to compare directly with the averaged potential energy values resulting from the direct integration of Equation (6.13). Several standard integration techniques were used to evaluate the guest-host configurational properties. These included:

- Simple Monte Carlo Integration
- Composite Trapeziodal Rule
- Gauss-Legendre Quadrature

The simple Monte Carlo integration scheme is best described as a elementary application of the mean value theorem of integrable calculus, which in this context is expressed as:

$$Z_{Ji} = \int_V e^{-U/kT} dV \cong \langle e^{-U/kT} \rangle V \pm \left(\frac{\langle e^{-2U/kT} \rangle - \langle e^{-U/kT} \rangle^2}{N} \right)^{1/2} \tag{6.14}$$

where N is the number of random guest configurational samples. The averages $\langle e^{-U/kT} \rangle$ and $\langle e^{-2U/kT} \rangle$ are given by

$$\langle e^{-U/kT} \rangle \equiv \frac{1}{N}\sum_{k=1}^{N} e^{-U/kT} \qquad \langle e^{-2U/kT} \rangle \equiv \frac{1}{N}\sum_{k=1}^{N} e^{-2U/kT} \tag{6.15}$$

Applying the simple Monte Carlo integration scheme to the configurational integral of a spherically symmetric guest molecule results in a significant simplification of Equation (6.6). Here we have chosen not to include the variance term as a matter of convenience

$$Z_{Ji} \equiv \frac{2\pi^2 R}{N}\sum_{k=1}^{N} e^{-U(r_k,\theta_k,\phi_k)/kT} r_k^2 \sin\theta_k \tag{6.16}$$

Similarly, for an asymmetric guest molecule we can write

$$Z_{Ji} \cong \frac{\pi^3 R}{N}\sum_{k=1}^{N} e^{-U(r_k,\theta_k,\phi_k,\alpha_k,\beta_k,\gamma_k)/kT} r_k^2 \sin\theta_k \sin\beta_k \tag{6.17}$$

The major advantage associated with simple Monte Carlo integration is that it is extremely easy to implement and its accuracy, proportional to $N^{-1/2}$, is independent of the dimensionality of the integration. One disadvantage, however, of using simple Monte Carlo integration, is that it is ill-suited for estimating positionally averaged potential energy profiles within the different host lattice cavities.

Since standard numerical integration methods are set up to use some sort of one, two, or three-dimensional grid, they are better suited to yield positionally averaged information such as angle averaged potential energy profiles. This is an advantage in that the resulting potential profiles can be directly compared to those derived from the Lennard-Jones Devonshire spherical cell approximation.

The composite trapezoidal rule was implemented as a method for the estimation of the configurational partition function, a multi-interval 10-point Gauss-Legendre quadrature formula, however, was found to be a much more efficient technique in terms of the number of grid points dictated for a given level of accuracy. The flexibility associated with the use of a multi-interval integration method

$$\int_a^b f(x)dx = \int_a^{b/n} f(x)dx + \int_{b/n}^{2b/n} f(x)dx + \cdots + \int_{(n-1)b/n}^{b} f(x)dx \qquad (6.18)$$

overwhelmed the advantages of a single-interval, higher-order formula in that the accuracy of the integration was not restricted by the choice of the integration formula.

The actual evaluation of the multi-dimensional configurational partition function involved the simple repeated application of the one-dimensional 10-point Gauss-Legendre quadrature formula discussed extensively by Carnahan et al. (1969).

A subdivision of each dimension into 4 intervals was usually found to return values of sufficient accuracy, usually on the order of 1 part in 10,000. However, for the five and six dimensional integrations associated with asymmetric guest molecules, computational restrictions (cpu time) commonly allowed for only two or one subdivisions, respectively. For example, in the calculation of the configurational integral of cyclopropane, the use of a single interval for each dimension, corresponding to 10^6 Gauss points, required approximately 12 minutes of cpu time on the M.I.T. Cray 2 - Supercomputer Facility.

7. INTERMOLECULAR POTENTIAL FUNCTIONS

7.1 Guest-Host Intermolecular Potential Interactions

In the evaluation of any configurational property, the intermolecular interaction potential energy must be accurately represented. The thermodynamic properties of water clathrates depend critically on the exact value of the configurational partition function of the guest molecules within the host lattice cavities which is rewritten here for convenience.

$$Z_{Ji} = \frac{1}{8\pi^2} \int_V e^{-U(r,\theta,\phi,\alpha,\beta,\gamma)/kT} r^2 \sin\theta \, d\theta \, d\phi \, dr \, d\alpha \sin\beta \, d\beta \, d\gamma \tag{7.1}$$

Generally, the total interaction potential between each guest molecule (J) and all host molecules is modeled as being pairwise additive

$$U(r,\theta,\phi,\alpha,\beta,\gamma) = \sum_{k=1}^{N} U_{Jk}(r,\theta,\phi,\alpha,\beta,\gamma)_{Jk} \tag{7.2}$$

where the sum is over all of the N interacting host water molecules.

Van der Waals and Platteeuw chose to model the guest-host interaction using the Lennard-Jones (6-12) interaction potential, illustrated in Figure 7.1, in the development of the spherically symmetric cell potential model.

$$U(r) = 4\varepsilon\left(\left(\frac{\sigma}{r}\right)^{12} - \left(\frac{\sigma}{r}\right)^{6}\right) \tag{7.3}$$

where r is the usual distance between molecular centers, σ is the collision diameter, and ε is the characteristic energy. The pure component Lennard-Jones parameters were taken from those

derived from viscosity and viral coefficient data (Hirschfelder et al., 1954). The actual Lennard-Jones parameters for the guest-host interactions were determined using the empirical Berthelot geometric mean approximation for ε, and the hard sphere approximation for σ.

$$\sigma = \frac{(\sigma_{guest} + \sigma_{host})}{2} \tag{7.4}$$

$$\varepsilon = \left(\varepsilon_{guest}\varepsilon_{host}\right)^{1/2} \tag{7.5}$$

The first of these "mixing" rules is unquestionably exact for a pair of hard sphere molecules. The second rule is based on a simple interpretation of the dispersion forces in terms of molecular polarizabilities (Hirschfelder et al., 1954). Using Equations (7.4) and (7.5) coupled with the L-J (6-12) potential with the Lennard-Jones Devonshire spherical cell approximation yielded reasonably good equilibrium dissociation pressures for the noble gas hydrates of Ar, Kr, and Xe.

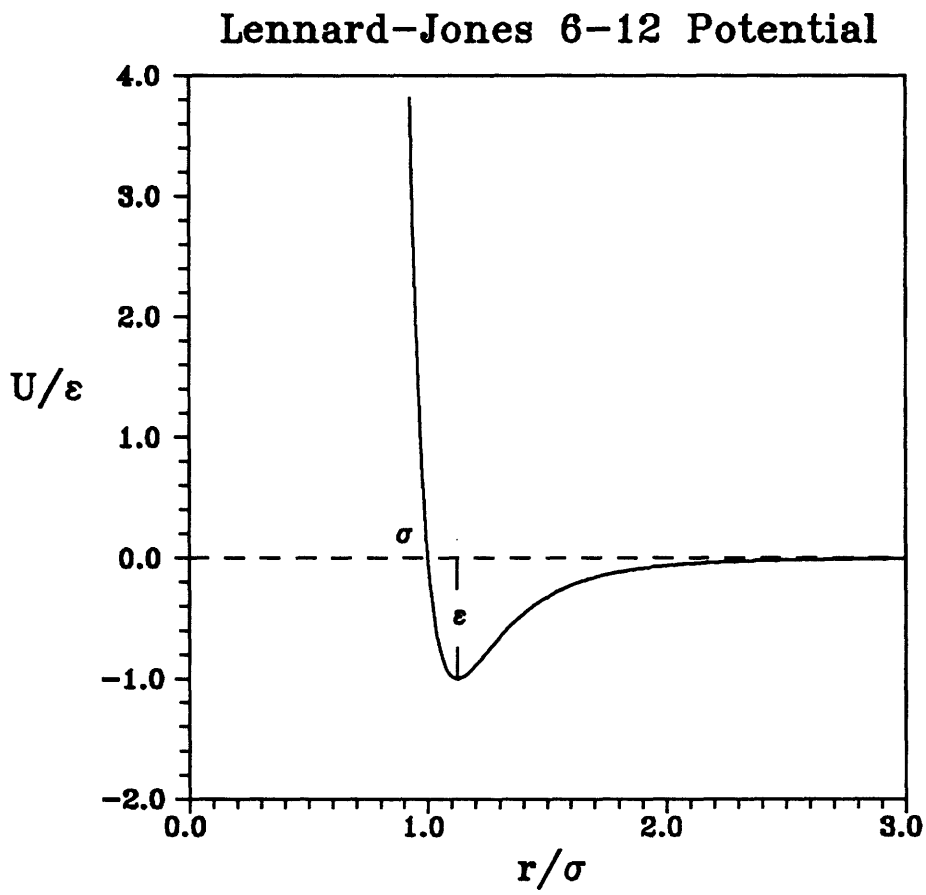

Figure 7.1 Lennard-Jones (6-12) Intermolecular Potential

Discrepancy between theory and experiment for the more complex guest molecules directed McKoy and Sinanoglu (1963) to explore several different potential models in the evaluation of the guest-host configurational partition function. The Lennard-Jones (6-12), (7-28), and Kihara potentials were used with the LJD spherical cell approximation. They found the Kihara potential, with its third parameter (a), to yield the best fits to experimental dissociation pressure data. It has since been extensively used in the modeling of guest-host intermolecular interactions in many water clathrate systems. The Kihara model is illustrated in Figure 7.2.

$$U(r) = \infty \qquad r \leq 2a$$

$$U(r) = 4\varepsilon\left(\left(\frac{(\sigma - 2a)}{(r - 2a)}\right)^{12} - \left(\frac{(\sigma - 2a)}{(r - 2a)}\right)^{6}\right) \qquad r > 2a \tag{7.6}$$

where $2a$ is the molecular hard core diameter, σ is the collision diameter, and ε is the characteristic energy. The spherically-averaged (McKoy and Sinanoglu, 1963) LJD form of the Kihara potential is shown here

$$W(r) = 2z\varepsilon\left(\frac{\sigma^{12}}{R^{11}r}\left(\delta^{10} + \frac{a}{R}\delta^{11}\right) - \frac{\sigma^{6}}{R^{5}r}\left(\delta^{4} + \frac{a}{R}\delta^{5}\right)\right) \tag{7.7}$$

where

$$\delta^{N} \equiv \frac{\left(\left(1 - \frac{r}{R} - \frac{a}{R}\right)^{-N} - \left(1 + \frac{r}{R} - \frac{a}{R}\right)^{-N}\right)}{N} \tag{7.8}$$

and z is the coordination number of the cell and R is the radius. Generally, only the first shell of water molecules is considered in the calculation of the total guest-host intermolecular interaction energies. Thus for the structure I hydrates, z = 20 for the pentagonal dodecahedral

cavities and z = 24 for the tetrakaidecahedral cavities. Similarly, for the structure II hydrates, z = 20 for the pentagonal dodecahedral cavities and z = 28 for the hexakaidecahedral cavities, respectively. One should also note that if a = 0, the familiar LJ (6-12) spherically-averaged potential results.

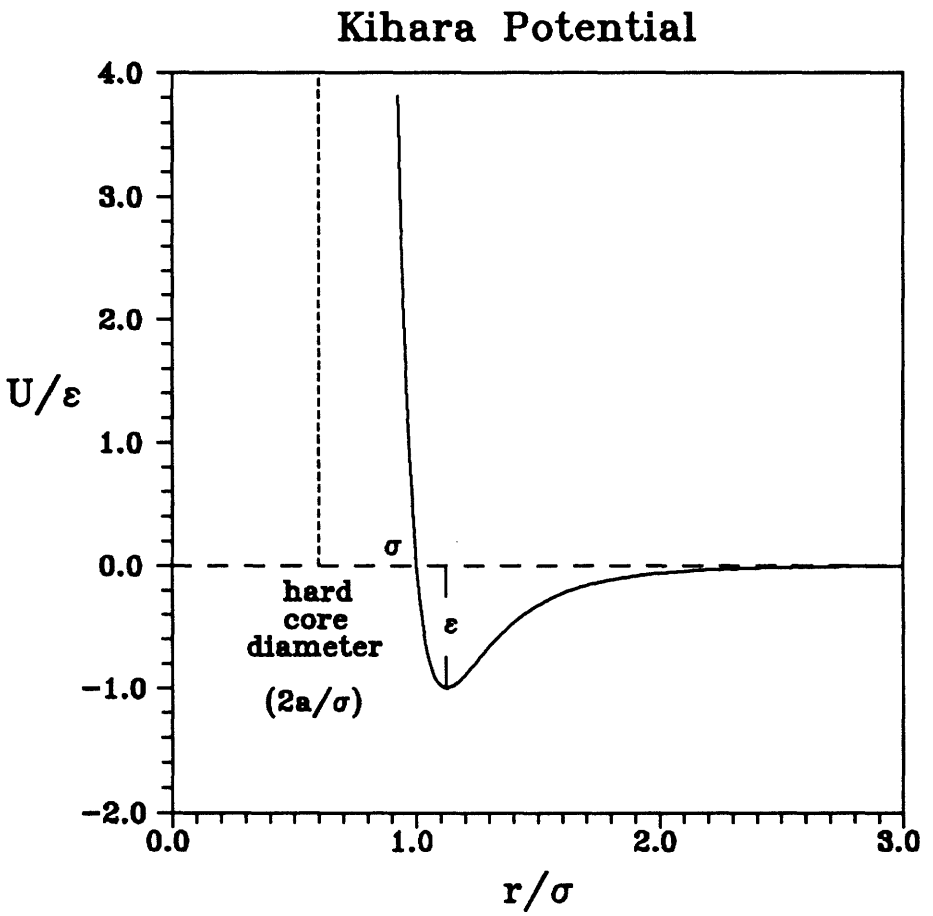

Figure 7.2 Spherical Core Kihara Intermolecular Potential

Generally, however, the use of any of these intermolecular potential functions, coupled with the spherically symmetric Lennard-Jones Devonshire approximation, has required the use of non-unique potential parameters derived from the simple fitting of experimental dissociation pressure data. And as might be expected, the Kihara potential, with its three adjustable parameters, has proved to yield better results than the simple two parameter Lennard-Jones (6-12) potential. Unfortunately, this does not mean that the Kihara potential provides a more physically realistic potential than the Lennard-Jones (6-12) potential but only that it is empirically superior.

Although, these empirically based potential functions provide us with a means of correlating certain macroscopic properties, they provide little insight into the true nature of the potential of interaction. However, with the continuing advances occurring with computer hardware, analytical intermolecular potential functions between guest and host molecules derived from molecular orbital (MO) quantum mechanical calculations and first principles (*ab initio*) become a viable alternative in the representation of the interaction potential (Maitland et al, 1981). The basis of these *ab initio* type calculations involves the evaluation of the potential in terms of fundamental physical constants. Generally, the Schrödinger equation is solved numerically given certain simplifying assumptions. The complexity of the many-body Schrödinger wave equation requires the use of the Born-Oppenheimer approximation in which the nuclei of each molecule is assumed fixed relative to the motion of the electrons. The motion of the electrons are usually further restricted via the Hartree-Fock approximation which involves the motion of a single electron in the spherically averaged potential field produced by the remaining electrons. The resulting approximated wave functions are then used to construct the interaction potential energy surfaces which are then often fit to empirical expressions.

The study of hydrophobic behavior has resulted in the development of a number of models involving interactions with water. In the modeling of biological systems involving macromolecules, Carozzo et al. (1978), Goodfellow et al. (1982), and Mezei et al. (1984) developed analytic potentials from *ab initio* computations for the interaction between

biomolecules. Dashevsky and Sarkisov (1974) studied the solvation and hydrophobic interaction of non-polar molecules in water in the approximation of interatomic potentials. Clementi et al. (1972, 1980), Kistenmacher et al. (1973a,b, 1974a,b), and Corongiu (1978) examined the structure of several ionic molecular complexes in aqueous solutions where the modeling of the water interaction was critical.

Swaminathan et al. (1978) performed Monte Carlo studies on dilute aqueous solutions of methane. The methane-water interaction energy was described using an analytical potential function representative of *ab initio* molecular orbital (MO) calculations. Bolis and Clementi (1981) and Owicki and Scheraga (1977) also studied methane in aqueous solution using Monte Carlo simulation. Again, the methane-water interaction were represented with an analytic function fitted to *ab initio* MO computations.

Alagoni and Tani (1985) performed Monte Carlo studies on the dilute aqueous solution of argon. The argon-water intermolecular potential energy function was also based on the results of *ab initio* MO calculations.

The major problem associated with these analytic potential functions derived for *ab initio* quantum mechanical type calculations involves the fact that they are generally only performed on a pair of molecules. This corresponds to an environment which is indicative of a molecular beam type experiment, In other words, the potential energy functions are obtained for the extreme low density region. Additionally, the calculations are also usually of limited range in terms of intermolecular distances. Typical calculations only consider separations less than 5 - 7 Å. The nature of the interactions at long range is often ignored. At best, the functions are forced to give the correct asymptotic behavior (r^{-6}).

In terms of representing the actual intermolecular potentials associated with the modeling of the guest-host interactions in the water clathrate systems, the work of Jorgensen (1981a,b,c, 1982) on transferable intermolecular potential functions (TIPS) is probably the most applicable.

By constructing a transferable potential function they were able to obtain a single set of parameters for atoms or groups of atoms that could be used to construct potential functions for a variety of different systems. These potential energy functions are modeled as

$$\Delta U_{ab} = \sum_a \sum_b \frac{q_a q_b}{4\pi\varepsilon_0 r_{ab}} + 4\varepsilon_{ab}\left(\left(\frac{\sigma_{ab}}{r_{ab}}\right)^{12} - \left(\frac{\sigma_{ab}}{r_{ab}}\right)^{6}\right) \tag{7.9}$$

where each site has three parameters, a charge in electrons, q_a or q_b, and binary mixture Lennard-Jones parameters σ_{ab} and ε_{ab}. $\varepsilon_0 = 8.8452 \times 10^{-12}$ $C^2N^{-1}m^{-2}$ is the permittivity of free space. Geometric-mean or Berthelot type mixing rules are used for both σ_{ab} and ε_{ab}.

$$\sigma_{ab} = (\sigma_a \sigma_b)^{1/2} \qquad \varepsilon_{ab} = (\varepsilon_a \varepsilon_b)^{1/2} \tag{7.10}$$

For the vast majority of water clathrate systems, the guests are non-polar. This eliminates the first term in Equation (7.9) thus resulting in a pure Lennard-Jones (6-12) type intermolecular interaction.

Standard geometries for the various functionalities are used (Bowen et al., 1958). Jorgensen's (1981) summarized functional geometries are tabulated in Table 7.2. Jorgensen also adopted the H_2O monomer experimental geometry (r(OH) = 0.9572 Å, ∠HOH = 104.52°) throughout his study.

Bickes et al. (1975) used the results of molecular beam scattering experiments, specifically the measured differential collision cross sections, to estimate a set of Lennard-Jones (6-12) parameters σ_{ab} and ε_{ab} for a number of different molecular pairs involving water. These parameters are listed in Table 7.3. The theoretical neon-water Lennard-Jones potential ($\sigma_{Ne\text{-}w}$ = 2.89 Å, $\varepsilon_{Ne\text{-}w}/k$ = 89.3 K) based on Hartree-Fock *ab initio* molecular orbital calculations (Losonczy et al., 1973) show surprisingly good agreement with those derived from the measured differential collision cross sections ($\sigma_{Ne\text{-}w}$ = 2.85 Å, $\varepsilon_{Ne\text{-}w}/k$ = 64 K)

TIPS Parameters for Alcohols and Ethers Jorgensen (1981)			
site	q_a (electrons)	σ_a (Å)	ε_a/k (K)
O in H_2O	- 0.80	3.215	59.78
O in ROH	- 0.685	3.083	87.94
O in ROR´	- 0.58	3.047	98.29
H in H_2O	0.40	0.0	0.0
H in ROH	0.40	0.0	0.0
CH_4	0.00	3.730	147.94
CH_3	*b*	3.861	91.15
CH_2	*b*	3.983	57.48
CH	*b*	4.252	24.47
C	*b*	4.436	13.20
*Charges chosen to achieve neutrality of the monomers. R = Non-hydrogen site			

Table 7.1 TIPS Potential Parameters

An accurate representation of the intermolecular interaction potential is usually unknown for the vast majority of water clathrate systems. This requires not only that a functional form be selected but also that the parameters need to be estimated, usually through an appropriate set of mixing rules and the pure component potential parameters. The validity of these mixing rules and the selected potential function often goes without question. Therefore, using the mixed Lennard-Jones (6-12) parameters estimated from the experimentally measured differential collision cross sections (Bickes et al., 1975) and the pure parameters for Neon and Argon approximated from viscosity data (Reid et al., 1987), the Lennard-Jones (6-12) parameters for water were derived from the standard guest-host mixing rules, specifically, the Berthelot geometric mean approximation for ε, and the hard sphere approximation for σ. The results are shown in Table 7.4. Quite obviously, blind, unjustified usage of these mixing rules, can lead to an improper representation of the guest-host intermolecular interaction potential. For example, this is especially true when one tries to rationalize the potential parameters which have been fitted in an *ad hoc* manner to match experimental dissociation pressure data.

Standard Geometric Parameters for Saturated Alcohols and Ethers Jorgensen (1981) r = bond length ∠ = bond angle					
alcohols		ethers		general	
r(OH)	0.945 Å	r(CO)	1.410 Å	r(CC)	1.535 Å
r(CO)	1.430 Å	$r(CC_o)$	1.516 Å	∠CCC	109.47°
$r(CC_o)$	1.512 Å	∠COC	112.0°		
∠COH	108.5°				
∠CCO	107.8°				

Table 7.2 Standard Geometrical Functional Parameters

Lennard-Jones (6-12) Potential Parameters Molecular Beam Scattering Bickes et al. (1975)		
System	σ_{ab} (Å)	ϵ_{ab}/k (K)
H_2+H_2O	2.92 ± 0.06	137 ± 12
He+H_2O	2.98 ± 0.07	29 ± 3
Ne+H_2O	2.85 ± 0.03	64 ± 2
Ar+H_2O	2.93 ± 0.22	164 ± 11
H_2O+H_2O	2.75	390 ± 22
Errors represent lower limits, they do not necessarily indicate the dependence of the results on the assumed potential model.		

Table 7.3 Lennard-Jones (6-12) Potential Parameters - Molecular Scattering

Lennard-Jones (6-12) Mixing Rule Examination Derived H_2O-H_2O Potential Parameters		
System	Hard Sphere Approximation $\sigma_{w-w} = 2\sigma_{w-g} - \sigma_{g-g}$	Geometric-Mean (Berthelot) $\varepsilon_{w-w}/k = (\varepsilon_{w-g}/k)^2/\varepsilon_{g-g}/k$
H_2O - Ne	2.880 Å	124.9 K
H_2O - Ar	2.318 Å	288.3 K
$\sigma_{Ne-Ne} = 2.820$ Å, $\varepsilon_{Ne-Ne}/k = 32.8$ K, $\sigma_{Ar-Ar} = 3.542$ Å, $\varepsilon_{Ar-Ar}/k = 93.3$ K Reid, Prausnitz, and Poling (1987)		

Table 7.4 Lennard-Jones (6-12) Mixing Rule Examination

7.2 H_2O- H_2O Intermolecular Potential Interactions

The host water lattice is assumed rigid in this work in the evaluation of the guest-host configurational partition function. With this assumption, the evaluation of the configurational properties requires only a description of the guest-host interaction potential and possibly the guest-guest interaction potential. The molecular dynamics simulation of the entire water clathrate structure, on the other hand, also requires that the host-host or H_2O-H_2O interaction potential be specified. Without a good representative model for the host-host interactions, it would be impossible to model the coupling of the lattice dynamics of the hydrogen-bonded host framework with the motion of the guests within the various cavities.

Several intermolecular potential functions of the H_2O-H_2O interaction have been quite successful in the modeling of the various properties of liquid water and ice (Bernal and Fowler, 1933; Berendsen et al., 1981; Clementi and Popkie, 1972; Clementi et al., 1980; Clementi and Habitz, 1983; Egelstaff and Root, 1983; Jorgensen, 1981a,b,c; Jorgensen et al., 1983; Kistenmacher et al., 1973a,b, 1974a,b; Lie and Clementi, 1975; Matsuoka et al., 1976; Stillinger and Rahman, 1978; Stillinger and Weber, 1983). Morse and Rice (1982) examined a number of the potential models in the prediction of ice structures. Tse, Klein, and McDonald (1983a,b, 1984b) used the simple point charge (SPC) model proposed by Berendsen et al. (1981) in their computer simulation studies of several structure I clathrate hydrates.

Since the simple point charge (SPC) model has been extensively used in the molecular dynamics modeling of a number of different water clathrate systems, it was therefore chosen to represent the H_2O-H_2O interaction potential in this work.
Furthermore, the computation simplicity associated with use of a three site model, as compared to four and five site models, offered an attractive numerical benefit.

The SPC model, represented in a TIPS format by Equation (7.9) is best described as a simple three-site model involving a Lennard-Jones (6-12) interaction between oxygen centers, and electrostatic interactions between separated charges centered on the hydrogen and oxygen positions. The potential parameters for the SPC model are given in Table 7.5.

Simple Point Charge (SPC) Model for Water Berendsen (1981)			
site	q_i (electrons)	σ_i (Å)	ϵ_i/k (K)
O in H_2O	- 0.82	3.16	78.2
H in H_2O	0.41	0.0	0.0
r(OH) = 1.0 Å, ∠HOH = 109.47°			

Table 7.5 Simple Point Charge (SPC) Model for Water

8. CONFIGURATIONAL RESULTS

8.1 Lattice Summation

When the potential energy between two atoms can be expressed as a inverse power series in separation, r_{ij} ,

$$U(r_{ij}) = \frac{\lambda_1}{r_{ij}^{s_1}} + \frac{\lambda_2}{r_{ij}^{s_2}} + \frac{\lambda_3}{r_{ij}^{s_3}} + \cdots \tag{8.1}$$

then the total potential energy of an atom within an infinite cubic crystal is given by

$$\sum_{i=-\infty}^{\infty}\sum_{j=-\infty}^{\infty}\sum_{k=-\infty}^{\infty}\sum_{n=1}^{\rho} \lambda_1\left[(x_c-x_n+i)^2+(y_c-y_n+j)^2+(z_c-z_n+k)^2\right]^{-s_1/2}+\cdots \tag{8.2}$$

where the subscript c denotes the atom of interest and the subscript n denotes the remaining interacting atoms within the unit cell of the cubic crystal. The number of atoms within the unit cell is given by ρ. Recasting this expression into a more compact form, yields

$$U(Total) = \frac{\lambda_1 A_{s_1}}{d_0^{s_1}} + \frac{\lambda_2 A_{s_2}}{d_0^{s_2}} + \frac{\lambda_3 A_{s_3}}{d_0^{s_3}} + \cdots \tag{8.3}$$

where the potential energy constant, A_{s_n} , is defined by

$$A_{s_n} = \sum_{i=-\infty}^{\infty}\sum_{j=-\infty}^{\infty}\sum_{k=-\infty}^{\infty}\sum_{n=1}^{\rho} d_0^{s_n}\left[(x_c-x_n+i)^2+(y_c-y_n+j)^2+(z_c-z_n+k)^2\right]^{-s_n/2} \tag{8.4}$$

and d_0 is a normalizing distance, usually defined as the minimum nearest neighbor distance.

The errors associated with the finite limits imposed on the direct summation of the potential energy series can be estimated by the conversion of the residual discrete summations to continuous integrations beyond a certain radius R. With this approach, the error can be estimated by

$$A_{s_\infty} - A_{s_R} \approx \int_R^\infty \frac{4\pi\rho r^2}{(r/d_0)^s}\,dr = d_0^s \int_R^\infty 4\pi\rho r^{2-s}\,dr \tag{8.5}$$

where A_{s_∞} is the potential energy constant associated with a truly infinite lattice sum (Equation (8.4)) and A_{s_R} is the potential energy constant associated with the truncation of the series at a radial value of R, depicted in the two-dimensional analog of the lattice summation diagram illustrated in Figure 8.1. The integration of Equation (8.5) yields

$$\Delta A_s \equiv A_{s_\infty} - A_{s_R} \approx d_0^s 4\pi\rho \frac{R^{3-s}}{s-3} \qquad s>3 \tag{8.6}$$

or equivalently

$$\log_{10}\Delta A_s \approx \log_{10}\left[d_0^s 4\pi\rho/(s-3)\right] + \log_{10}\left[R^{3-s}\right] \tag{8.7}$$

which further simplifies to

$$\log_{10}\Delta A_s \approx \log_{10}\left[d_0^s 4\pi\rho/(s-3)\right] + (3-s)\log_{10}R \tag{8.8}$$

This simple linear expression relating the logarithm of the potential energy constant error, ΔA_s, is shown graphically in Figures 8.2, 8.3, 8.4, and 8.5 for the four types of water clathrate cavities. The potential energy constant error associated with the truncation of the series at a finite limit for a guest molecule located at the center of a pentagonal dodecahedron in a Structure I water clathrate is illustrated in Figure 8.2. Similarly, the potential energy constant errors associated with the other various guest-host configurations are shown in Figure 8.3, Figure 8.4, and Figure 8.5. It is

Two-Dimensional Lattice-Summation Diagram

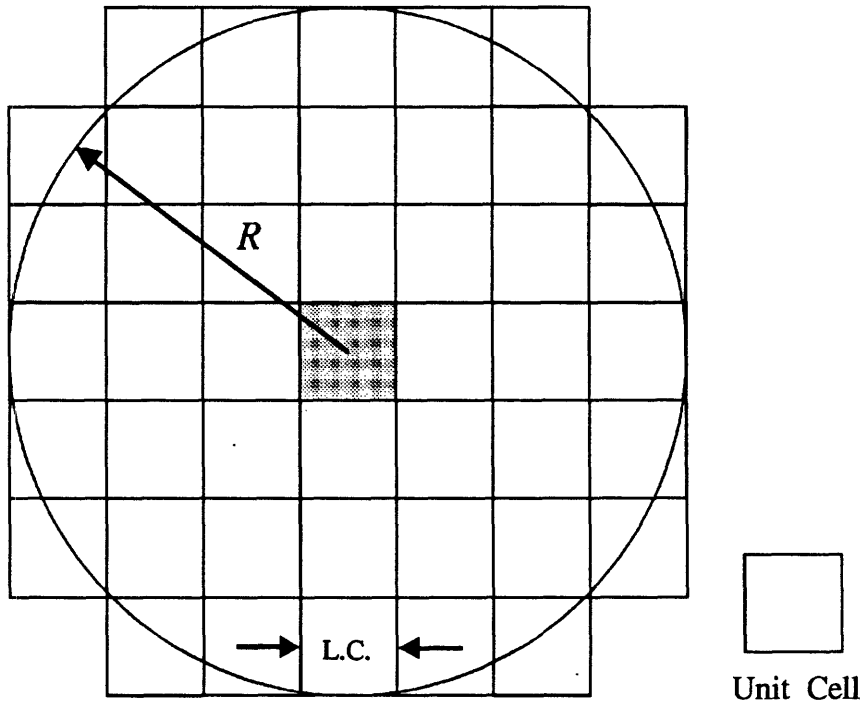

L.C. - Lattice Constant

Figure 8.1 Two-Dimensional Lattice-Summation Diagram

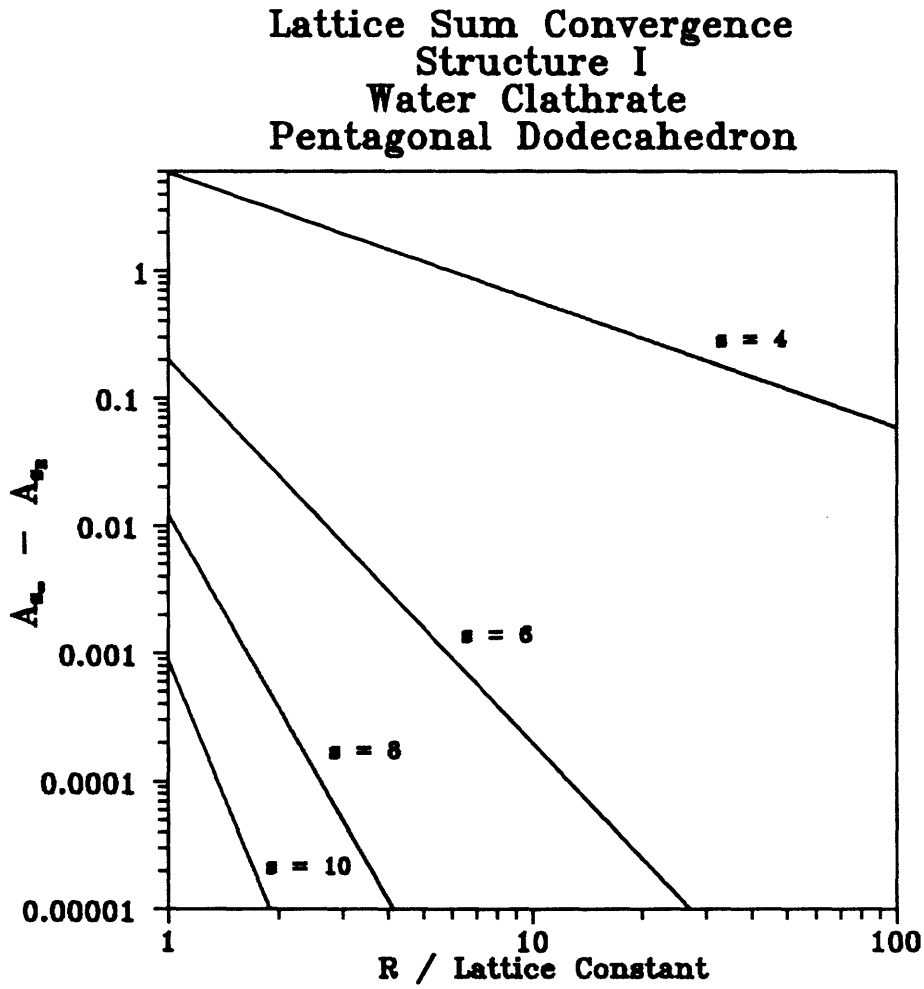

Figure 8.2 Lattice Sum Convergence - Structure I Pentagonal Dodecahedron

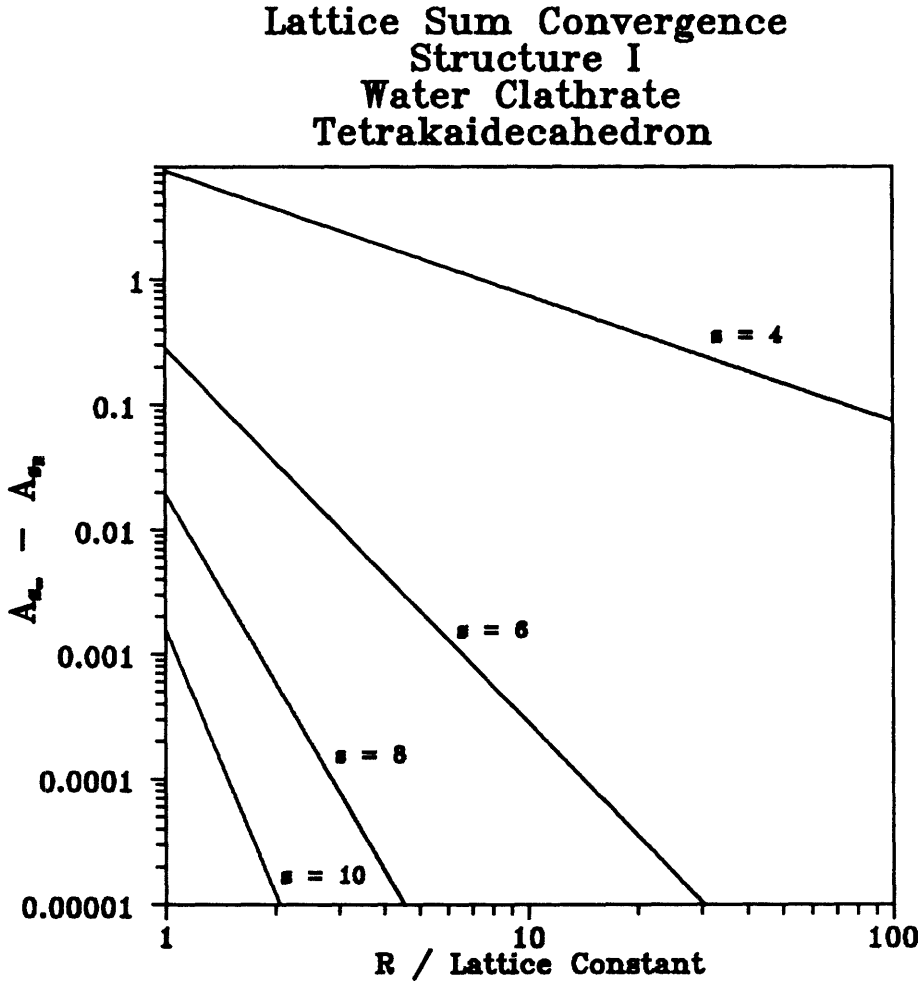

Figure 8.3 Lattice Sum Convergence - Structure I Tetrakaidecahedron

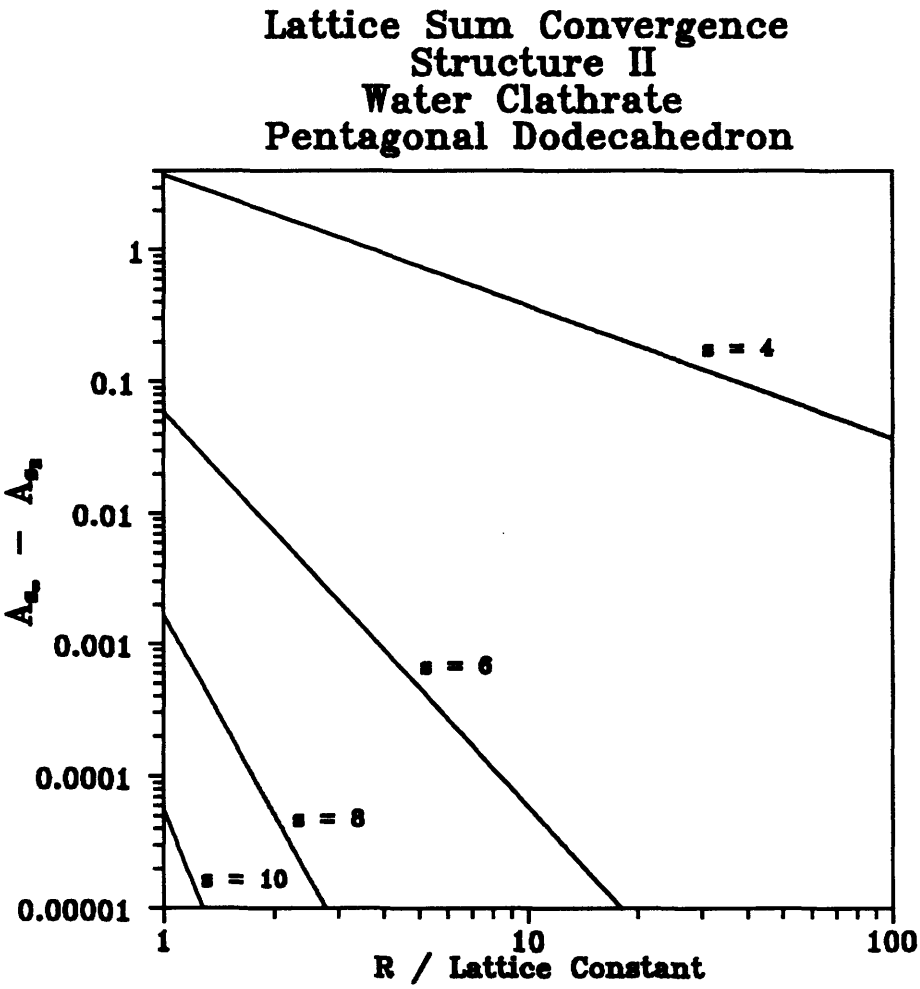

Figure 8.4 Lattice Sum Convergence - Structure II Pentagonal Dodecahedron

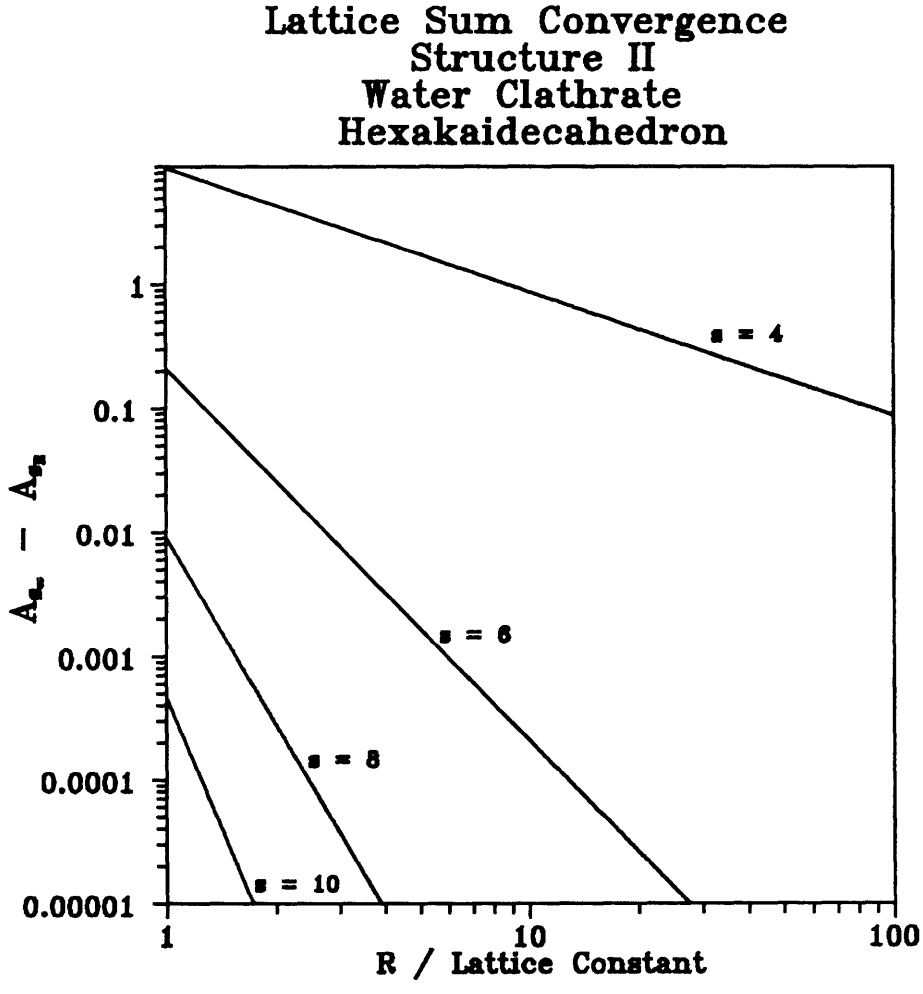

Figure 8.5 Lattice Sum Convergence - Structure II Hexakaidecahedron

obvious that for integral values of $s > 6$ the convergence of the series is rapid and the direct summation of the series is applicable. However, for a value of $s = 5$, the summation requires considerable effort while for, value of $s = 4$, the direct summation is completely intractable. Using the M.I.T. Cray 2 Supercomputer facility, we estimated that it would take over 10^6 years to converge the potential energy constant to five decimals of precision.

Hirschfelder, Curtis, and Bird (1954) tabulated the potential energy constants for several simple crystalline structures, specifically, the face-centered cubic, body-centered cubic, and simple cubic structures. These potential energy constants were calculated by Lennard-Jones (1924) and Lennard-Jones and Ingham (1925) using elaborate transformations involving the Euler-Maclauren sum formula for the Riemann zeta-function. They were able to calculate the potential energy constants to 5 decimal precision for the three cubic structures for values of s ranging from 4 to 30. Unfortunately, the structure I and II water clathrate structures are much more complex and thus do not easily lend themselves to a similar treatment.

8.1.1 Potential Energy Constants / Guest-Host Interactions

The potential energy constants, A_s, for the water clathrate guest-host interactions are given in Table 8.1. These constants were calculated from the direct summation of the series using double precision arithmetic. For these calculations, the guest molecules were always located at the center of their respective cavities and were assumed to be spherical. The host water molecules were positioned at the crystallographic locations (McMullan and Jeffrey, 1965; Mak and McMullan, 1965) of the oxygen atoms. The hydrogen atoms were not considered.

8.1.2 Potential Energy Constants / Guest-Guest Interactions

The potential energy constants, A_s, for the water clathrate guest-guest interactions are given in Tables 8.2 and 8.3. Again, the guest molecules were always located at the center of their respective cavities, which were assumed to be at full occupancy. Only single site spherical guests were considered. The guest-guest interactions were subdivided into four types per clathrate structure, specifically:

Structure I

1) The interaction of a guest within a pentagonal dodecahedron with guests within other pentagonal dodecahedrons.

2) The interaction of a guest within a pentagonal dodecahedron with guests within tetrakaidecahedrons.

3) The interaction of a guest within a tetrakaidecahedron with guests within pentagonal dodecahedrons.

4) The interaction of a guest within a tetrakaidecahedron with guests within other tetrakaidecahedrons.

Structure II

1) The interaction of a guest within a pentagonal dodecahedron with guests within other pentagonal dodecahedrons.

2) The interaction of a guest within a pentagonal dodecahedron with guests within hexakaidecahedrons.

3) The interaction of a guest within a hexakaidecahedron with guests within pentagonal dodecahedrons.

4) The interaction of a guest within a hexakaidecahedron with guests within other hexakaidecahedrons.

The first interaction type given under the structure I category in Table 8.2 for pentagonal dodecahedrons corresponds to a body-centered cubic type structure. For this situation, the potential energy constants tabulated by Hirschfelder, Curtis, and Bird (1954) in Table 13.9-2 on p. 1040 can be compared with those calculated here by direct summation. Discrepancies exist only in the last one or two decimal values for some of the constants particularly at values of s less than 10. Examination of the convergence properties of these series, suggests that the values determined in this work from direct summation to be correct.

Potential Energy Constants - A_x Water Clathrate Guest-Host Interactions				
	Structure I		*Structure II*	
x	*Pentagonal Dodecahedron*	*Tetrakaidecahedron*	*Pentagonal Dodecahedron*	*Hexakaidecahedron*
5	21.93721	22.72571	19.87255	34.69343
6	19.38596	19.19966	17.24331	30.06453
7	18.20575	17.38725	15.89227	27.99541
8	17.50893	16.21892	14.99768	26.87150
9	17.01950	15.35567	14.30543	26.17033
10	16.63077	14.66220	13.71773	25.67964
11	16.29618	14.07625	13.19191	25.30135
12	15.99366	13.56598	12.70760	24.98635
13	15.71220	13.11345	12.25439	24.70874
14	15.44601	12.70766	11.82653	24.45431
15	15.19191	12.34125	11.42063	24.21504
16	14.94808	12.00888	11.03447	23.98634
17	14.71339	11.70645	10.66649	23.76546
18	14.48712	11.43064	10.31549	23.55077
19	14.26875	11.17866	9.98048	23.34131
20	14.05789	10.94813	9.66058	23.13643
21	13.85420	10.73694	9.35501	22.93573
22	13.65742	10.54325	9.06307	22.73895
23	13.46728	10.36542	8.78407	22.54591
24	13.28354	10.20198	8.51739	22.35645
25	13.10598	10.05161	8.26243	22.17048
26	12.93441	9.91314	8.01865	21.98790
27	12.76860	9.78549	7.78550	21.80863
28	12.60836	9.66771	7.56249	21.63261
29	12.45350	9.55892	7.34913	21.45977
30	12.30385	9.45836	7.14497	21.29005
d_0	0.31800	0.33717	0.21651	0.26770
d_0 = *Fractional Distance Between Nearest Neighboring Host Water Molecules*				

Table 8.1 Potential Energy Constants / Guest-Host Interactions

Potential Energy Constants - A_s Structure I - Water Clathrate Guest-Guest Interactions				
s	*Pentagonal Dodecahedron*		*Tetrakaidecahedron*	
	Pentagonal Dodecahedron	*Tetrakaidecahedron*	*Pentagonal Dodecahedron*	*Tetrakaidecahedron*
5	14.75840	15.11660	5.03886	6.77733
6	12.25367	13.41525	4.47175	5.14048
7	11.05424	12.72028	4.24009	4.28668
8	10.35520	12.38994	4.12998	3.74916
9	9.89459	12.21937	4.07312	3.37400
10	9.56440	12.12665	4.04222	3.09581
11	9.31326	12.07446	4.02482	2.88183
12	9.11418	12.04436	4.01479	2.71351
13	8.95181	12.02668	4.00889	2.57926
14	8.81677	12.01617	4.00539	2.47125
15	8.70298	12.00985	4.00328	2.38389
16	8.60625	12.00602	4.00201	2.31298
17	8.52353	12.00370	4.00123	2.25531
18	8.45250	12.00227	4.00076	2.20833
19	8.39135	12.00140	4.00047	2.17003
20	8.33860	12.00086	4.00029	2.13880
21	8.29305	12.00053	4.00018	2.11331
22	8.23568	12.00033	4.00011	2.09251
23	8.21962	12.00020	4.00007	2.07553
24	8.19016	12.00013	4.00004	2.06166
25	8.16465	12.00008	4.00003	2.05035
26	8.14258	12.00005	4.00002	2.04111
27	8.12347	12.00003	4.00001	2.03356
28	8.10692	12.00002	4.00001	2.02740
29	8.09259	12.00001	4.00000	2.02238
30	8.08019	12.00001	4.00000	2.01827
d_o	0.86602	0.55901	0.55901	0.50000
d_o = Fractional Distance Between Nearest Neighboring Cavities				

Table 8.2 Potential Energy Constants / Structure I Guest-Guest Interactions

Potential Energy Constants - A_s Structure II - Water Clathrate Guest-Guest Interactions				
s	*Pentagonal Dodecahedron*		*Hexakaidecahedron*	
	Pentagonal Dodecahedron	*Hexakaidecahedron*	*Pentagonal Dodecahedron*	*Hexakaidecahedron*
5	8.09672	7.88952	15.77903	6.31274
6	6.92768	6.91143	13.82287	5.11677
7	6.45406	6.49268	12.98537	4.59448
8	6.23392	6.28271	12.56542	4.33191
9	6.12419	6.16805	12.3361	4.19037
10	6.06724	6.10214	12.20428	4.11102
11	6.03690	6.06299	12.12599	4.06547
12	6.02045	6.03924	12.07847	4.0389
13	6.01142	6.02460	12.04921	4.02325
14	6.00641	6.01550	12.03101	4.01396
15	6.00362	6.00980	12.0196	4.00841
16	6.00205	6.00621	12.01242	4.00508
17	6.00116	6.00394	12.00789	4.00307
18	6.00066	6.00251	12.00501	4.00186
19	6.00038	6.00160	12.00319	4.00113
20	6.00022	6.00102	12.00203	4.00069
21	6.00012	6.00065	12.00129	4.00042
22	6.00007	6.00041	12.00083	4.00026
23	6.00004	6.00026	12.00053	4.00016
24	6.00002	6.00017	12.00034	4.00009
25	6.00001	6.00011	12.00021	4.00006
26	6.00001	6.00007	12.00014	4.00004
27	6.00000	6.00004	12.00009	4.00002
28	6.00000	6.00003	12.00006	4.00001
29	6.00000	6.00002	12.00004	4.00001
30	6.00000	6.00001	12.00002	4.00000
d_0	0.35355	0.41457	0.41457	0.43301
d_0 = Fractional Distance Between Nearest Neighboring Cavities				

Table 8.3 Potential Energy Constants / Structure II Guest-Guest Interactions

8.2 Lattice Summation Results

If the Lennard-Jones (6-12) intermolecular potential is used to model the various guest-type interactions within the water clathrate system, then the total potential energy of a guest molecule located at the center of a given cavity within a rigid host lattice is given by

$$U = \left(\frac{4\varepsilon\sigma^{12}A_{12}}{d_0^{12}} - \frac{4\varepsilon\sigma^{6}A_{6}}{d_0^{6}} \right)_{guest\text{-}host} + \left(\frac{4\varepsilon\sigma^{12}A_{12}}{d_0^{12}} - \frac{4\varepsilon\sigma^{6}A_{6}}{d_0^{6}} \right)_{guest\text{-}guest} \tag{8.9}$$

where the first term solely represents the usual guest-host interactions, with the exception that the all of the subsequent water shell contributions are included. The second term, has been added to represent the usually ignored guest-guest interactions. As discussed in Section 8.1.2, since there are two types of cavities in the different water clathrate structures, the guest-guest interaction term actually consists of two separate terms, specifically one to model the interactions of guest molecules within like cavities, and one to model the interactions with guest molecules in unlike cavities.

$$U_{guest\text{-}guest} = \left(\frac{4\varepsilon\sigma^{12}A_{12}}{d_0^{12}} - \frac{4\varepsilon\sigma^{6}A_{6}}{d_0^{6}} \right)_{like\ cavities} \tag{8.10}$$

$$+ \left(\frac{4\varepsilon\sigma^{12}A_{12}}{d_0^{12}} - \frac{4\varepsilon\sigma^{6}A_{6}}{d_0^{6}} \right)_{unlike\ cavities}$$

In the case of a structure I water clathrate, the first term could represent either the interactions of a guest within a pentagonal dodecahedron with all the neighboring guests also located in pentagonal dodecahedrons or similarly a guest within a tetrakaidecahedron with all the neighboring guests also located in tetrakaidecahedrons. The second term would represent the remaining unlike interactions. For a guest molecule that only fills the large cavities within a water clathrate structure, the second term involving these unlike interactions would disappear leaving only those like interactions.

The guest-host interactions can also be similarly modeled by the sum of two terms

$$U_{guest-host} = \left(\frac{4\varepsilon\sigma^{12}A'_{12}}{d_0^{12}} - \frac{4\varepsilon\sigma^{6}A'_{6}}{d_0^{6}} \right)_{guest-host,\,1^{st}\,shell} + \left(\frac{4\varepsilon\sigma^{12}(A_{12} - A'_{12})}{d_0^{12}} - \frac{4\varepsilon\sigma^{6}(A_{6} - A'_{6})}{d_0^{6}} \right)_{guest-host,\,residual} \tag{8.11}$$

where the first shell potential energy constants, A'_s , are given in Table 8.4. In this case, the first term involves the interactions of a guest molecule situated at the center of a given cavity with the first shell of neighboring water molecules, while the second term captures the residual contributions to the total potential energy of the usually neglected subsequent water shells.

First Shell Potential Energy Constants - A_1' Water Clathrate Guest-Host Interactions				
	Structure I		*Structure II*	
x	*Pentagonal Dodecahedron*	*Tetrakaidecahedron*	*Pentagonal Dodecahedron*	*Hexakaidecahedron*
5	18.11488	18.09507	16.43662	26.61284
6	17.77499	17.23449	15.82105	26.35025
7	17.44653	16.45583	15.23417	26.09239
8	17.12911	15.75069	14.67457	25.83918
9	16.82235	15.11157	14.14091	25.59054
10	16.52589	14.53177	13.63191	25.34638
11	16.23940	14.00533	13.14637	25.10663
12	15.96254	13.52689	12.68313	24.87120
13	15.69498	13.09169	12.24112	24.64001
14	15.43641	12.69545	11.81928	24.41299
15	15.18653	12.33435	11.41664	24.19007
16	14.94505	12.00496	11.03227	23.97117
17	14.71168	11.70421	10.66527	23.75621
18	14.48615	11.42936	10.31482	23.54512
19	14.26820	11.17793	9.98011	23.33784
20	14.05757	10.94770	9.66037	23.13430
21	13.85402	10.73670	9.35490	22.93442
22	13.65732	10.54311	9.06300	22.73815
23	13.46722	10.36534	8.78403	22.54541
24	13.28351	10.20193	8.51737	22.35614
25	13.10597	10.05159	8.26242	22.17029
26	12.93439	9.91312	8.01865	21.98778
27	12.76859	9.78548	7.78550	21.80856
28	12.60835	9.66770	7.56249	21.63257
29	12.45350	9.55892	7.34913	21.45974
30	12.30385	9.45836	7.14497	21.29003
d_0	0.31800	0.33717	0.21651	0.26770
d_0 = Fractional Distance Between Nearest Neighboring Host Water Molecules				

Table 8.4 First Shell Potential Energy Constants / Guest-Host Interactions

Using the results previously given for the various guest-host lattice summation configurations, the contributions to the total potential energy by the inclusion of the subsequent water shell interactions and the various guest-guest interactions were examined for a number of systems. As a means of estimating the effect these potential energy changes had on the guest configurational integral, or equivalently the Langmuir constant, the mean value theorem was used. Specifically, a general Langmuir constant, C, was expressed as

$$C = (kT)^{-1}\langle e^{-U/kT}\rangle V_f \approx (kT)^{-1} e^{\langle -U/kT\rangle} V_f \tag{8.12}$$

which enables us to write the ratio of two Langmuir constants as, for example

$$\frac{C_{total}}{C_{shell\,1}} \approx \frac{e^{\langle -U_{total}/kT\rangle} V_{f,total}}{e^{\langle -U_{shell\,1}/kT\rangle} V_{f,shell\,1}} \tag{8.13}$$

Assuming the free volumes associated with the different potential energies to be approximately equal, the Langmuir constant ratio was approximated as

$$\frac{C_{total}}{C_{shell\,1}} \approx \frac{e^{\langle -U_{total}/kT\rangle}}{e^{\langle -U_{shell\,1}/kT\rangle}} \tag{8.14}$$

where the average potential energies, $\langle U/kT\rangle$, are for the sake of comparison assumed to be equal to the value of the potential energy at the center of the assorted cavities.

To further enhance the presentation of the various effects subsequent water shells and the inclusion of guest-guest interactions have on the value of the configurational integral, or equivalently, the Langmuir constant, the total guest-host interaction potentials at the center of each of the various cavities have been tabulated as simple functions of the guest-host Lennard-Jones parameters σ and ε. Specifically, the results for the structure I pentagonal dodecahedron are given in Tables 8.5a and 8.5b., while the results for the structure I tetrakaidecahedron are given in Tables 8.6a and 8.6b. Similarly, the

results for the structure II pentagonal dodecahedron are given in Tables 5.7a and 5.7b, and finally, the results for the structure II hexakaidecahedron are given in Tables 5.8a and 5.8b.

The format of the tables is self evident. One notes that the contribution of the subsequent water shells to the total potential energy is quite significant in that it is approximately ten percent of the total potential energy for values of $\sigma < 3.0$ and increases to about the same magnitude of the 1st shell interaction at larger σ values. The contribution of the guest-guest interactions is also quite significant, usually on the order of two to three percent of the total. However, the inclusion of the guest-guest interactions in the calculation of the total potential energy is probably not truly justified in that the error in estimating the guest-host potential energy constant, ε, is definitely great enough as to overwhelm the contribution of the guest-guest interactions.

The effect these additional contributions have on the actual Langmuir constant is quite apparent. The actual change can range from a factor of 1.5 to several orders of magnitude, thus making the inclusion of these "additional" interactions essential in the characterization of the guest-host configurational partition function.

Lattice Summation Results Structure I - Water Clathrate Pentagonal Dodecahedron T = 273.15 K Lennard-Jones (6-12) Potential ε/k = 100 K						
σ	Potential Energy - Cell Center					Langmuir Constant Ratio
	Guest - Host		Guest - Guest		Total	
Å	Shell 1	Shell > 1	Small Cavity	Large Cavity	U/kT	Total / Shell 1
2.9	-4.0976	-0.4460	-0.0083	-0.1256	-4.6775	1.7806
3.0	-4.7892	-0.5462	-0.0102	-0.1537	-5.4993	2.0342
3.1	-5.4959	-0.6643	-0.0124	-0.1869	-6.3594	2.3716
3.2	-6.1734	-0.8027	-0.0151	-0.2257	-7.2169	2.8309
3.3	-6.7563	-0.9642	-0.0181	-0.2708	-8.0095	3.5014
3.4	-7.1507	-1.1515	-0.0217	-0.3232	-8.6470	4.4653
3.5	-7.2257	-1.3678	-0.0258	-0.3834	-9.0027	5.9120
3.6	-6.8034	-1.6162	-0.0305	-0.4525	-8.9027	8.1602
3.7	-5.6451	-1.9004	-0.0360	-0.5313	-8.1127	11.7950
3.8	-3.4357	-2.2239	-0.0422	-0.6208	-6.3226	17.9372
3.9	0.2355	-2.5907	-0.0493	-0.7218	-3.1263	28.8404
4.0	5.8989	-3.0048	-0.0573	-0.8353	2.0015	49.2754
Langmuir constant ratio approximated as $e^{-U_{Guest}/kT} / e^{-U_{Host}/kT}$						

Table 8.5a Lattice Summation Results - Structure I Pentagonal Dodecahedron

Lattice Summation Results Structure I - Water Clathrate Pentagonal Dodecahedron T = 273.15 K Lennard-Jones (6-12) Potential ε/k = 180 K						
σ	Potential Energy - Cell Center					Langmuir Constant Ratio
	Guest - Host		Guest - Guest		Total	
Å	Shell 1	Shell > 1	Small Cavity	Large Cavity	U/kT	Total / Shell 1
2.9	-7.3756	-0.8028	-0.0150	-0.2261	-8.4196	2.8403
3.0	-8.6206	-0.9831	-0.0184	-0.2767	-9.8988	3.5902
3.1	-9.8925	-1.1957	-0.0224	-0.3364	-11.4470	4.7324
3.2	-11.1122	-1.4449	-0.0271	-0.4062	-12.9904	6.5418
3.3	-12.1614	-1.7356	-0.0326	-0.4875	-14.4170	9.5417
3.4	-12.8712	-2.0727	-0.0390	-0.5817	-15.5646	14.7822
3.5	-13.0063	-2.4620	-0.0464	-0.6902	-16.2049	24.4975
3.6	-12.2461	-2.9092	-0.0549	-0.8146	-16.0248	43.7587
3.7	-10.1611	-3.4207	-0.0647	-0.9564	-14.6029	84.9288
3.8	-6.1843	-4.0031	-0.0759	-1.1174	-11.3807	180.6175
3.9	0.4239	-4.6633	-0.0887	-1.2992	-5.6273	424.6226
4.0	10.6180	-5.4086	-0.1032	-1.5036	3.6027	1113.612
Langmuir constant ratio approximated as $e^{-U_{Guest}/kT} / e^{-U_{Guest\ 1}/kT}$						

Table 8.5b Lattice Summation Results - Structure I Pentagonal Dodecahedron

Lattice Summation Results Structure I - Water Clathrate Tetrakaidecahedron T = 273.15 K Lennard-Jones (6-12) Potential ε/k = 100 K						
σ	Potential Energy - Cell Center					Langmuir Constant Ratio
	Guest - Host		Guest - Guest		Total	
Å	Shell 1	Shell > 1	Small Cavity	Large Cavity	U/kT	Total / Shell 1
2.9	-3.0177	-0.3720	-0.0419	-0.0939	-3.5255	1.662
3.0	-3.6008	-0.4525	-0.0512	-0.1149	-4.2194	1.857
3.1	-4.2431	-0.5460	-0.0623	-0.1397	-4.9910	2.113
3.2	-4.9338	-0.6535	-0.0752	-0.1686	-5.8311	2.453
3.3	-5.6533	-0.7762	-0.0903	-0.2023	-6.7221	2.912
3.4	-6.3714	-0.9147	-0.1077	-0.2413	-7.6351	3.539
3.5	-7.0428	-1.0696	-0.1278	-0.2862	-8.5265	4.409
3.6	-7.6037	-1.2408	-0.1508	-0.3376	-9.3329	5.636
3.7	-7.9655	-1.4275	-0.1771	-0.3961	-9.9663	7.395
3.8	-8.0086	-1.6283	-0.2069	-0.4625	-10.3063	9.951
3.9	-7.5744	-1.8403	-0.2406	-0.5374	-10.1927	13.712
4.0	-6.4552	-2.0594	-0.2784	-0.6213	-9.4143	19.281
4.1	-4.3823	-2.2794	-0.3208	-0.7150	-7.6976	27.529
4.2	-1.0125	-2.4920	-0.3679	-0.8191	-4.6914	39.603
4.3	4.0897	-2.6856	-0.4200	-0.9340	0.0502	56.801
4.4	11.4715	-2.8451	-0.4775	-1.0601	7.0888	80.055
4.5	21.8158	-2.9512	-0.5405	-1.1977	17.1264	108.782
Langmuir constant ratio approximated as $e^{-U_{guest/host}/kT} / e^{-U_{Guest}/kT}$						

Table 8.6a Lattice Summation Results - Structure I Tetrakaidecahedron

Lattice Summation Results Structure I - Water Clathrate Tetrakaidecahedron T = 273.15 K Leonard-Jones (6-12) Potential ε/k = 180 K						
σ	Potential Energy - Cell Center					Langmuir Constant Ratio
	Guest - Host		Guest - Guest		Total	
Å	Shell 1	Shell > 1	Small Cavity	Large Cavity	U/KT	Total / Shell 1
2.9	-5.4319	-0.6696	-0.0754	-0.1691	-6.3459	2.494
3.0	-6.4814	-0.8145	-0.0922	-0.2069	-7.5950	3.045
3.1	-7.6376	-0.9827	-0.1121	-0.2514	-8.9839	3.843
3.2	-8.8808	-1.1763	-0.1354	-0.3035	-10.4960	5.029
3.3	-10.1760	-1.3971	-0.1625	-0.3642	-12.0998	6.847
3.4	-11.4685	-1.6465	-0.1939	-0.4344	-13.7432	9.726
3.5	-12.6771	-1.9253	-0.2301	-0.5152	-15.3476	14.447
3.6	-13.6867	-2.2334	-0.2715	-0.6077	-16.7992	22.479
3.7	-14.3379	-2.5695	-0.3188	-0.7131	-17.9393	36.649
3.8	-14.4156	-2.9309	-0.3725	-0.8325	-18.5514	62.543
3.9	-13.6340	-3.3125	-0.4331	-0.9672	-18.3468	111.367
4.0	-11.6193	-3.7069	-0.5012	-1.1184	-16.9458	205.706
4.1	-7.8882	-4.1030	-0.5774	-1.2871	-13.8556	390.494
4.2	-1.8225	-4.4855	-0.6622	-1.4743	-8.4445	751.482
4.3	7.3615	-4.8340	-0.7561	-1.6811	0.0903	1438.266
4.4	20.6488	-5.1212	-0.8595	-1.9081	12.7599	2667.487
4.5	39.2684	-5.3121	-0.9728	-2.1558	30.8276	4632.341
Langmuir constant ratio approximated as $e^{-U_{Shell\,1}/kT}$ / $e^{-U_{Shell\,1}/kT}$						

Table 8.6b Lattice Summation Results - Structure I Tetrakaidecahedron

Lattice Summation Results Structure II - Water Clathrate Pentagonal Dodecahedron T = 273.15 K Lennard-Jones (6-12) Potential ε/k = 100 K						
σ Å	Potential Energy - Cell Center					Langmuir Constant Ratio
	Guest - Host		Guest - Guest		Total	
	Shell 1	Shell > 1	Small Cavity	Large Cavity	U/kT	Total / Shell 1
2.5	-1.8972	-0.1832	-0.0470	-0.0181	-2.1454	1.282
2.6	-2.3522	-0.2317	-0.0593	-0.0228	-2.6661	1.369
2.7	-2.8763	-0.2905	-0.0743	-0.0286	-3.2698	1.482
2.8	-3.4676	-0.3611	-0.0923	-0.0356	-3.9566	1.631
2.9	-4.1177	-0.4454	-0.1137	-0.0439	-4.7207	1.828
3.0	-4.8099	-0.5454	-0.1391	-0.0538	-5.5482	2.092
3.1	-5.5154	-0.6634	-0.1689	-0.0654	-6.4130	2.454
3.2	-6.1890	-0.8016	-0.2036	-0.0790	-7.2733	2.957
3.3	-6.7637	-0.9629	-0.2440	-0.0949	-8.0655	3.676
3.4	-7.1437	-1.1499	-0.2907	-0.1133	-8.6977	4.730
3.5	-7.1958	-1.3658	-0.3442	-0.1346	-9.0404	6.326
3.6	-6.7382	-1.6139	-0.4052	-0.1590	-8.9163	8.830
3.7	-5.5280	-1.8976	-0.4744	-0.1870	-8.0870	12.923
3.8	-3.2443	-2.2206	-0.5524	-0.2188	-6.2362	19.923
3.9	0.5313	-2.5868	-0.6399	-0.2549	-2.9503	32.511
4.0	6.3385	-3.0002	-0.7373	-0.2955	2.3054	56.431
Langmuir constant ratio approximated as $e^{U_{Guest-Host}/kT} / e^{U_{Guest-Host}/kT}$						

Table 8.7a Lattice Summation Results - Structure II Pentagonal Dodecahedron

Lattice Summation Results Structure II - Water Clathrate Pentagonal Dodecahedron T = 273.15 K Lennard-Jones (6-12) Potential ε/k = 180 K						
σ	Potential Energy - Cell Center					Langmuir Constant Ratio
	Guest - Host		Guest - Guest		Total	
Å	Shell 1	Shell > 1	Small Cavity	Large Cavity	U/kT	Total / Shell 1
2.5	-3.4150	-0.3298	-0.0845	-0.0325	-3.8618	1.563
2.6	-4.2339	-0.4171	-0.1068	-0.0411	-4.7989	1.760
2.7	-5.1774	-0.5229	-0.1338	-0.0515	-5.8856	2.030
2.8	-6.2416	-0.6500	-0.1662	-0.0641	-7.1218	2.411
2.9	-7.4119	-0.8017	-0.2047	-0.0790	-8.4973	2.961
3.0	-8.6578	-0.9818	-0.2503	-0.0968	-9.9867	3.777
3.1	-9.9277	-1.1940	-0.3039	-0.1177	-11.5434	5.031
3.2	-11.1402	-1.4429	-0.3666	-0.1422	-13.0919	7.041
3.3	-12.1747	-1.7331	-0.4393	-0.1708	-14.5180	10.415
3.4	-12.8587	-2.0698	-0.5232	-0.2040	-15.6558	16.396
3.5	-12.9524	-2.4585	-0.6195	-0.2423	-16.2726	27.668
3.6	-12.1288	-2.9050	-0.7293	-0.2863	-16.0494	50.433
3.7	-9.9504	-3.4157	-0.8539	-0.3366	-14.5566	100.104
3.8	-5.8397	-3.9972	-0.9944	-0.3938	-11.2251	218.193
3.9	0.9563	-4.6563	-1.1518	-0.4587	-5.3106	526.808
4.0	11.4093	-5.4003	-1.3272	-0.5320	4.1498	1421.472
Langmuir constant ratio approximated as $e^{-U_{Shell\ 1}/kT} / e^{-U_{Shell\ 1}/kT}$						

Table 8.7b Lattice Summation Results - Structure II Pentagonal Dodecahedron

Lattice Summation Results Structure II - Water Clathrate Hexakaidecahedron T = 273.15 K Lennard-Jones (6-12) Potential ε/k = 100 K						
σ	Potential Energy - Cell Center					Langmuir Constant Ratio
	Guest - Host		Guest - Guest		Total	
Å	Shell 1	Shell > 1	Small Cavity	Large Cavity	U/kT	Total / Shell 1
2.9	-2.1866	-0.3261	-0.0878	-0.0251	-2.6256	1.551
3.0	-2.6435	-0.3995	-0.1075	-0.0307	-3.1813	1.712
3.1	-3.1660	-0.4862	-0.1308	-0.0374	-3.8203	1.924
3.2	-3.7561	-0.5878	-0.1580	-0.0452	-4.5471	2.206
3.3	-4.4133	-0.7066	-0.1898	-0.0543	-5.3639	2.587
3.4	-5.1336	-0.8445	-0.2267	-0.0648	-6.2696	3.114
3.5	-5.9084	-1.0040	-0.2692	-0.0770	-7.2586	3.858
3.6	-6.7227	-1.1876	-0.3181	-0.0911	-8.3195	4.937
3.7	-7.5532	-1.3981	-0.3740	-0.1072	-9.4325	6.548
3.8	-8.3659	-1.6384	-0.4376	-0.1255	-10.5674	9.038
3.9	-9.1131	-1.9116	-0.5097	-0.1464	-11.6808	13.035
4.0	-9.7298	-2.2211	-0.5911	-0.1699	-12.7119	19.730
4.1	-10.1294	-2.5705	-0.6825	-0.1965	-13.5789	31.485
4.2	-10.1984	-2.9634	-0.7849	-0.2263	-14.1729	53.225
4.3	-9.7904	-3.4037	-0.8989	-0.2596	-14.3525	95.791
4.4	-8.7182	-3.8954	-1.0254	-0.2967	-13.9358	184.483
4.5	-6.7457	-4.4428	-1.1652	-0.3379	-12.6915	382.173
Langmuir constant ratio approximated as $e^{-U_{Shell\,>1}/kT}$ / $e^{-U_{Shell\,1}/kT}$						

Table 8.8a Lattice Summation Results - Structure II Hexakaidecahedron

Lattice Summation Results Structure II - Water Clathrate Hexakaidecahedron T = 273.15 K Lennard-Jones (6-12) Potential ε/k = 180 K						
σ	Potential Energy - Cell Center					Langmuir Constant Ratio
	Guest - Host		Guest - Guest		Total	
Å	Shell 1	Shell > 1	Small Cavity	Large Cavity	U/kT	Total / Shell 1
2.9	-3.9359	-0.5870	-0.1581	-0.0451	-4.7261	2.204
3.0	-4.7583	-0.7192	-0.1936	-0.0553	-5.7263	2.633
3.1	-5.6988	-0.8751	-0.2354	-0.0672	-6.8765	3.247
3.2	-6.7610	-1.0581	-0.2844	-0.0813	-8.1848	4.153
3.3	-7.9439	-1.2718	-0.3416	-0.0977	-9.6550	5.535
3.4	-9.2405	-1.5201	-0.4080	-0.1167	-11.2852	7.727
3.5	-10.6352	-1.8071	-0.4846	-0.1387	-13.0656	11.364
3.6	-12.1009	-2.1377	-0.5726	-0.1640	-14.9751	17.711
3.7	-13.5958	-2.5165	-0.6732	-0.1929	-16.9784	29.447
3.8	-15.0587	-2.9490	-0.7877	-0.2259	-19.0213	52.597
3.9	-16.4036	-3.4409	-0.9175	-0.2634	-21.0254	101.677
4.0	-17.5136	-3.9980	-1.0640	-0.3059	-22.8815	214.404
4.1	-18.2329	-4.6269	-1.2286	-0.3537	-24.4420	497.254
4.2	-18.3572	-5.3341	-1.4128	-0.4073	-25.5113	1279.391
4.3	-17.6227	-6.1266	-1.6180	-0.4673	-25.8346	3684.581
4.4	-15.6928	-7.0118	-1.8457	-0.5341	-25.0844	11987.325
4.5	-12.1422	-7.9970	-2.0973	-0.6082	-22.8448	44470.175
Langmuir constant ratio approximated as $e^{-U_{Shell}/kT} / e^{-U_{Guest}/kT}$						

Table 8.8b Lattice Summation Results - Structure II Hexakaidecahedron

8.3 Full Integration versus Lennard-Jones and Devonshire Approximation

In order to elucidate the inadequacies associated with the use of spherically symmetric Lennard-Jones Devonshire smooth cell approximation, we have performed multi-dimensional integrations over the various water clathrate cavities while accounting for the asymmetries of the host lattice using the complete crystallographic structural data as described earlier in Chapter 4. Using the methods outlined previously in Section 6.2, the configurational partition functions were evaluated for a number of systems. Additionally, the angle-averaged potential energy profiles were calculated in order to compare with those determined via the Lennard-Jones Devonshire approximation.

A sample angle-averaged potential energy profile of a spherical guest within the structure II pentagonal dodecahedron is shown in Figure 8.6. Similarly, the angle-averaged profile of a spherical guest within the structure II hexakaidecahedron is shown in Figures 8.7 and 8.8. Due to the similar geometry of the various cavities, the structure I water clathrate cavity profiles have not been included in the figures even though calculations were made.

The dashed curves in each of these figures represent the Lennard-Jones Devonshire spherical cell approximation as given by Equation (7.7). Only the first shell of water molecules were included. The family of solid curves represents the full three-dimensional integration over the rigid host lattice. The upper most solid line represents the first shell interaction only. The five additional solid lines represents the inclusion of subsequent water shell interactions in the potential energy calculations. The convergence of the potential energy as a function of these succeeding interactions is clearly illustrated in each of the figures. Again, it

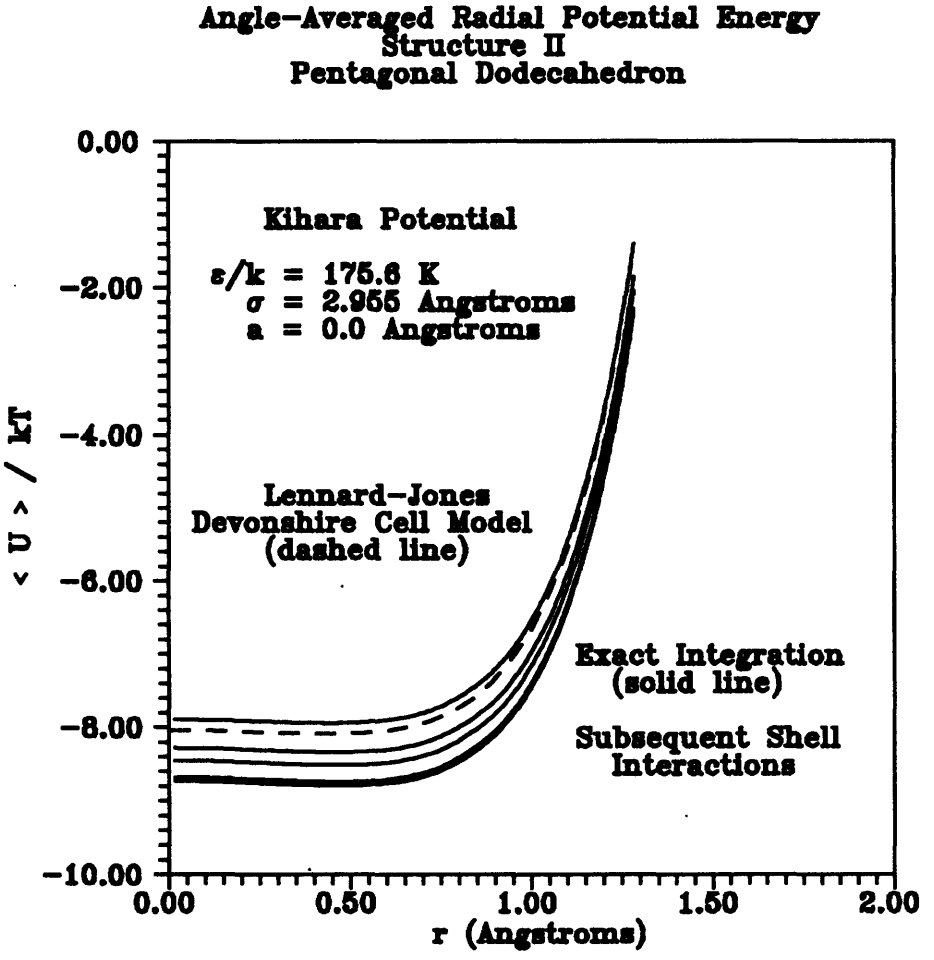

Figure 8.6 Angle-Averaged Potential Energy - Structure II Dodecahedron

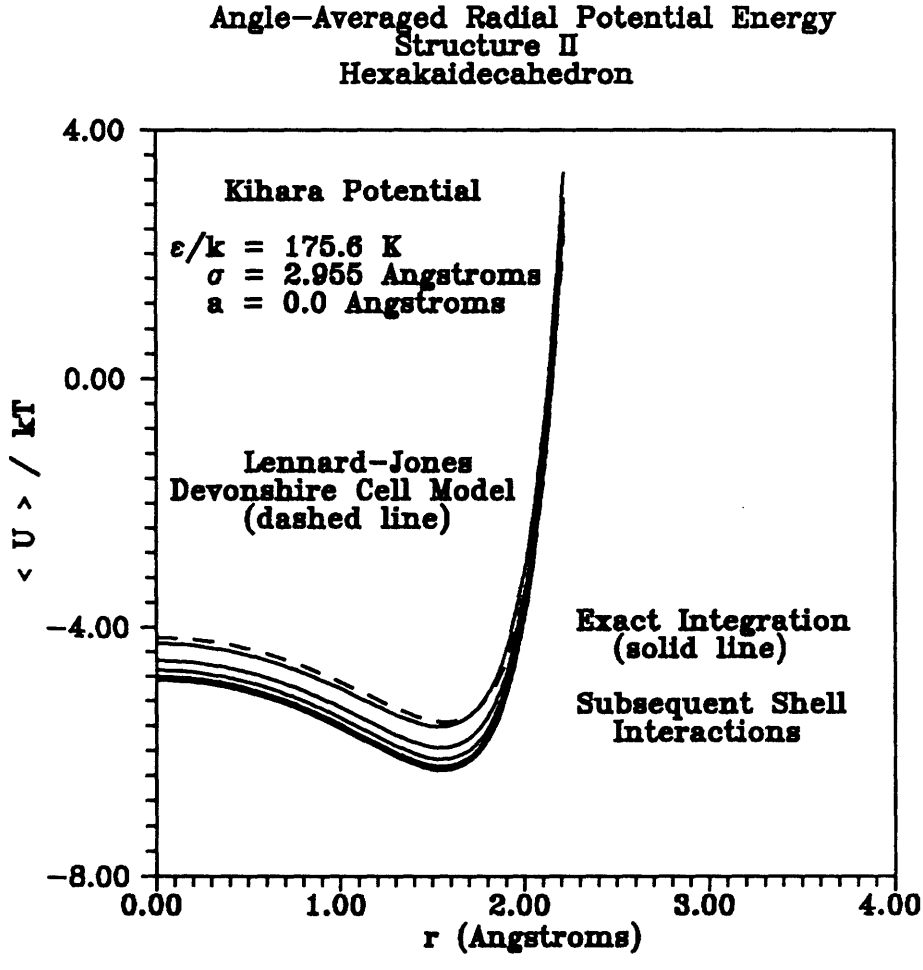

Figure 8.7 Angle-Averaged Potential Energy - Structure II Hexakaidecahedron

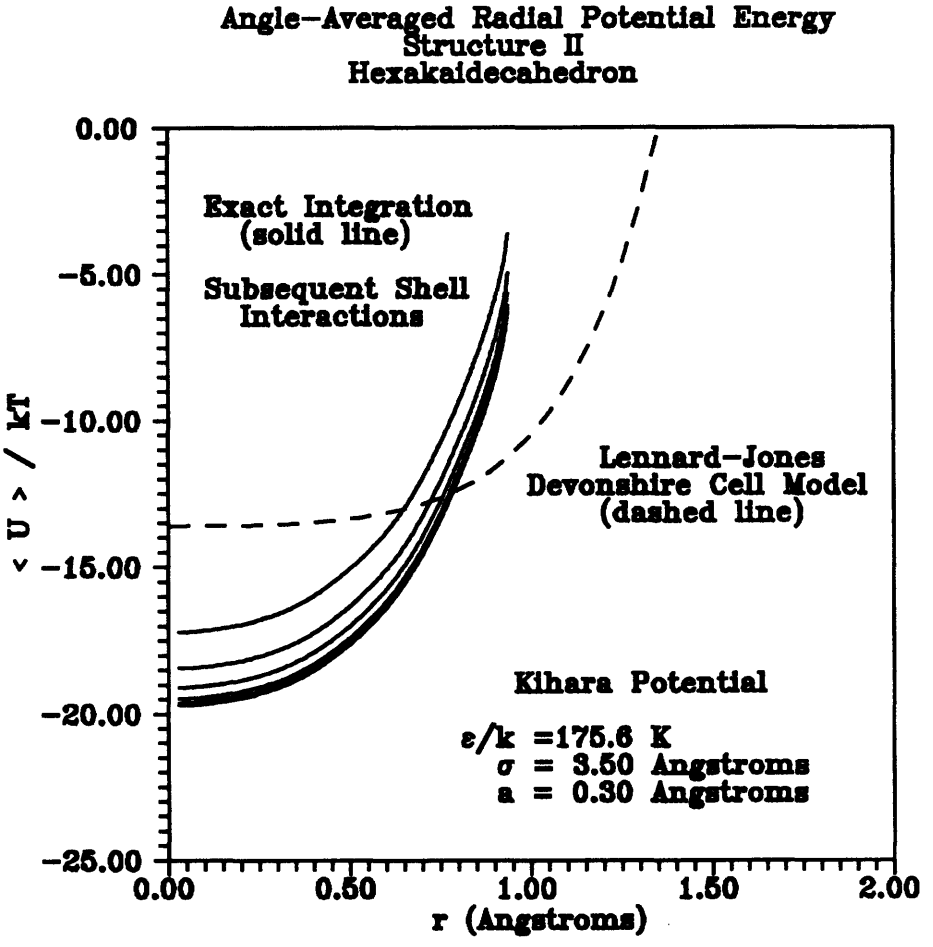

Figure 8.8 Angle-Averaged Potential Energy - Structure II Hexakaidecahedron

should be noted that the inclusion of these additional water shell interactions has a rather significant effect on the potential energy profile, and must therefore be considered in the configurational partition function evaluation.

It is quite obvious from Figure 8.6, and Figure 8.7, that for the smaller guest molecules ($\sigma < 3.0$), the Lennard-Jones Devonshire approximation does a remarkably good job in describing the potential energy profiles within the different water clathrate cavities. Of course, the addition of the subsequent water shell interactions would be still be necessary in order to accurately capture their important contributions. For the larger guest molecules ($\sigma = 3.5$), as depicted in Figure 8.8, the Lennard-Jones Devonshire approximation is completely inadequate in describing the potential energies and is therefore incapable of providing reliable estimates of the configurational partition function.

In an attempt to further elucidate the inadequacies of the Lennard-Jones Devonshire approximation in regard to the asymmetries of the host lattice, we have performed calculations for a wide range of Kihara intermolecular potential parameters following the Q^* convention first proposed by John and Holder (1985).

$$Q^* \equiv \frac{C(EXACT)}{C(LJD)} \tag{8.15}$$

Using the definition above we have compared the Langmuir constant determined through the use of the Lennard-Jones Devonshire approximation (*C(LJD)*) with those determined from the complete three-dimensional integration over the host lattice (*C(EXACT)*). For the sake of comparison with John and Holder's results only the first shell interactions were included.

The results for the structure I pentagonal dodecahedron are illustrated in Figure 8.9. The symbols represent the actual calculations while the solid lines are simple cubic splines through the data points. The results for the structure I tetrakaidecahedron are similarly pictured in Figure 8.10. Additionally, the results for the structure II pentagonal dodecahedron and hexakaidecahedron are given in Figures 8.11 and 8.12.

It is clearly evident from the various figures that their exists appreciable deviation between the *LJD* value and that determined from the more complete three dimensional integrations. We know that for the larger more asymmetric water clathrate formers, the use of the Lennard-Jones Devonshire approximation results in estimates of the dissociation pressure which are far below those determined experimentally. The inverse relationship between the Langmuir constant of the guest molecule and its fugacity, as dictated by van der Waals and Platteeuw model (Equation (5.25)) requires smaller Langmuir constants if we are to better predict these dissociation pressures. The decreasing nature of the "exact" Langmuir constants as illustrated in Figures 8.9, 8.10, 8.11, and 8.12 is therefore in accord with the theory. Probably the most interesting point illustrated in these figures, involves the fact that they exhibit a completely different behavior than those reported by John and Holder (1985). The results of their three-dimensional integrations illustrated in Figures 8.13, 8.14, 8.15, and 8.16 instead demonstrate a nearly opposite trend. For the same range of potential parameters they observed an increasing Langmuir constant ratio for increasing values of σ. The magnitude of the changes were also of a much lesser value, usually on the order of a factor of two or three. Using questionable reasoning they, however, discounted their results in favor of an empirical correlation for Q^* which instead gave the theoretically correct downward trend similar to the results reported here. Apparently, their integrations are not correct as the authors did not report any checks of their integration procedures. We used simple Monte Carlo integrations to test the results of our multi-dimensional Gaussian-Legendre

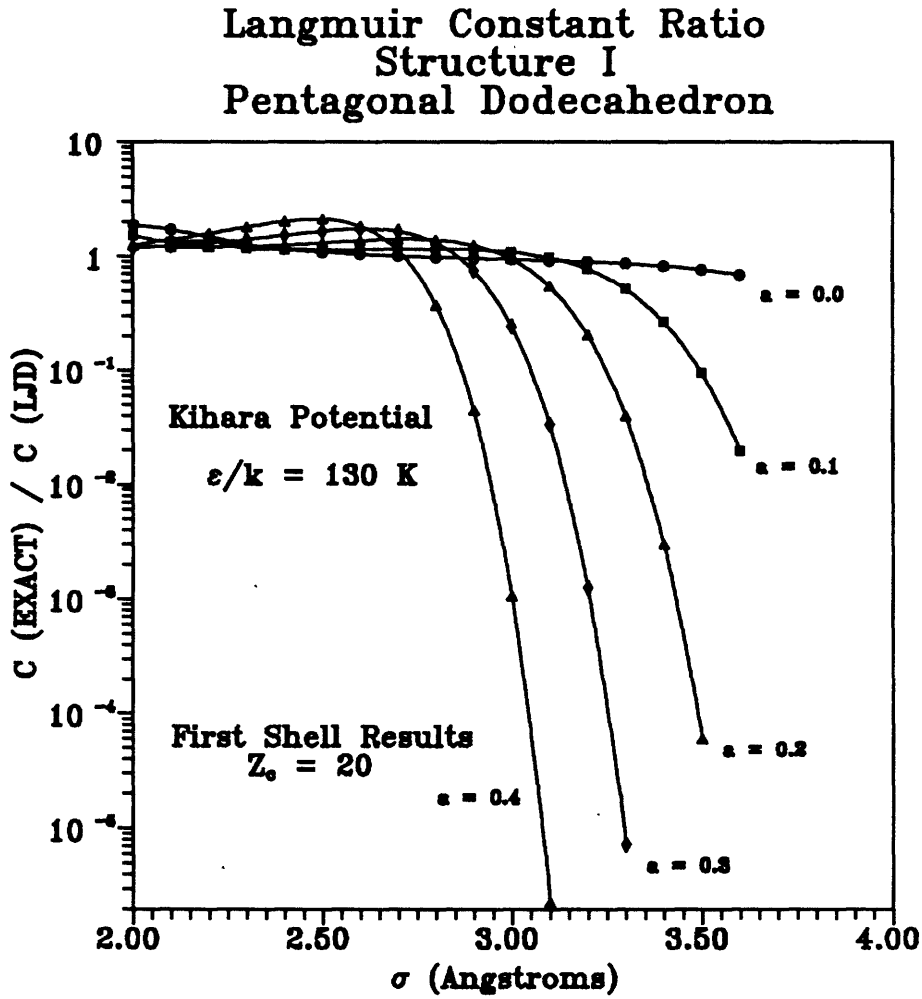

Figure 8.9 Langmuir Constant Ratio - Structure I Pentagonal Dodecahedron

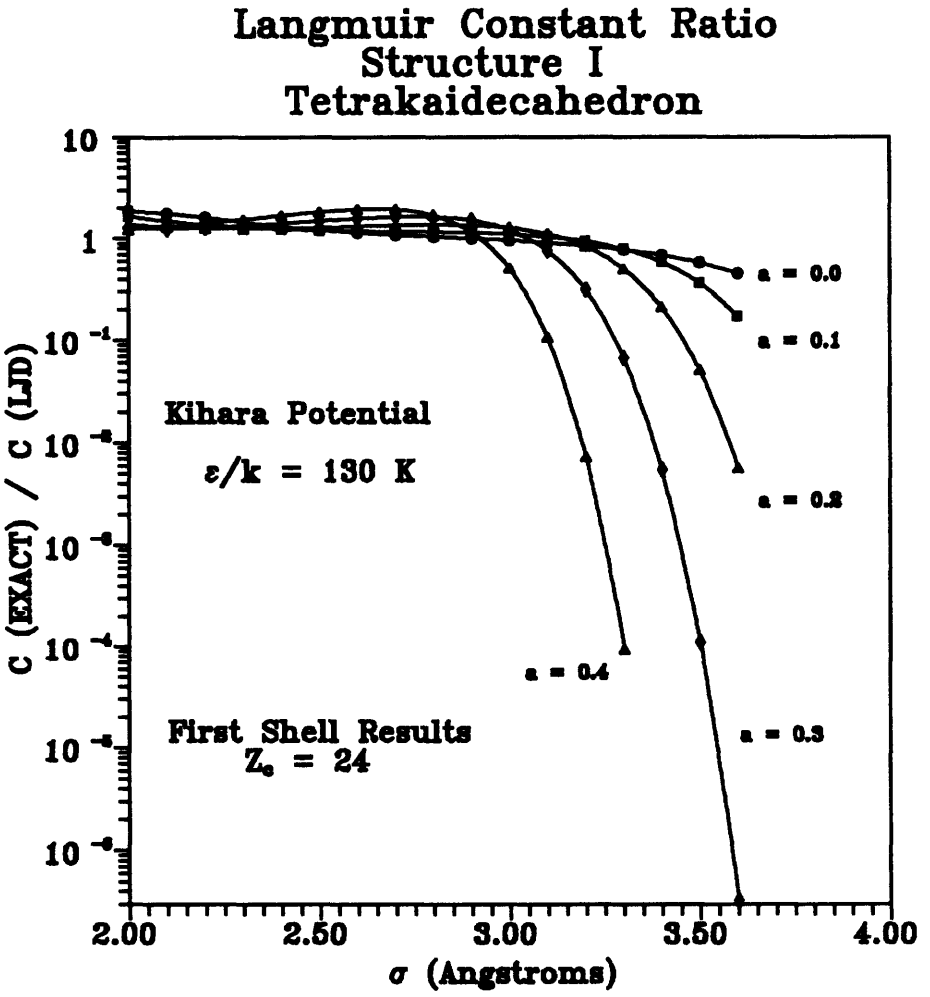

Figure 8.10 Langmuir Constant Ratio - Structure I Tetrakaidecahedron

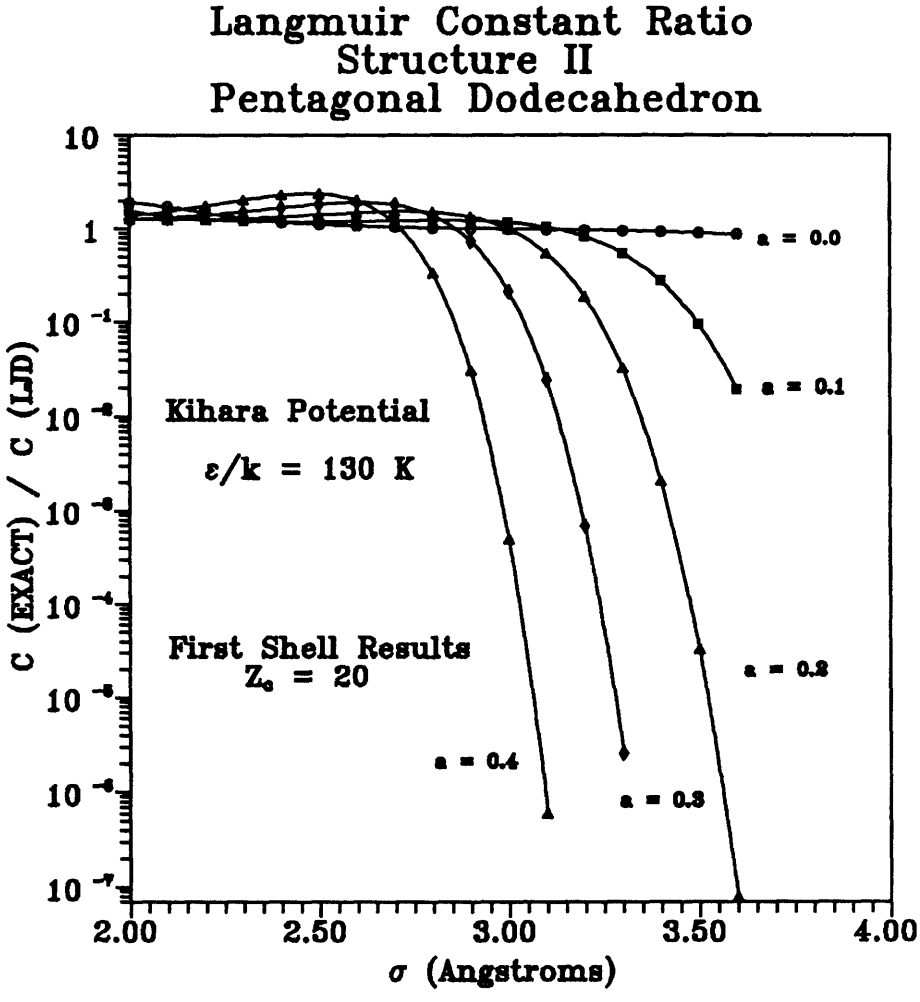

Figure 8.11 Langmuir Constant Ratio - Structure II Pentagonal Dodecahedron

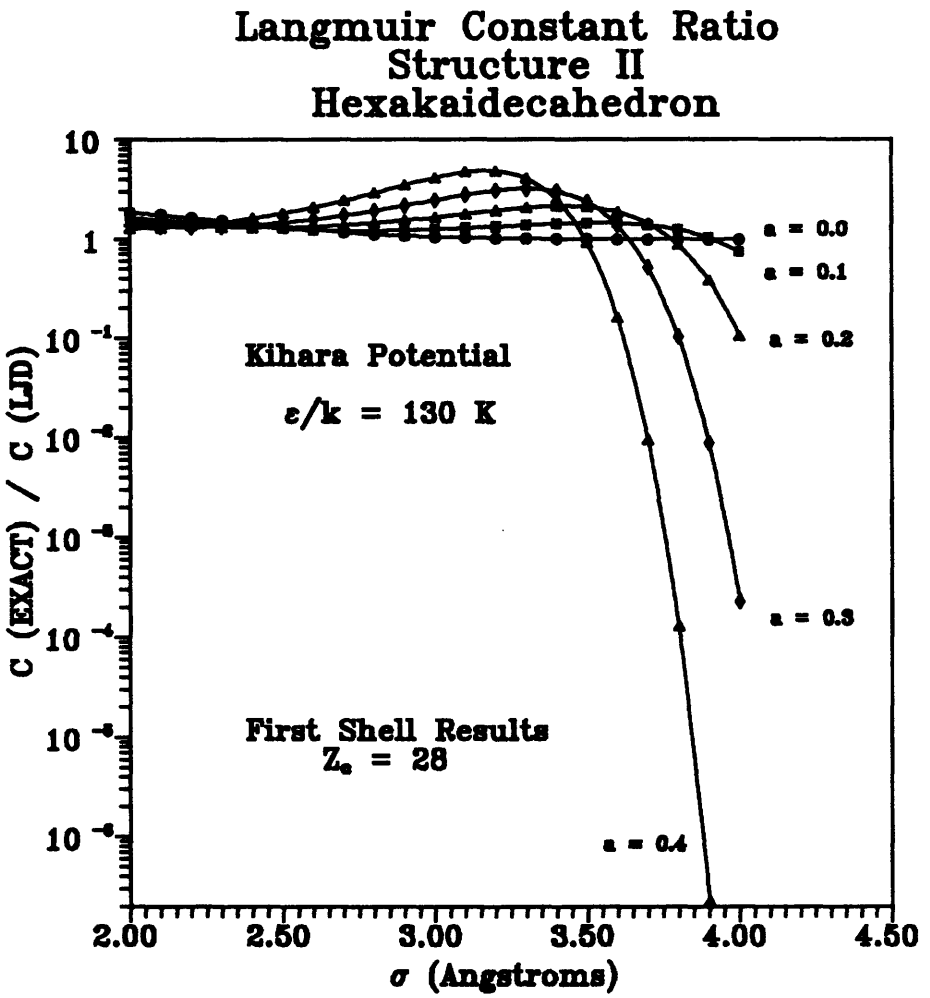

Figure 8.12 Langmuir Constant Ratio - Structure II Hexakaidecahedron

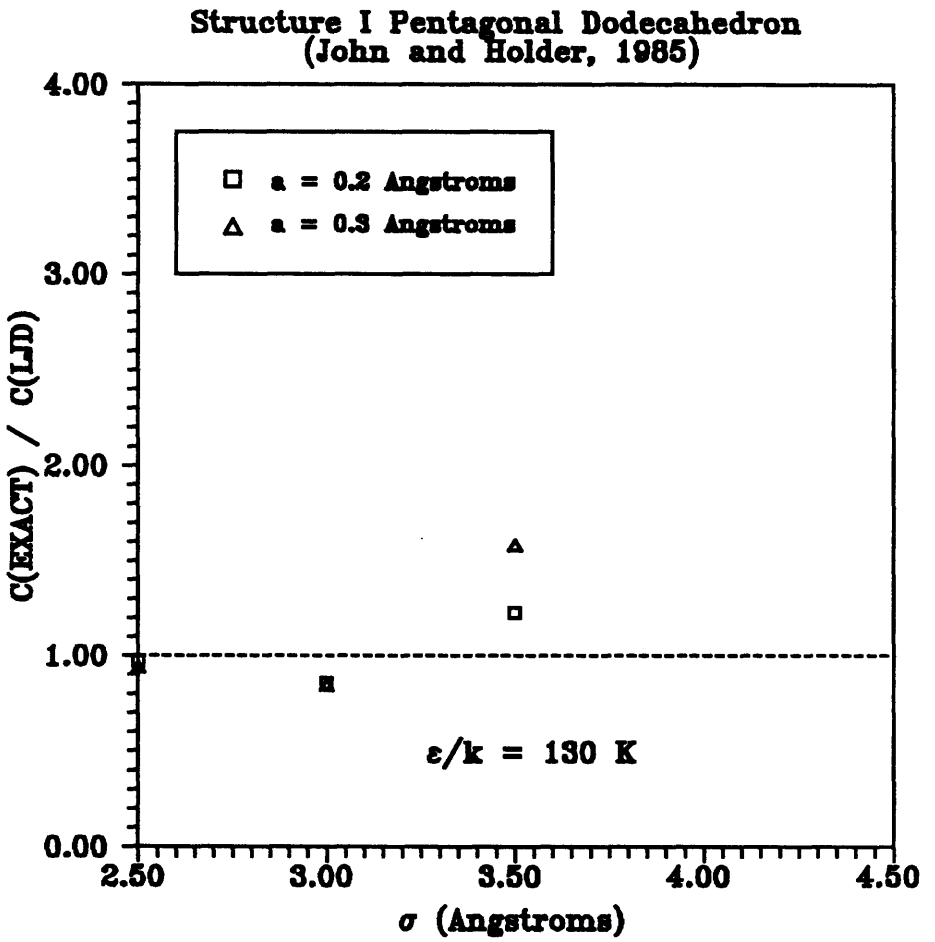

Figure 8.13 Structure I Pentagonal Dodecahedron (John and Holder, 1985)

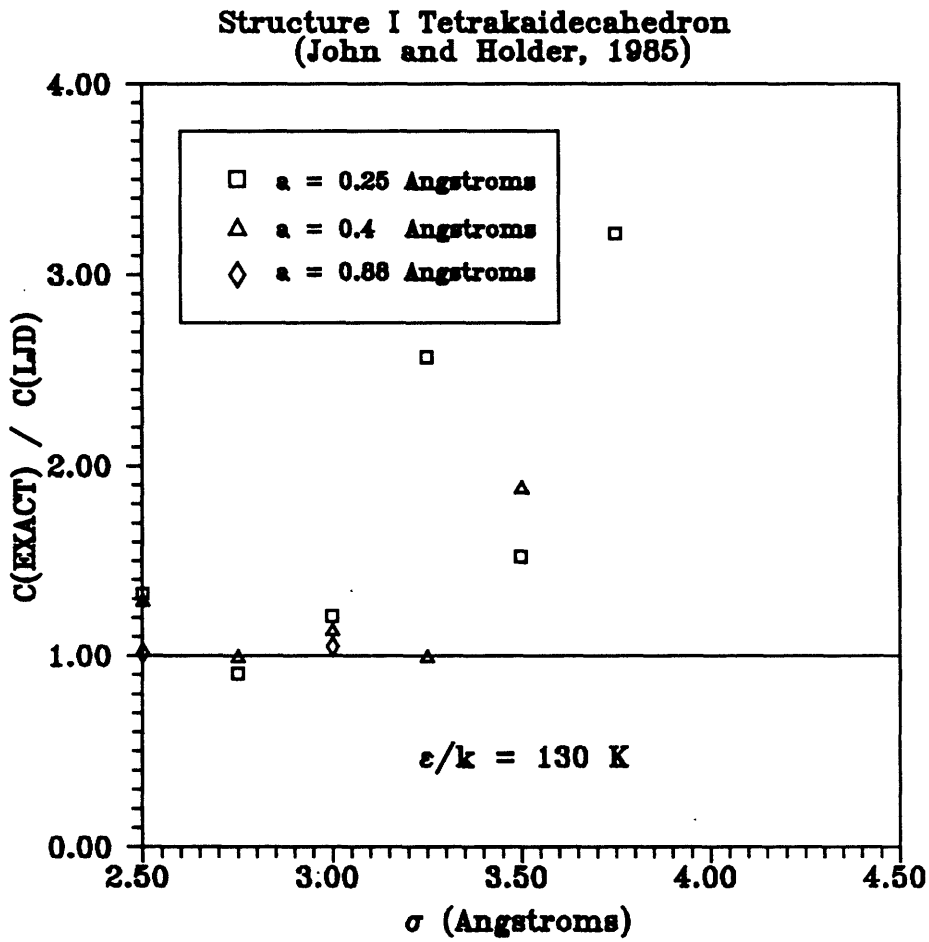

Figure 8.14 Structure I Tetrakaidecahedron (John and Holder, 1985)

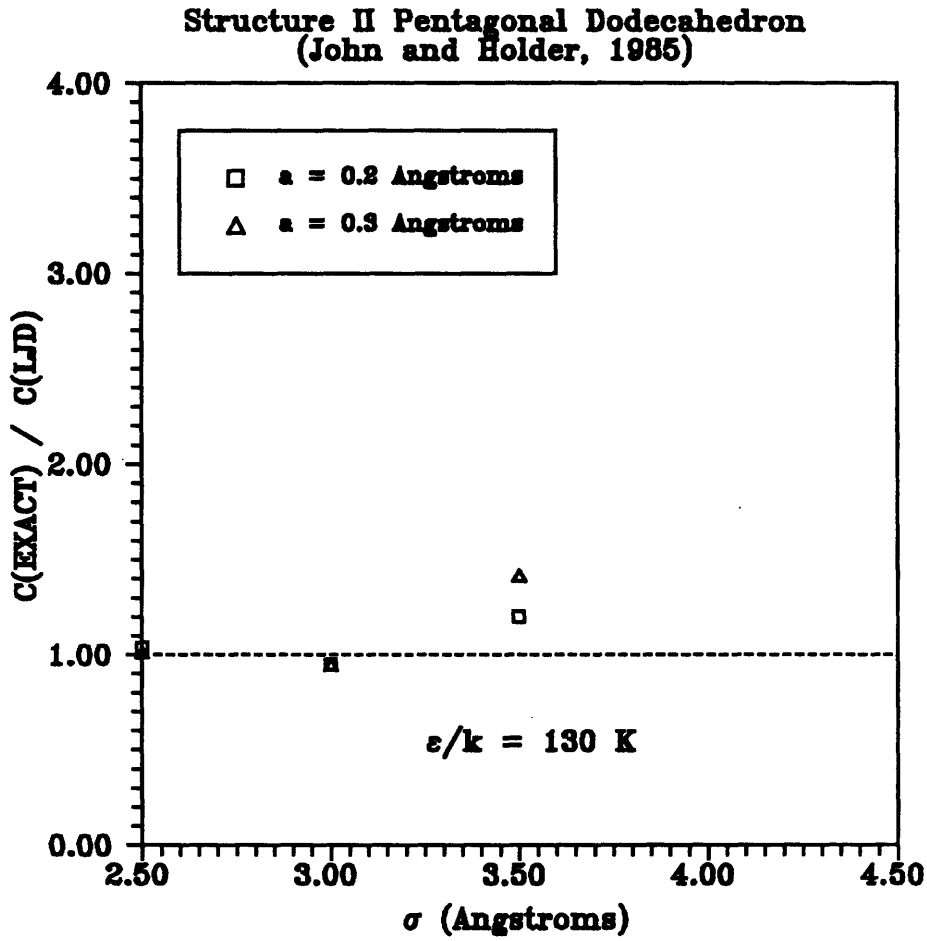

Figure 8.15 Structure II Pentagonal Dodecahedron (John and Holder, 1985)

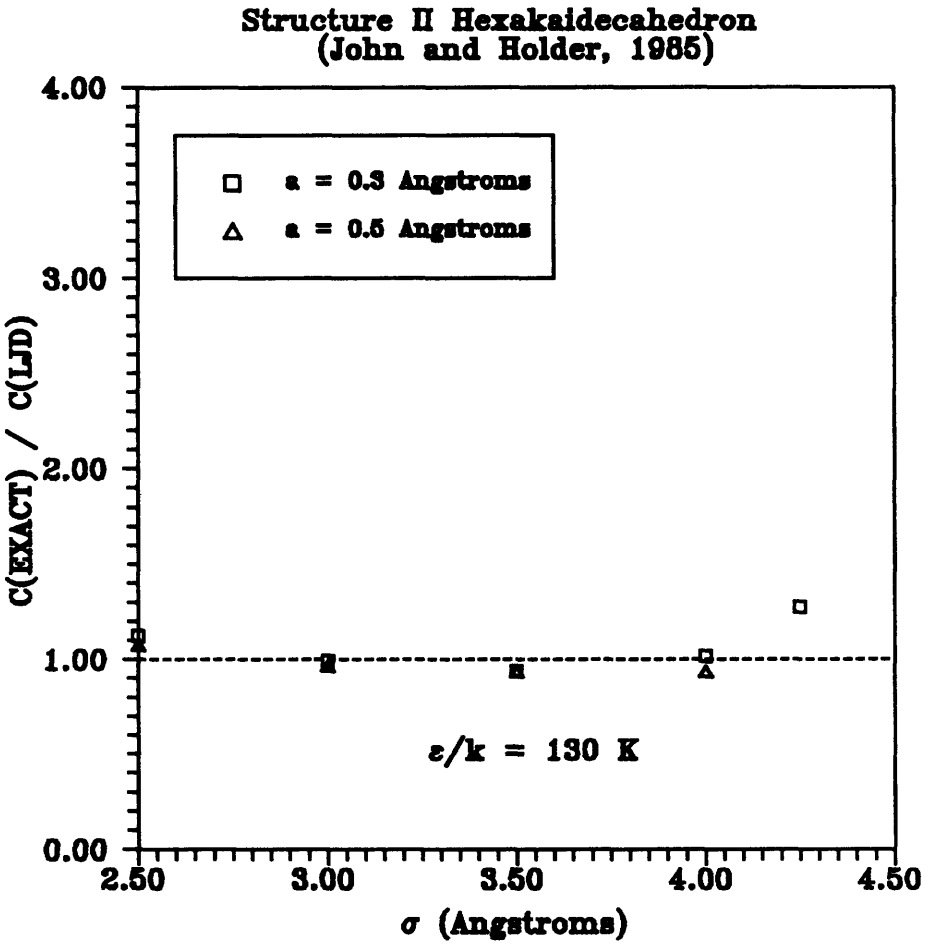

Figure 8.16 Structure II Hexakaidecahedron (John and Holder, 1985)

quadrature. The additional potential energy profiles reported previously, also provided us with a quantitative check of our methods. In particular, the excellent agreement exhibited between the *LJD* model and the exact integration for the smaller guests provided us with a positive verification of our integration methods. Furthermore, by setting the intermolecular potential energy parameter, ε, to zero, we were able to equate the configurational partition function to the known integration volume.

Given the importance of including the host lattice asymmetries in the evaluation of the configurational partition function, the inclusion of the subsequent water shell interactions is additionally important. A good example of this is illustrated in Figure 8.17. Using complete three-dimensional integrations the Langmuir constant was calculated as a simple function of coordination number for a sample system. Again, as explained in Section 8.2, the effect can be quite large. In fact, in Figure 8.17 we observe a change of more than an order of magnitude in the value of the Langmuir constant.

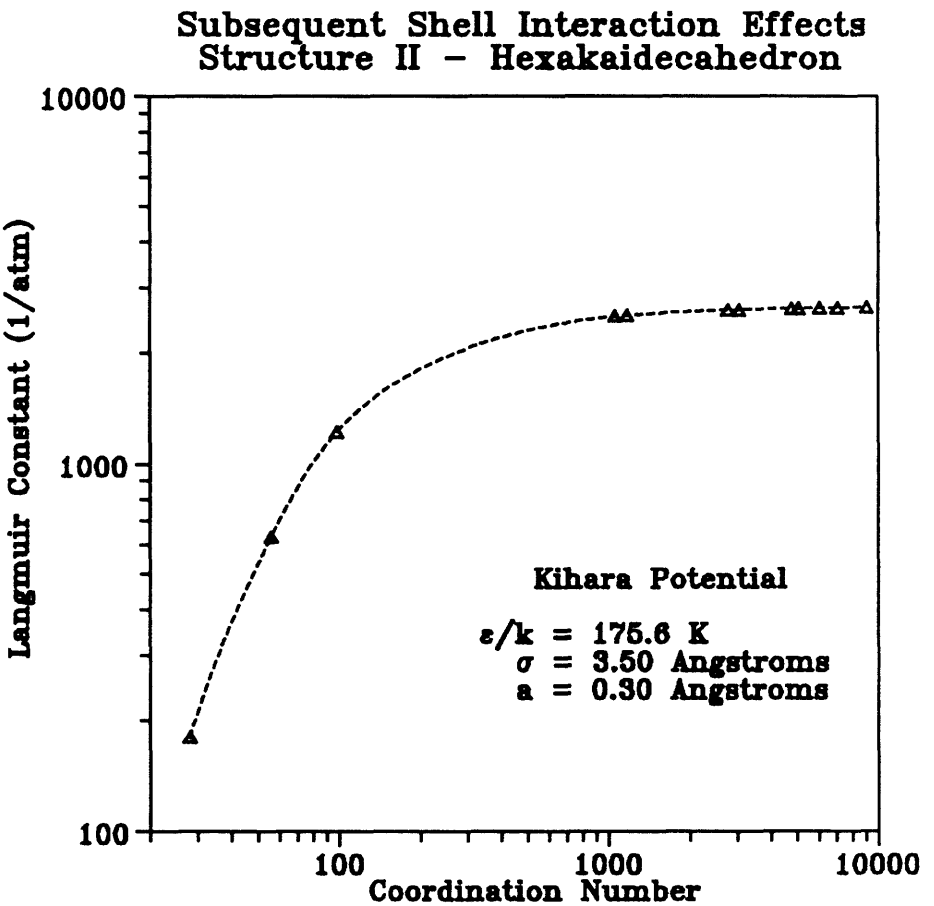

Figure 8.17 Subsequent Water Shell Contributions

9. MOLECULAR SIMULATION OF PHASE EQUILIBRIA IN WELL-DEFINED MODEL SYSTEMS

The modeling of the three-phase dissociation pressures of water clathrate systems is often of great concern for those involved in the various gas processing industries. In an attempt to further our understanding of the importance of the true configurational characteristics of the guest-host interaction, we have chosen to model two rather unique water clathrate systems. We have restricted this portion of our study to structure I water clathrates in which only the large cavities are occupied by the guest molecules, specifically, the ethane-water clathrate and cyclopropane-water clathrate.

In structure I clathrates the reference properties which correlate the chemical potential difference between water in a hypothetical empty hydrate lattice and water in either a water rich aqueous phase or solid ice phase are based upon actual experimental measurements. Whereas the structure II reference properties are based upon applications of Lennard-Jones and Devonshire Smooth Cell model to several model systems. Thus, we have limited our simulation studies to structure I systems.

Additionally, by restricting our study to those systems in which only the larger of the two cavity types are occupied, we can compare the Langmuir constants based upon our evaluation of the configurational partition function with those derived directly from dissociation pressure data.

9.1 Experimental Langmuir Constants

In Chapter 5, we derived using statistical mechanics an expression for the chemical potential difference of water in the hypothetical empty water clathrate and water in the "filled" clathrate phase. This expression, repeated here for completeness,

$$\frac{\Delta\mu_w^{\beta\text{-}H}}{kT} = \sum_i \nu_i \ln\left(1 + \sum_J C_{Ji} f_J\right) \tag{9.1}$$

can be applied to a number of different clathrate type systems. In terms of the structure I water clathrate system we know there are two of the smaller pentagonal dodecahedral cavities and six of the larger tetrakaidecahedral cavities for each unit cell comprised of forty six water molecules. Since ν_i is defined as the number of type i cavities per water molecule in the host lattice, we can write for a pure component structure I water clathrate system

$$\frac{\Delta\mu_w^{\beta\text{-}H}}{kT} = \frac{1}{23}\ln\left(1 + C_{J,1} f_J\right) + \frac{3}{23}\ln\left(1 + C_{J,2} f_J\right) \tag{9.2}$$

where $C_{J,1}$ is the Langmuir constant for a type J guest within the pentagonal dodecahedral cavity, $C_{J,2}$ is the Langmuir constant for a type J guest within the tetrakaidecahedral cavity, and f_J is the fugacity of component J. Several of the larger structure I water clathrate formers, specifically ethane and cyclopropane, are however, energetically limited to occupation of only the larger of the two cavity types, thereby reducing Equation (9.2) to the following expression.

$$\frac{\Delta\mu_w^{\beta\text{-}H}}{kT} = \frac{3}{23}\ln\left(1 + C_{J,2} f_J\right) \tag{9.3}$$

As previously discussed in Section 5.3, phase equilibrium requires that the chemical potential difference between water in hypothetical empty clathrate phase (β) and water in the "filled" clathrate phase (*H*) must equal the chemical potential difference of water in the hypothetical empty clathrate phase and water in either an aqueous liquid phase (*L*) or solid ice phase (α).

$$\Delta\mu_w^{\beta-H} = \Delta\mu_w^{\beta-L,\alpha} \tag{9.4}$$

This equilibrium constraint thereby allows us to rewrite Equation (9.3) upon simple rearrangement as

$$\frac{e^{(23/3)\Delta\mu_w^{\beta-L,\alpha}/kT} - 1}{f_J} = C_{J,2} \tag{9.5}$$

thus providing a rather simple means of relating the Langmuir constant of a type *J* guest in the larger tetrakaidecahedral cavity to f_J, the fugacity of guest component *J*, and $\Delta\mu_w^{\beta-H}$, the chemical potential difference between water in the hypothetical empty hydrate and water in either an aqueous liquid phase or ice phase.

In the following sections the "experimental" Langmuir constants derived from Equation (9.5) and the dissociation pressure data for the ethane and cyclopropane water clathrate systems are presented. The chemical potential difference $\Delta\mu_w^{\beta-H}$ was calculated using the method proposed by Holder et al. (1980) as previously discussed in Section 5.3. The Peng-Robinson equation of state (Peng et al., 1976) was used to estimate the fugacity of the guest component.

9.2 Configurational Langmuir Constants

In order to accurately account for the asymmetries associated with the interactions between the guest and the static host lattice, we have chosen to model the ethane and cyclopropane molecules as simple multi-site rigid bodies. The six orientational degrees of freedom associated with the guest within the clathrate cavity were considered directly in the evaluation of the configurational integral

$$Z_{Ji} = \frac{1}{8\pi^2} \int e^{-U(r,\theta,\phi,\alpha,\beta,\gamma)/kT} r^2 \sin\theta \, d\theta \, d\phi \, dr \, d\alpha \sin\beta \, d\beta \, d\gamma \qquad (9.6)$$

where the position and orientation of the guest is given by the spherical spatial coordinates r, θ, and ϕ, defined in reference to the center of a given cavity, and their Euler orientation angles α, β, and γ. The factor of $8\pi^2$ is simply a normalization constant.

The complexities associated with the modeling of these asymmetric guest molecules limited in several respects our evaluation of the "configurational" Langmuir constants. Specifically, due to the dimensionality of our integrations, we were restricted to a finite number of subsequent water shell interactions in the calculation of the total potential energy. Up to five shells were included in our integrations. The first shell consisted of the interaction energies associated with the 24 nearest neighboring water molecules while the second shell involved the interaction energies associated with the next 24 nearest neighboring water molecules. The third shell involved the interaction energies associated with the next 32 nearest neighboring water molecules and finally, the fourth shell involved the interaction energies associated with next 104 nearest neighboring water molecules. The fifth shell involved the interaction energies associated with the next 64 nearest water molecules. The adequacy of these five shells in the representation of the "infinite" lattice interaction, as previously discussed in chapter 8, was the basis for this restriction. The properties of these shells are listed in Table 9.1.

The configurational integrals were evaluated using the multi-interval 10-point Guassian-Legendre quadrature formula previously discussed in Section 6.2. The shear number of Gauss points involved in these integrations, however, required us to limit our number of integration intervals to one for each of the six dimensions. As it was, the integrations involved the evaluation of the total potential energy of the guest molecule over the four subsequent water shells for each of the required 10^6 Gauss points. Each integration consumed approximately 12 minutes of time on the MIT Cray 2 supercomputer facility. The evaluation of the configurational partition function for the ethane molecule was somewhat simpler in that its symmetry permitted us to eliminate the degree of rotational freedom associated with the Eulerian angle α, thus reducing the computational burden by about an order of magnitude.

Subsequent Water Shell Properties Structure I - Water Clathrate Tetrakaidecahedron			
Shell	Shell Coordination Number z_s	Total Coordination Number z_t	Average Distance from Center of Cell
1	24	24	4.33 Å
2	24	48	7.10 Å
3	32	80	8.33 Å
4	104	184	10.43 Å
5	64	248	12.62 Å
Based on a Cell Constant of 12.03 Å			

Table 9.1 Subsequent Water Shell Properties

9.3 Ethane-Water Clathrate System

In modeling the ethane-water clathrate system we chose to represent the ethane molecule using a rigid two interaction site Lennard-Jones (6-12) model as shown illustrated in Figure 9.1. As previously discussed in Section 7.1, the initial intermolecular interaction parameters ε and σ were taken from the TIPS model of Jorgensen (1981) since they were indicative of the parameters used by Tse et al. (1983; 1984) and Rodger (1989; 1990) in their molecular dynamics simulations of several similar structure I water clathrate systems. Only the interactions between the CH_3 sites and the O site on each of the static host water molecules were considered. The interactions between neighboring guest molecules were neglected.

Using the three-phase dissociation data for the ethane water clathrate system, as illustrated in Figure 9.2, Equation (9.5) was used to calculate the "experimental" Langmuir constants given in Table 9.2. The source of the experimental dissociation data is also given Table 9.2.

The TIPS based configurational Langmuir constants for the ethane molecule encaged within the larger tetrakaidecahedral cavity are shown in Figure 9.3. The lower most solid line represents the first shell interaction exclusively. The three additional dashed lines represent the inclusion of subsequent water shell interactions in the calculation of the potential energies, the upper most dashed line representing the inclusion of the intermolecular binary interactions between the guest ethane molecule and the nearest neighboring 248 host water molecules. Since these TIPS based Langmuir constants are nearly two orders of magnitude lower than the "experimentally" derived constants, we can rationally assume that these discrepancies are in all likelihood based upon improper choices of potential parameters.

If we examine the work of Bolis et al. (1983) which pertains to interactions between methane and water as determined from *ab initio* quantum mechanical calculations, we notice that they report for a specific conformation a minimum interaction energy of -2.719 kJ/mol. If we assume a correspondence between this minimum energy and the Lennard-Jones potential well depth, then we can reasonably conclude that the methane-water interaction is well represented by the ε/k value of 327 K as compared to the TIPS based value of 94 K. Since the TIPS model appears to significantly underestimate the well depth parameter for the methane-water system, we can assume that in all likelihood, the similarly derived intermolecular energy site parameter for the ethane-water system, are also undervalued. It should also be noted that due to the orientational dependency of the methane-water interaction, the reported ε/k value of 327 K should only strictly be considered an extreme upper limit.

For a given temperature and set of Lennard-Jones parameters, following the 10-point Gaussian-Legendre quadrature scheme to evaluate the configurational partition function, we obtained a predicted Langmuir constant to compare with the experimental values shown in Figure 9.3. The parameters were altered to minimize a suitable objective function. In this case, we selected the simple sum of the squares of the deviation between the experimental and predicted values. The resulting fitted constants along with the predicted plots are given in Figure 9.4.

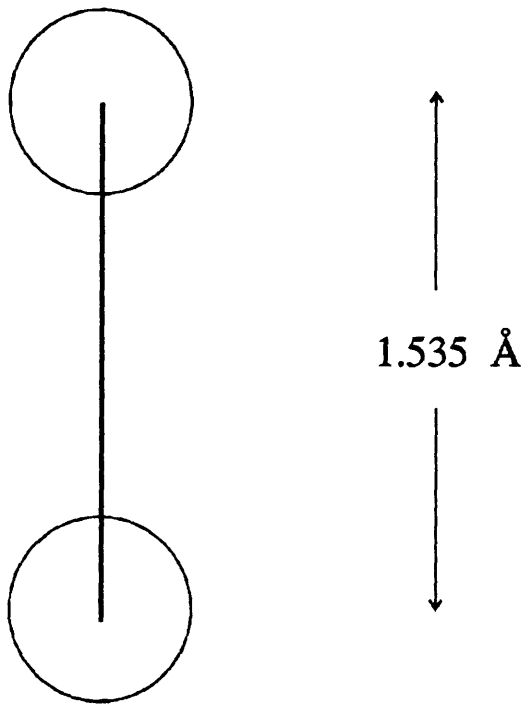

Figure 9.1 Ethane Model Representation

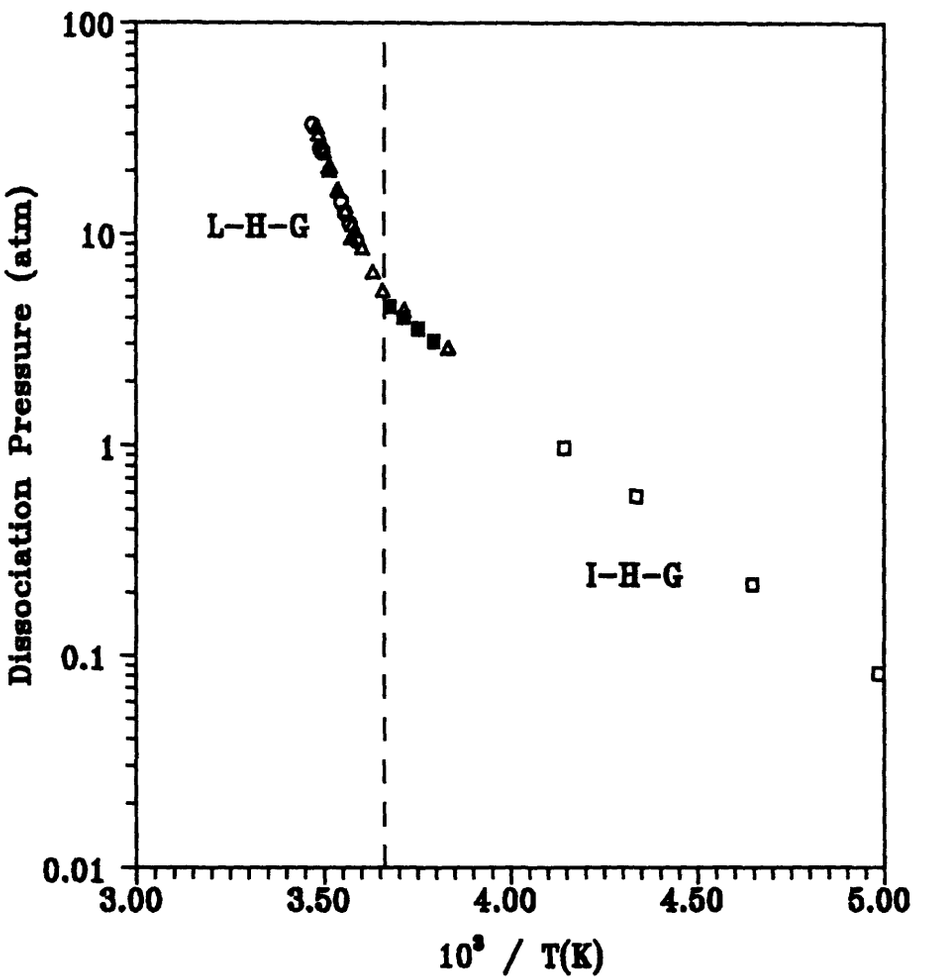

Figure 9.2 Ethane - Water Clathrate Three-Phase Equilibria

Experimental Ethane Langmuir Constants		
Temperature (Kelvin)	Dissociation Pressure (atm)	Langmuir Constant (atm^{-1})
288.2	33.161 [1]	7.64
286.5	25.660 [1]	8.24
286.0	24.772 [1]	8.24
282.0	14.310 [1]	10.31
281.1	12.633 [1]	10.94
280.2	11.251 [1]	11.55
278.8	9.376 [1]	12.62
240.8	0.968 [2]	194.04
229.9	0.575 [2]	445.24
215.5	0.218 [2]	1976.11
200.8	0.082 [2]	9329.50
272.0	4.511 [3]	19.01
269.3	3.994 [3]	22.79
266.5	3.525 [3]	27.52
263.5	3.089 [3]	33.65
287.4	32.553 [4]	7.43
284.7	21.013 [4]	8.71
282.8	16.447 [4]	9.57
279.9	9.594 [4]	13.09
287.0	30.144 [5]	7.62
285.8	25.041 [5]	8.10
284.5	20.278 [5]	8.85
284.4	21.094 [5]	8.55
282.8	16.195 [5]	9.69
281.1	12.997 [5]	10.68
279.7	11.160 [5]	11.33
279.1	10.343 [5]	11.75
277.5	8.642 [5]	12.71
275.4	6.600 [5]	14.59
273.4	5.376 [5]	15.93
269.3	4.355 [5]	21.00
260.9	2.865 [5]	38.70
260.8	2.906 [5]	38.26
[1] Holder and Hand (1982) [2] Falabella and Vanpee (1974) [3] Frost and Deaton (1946) [4] Reamer, Selleck, and Sage (1952) [5] Roberts, Brownscombe, Howe, and Ramser (1941)		

Table 9.2 Experimental Ethane Langmuir Constants

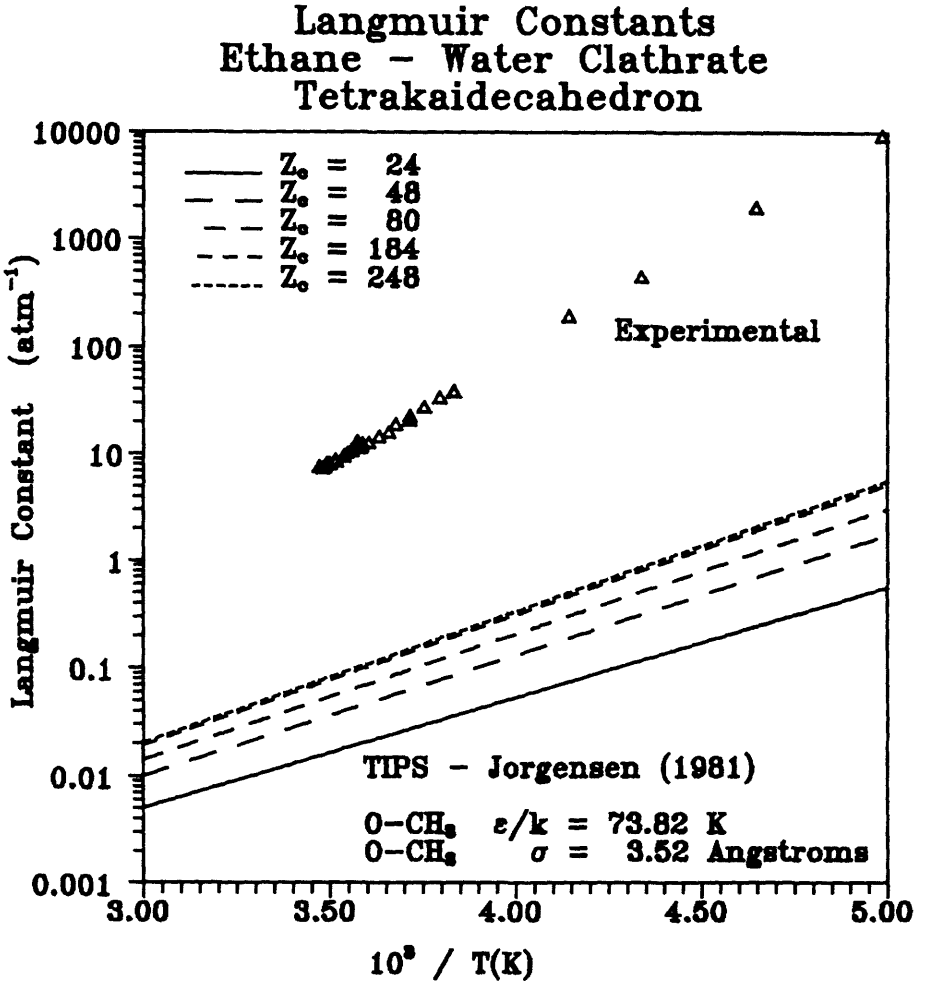

Figure 9.3 Ethane - Water Clathrate Langmuir Constants

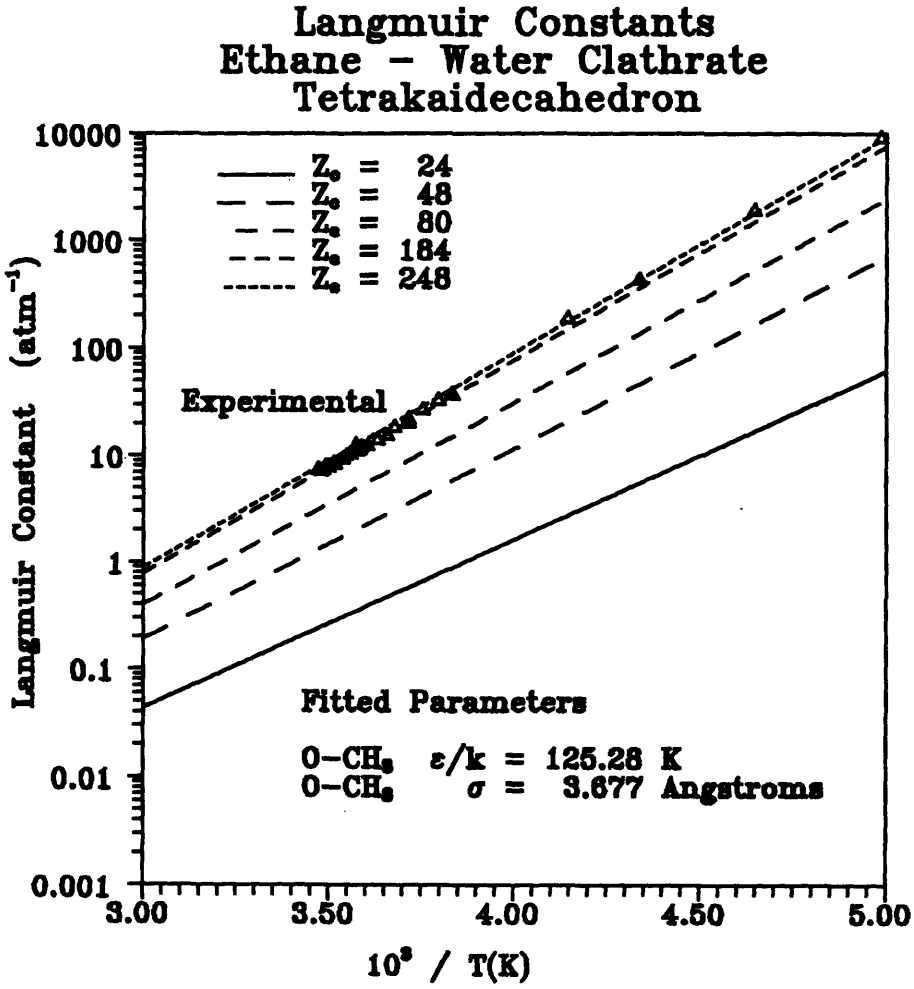

Figure 9.4 Fitted Ethane - Water Clathrate Langmuir Constants

9.4 Cyclopropane Water Clathrate System

In modeling the cyclopropane-water clathrate system we chose to represent the cyclopropane molecule using a rigid, three interaction site Lennard-Jones (6-12) model as shown illustrated in Figure 9.5. Again, the initial intermolecular interaction parameters ε and σ were taken from the TIPS model of Jorgensen (1981) since they were indicative of the parameters used by Tse et al. (1983; 1984) and Rodger (1989; 1990) in their molecular dynamics simulations of several similar structure I water clathrate systems. Only the interactions between the CH_2 sites and the O site on each of the static host water molecules were considered. The interactions between neighboring guest molecules were neglected.

Using the three-phase dissociation data for the cyclopropane water clathrate system, as illustrated in Figure 9.10, Equation (9.5) was used to calculate the "experimental" Langmuir constants given in Table 9.3. The source of the experimental dissociation data is also given Table 9.3.

The TIPS based configurational Langmuir constants for the cyclopropane molecule encaged within the larger tetrakaidecahedral cavity are shown in Figure 9.7. The lower most solid line represents the first shell interaction exclusively, The three additional dashed lines represent the inclusion of subsequent water shell interactions in the calculation of the potential energies, the upper most dashed line representing the inclusion of the intermolecular binary interactions between the guest cyclopropane molecule and the nearest neighboring 248 host water molecules. Since these TIPS based Langmuir constants are nearly three orders of magnitude lower than the "experimentally" derived constants, we can reasonably assume, following the arguments presented in the previous section, that the TIPS model also underestimates the potential well depth parameters for the cyclopropane-water system.

A similar treatment to obtain fitted potential parameters was followed for the cyclopropane-water system as described for the ethane-water system in Section 9.3. Results expressed in the form of a Langmuir constant versus inverse temperature plot are given in Figure 9.8.

One should note that the computational time for these fits was approximately an order of magnitude larger than for the ethane-water system due to the extra degree of rotational freedom of the non-linear cyclopropane guest.

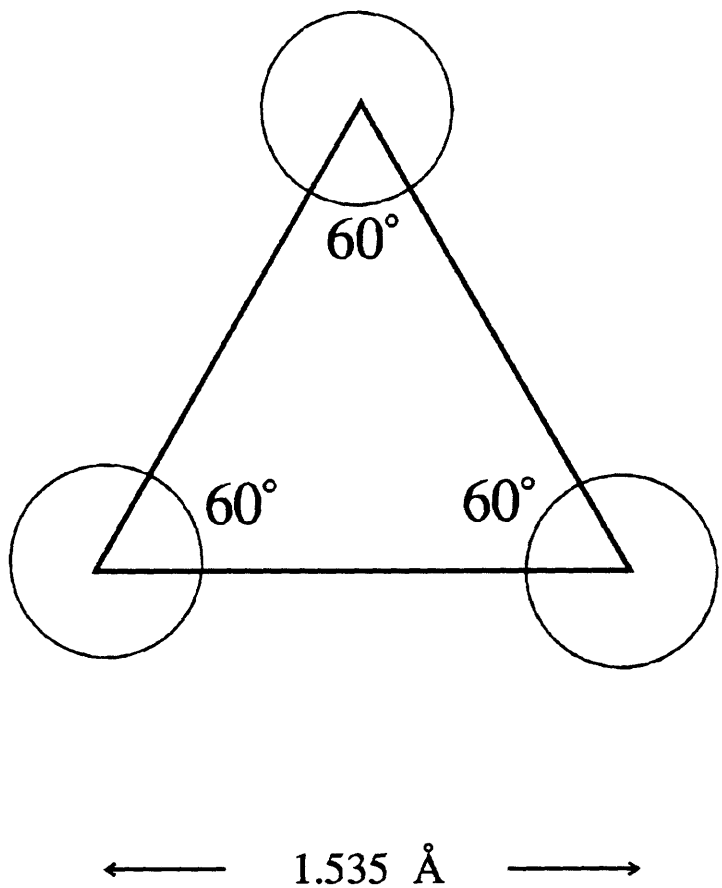

Figure 9.5 Cyclopropane Model Representation

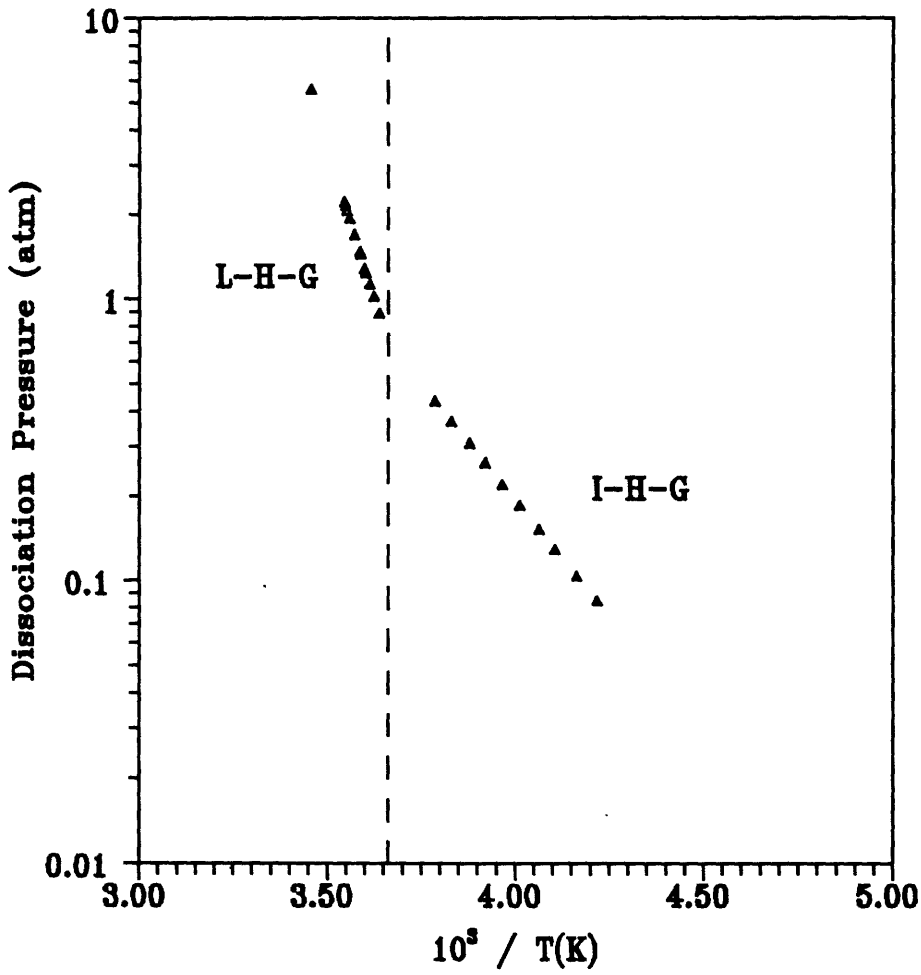

Figure 9.6 Cyclopropane - Water Clathrate Three-Phase Equilibria

Experimental Cyclopropane Langmuir Constants		
Temperature (Kelvin)	Dissociation Pressure (atm)	Langmuir Constant (atm^{-1})
289.4	5.587 [1]	20.52
282.2	2.218 [1]	32.97
281.9	2.163 [1]	33.21
281.6	2.071 [1]	34.08
281.1	1.939 [1]	35.34
280.0	1.699 [1]	37.84
278.9	1.477 [1]	40.83
278.8	1.445 [1]	41.47
277.9	1.282 [1]	44.40
277.7	1.237 [1]	45.49
276.9	1.132 [1]	47.48
276.0	1.020 [1]	50.06
275.0	0.888 [1]	54.38
264.2	0.436 [1]	121.20
261.1	0.370 [1]	153.04
257.9	0.309 [1]	197.02
255.1	0.263 [1]	247.02
252.2	0.220 [1]	315.84
249.3	0.186 [1]	402.14
246.2	0.153 [1]	527.87
243.6	0.130 [1]	663.70
240.2	0.104 [1]	902.75
237.2	0.085 [1]	1194.02
[1] Hafemann and Miller (1969)		

Table 9.3 Experimental Cyclopropane Langmuir Constants

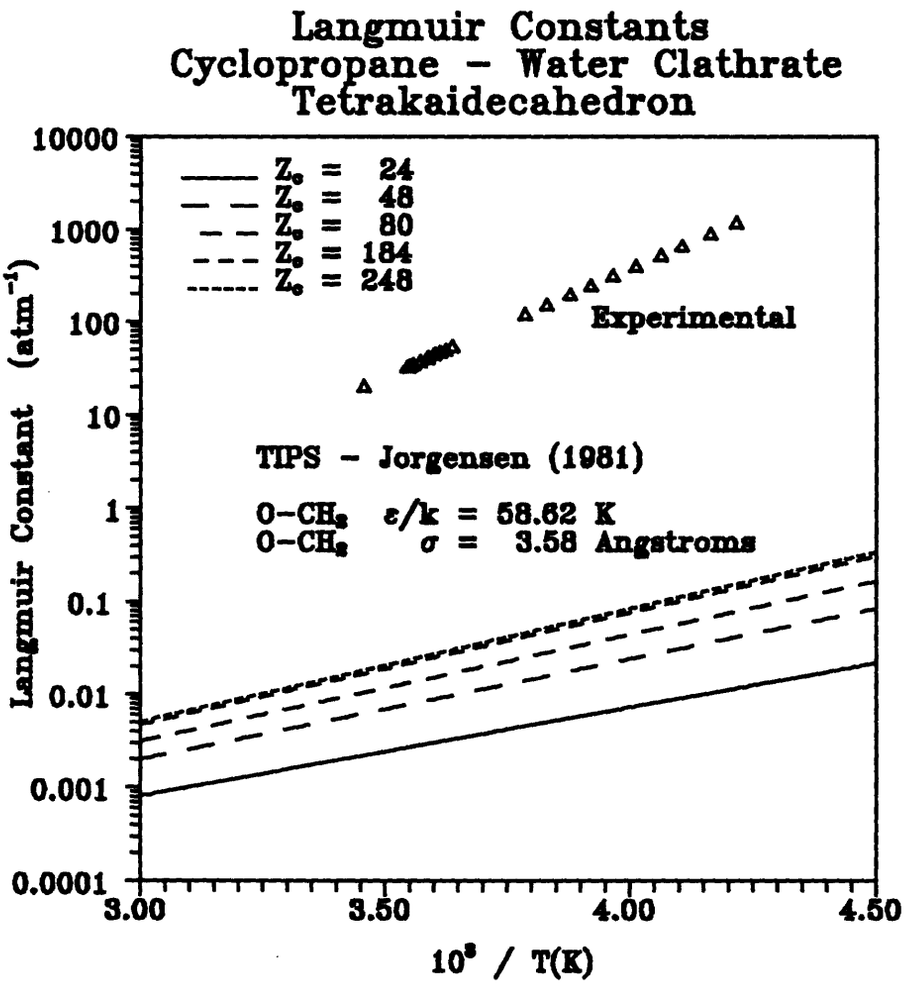

Figure 9.7 Cyclopropane - Water Clathrate Langmuir Constants

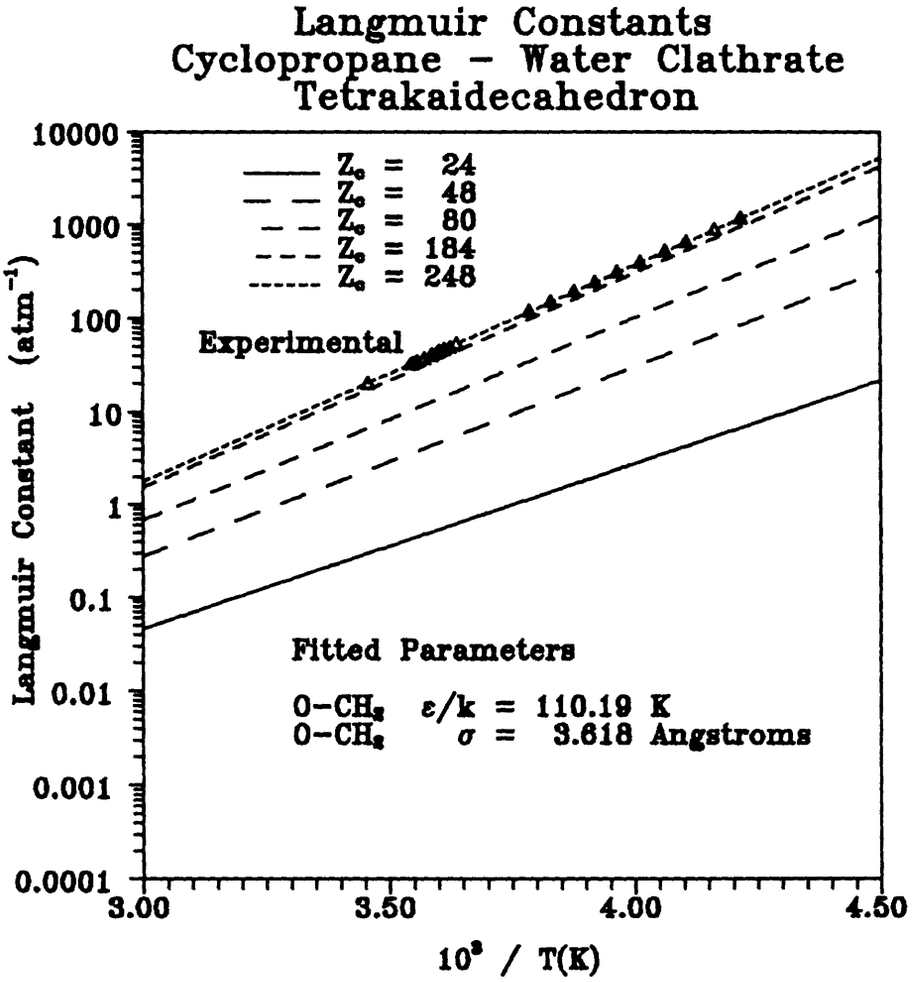

Figure 9.8 Fitted Cyclopropane - Water Clathrate Langmuir Constants

10. MOLECULAR DYNAMICS OF WATER CLATHRATES

Molecular Dynamics simulations of molecular systems have become an increasingly powerful tool in the study of the physical behavior of molecular liquids and solids. Thus, in an attempt to better understand the configurational characteristic of the guest-host interaction within the water clathrate structure we have performed constant volume and energy (NVE) simulations for both the methane and cyclopropane water clathrate systems.

10.1 Method of Constraints

The computational complexities associated with the modeling of molecular systems has resulted in the development of several algorithms which greatly simplify the construction of the relevant equations of motion. Allen and Tildesley (1987) discuss in great detail the different options available for the modeling of molecular systems, notwithstanding, constraint dynamics has become the predominate choice in recent years. Specifically, in terms of the modeling of water clathrate systems the *SHAKE* constraint algorithm by Ryckaert et al. (1977) has been used extensively by Tse et al. (1983; 1984; 1987) in their study of the dynamical properties of several different gas hydrates. Additionally, *RATTLE* (Anderson, 1983), the velocity version of *SHAKE*, has also been used recently by Rodger (1989; 1990) in the modeling of water clathrate systems. Nevertheless, we instead chose to implement the more recent differential constraint algorithm based on Gauss' principle of least constraint as proposed by Edberg et al. (1986).

The derivation of the constrained equations of motion for a rigid triatomic molecule (i.e. H_2O) using Gauss' principle of least constraint is simple and straightforward. The holonomic bonding constraints for a rigid triatomic molecule are given by

$$\begin{aligned} g_{12} &= r_{12}^2 - d_{12}^2 = 0 \\ g_{13} &= r_{13}^2 - d_{13}^2 = 0 \\ g_{23} &= r_{23}^2 - d_{23}^2 = 0 \end{aligned} \tag{10.1}$$

where

$$\begin{aligned} \boldsymbol{r}_{12} &= \boldsymbol{r}_1 - \boldsymbol{r}_2 \\ \boldsymbol{r}_{13} &= \boldsymbol{r}_1 - \boldsymbol{r}_3 \\ \boldsymbol{r}_{23} &= \boldsymbol{r}_2 - \boldsymbol{r}_3 \end{aligned} \tag{10.2}$$

and d_{12}, d_{13}, and d_{23} are the desired bond lengths within the three site molecule. Differentiating these equations with respect to time yields

$$\begin{aligned} \frac{\partial g_{12}}{\partial t} &= 2\boldsymbol{r}_{12}\dot{\boldsymbol{r}}_{12} = 0 \\ \frac{\partial g_{13}}{\partial t} &= 2\boldsymbol{r}_{13}\dot{\boldsymbol{r}}_{13} = 0 \\ \frac{\partial g_{23}}{\partial t} &= 2\boldsymbol{r}_{23}\dot{\boldsymbol{r}}_{23} = 0 \end{aligned} \tag{10.3}$$

while differentiating Equations (10.1) a second time with respect to time gives

$$\frac{\partial^2 g_{12}}{\partial t^2} = 2\dot{r}_{12}\,\dot{r}_{12} + 2\,r_{12}\,\ddot{r}_{12} = 0$$

$$\frac{\partial^2 g_{13}}{\partial t^2} = 2\dot{r}_{13}\,\dot{r}_{13} + 2\,r_{13}\,\ddot{r}_{13} = 0 \qquad (10.4)$$

$$\frac{\partial^2 g_{23}}{\partial t^2} = 2\dot{r}_{23}\,\dot{r}_{23} + 2\,r_{23}\,\ddot{r}_{23} = 0$$

or equivalently

$$\dot{r}_{12}\,\dot{r}_{12} + r_{12}\,\ddot{r}_{12} = 0$$

$$\dot{r}_{13}\,\dot{r}_{13} + r_{13}\,\ddot{r}_{13} = 0 \qquad (10.5)$$

$$\dot{r}_{23}\,\dot{r}_{23} + r_{23}\,\ddot{r}_{23} = 0$$

where

$$\dot{r}_{12} = \dot{r}_1 - \dot{r}_2$$

$$\dot{r}_{13} = \dot{r}_1 - \dot{r}_3 \qquad (10.6)$$

$$\dot{r}_{23} = \dot{r}_2 - \dot{r}_3$$

and

$$\ddot{r}_{12} = \ddot{r}_1 - \ddot{r}_2$$

$$\ddot{r}_{13} = \ddot{r}_1 - \ddot{r}_3 \qquad (10.7)$$

$$\ddot{r}_{23} = \ddot{r}_2 - \ddot{r}_3$$

Equations (10.5) are fundamental to the derivation of the constrained equations of motion. Specifically, since the constrained equations of motion for each site in a triatomic molecule are given by

$$\begin{aligned} m_1 \ddot{r}_1 &= F_1 - \lambda_{12} r_{12} - \lambda_{13} r_{13} \\ m_2 \ddot{r}_2 &= F_2 + \lambda_{12} r_{12} - \lambda_{23} r_{23} \\ m_3 \ddot{r}_3 &= F_3 + \lambda_{13} r_{13} + \lambda_{23} r_{23} \end{aligned} \qquad (10.8)$$

where λ_{12}, λ_{13}, and λ_{23} are undetermined Lagrangian multipliers. The substitution of Equations (10.8) into Equations (10.7) yields

$$\begin{aligned} \ddot{r}_{12} &= F_1 m_1^{-1} - F_2 m_2^{-1} - \lambda_{12} r_{12} (m_1^{-1} + m_2^{-1}) - \lambda_{13} r_{13} m_1^{-1} + \lambda_{23} r_{23} m_2^{-1} \\ \ddot{r}_{13} &= F_1 m_1^{-1} - F_3 m_3^{-1} - \lambda_{12} r_{12} m_1^{-1} - \lambda_{13} r_{13} (m_1^{-1} + m_3^{-1}) - \lambda_{23} r_{23} m_3^{-1} \\ \ddot{r}_{23} &= F_2 m_2^{-1} - F_3 m_3^{-1} + \lambda_{12} r_{12} m_2^{-1} - \lambda_{13} r_{13} m_3^{-1} - \lambda_{23} r_{23} (m_2^{-1} + m_3^{-1}) \end{aligned} \qquad (10.9)$$

The substitution of Equations (10.9) into the differential forms of the constraint equations (Equations (10.5)) results in the compact expression

$$A\lambda = b \qquad (10.8)$$

where the matrix A is defined as

$$\boldsymbol{A} = \begin{pmatrix} r_{12}^2(m_1^{-1} + m_2^{-1}) & r_{12}\cdot r_{13}\, m_1^{-2} & -r_{12}\cdot r_{23}\, m_3^{-1} \\ r_{13}\cdot r_{12}\, m_1^{-1} & r_{13}^2(m_1^{-1} + m_3^{-1}) & r_{13}\cdot r_{23}\, m_3^{-1} \\ -r_{23}\cdot r_{12}\, m_2^{-1} & r_{23}\cdot r_{13}\, m_3^{-1} & r_{23}^2(m_2^{-1} + m_3^{-1}) \end{pmatrix} \tag{10.9}$$

and the vectors λ and $\boldsymbol{b}$ are defined by

$$\lambda = \begin{pmatrix} \lambda_{12} \\ \lambda_{13} \\ \lambda_{23} \end{pmatrix} \tag{10.10}$$

and

$$\boldsymbol{b} = \begin{pmatrix} (\boldsymbol{F}_1 m_1^{-1} - \boldsymbol{F}_2 m_2^{-1})\cdot \boldsymbol{r}_{12} + \dot{r}_{12}^2 \\ (\boldsymbol{F}_1 m_1^{-1} + \boldsymbol{F}_3 m_3^{-1})\cdot \boldsymbol{r}_{13} + \dot{r}_{13}^2 \\ (\boldsymbol{F}_2 m_2^{-1} + \boldsymbol{F}_3 m_3^{-1})\cdot \boldsymbol{r}_{23} + \dot{r}_{23}^2 \end{pmatrix} \tag{10.11}$$

These resulting linear equations in λ define the principal advantage of using the differential forms of the constraint equations (Edberg et al., 1986), specifically, since the quadratic equations for λ associated with the SHAKE constrained dynamics algorithm (Ryckaert et al.,1977) are much more complex and generally involve an iterative type solution.

10.1.1 Penalty Functions

Since the bond length constraints are applied in differential form, the bond length values d_{12}, d_{13}, and d_{23} should remain constant throughout the simulation. However, the error associated with the numerical integration of the constrained equations of motion eventually induces the various bond lengths and bond angles to drift away from their desired values. In order to solve this problem, we have adopted to use the penalty function approach of Edberg (1986).

The positional penalty function defined by

$$\Phi = \sum (r_{\alpha\beta}^2 - d_{\alpha\beta}^2)^2 \tag{10.12}$$

is a measure of the deviation in the different bond constraints. The velocity penalty function defined by

$$\Psi = \sum (\boldsymbol{r}_{\alpha\beta} \cdot \dot{\boldsymbol{r}}_{\alpha\beta})^2 \tag{10.13}$$

is a measure of the speed at which the bond constraints are changing. In terms of a rigid triatomic molecule the positional penalty function is written

$$\Phi = (r_{12}^2 - d_{12}^2)^2 + (r_{13}^2 - d_{13}^2)^2 + (r_{23}^2 - d_{23}^2)^2 \tag{10.14}$$

or in terms of its cartesian coordinates as

$$\begin{aligned}\Phi = &((x_1-x_2)^2+(y_1-y_2)^2+(z_1-z_2)^2-d_{12}^2)^2+\\ &((x_1-x_3)^2+(y_1-y_3)^2+(z_1-z_3)^2-d_{13}^2)^2+\\ &((x_2-x_3)^2+(y_2-y_3)^2+(z_2-z_3)^2-d_{23}^2)^2\end{aligned} \tag{10.15}$$

In terms of a rigid triatomic molecule the velocity penalty function is written

$$\Psi = (\boldsymbol{r}_{12}\cdot\dot{\boldsymbol{r}}_{12})^2 + (\boldsymbol{r}_{13}\cdot\dot{\boldsymbol{r}}_{13})^2 + (\boldsymbol{r}_{23}\cdot\dot{\boldsymbol{r}}_{23})^2 \tag{10.16}$$

or in terms of its cartesian coordinates as

$$\begin{aligned}\Psi = &((x_1-x_2)(\dot{x}_1-\dot{x}_2)+(y_1-y_2)(\dot{y}_1-\dot{y}_2)+(z_1-z_2)(\dot{z}_1-\dot{z}_2))^2+\\ &((x_1-x_3)(\dot{x}_1-\dot{x}_3)+(y_1-y_3)(\dot{y}_1-\dot{y}_3)+(z_1-z_3)(\dot{z}_1-\dot{z}_3))^2+\\ &((x_2-x_3)(\dot{x}_2-\dot{x}_3)+(y_2-y_3)(\dot{y}_2-\dot{y}_3)+(z_2-z_3)(\dot{z}_2-\dot{z}_3))^2\end{aligned} \tag{10.17}$$

These penalty functions are monitored during the course of a simulation for each molecule. When their values become sufficiently large, on the order of 10^{-8}, the positions and velocities of the various molecular sites are adjusted to new values corresponding to the potential minimum. A standard nonlinear minimization routine was used to implement this adjustment (Press et al., 1986).

10.2 Gear Predictor-Corrector Integration

The constrained equations of motion were numerically integrated using the 5-value Gear second-order predictor-corrector algorithm (Gear, 1971). The basis of the method involves a simple Taylor expansion about time *t*:

$$\boldsymbol{r}^p(t+\delta t) = \boldsymbol{r}(t) + \delta t\,\boldsymbol{v}(t) + \frac{1}{2}\delta t^2\,\boldsymbol{a}(t) + \frac{1}{6}\delta t^3\,\boldsymbol{b}(t) + \frac{1}{24}\delta t^4\,\boldsymbol{c}(t)$$

$$\boldsymbol{v}^p(t+\delta t) = \boldsymbol{v}(t) + \delta t\,\boldsymbol{a}(t) + \frac{1}{2}\delta t^2\,\boldsymbol{b}(t) + \frac{1}{6}\delta t^3\,\boldsymbol{c}(t)$$

$$\boldsymbol{a}^p(t+\delta t) = \boldsymbol{a}(t) + \delta t\,\boldsymbol{b}(t) + \frac{1}{2}\delta t^2\,\boldsymbol{c}(t) \qquad (10.18)$$

$$\boldsymbol{b}^p(t+\delta t) = \boldsymbol{b}(t) + \delta t\,\boldsymbol{c}(t)$$

$$\boldsymbol{c}^p(t+\delta t) = \boldsymbol{c}(t)$$

where **r** is the position vector, **v** is the velocity vector, **a** is the acceleration vector, **b** is the third time derivative vector, and **c** is the fourth time derivative vector. The superscipt *p* refers to the "predicted" values. The correction step involves the calculation of forces or equivalently the accelerations at a time $t+\delta t$. The error between the calculated acceleration and predicted corrections

$$\Delta\boldsymbol{a}(t+\delta t) = \boldsymbol{a}^c(t+\delta t) - \boldsymbol{a}^p(t+\delta t) \qquad (10.19)$$

is used with the results of the predictor step to make the corrector step

$$
\begin{aligned}
\boldsymbol{r}^c(t+\delta t) &= \boldsymbol{r}^p(t+\delta t) + c_0\Delta\ (t+\delta t) \\
\boldsymbol{v}^c(t+\delta t) &= \boldsymbol{v}^p(t+\delta t) + c_1\Delta\ (t+\delta t) \\
\boldsymbol{a}^c(t+\delta t) &= \boldsymbol{a}^p(t+\delta t) + c_2\Delta\ (t+\delta t) \\
\boldsymbol{b}^c(t+\delta t) &= \boldsymbol{b}^p(t+\delta t) + c_3\Delta\ (t+\delta t) \\
\boldsymbol{c}^c(t+\delta t) &= \boldsymbol{c}^p(t+\delta t) + c_4\Delta\ (t+\delta t)
\end{aligned}
\qquad (10.20)
$$

where the superscript c refers to the "corrected" values. The values of the coefficients c_0, c_1, c_2, c_3, and c_4 are given in Table 10.1.

Gear Pred ctor-Corrector Coefficients 5-valu Second Order Equation	
c_0	19/120
c_1	3/4
c_2	1
c_3	1/2
c_4	1/12
Gear (1971)	

Table 10.1 Gear Predictor-Corrector Coefficients

10.3 Simulation Temperature History

The classical equipartition principle equates an energy of kT/2 for every degree of freedom within a system. For an atomic system, there are three translational degrees of freedom for each atom, thus for a system of N atoms the system temperature (T) is defined by the total kinetic energy of the ensemble as:

$$\frac{3}{2}NkT = \frac{1}{2}\sum_{i=1}^{N} m_i v_i^2 \quad . \tag{10.21}$$

where m_i and v_i are the mass and velocity of atom i, respectively. In addition, the atomic temperature within a molecular system is given by

$$T_{atomic} = \frac{\sum m_{site} v_{site}^2}{(3N_s - N_c)k} \tag{10.22}$$

where m_{site} and v_{site} are the mass and velocity of site i. N_s is the total number of atoms or sites and N_c is the total number of system constraints. Usually, this includes the total number of independent internal constraints dictated by the fixed bond lengths and angles and the three additional global constraints associated with maintaining the overall linear momentum of the simulation cell at a value of zero. The molecular temperature is given similarly by

$$T_{molecular} = \frac{\sum m_{mol} v_{mol}^2}{(3N_m - 3)k} \tag{10.23}$$

where N_m is the total number of molecules in the system and m_{mol} and v_{mol} are again the molecular mass and velocity.

10.4 Methane-Water Clathrate Simulation

Constant volume and energy (NVE) molecular dynamics calculations have been use to study the configurational characteristics of the fully occupied structure I methane-water clathrate. The simulations involved a single structure I unit cell (*Pm3n*) with a lattice constant of 12.03 Å. The two smaller pentagonal dodecahedral cavities as well as the six larger tetrakaidecahedral cavities were assumed to be fully occupied by methane molecules. The initial positions of the 46 water molecules were taken from the work described earlier in chapter 4. As discussed previously in chapter 7, the simple point charge (SPC) model (Berendsen et al., 1983) was used to model the binary intermolecular interactions between the host water molecules. TIPS (Jorgensen, 1983) based single site Lennard-Jones (6-12) intermolecular potential functions were used to model the CH_4 - CH_4 and CH_4 - O interactions. Interactions between the water hydrogens and the methane molecules were ignored. Specifically, the . The potential parameters for these simple single site models are given in Table 10.2. Standard periodic boundary conditions were used to simulate an infinite system. The electrostatic interactions were handled via the minimum image convention due to computer resource limitations.

Using the Gear Predictor-Corrector algorithm, as previously discussed in section 10.3, the differentially constrained equations of motion were integrated using a time step of 1.34 fs. This time step was derived from the simple scaling of the intermolecular forces with respect to SPC electrostatic force. The trajectories of all of the molecules were followed for a total of 30-40 ps. The molecular temperature of the system was maintained by the scaling of the molecular velocities every 25-50 time steps during the equilibration portion of the simulation. During the actual dynamic portion of the simulation, the velocities were scaled every 500-1000 time steps. Energy conservation disparities between velocity rescalings were always less than 0.1 percent.

Methane-Water Clathrate Simulation Lennard-Jones (6-12) Parameters		
Interaction Type	σ (Å)	ε/k (K)
CH_4 - O	3.463	94.04
CH_4 - CH_4	3.730	147.94
TIPS (Jorgensen, 1983)		

Table 10.2 Methane-Water Clathrate Potential Parameters

A sample of the atomic temperature simulation history is illustrated in Figure 10.1. The corresponding molecular temperature simulation history is shown in Figure 10.2. The reported relative time interval was randomly taken from the dynamic history file of an equilibrated simulation.

In order to develop a more comprehensive physical and quantitative description of the intermolecular characteristics of water clathrate systems we have used the results of our molecular dynamic simulations to illustrate the various motions within the hydrate structure. These illustrations serve to highlight many of the adequacies and inadequacies of the previous simplistic treatments used in the modeling of the guest-host configurational partition function.

The dynamics of an oxygen atom within the host water lattice are shown in Figures 10.3, 10.4, 10.5, 10.6, 10.7, and 10.8. Specifically, a small sample of the X trajectory of a random host oxygen is depicted in Figure 10.3. The corresponding Y and Z trajectories are illustrated in Figures 10.4 and 10.5. The same trajectory of the oxygen atom within the X-Y, X-Z, and Y-Z planes are given in Figures 10.6, 10.7, and 10.8. The extreme localization of the oxygen atoms within the host lattice structure is quite apparent from the previous figures. The overall rigidity of the host water lattice, however, is difficult to assess without further study.

The motion of the methane molecules within the various cavities within the fully occupied structure I host lattice is illustrated in Figures 10.9, 10.10, 10.11, 10.12, 10.13 and 10.14. The trajectories of each of the methane molecules within the structure I unit cell are shown, specifically, in Figures 10.9, 10.10, and 10.11. The X-Y, X-Z, and Y-Z trajectories of the eight methane molecules are shown, similarly in Figures 10.12, 10.13, and 10.14. The localization of the methane guest molecules within the various cavities is quite apparent. As would be expected, the motion within the larger tetrakaidecahedral cavities is less restricted than the motion within

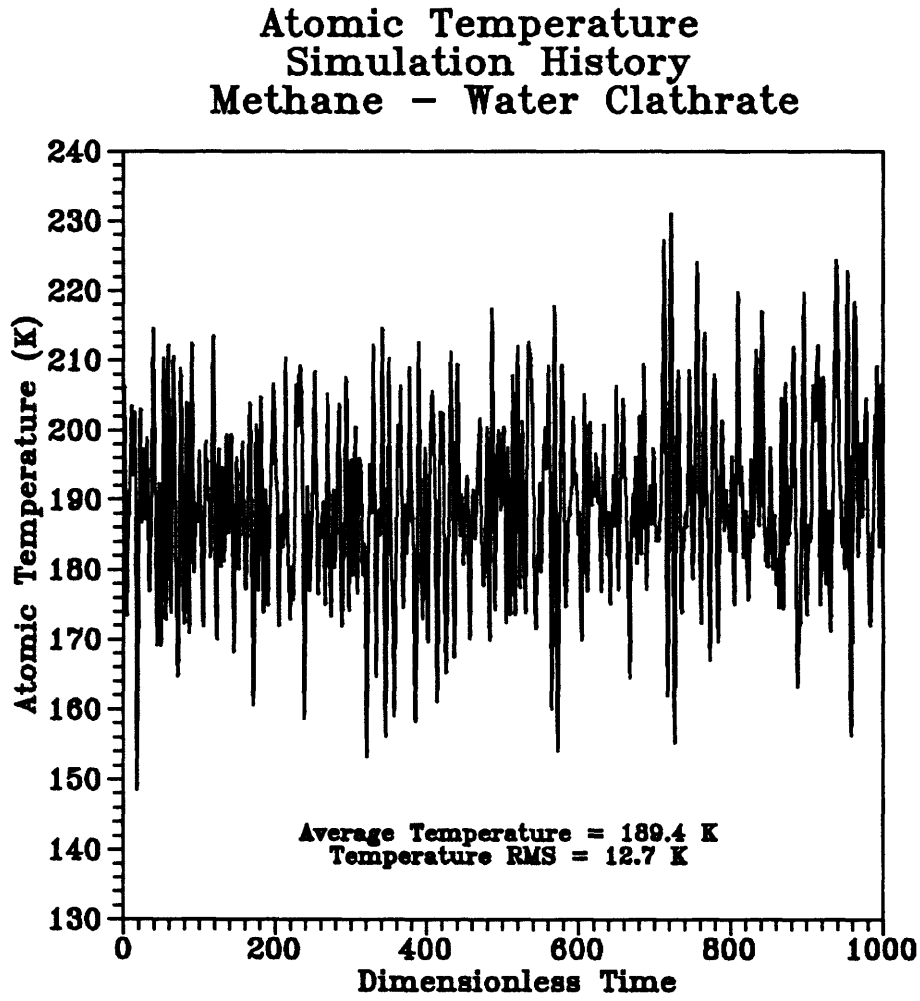

Figure 10.1 Atomic Temperature Simulation History - Methane Clathrate

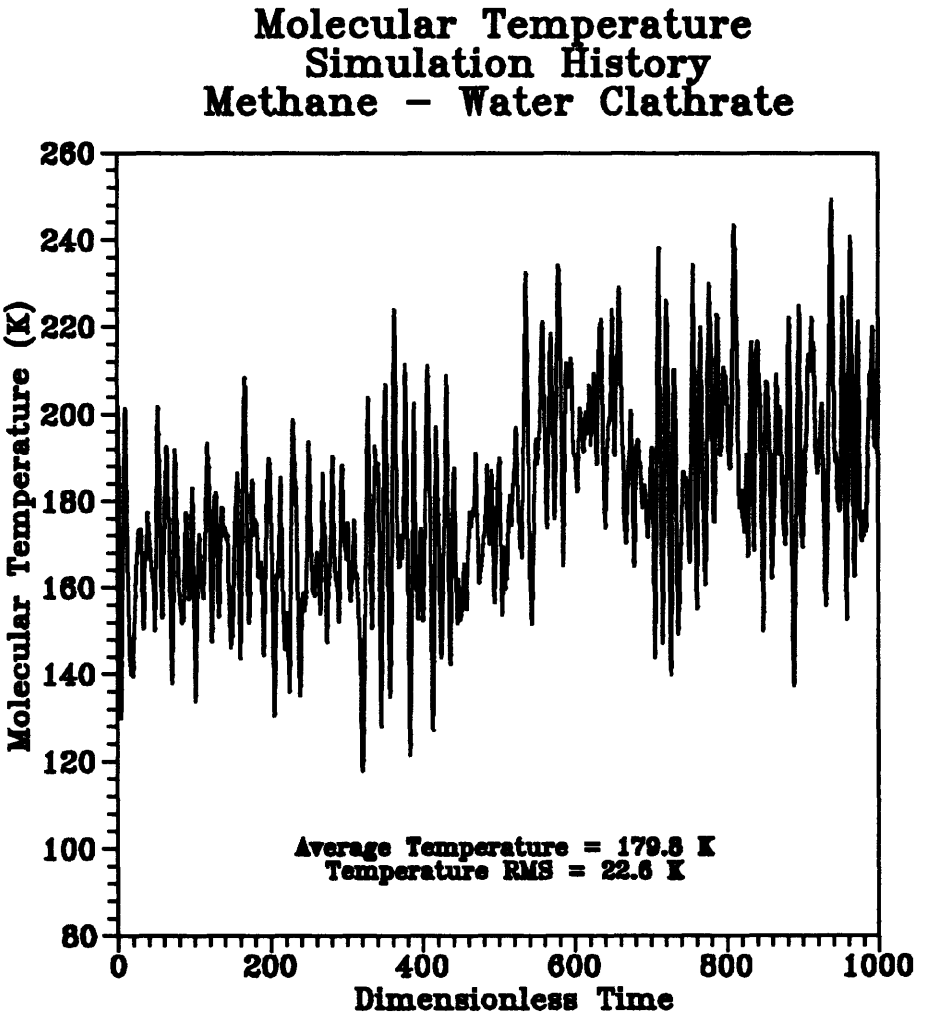

Figure 10.2 Molecular Temperature Simulation History - Methane Clathrate

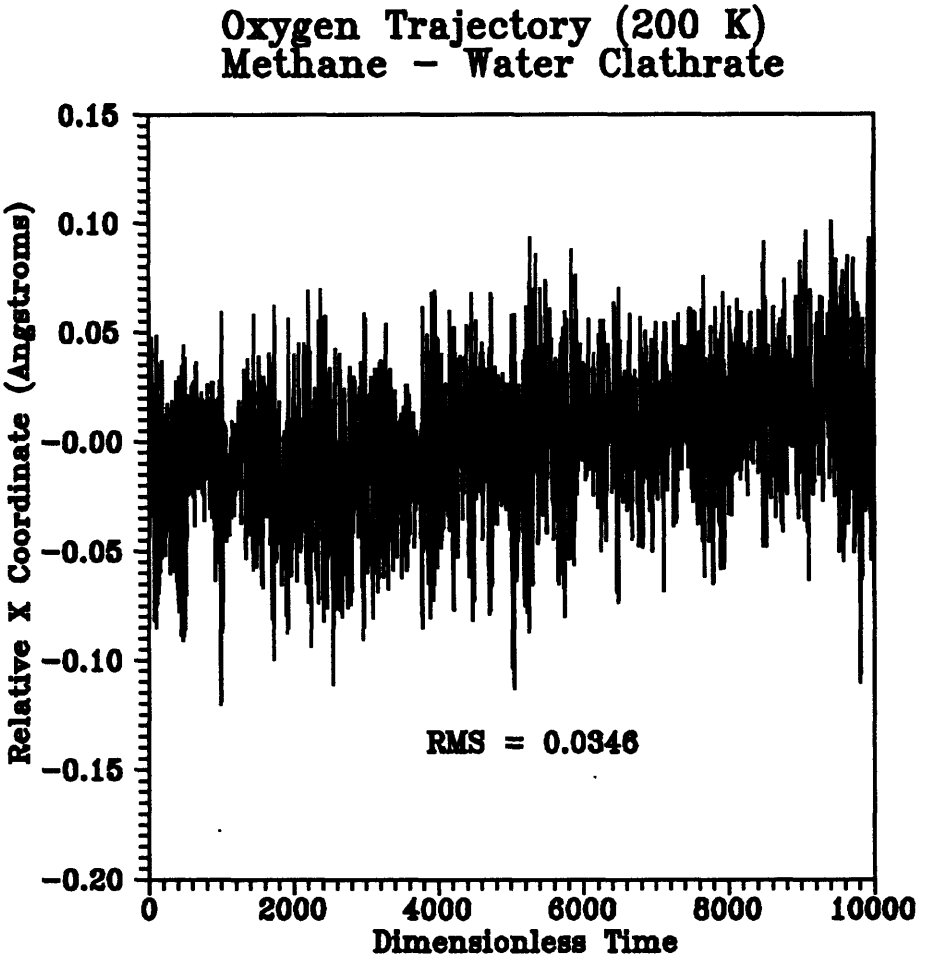

Figure 10.3 Oxygen X Trajectory - Methane Clathrate

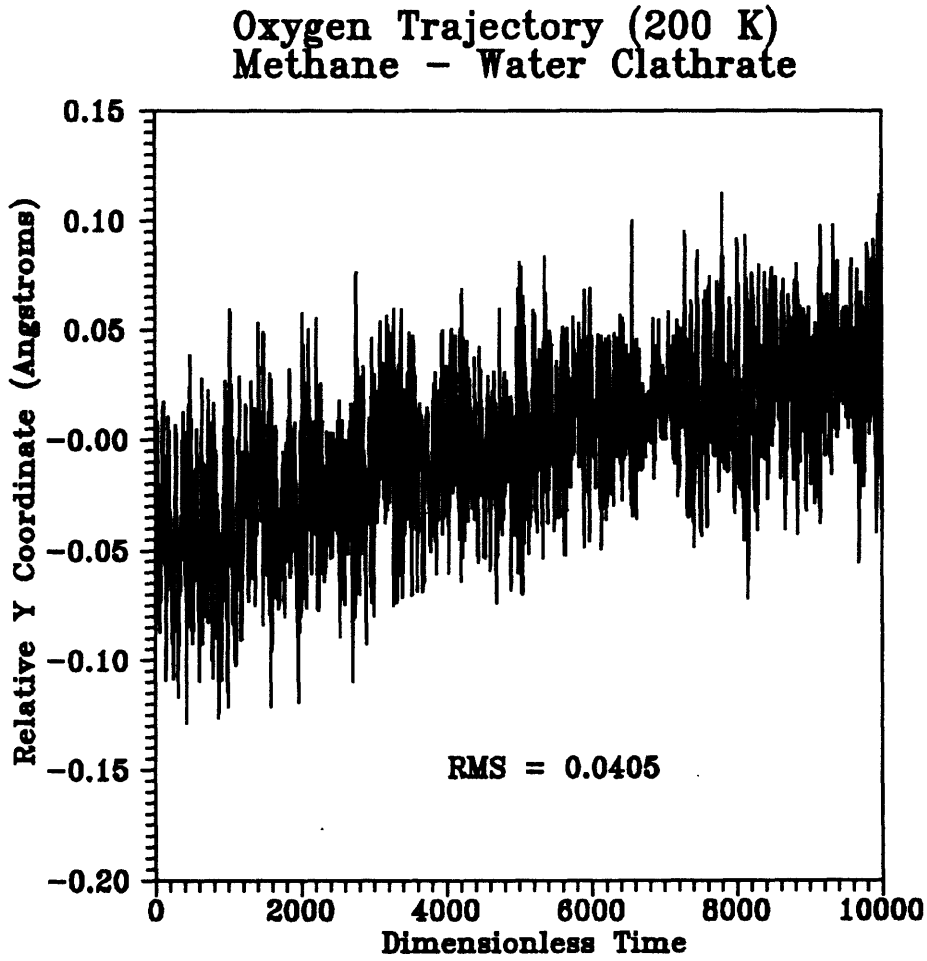

Figure 10.4 Oxygen Y Trajectory - Methane Clathrate

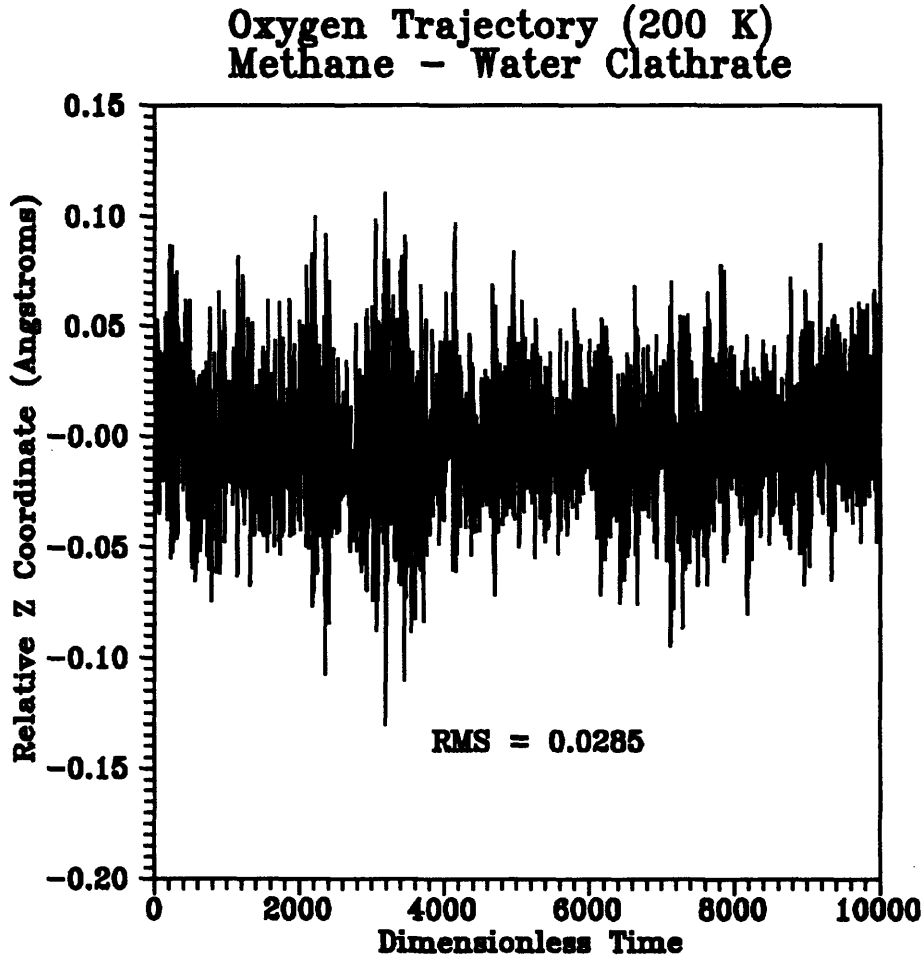

Figure 10.5 Oxygen Z Trajectory - Methane Clathrate

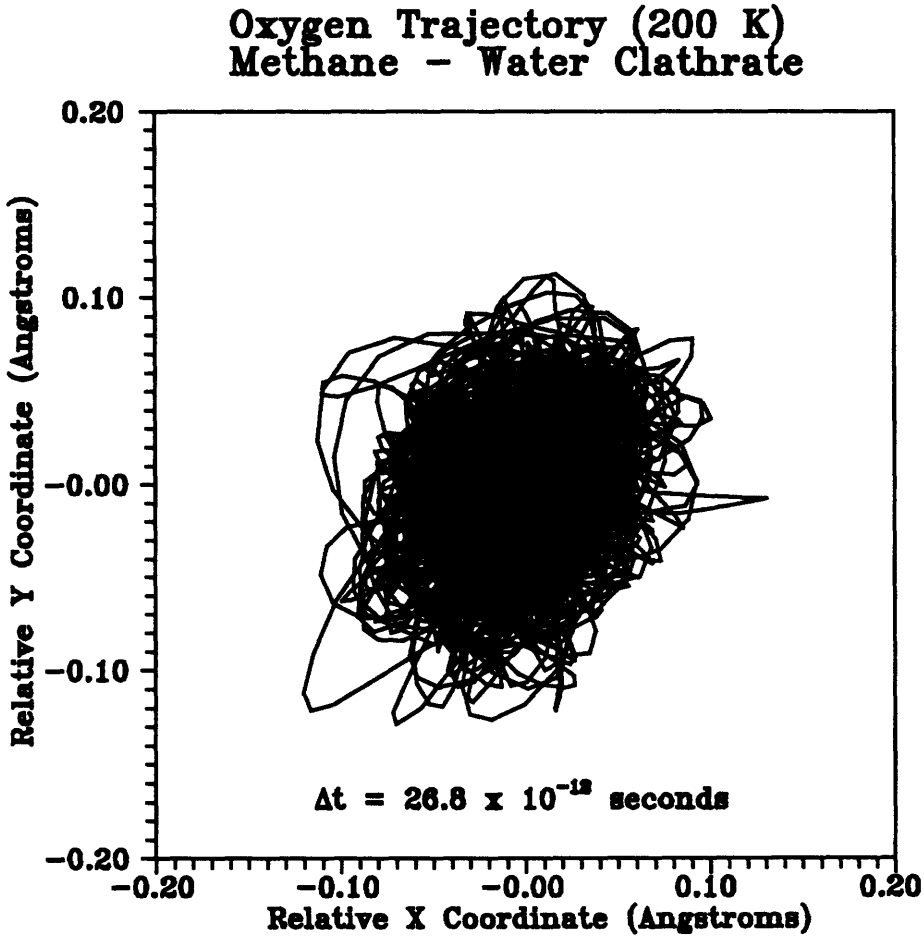

Figure 10.6 Oxygen X-Y Trajectory - Methane Clathrate

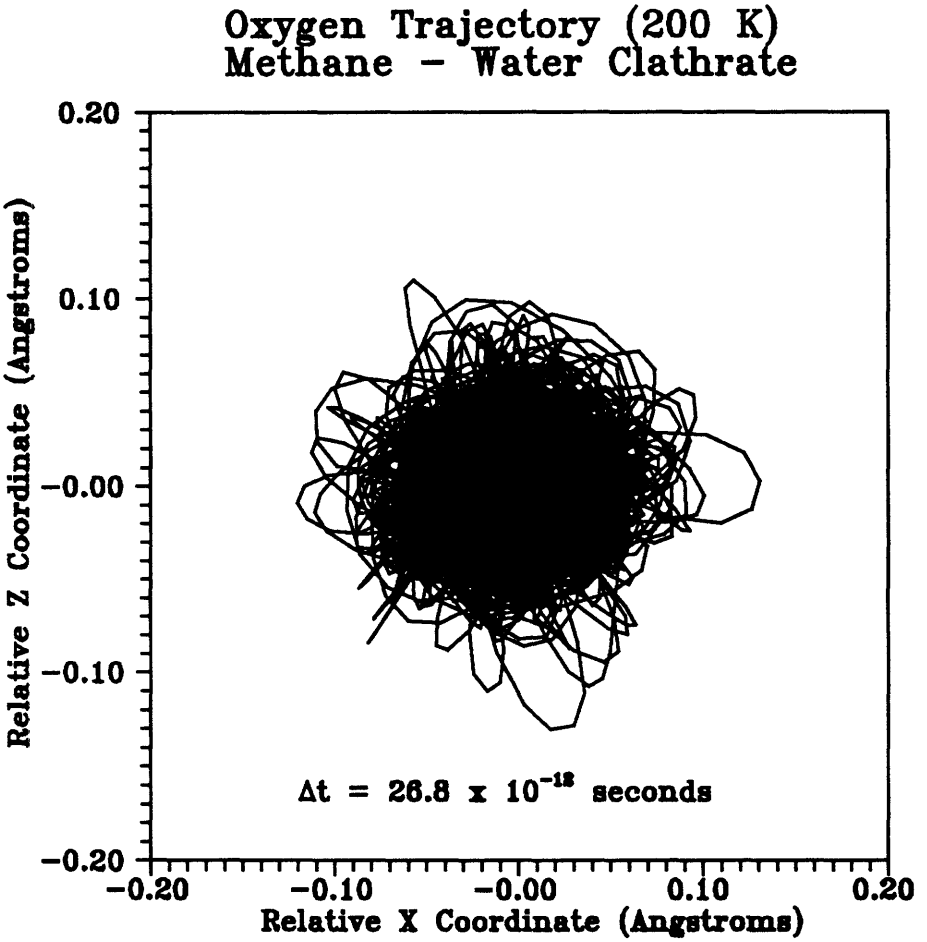

Figure 10.7 Oxygen X-Z Trajectory - Methane Clathrate

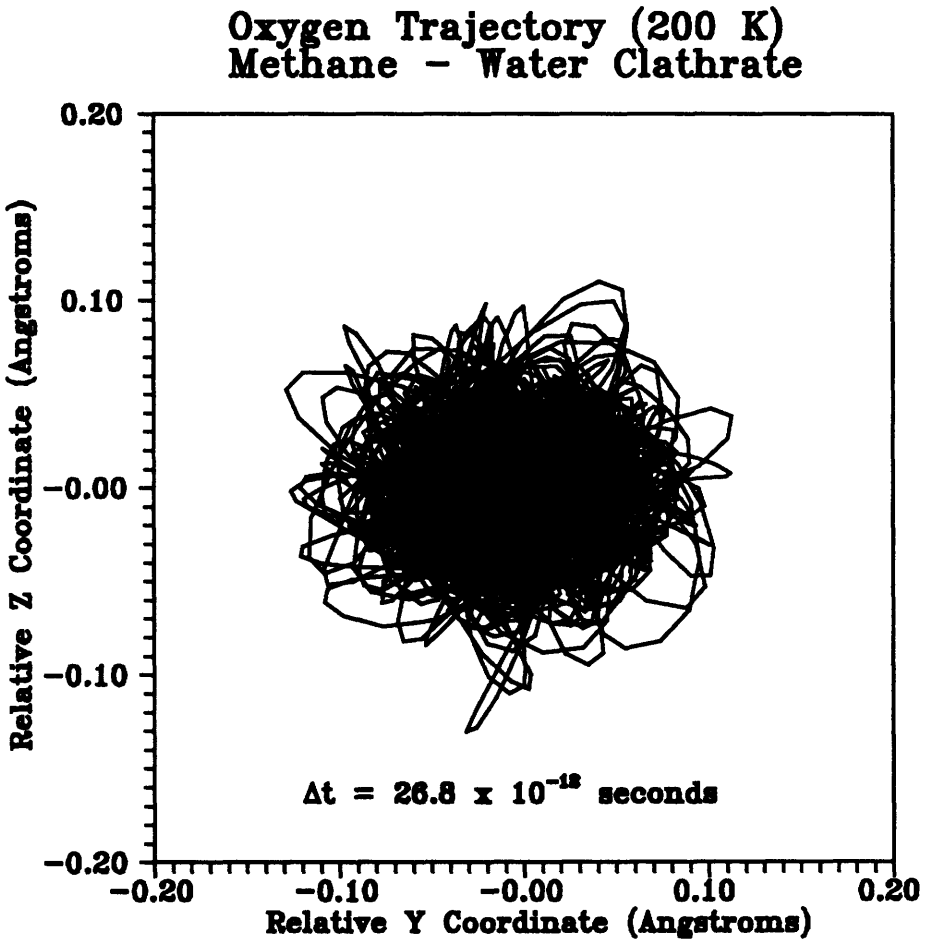

Figure 10.8 Oxygen Y-Z Trajectory - Methane Clathrate

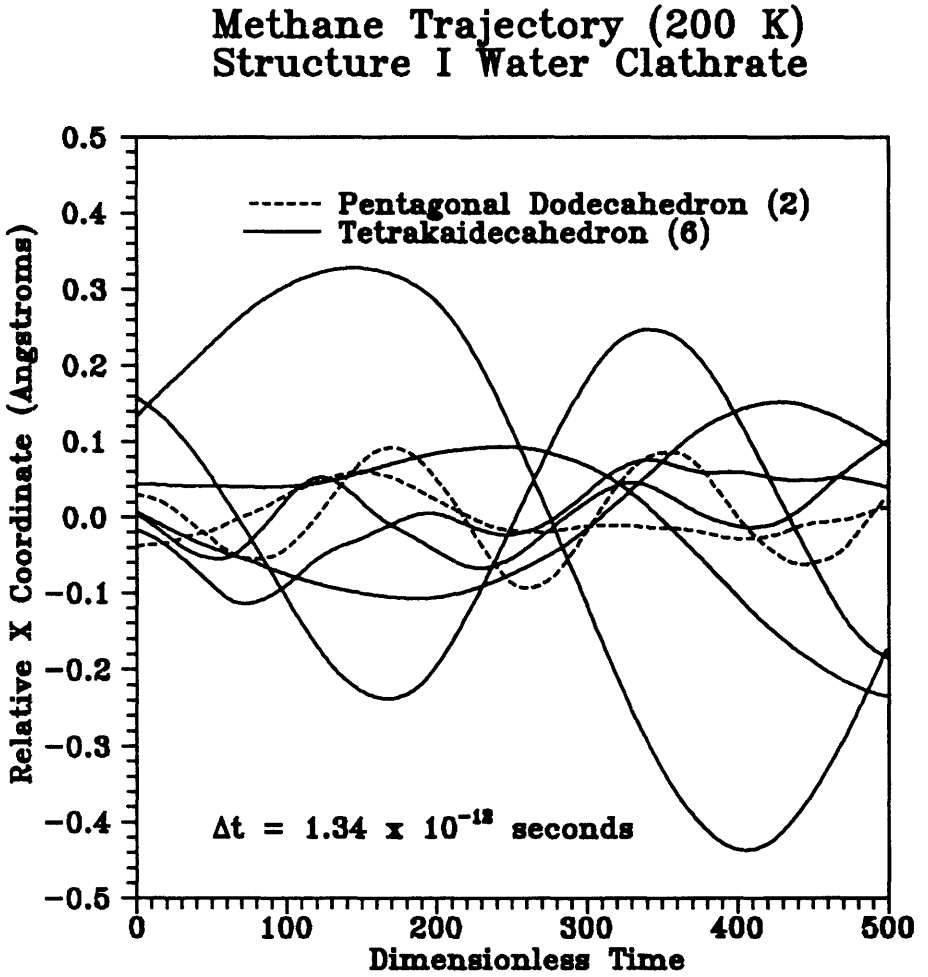

Figure 10.9 Methane X Trajectory - Structure I Water Clathrate

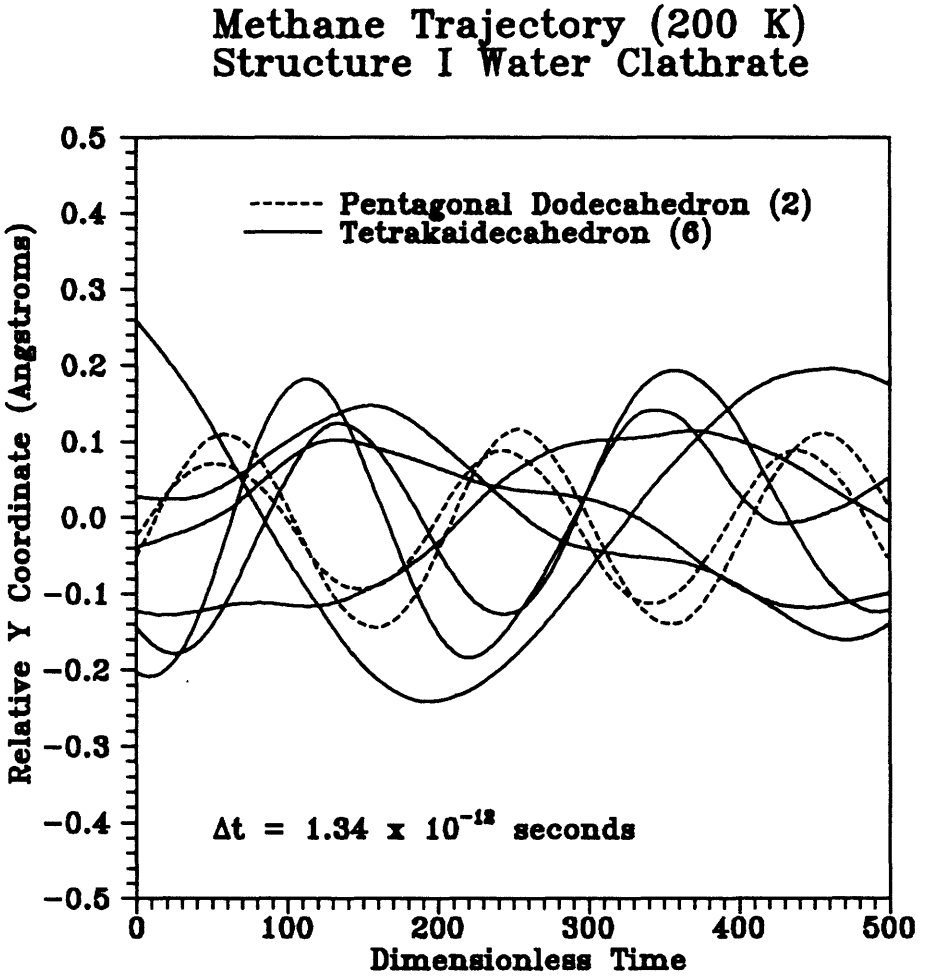

Figure 10.10 Methane Y Trajectory - Structure I Water Clathrate

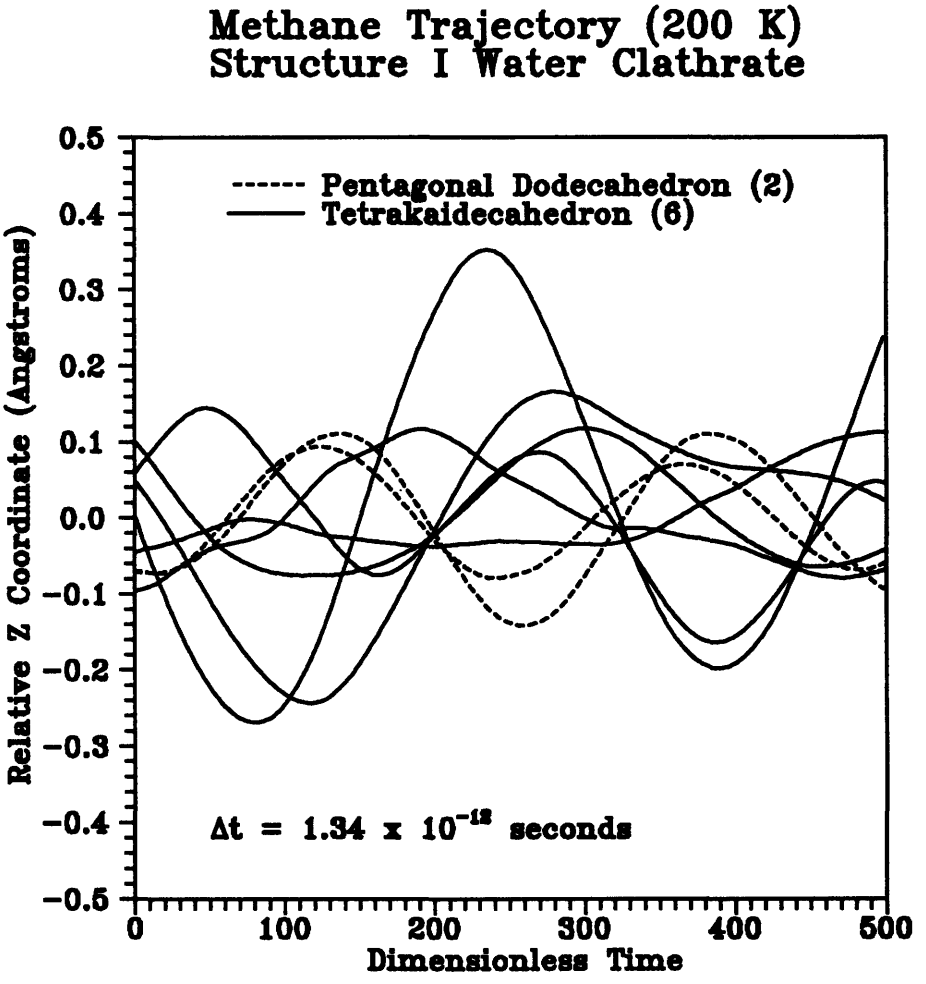

Figure 10.11 Methane Z Trajectory - Structure I Water Clathrate

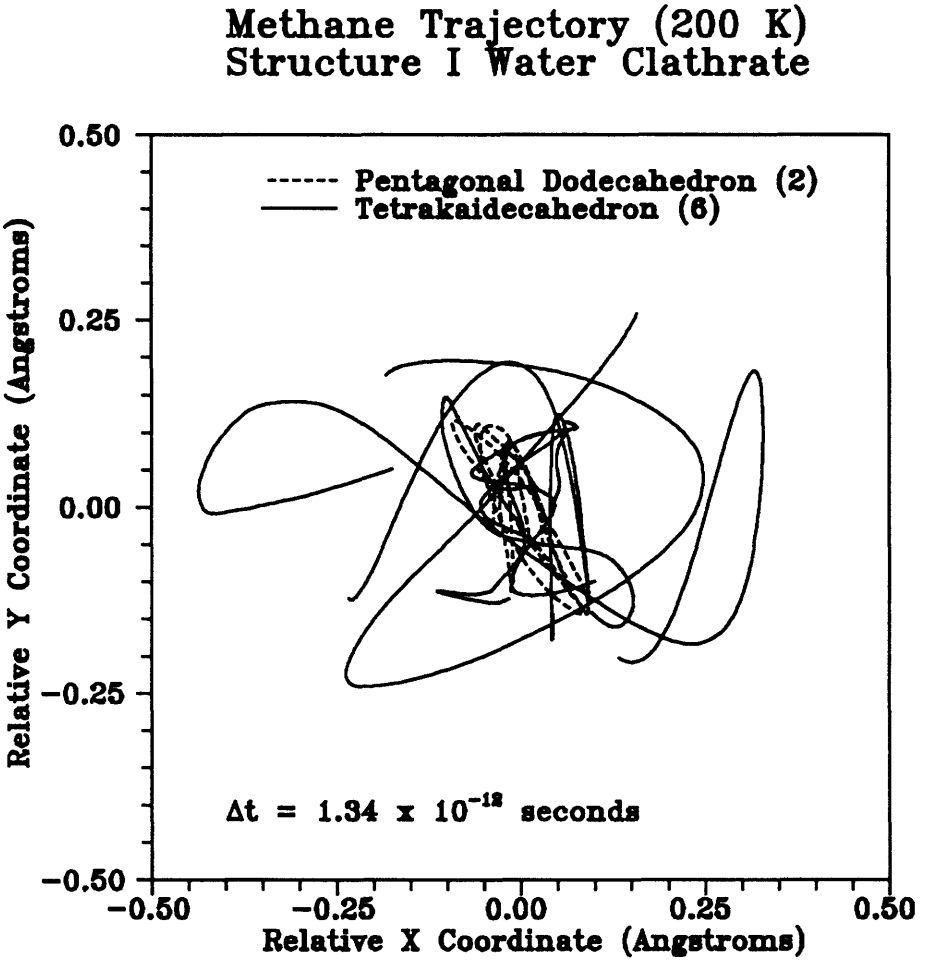

Figure 10.12 Methane X-Y Trajectory - Structure I Water Clathrate

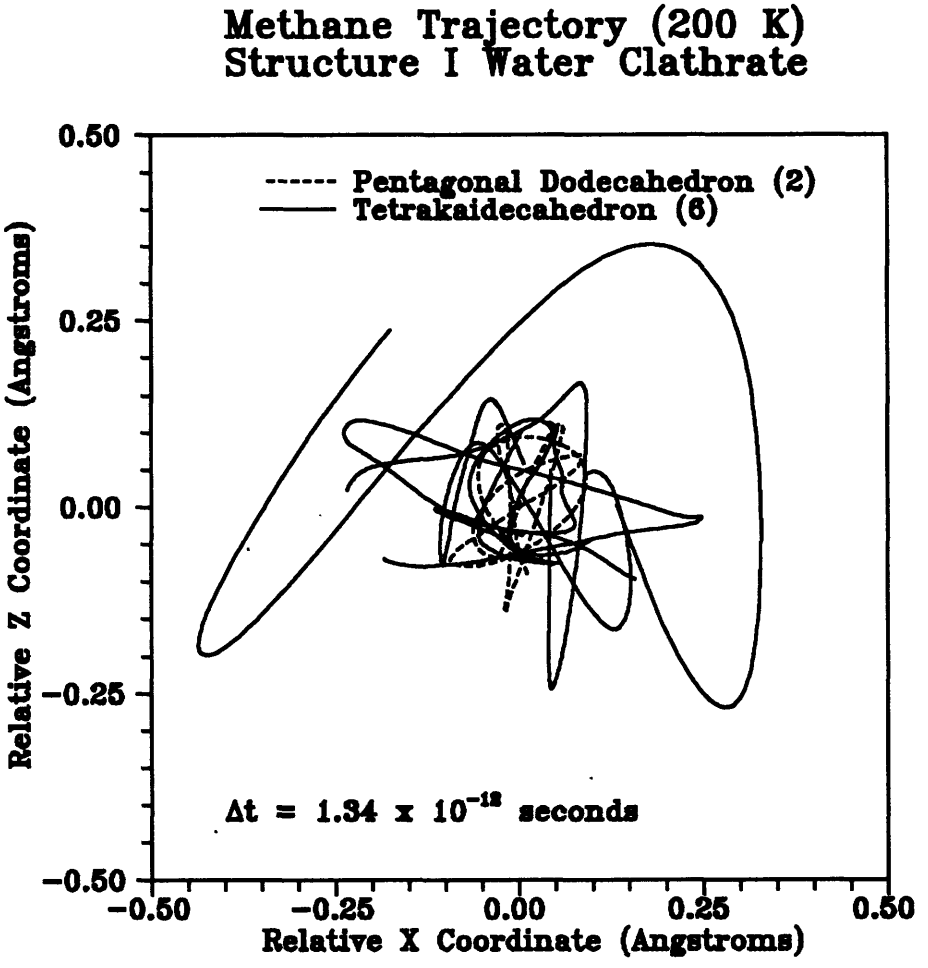

Figure 10.13 Methane X-Z Trajectory - Structure I Water Clathrate

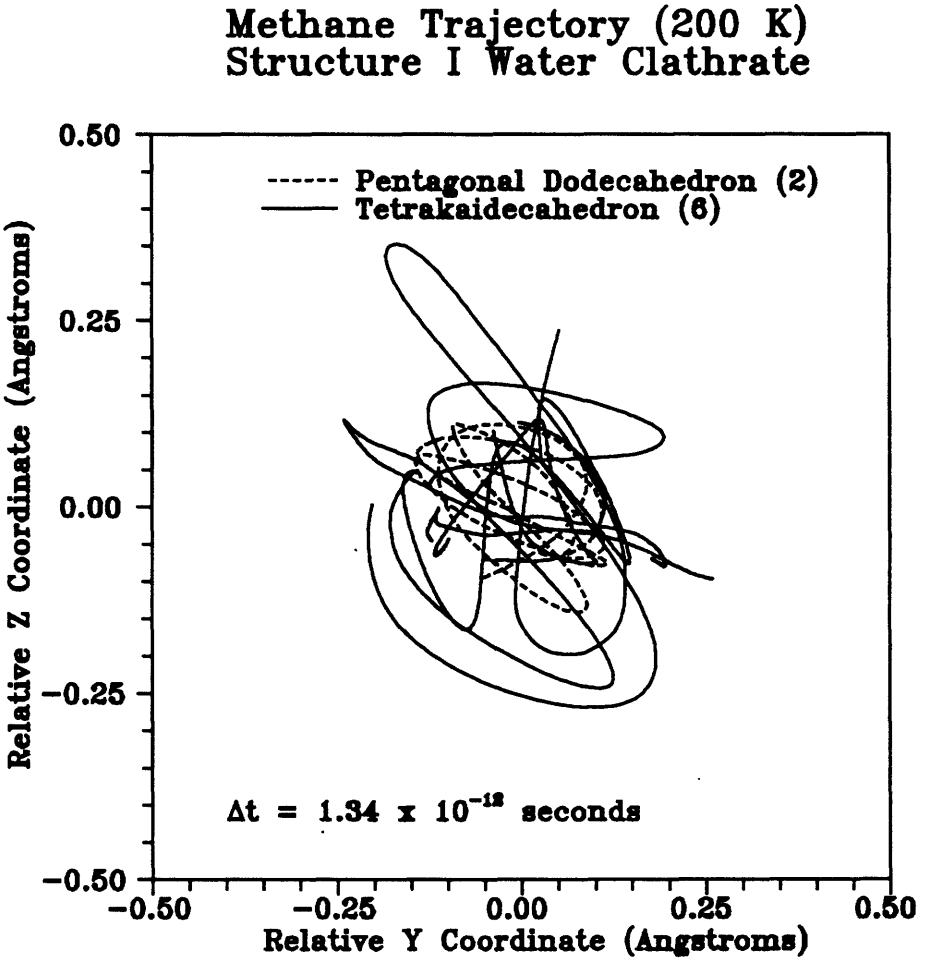

Figure 10.14 Methane Y-Z Trajectory - Structure I Water Clathrate

the smaller pentagonal dodecahedral cavities. The range of the localizations is also consistent with the range dictated by the spherical cavity potentials resulting from the simplistic Lennard-Jones and Devonshire spherical cell model.

A space-filling representation of a methane molecule within the structure I pentagonal dodecahedral cavity is depicted as a function of time in Figures 10.15a and 10.15b. For the purpose of illustration, only those host water molecules with a normalized Z position less than zero are shown. This also explains the abrupt appearances and disappearances of additional host water molecules. Similarly, a space-filling representation of a methane molecule within the structure I tetrakaidecahedral cavity is depicted as a function of time in Figures 10.16a and 10.16b.

$\Delta t = 0$ fs

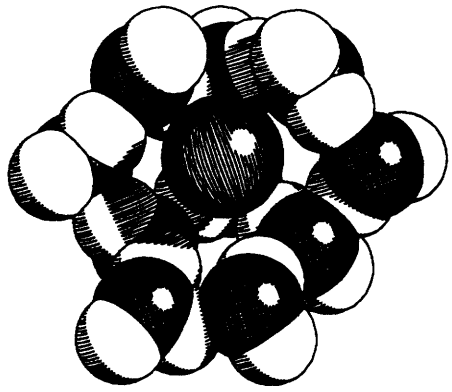

$\Delta t = 26.8$ fs

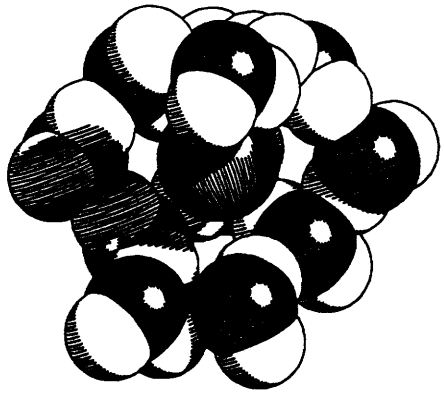

Figure 10.15a Methane Clathrate Simulation - Pentagonal Dodecahedron

Δt = 53.6 fs

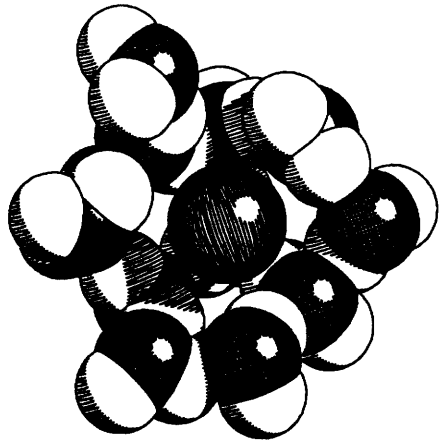

Δt = 80.4 fs

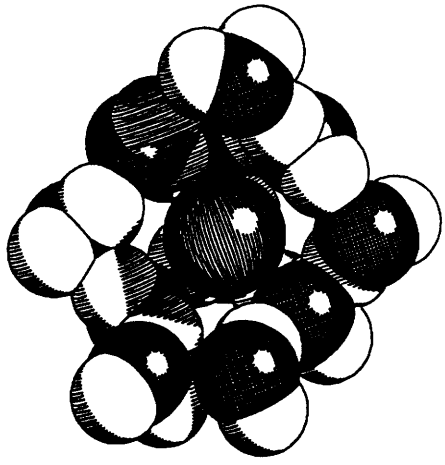

Figure 10.15b Methane Clathrate Simulation - Pentagonal Dodecahedron

$\Delta t = 0$ fs

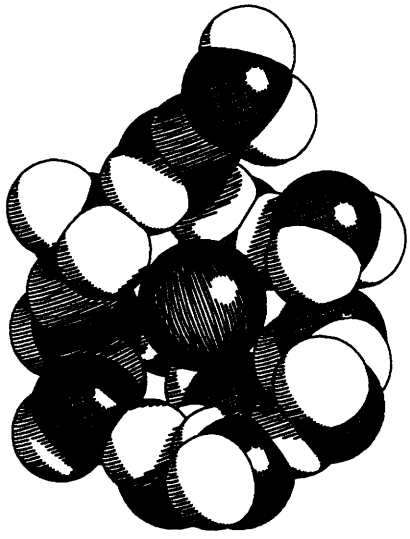

$\Delta t = 26.8$ fs

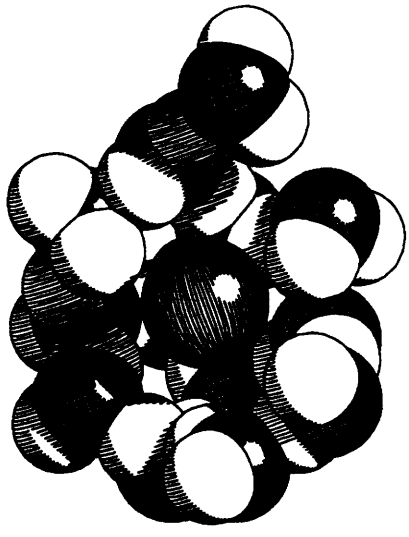

Figure 10.16a Methane Clathrate Simulation - Tetrakaidecahedron

Δt = 53.6 fs

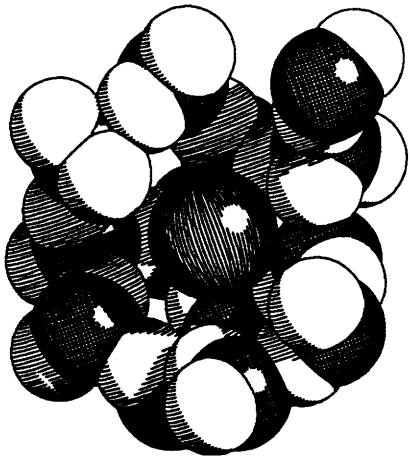

Δt = 80.4 fs

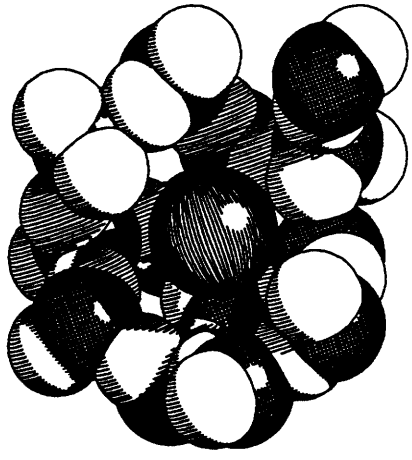

Figure 10.16b Methane Clathrate Simulation - Tetrakaidecahedron

10.5 Cyclopropane-Water Clathrate Simulation

Constant volume and energy (NVE) molecular dynamics calculations have been use to study the configurational characteristics of the fully occupied structure I cyclopropane-water clathrate. The simulations involved a single structure I unit cell (*Pm3n*) with a lattice constant of 12.03 Å. The six larger tetrakaidecahedral cavities were assumed to be fully occupied by cyclopropane molecules. The two smaller pentagonal dodecahedral cavities were assumed to be unoccupied. The initial positions of the 46 water molecules were taken from the work described earlier in chapter 4. The simple point charge (SPC) model (Berendsen et al., 1983) was used to simulate the binary intermolecular interactions between water molecules. A three site, TIPS (Jorgensen, 1983) based, Lennard-Jones (6-12) intermolecular potential functions were used to model the CH_2 - CH_2 and CH_2 - O interactions. Interactions between the water hydrogens and the CH_2 sites were ignored. The potential parameters are given in Table 10.3. Standard periodic boundary conditions were used to simulate an infinite system. The electrostatic interactions again were handled via the minimum image convention.

Using the Gear Predictor-Corrector algorithm, as previously discussed in section 10.3, the differentially constrained equations of motion were integrated using a time step of 1.34 fs. The trajectories of all of the molecules were followed for a total of 30-40 ps. The molecular temperature of the system was maintained by the scaling of the molecular velocities every 25-50 time steps during the equilibration portion of the simulation. During the actual dynamic portion of the simulation, the velocities were scaled every 500-1000 time steps. The energy conservation between velocity rescalings was always less than 0.1 percent.

Cyclopropane-Water Clathrate Simulation Lennard-Jones (6-12) Parameters		
Interaction Type	σ (Å)	ε/k (K)
CH_2 - O	3.579	58.62
CH_2 - CH_2	3.983	57.48
TIPS (Jorgensen, 1983)		

Table 10.3 Cyclopropane-Water Clathrate Simulation Parameters

A sample of the atomic temperature simulation history is illustrated in Figure 10.17. The corresponding molecular temperature simulation history is shown in Figure 10.18. Again, the reported relative time interval was randomly taken from the dynamic history file of an equilibrated simulation.

In order to develop a more comprehensive physical and quantitative description of the intermolecular characteristics of water clathrate systems we have used the results of our molecular dynamic simulations to illustrate the various motions within the hydrate structure. These illustrations serve to highlight many of the adequacies and inadequacies of the previous simplistic treatments used in the modeling of the guest-host configurational partition function.

The dynamics of an water molecule within the host lattice is shown in Figures 10.19, 10.20, and 10.21. A small sample of the X trajectory of a random host water molecule is depicted in Figure 10.19. The corresponding Y and Z trajectories are illustrated in Figures 10.20 and 10.21. The extreme localization of the water molecule within the host lattice structure is quite apparent. Again, the overall rigidity of the host water lattice, however, is difficult to assess without further study.

The motion of the cyclopropane molecule within the tetrakaidecahedral cavity within the fully occupied structure I host lattice is illustrated in Figures 10.22, 10.23, 10.24, 10.25, 10.26 and 10.27. The trajectories of each of the three CH_2 sites making up the cyclopropane molecule are shown in Figures 10.22, 10.23, and 10.24. The X-Y, X-Z, and Y-Z trajectories of the various sites are shown, similarly in Figures 10.25, 10.26, and 10.27. The localization of the cyclopropane guest molecules within the tetrakaidecahedral cavity is quite pronounced. In fact, the rotational motion of the guest is restricted severely as indicted by the torsional rocking motion exhibited. This rotational restriction highlights the inadequacies associated with using the Lennard-Jones Devonshire spherical

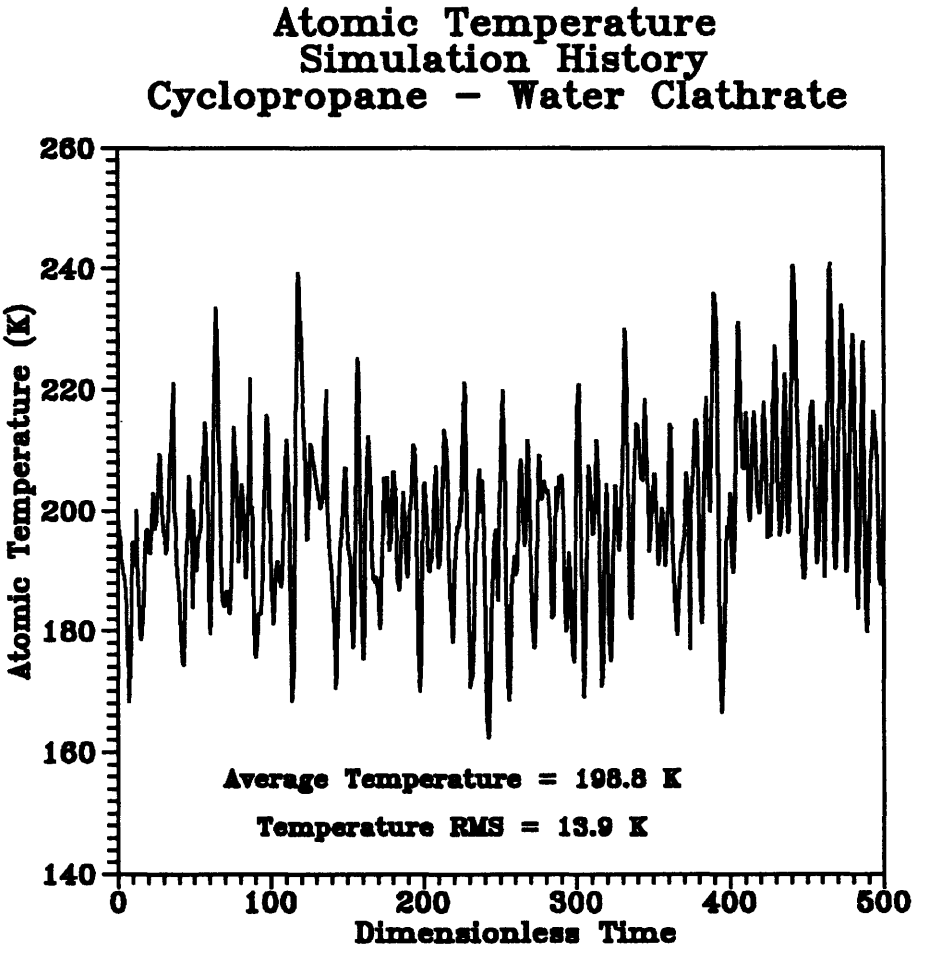

Figure 10.17 Atomic Temperature Simulation History - Cyclopropane Clathrate

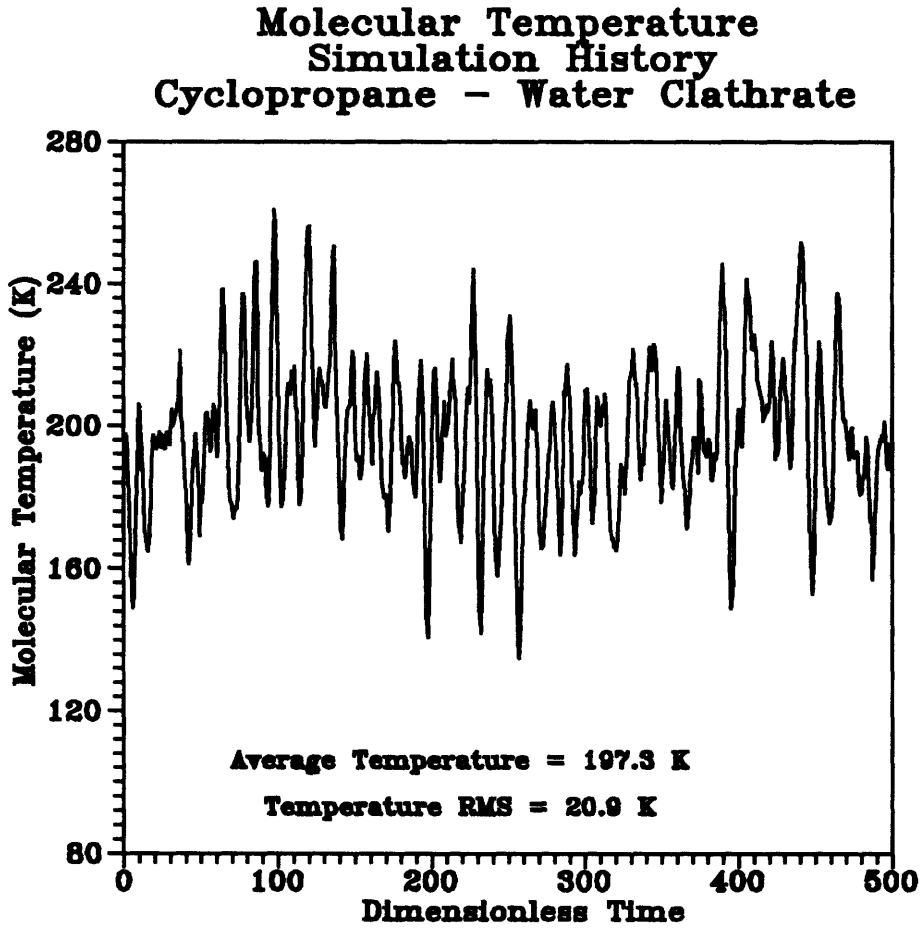

Figure 10.18 Molecular Temperature Simulation History - Cyclopropane Clathrate

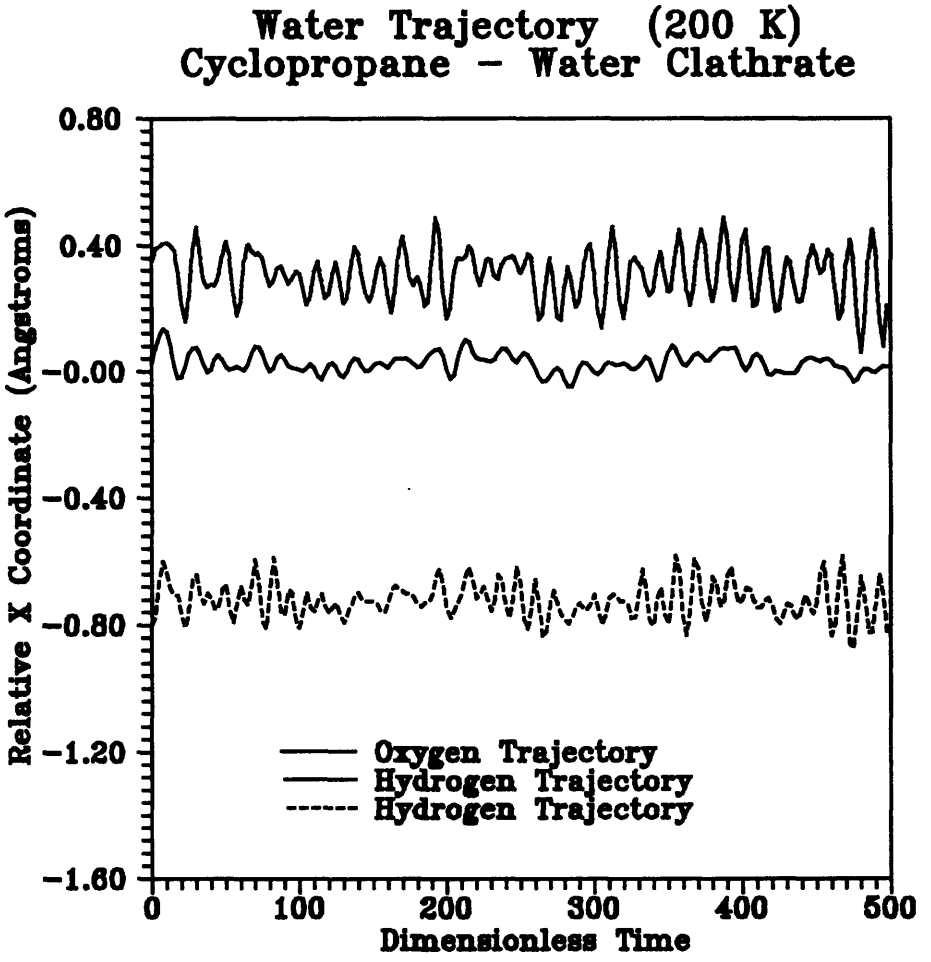

Figure 10.19 Sample Water X Trajectory - Cyclopropane Clathrate

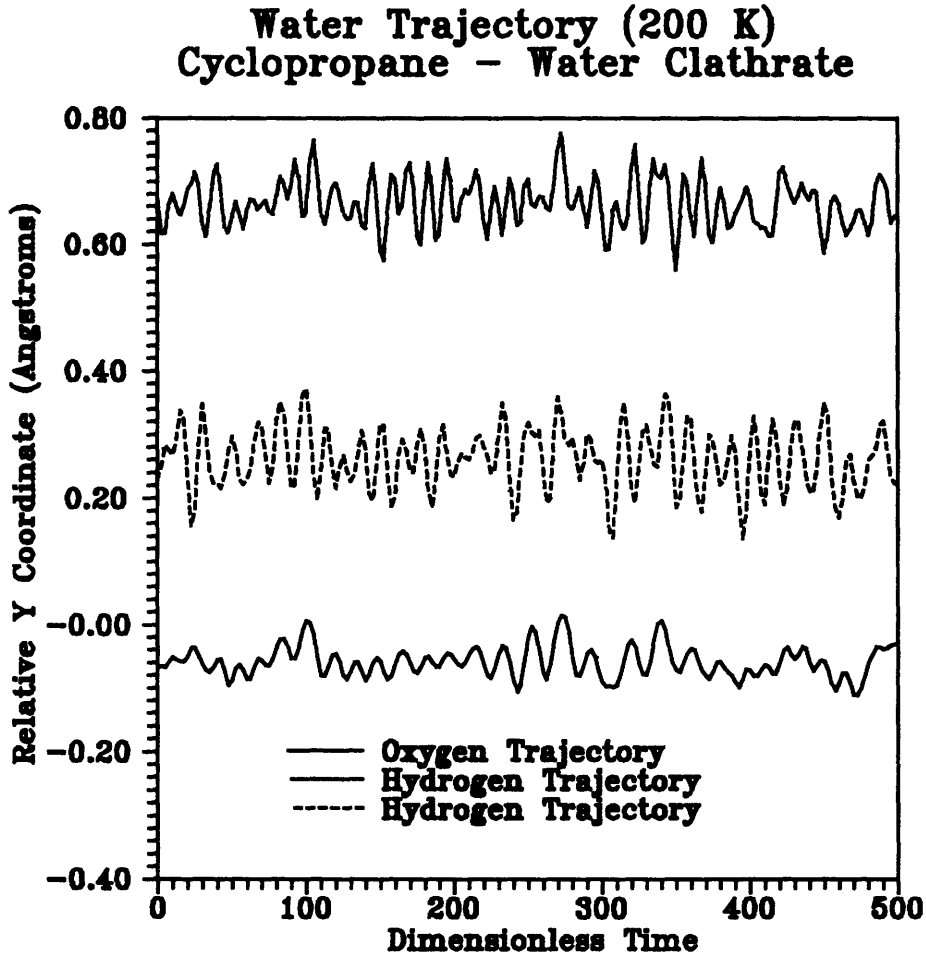

Figure 10.20 Sample Water Y Trajectory - Cyclopropane Clathrate

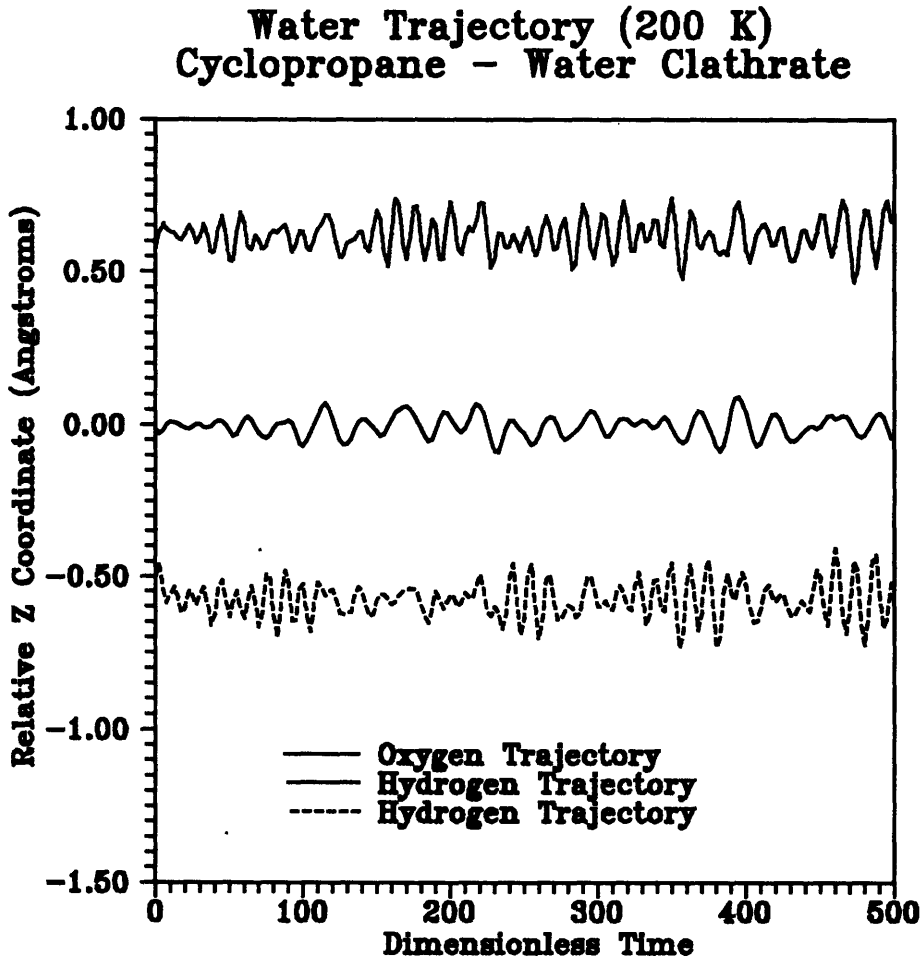

Figure 10.21 Sample Water Z Trajectory - Cyclopropane Clathrate

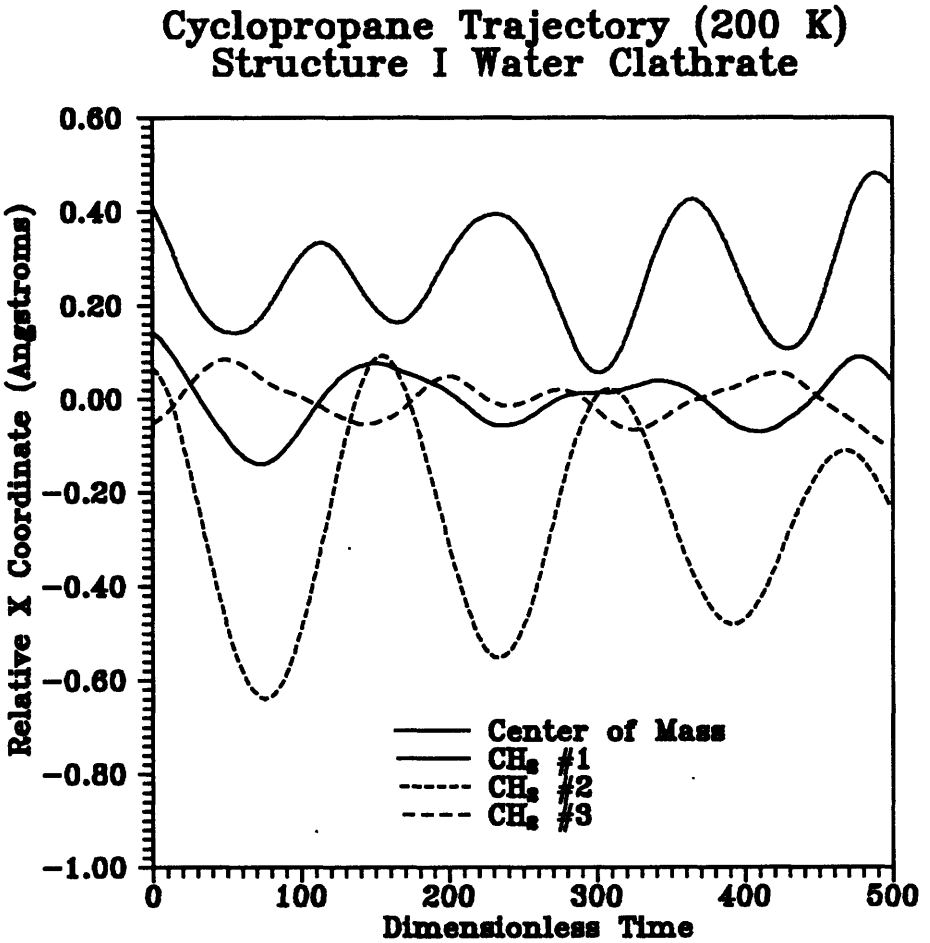

Figure 10.22 Cyclopropane X Trajectory - Structure I Water Clathrate

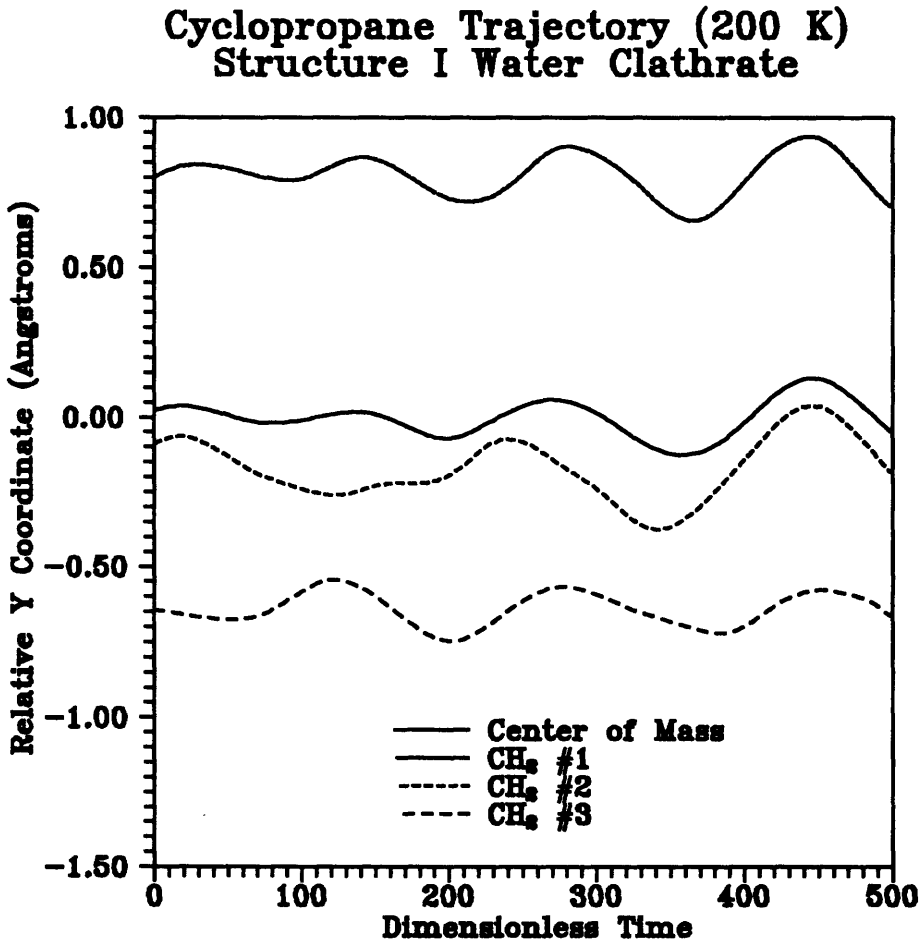

Figure 10.23 Cyclopropane Y Trajectory - Structure I Water Clathrate

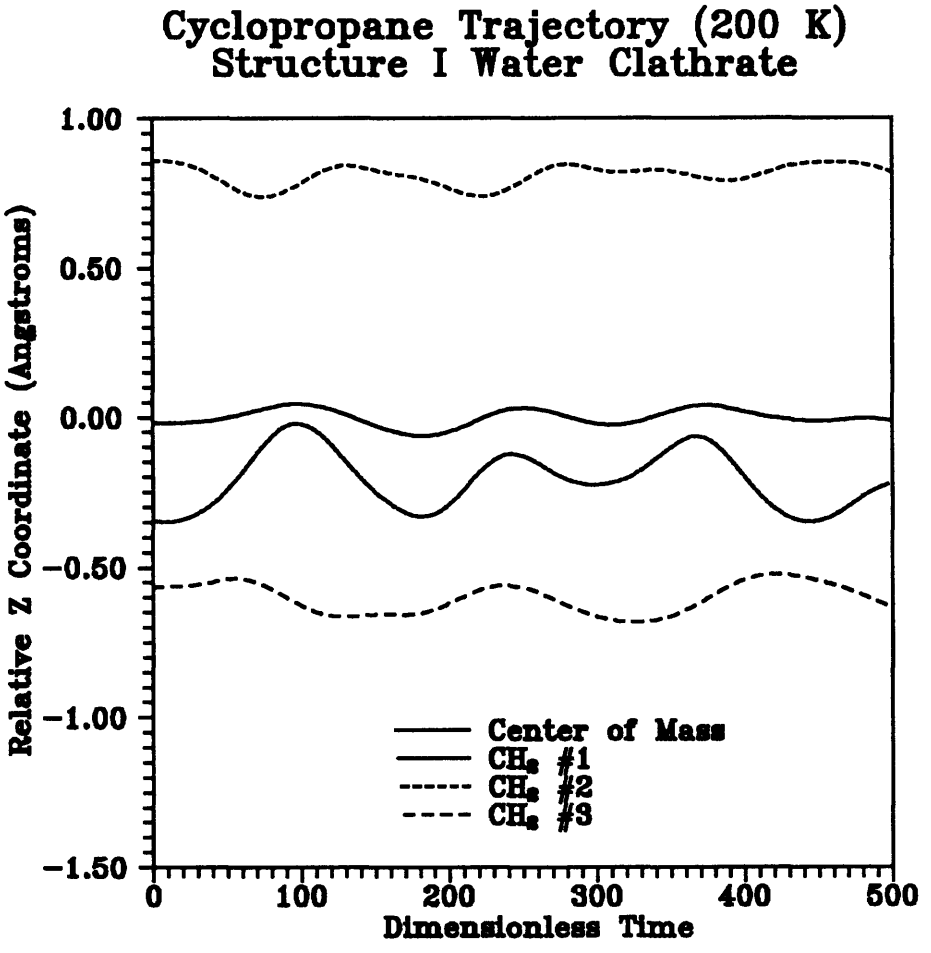

Figure 10.24 Cyclopropane Z Trajectory - Structure I Water Clathrate

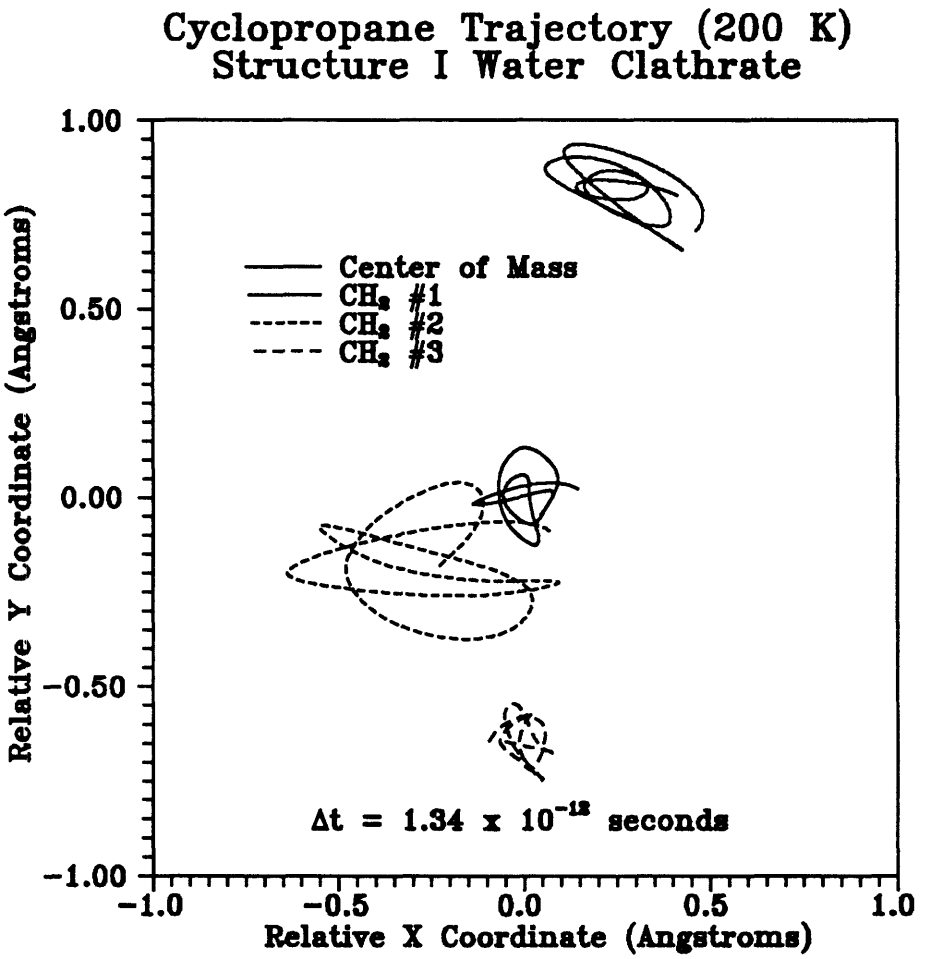

Figure 10.25 Cyclopropane X-Y Trajectory - Structure I Water Clathrate

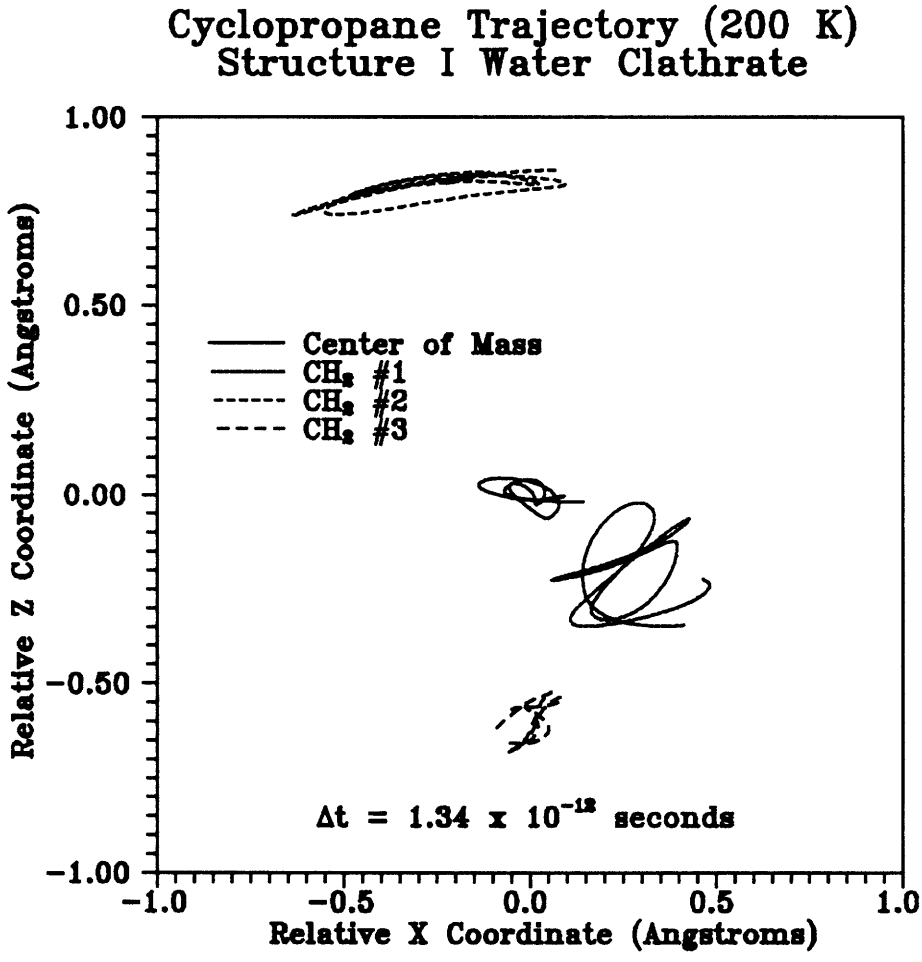

Figure 10.26 Cyclopropane X-Z Trajectory - Structure I Water Clathrate

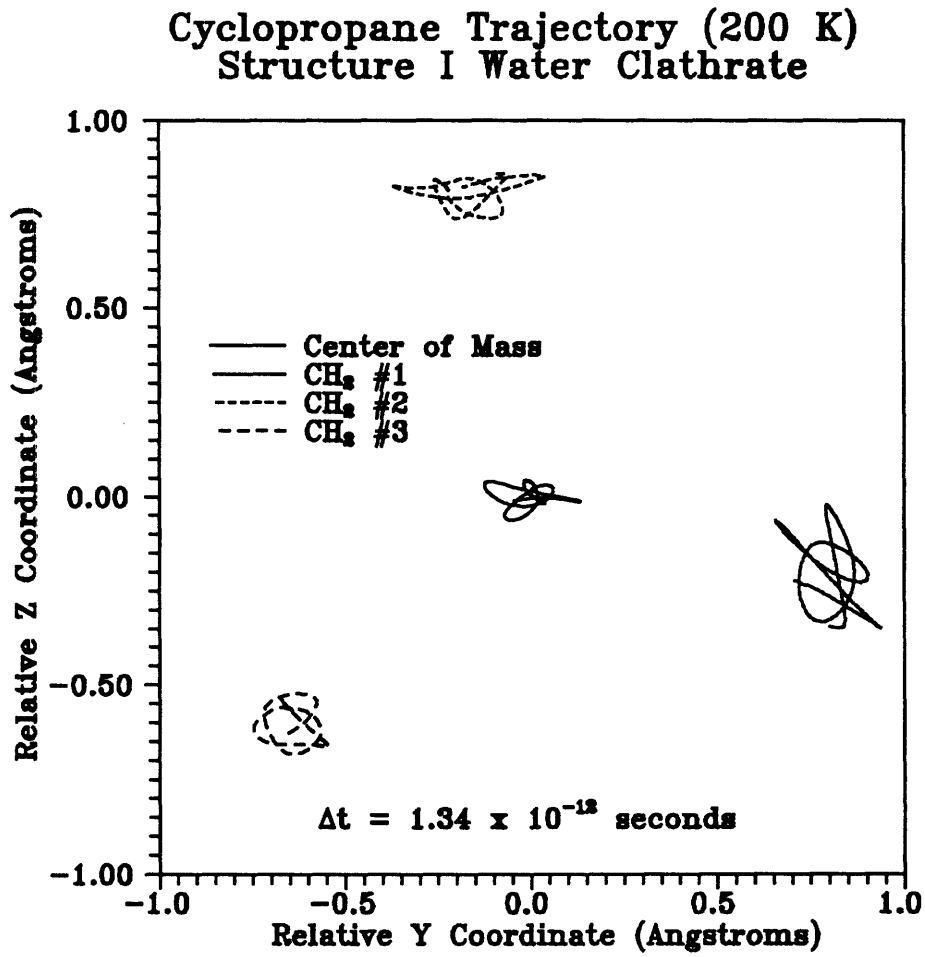

Figure 10.27 Cyclopropane Y-Z Trajectory - Structure I Water Clathrate

cell model to characterize the interactions between the host water lattice and the larger more asymmetric guest molecules.

A space-filling representation of a cyclopropane molecule within the structure I tetrakaidecahedral cavity is depicted as a function of time in Figures 10.28a - 10.28e. For the purpose of illustration, only those host water molecules with a normalized Z position less than zero are shown. This also explains the abrupt appearances and disappearances of additional host water molecules. It is quite apparent from these illustrations that the cyclopropane molecule is rotationally hindered within the tetrakaidecahedral cavity. It appears to undergo a rocking motion, somewhat analogous to a torsional oscillation.

$\Delta t = 0$ fs

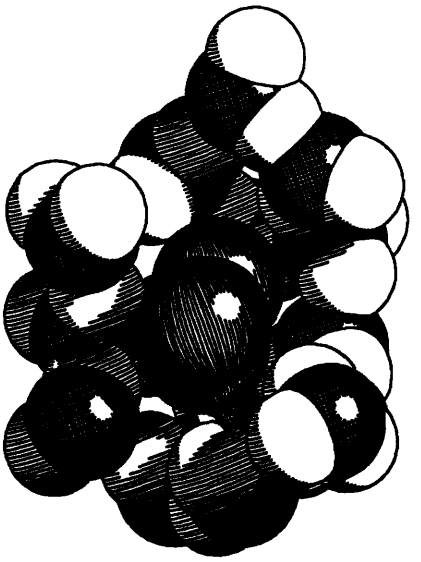

$\Delta t = 13.4$ fs

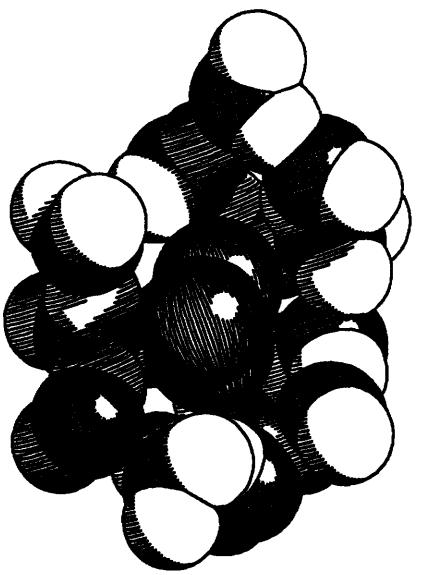

Figure 10.28a Cyclopropane Clathrate Simulation - Tetrakaidecahedron

Δt = 26.8 fs

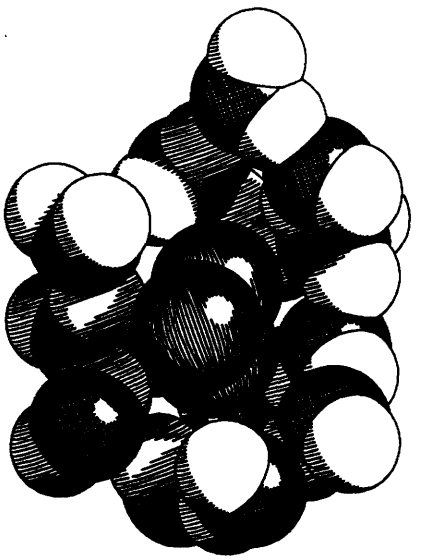

Δt = 40.2 fs

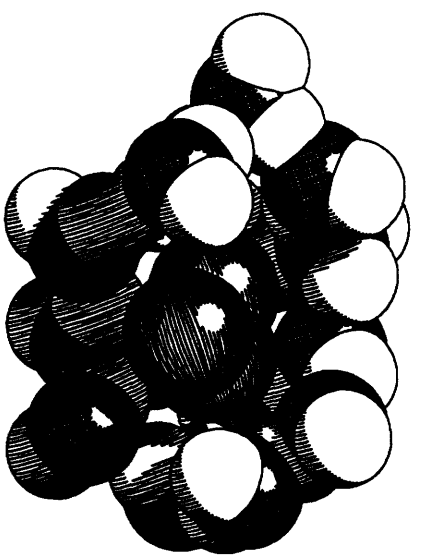

Figure 10.28b Cyclopropane Clathrate Simulation - Tetrakaidecahedron

Δt = 53.6 fs

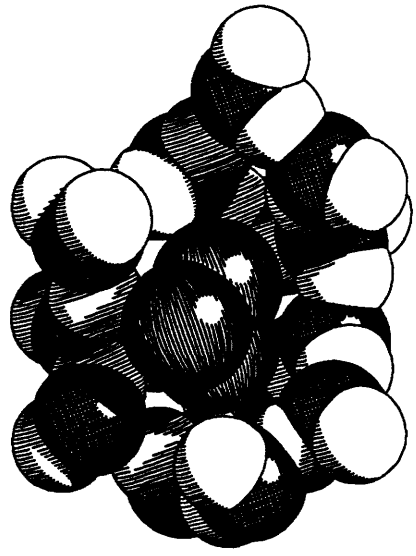

Δt = 67.0 fs

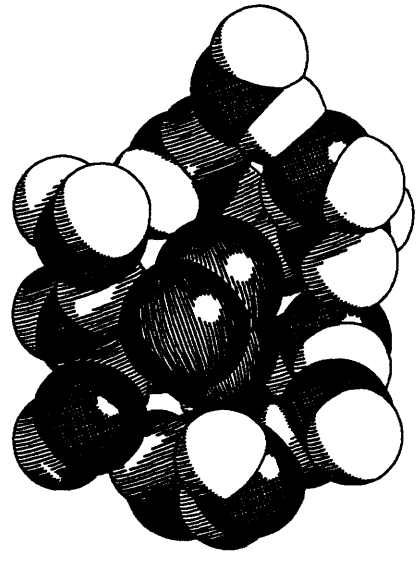

Figure 10.28c Cyclopropane Clathrate Simulation - Tetrakaidecahedron

Δt = 80.4 fs

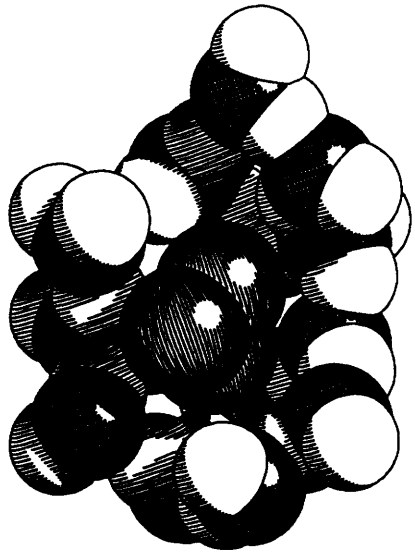

Δt = 93.8 fs

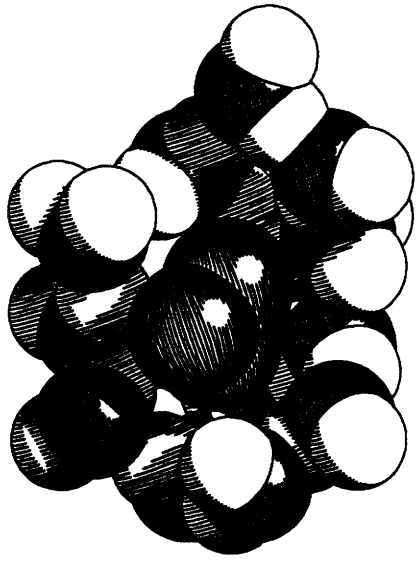

Figure 10.28d Cyclopropane Clathrate Simulation - Tetrakaidecahedron

Δt = 107.2 fs

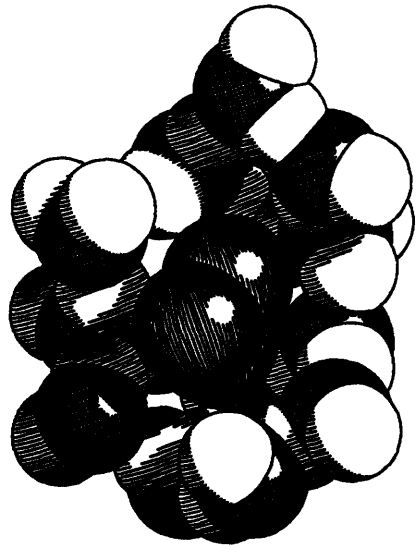

Δt = 120.6 fs

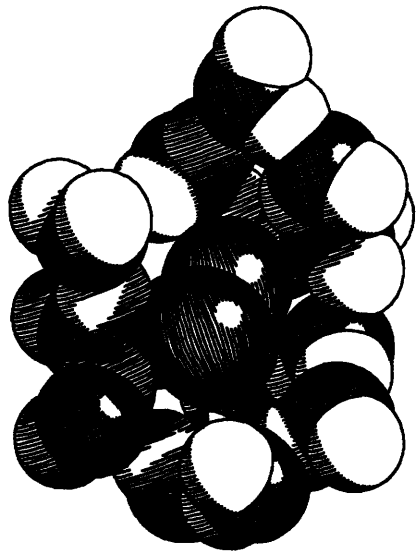

Figure 10.28e Cyclopropane Clathrate Simulation - Tetrakaidecahedron

10.6 Lattice Distortions

In order to better understand the free energy considerations involved in the development of the van der Waals and Platteeuw clathrate model we have used the results of our molecular dynamics simulations to investigate the host lattice distortions associated with the methane and cyclopropane clathrate systems. In particular we have utilized the dynamic trajectories of the host water molecules to determine the radial distribution functions of the host oxygen atoms about the various cavity centers. The functions were derived from the host water molecule configuration histories which consisted of more than 10000 saved configurations. The actual cavity-host pair distribution functions were calculated using the definition for g(r) given by

$$N(r+\Delta r/2) - N(r-\Delta r/2) = 4\pi\rho \int_{r-\Delta r/2}^{r+\Delta r/2} g(r)\, r^2\, dr \equiv \Delta N \tag{10.24}$$

where for small values of Δr can be rearranged to yield the approximate expression

$$g(r) = \frac{\Delta N(r)}{\frac{4\pi}{3}\rho\,(\Delta r)^3\left(3\left(\frac{r}{\Delta r}\right)^2 + \frac{1}{4}\right)} \tag{10.25}$$

where the bin width, Δr, was set at 0.1 Å, and the system density, ρ, defined as the number of host water molecules (oxygen sites) per $Å^3$, was simply equal to 0.02642 or $(46/(12.03)^3)$.

In order to establish a relative reference point to which the dynamically derived distributions could be compared, we constructed, using the crystallographic based equilibrium oxygen positions previously described in chapter 4, "static" cavity radial

distribution functions of the oxygen atoms about the centers of the various cavities within the structure I host lattice. The "static" cavity-host radial distribution functions referenced to the centers of the smaller pentagonal dodecahedral cavities is illustrated in Figure 10.29. The static distribution about the centers of the larger tetrakaidecahedral cavities is shown in Figure 10.30.

The cavity-host radial distribution functions associated with the methane-water clathrate system are given in Figures 10.31 and 10.32. The corresponding cyclopropane-water clathrate cavity-host radial distribution functions are shown in Figures 10.33 and 10.34. The statistical noise inherent to these distribution functions stems from the small number of cavities involved in the calculation of g(r). Still, these results compare favorably to the cavity-radial distribution functions reported by Rodger (1990), with the exception of the noise level. The similarity between the number of configurations used in this work and the number used by Rodger in the determination of the cavity-host radial distribution functions, however has led us to believe that Rodger's results were somehow smoothed.

It is quite apparent from our results that the structure I host water lattice is far from being a completely rigid structure, we notice however, that the differences between the dispersion of the host water molecules about their equilibrium positions within the two very different clathrate systems, are statistically insignificant. This suggests that the lattice distortions associated with the larger, more asymmetric guests, such as cyclopropane, are no more appreciable than those associated with the smaller guests. Although, far from being conclusive, these results appear to be consistent with the primary assumption used by van der Waals and Platteeuw in the development of the clathrate model. Specifically, the contribution of the host water molecules to the total system free energy truly seems to be independent of the mode of occupation of the various cavities.

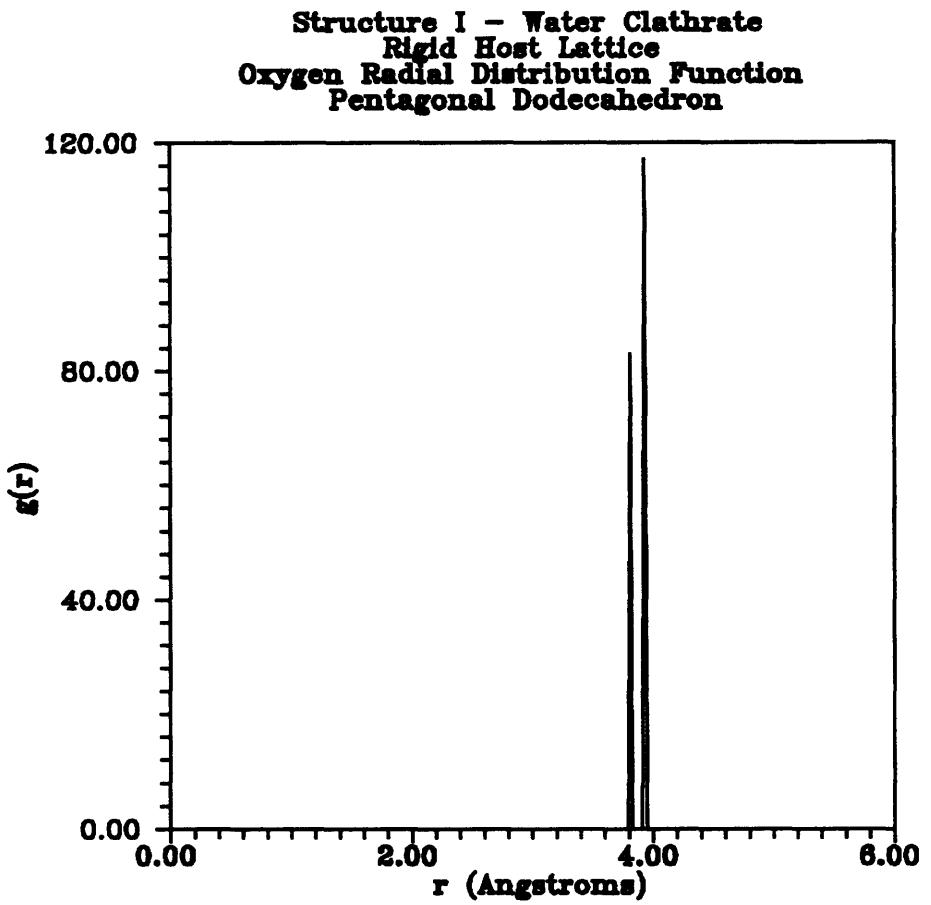

Figure 10.29 Static Oxygen Radial Distribution - Dodecahedron

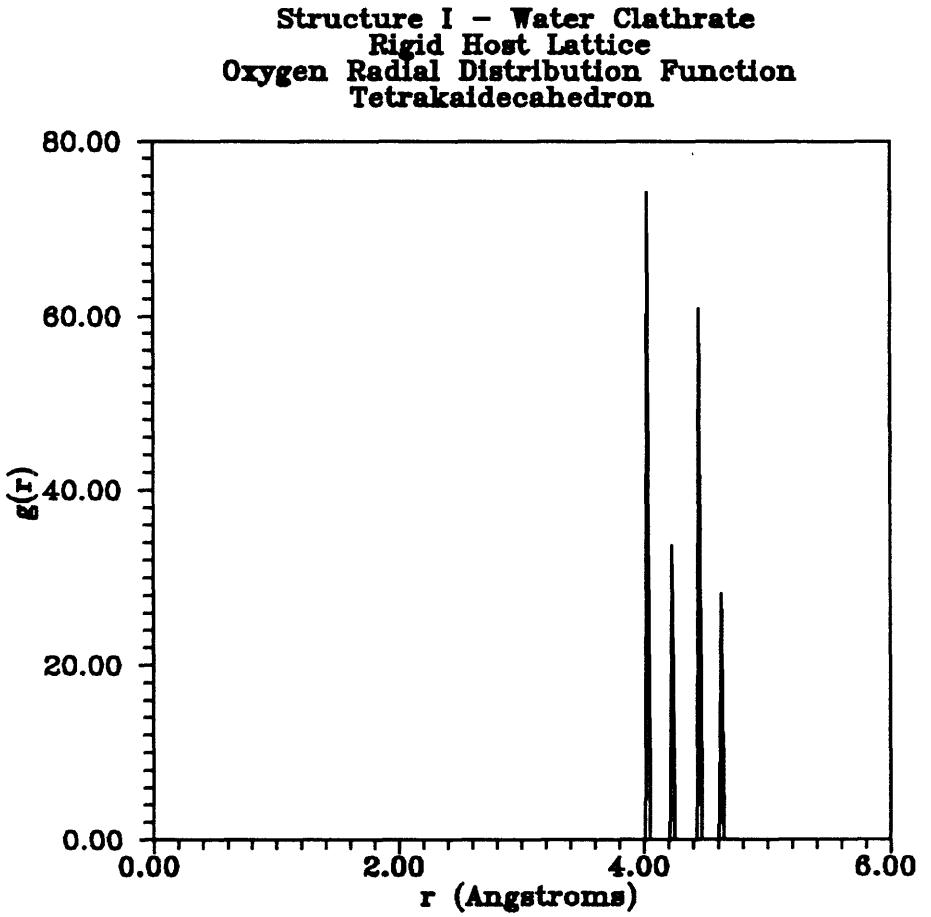

Figure 10.30 Static Oxygen Radial Distribution - Tetrakaidecahedron

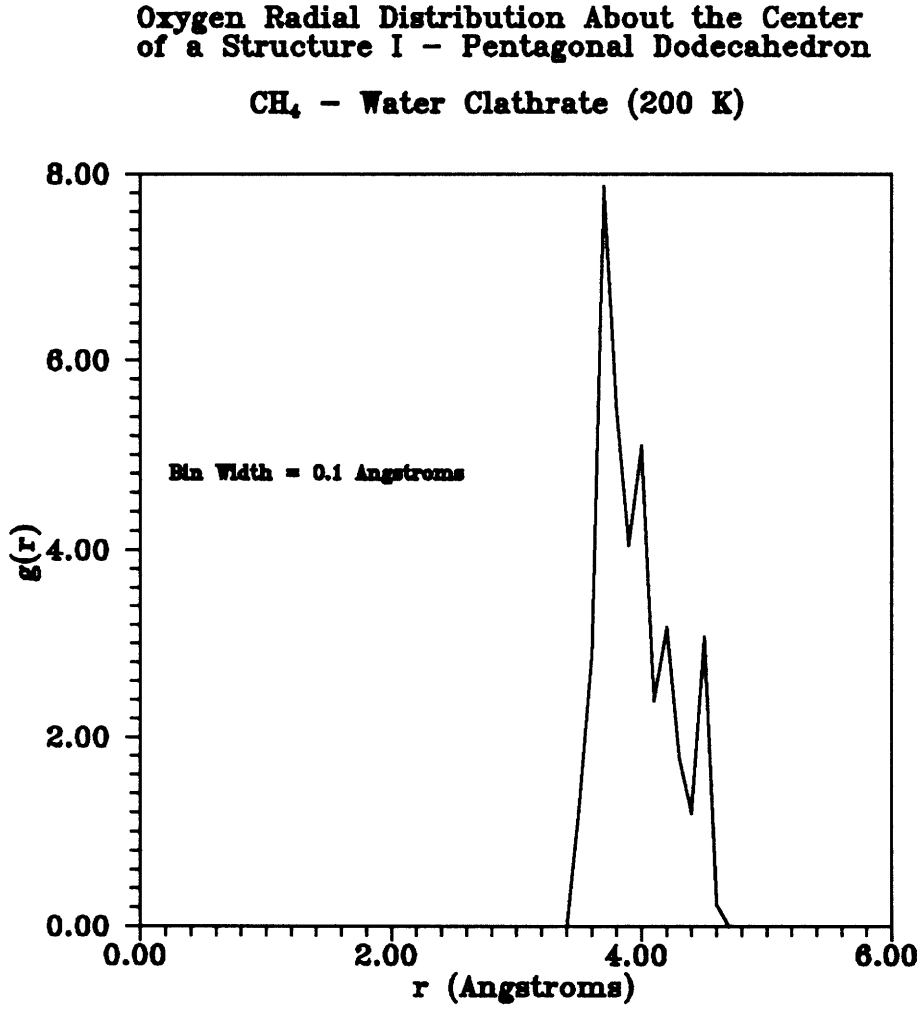

Figure 10.31 Dodecahedron Oxygen Radial Distribution - Methane

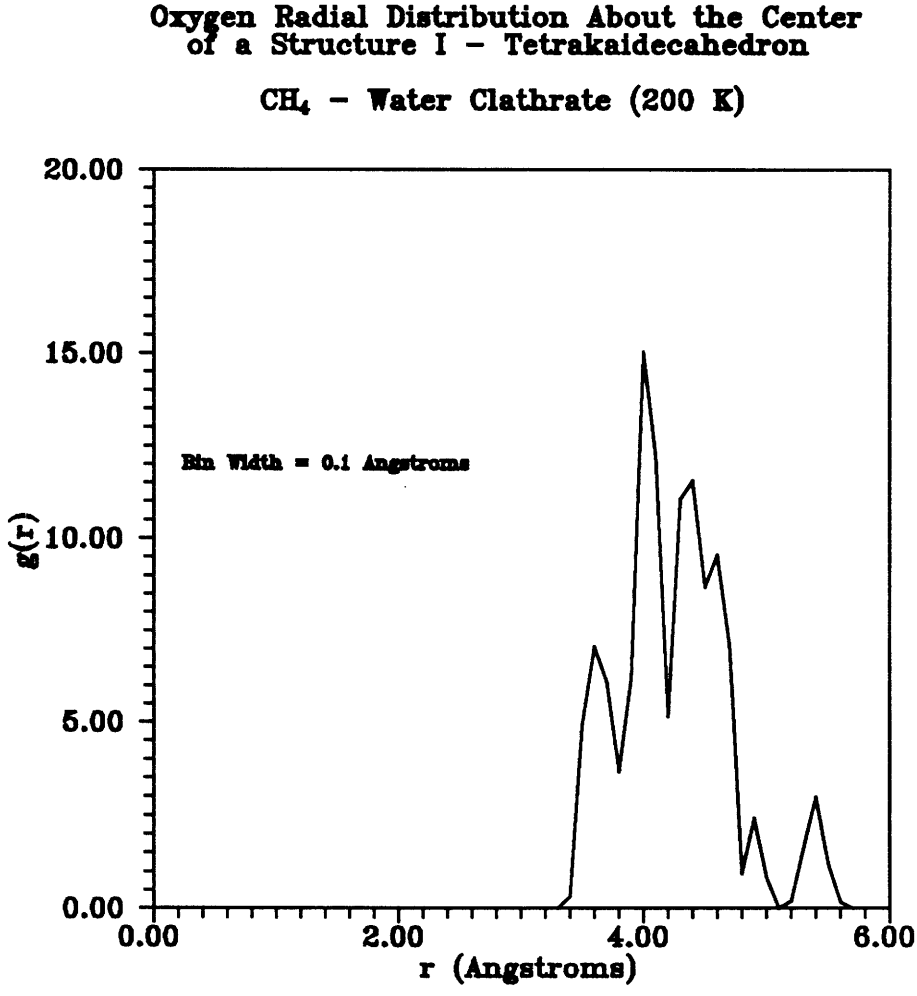

Figure 10.32 Tetrakaidecahedron Oxygen Radial Distribution - Methane

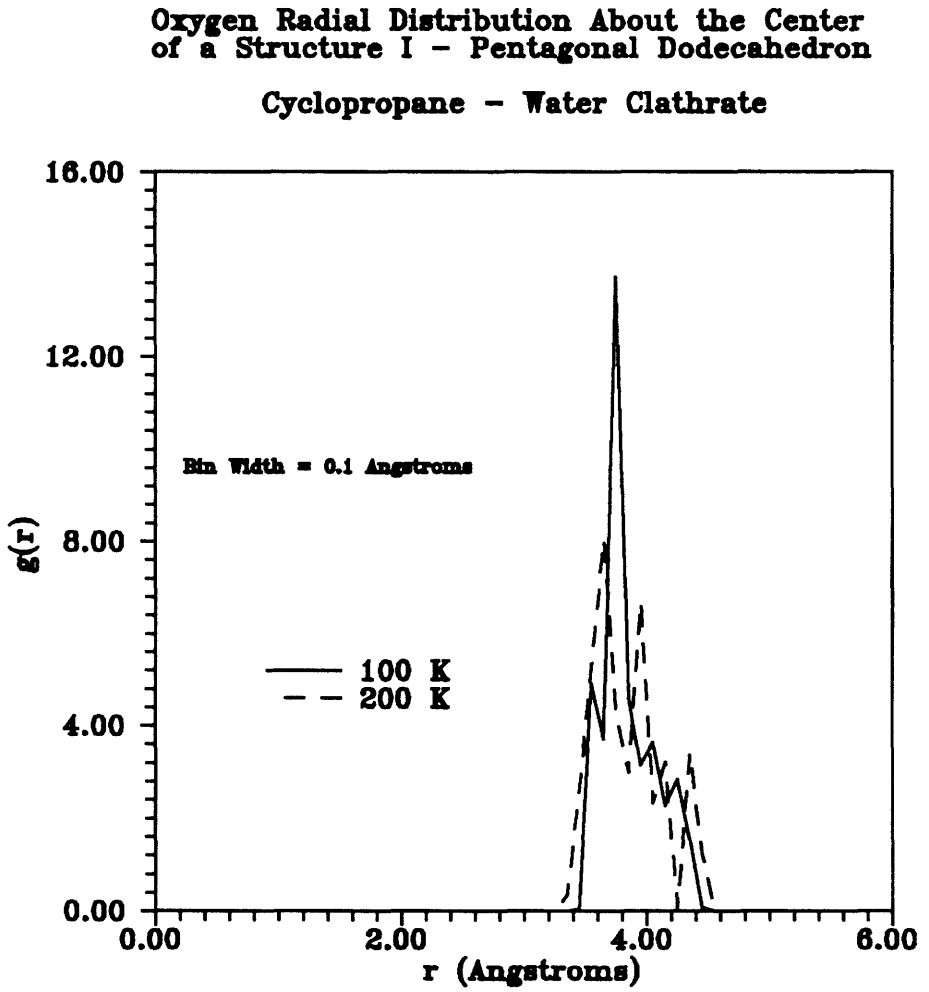

Figure 10.33 Dodecahedron Oxygen Radial Distribution - Cyclopropane

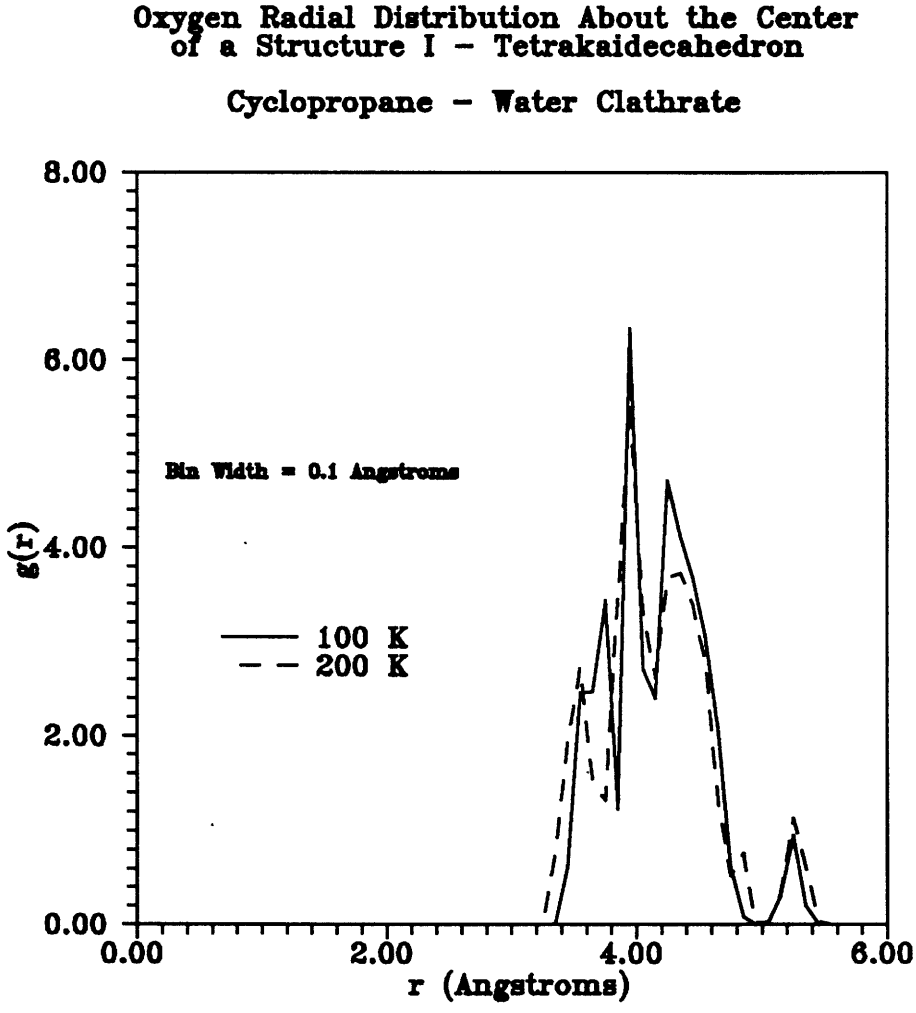

Figure 10.34 Tetrakaidecahedron Oxygen Radial Distribution - Cyclopropane

10.7 Liquid Phase Simulation

In an attempt to better understand the clustering phenomenon associated with clathrate nucleation we have performed constant volume and energy (NVE) molecular dynamics calculations on a liquid system consisting of 368 water molecules. The system was initially prepared by "melting" the unoccupied structure I unit cell as previously described in Chapter 4. The resulting disordered liquid consisting of 46 water molecules was then compressed to a density corresponding to 1 g/cm^3. This single unit cell was then duplicated eight times in order to construct a larger unit cell consisting of a total of 368 water molecules. The simple point charge (SPC) model (Berendsen et al., 1983) was used to simulate the binary interactions between water molecules. Standard periodic boundary conditions were used to simulate an infinite system. Again, the electrostatic interactions were handled via the minimum image convention. Using the Gear Predictor-Corrector algorithm as previously discussed in section 10.3, the differentially constrained equations of motion were integrated using a time step of 1.34 fs. The trajectories of all of the water molecules were followed for a total of 50-60 ps. A molecular system temperature of 300 K was maintained by the scaling of the molecular velocities every 25-50 time steps during the equilibration portion of the simulation. During the actual dynamic portion of the simulation, the velocities were scaled every 500-1000 time steps. Again, the energy conservation between rescalings was always less than 0.1 percent

Without exception, the results of the MD calculations indicated the liquid system always tended to approach a well-ordered ice structure. Attempts were made to remelt the system by drastically increasing the system temperature, however, the system would continue to approach that of a well-ordered solid system following a drop in the system temperature.

10.8 Solid Nucleation Phenomenon

The results of the pure liquid water molecular dynamics simulations prohibited further studies of mixed systems. These more complex simulations involving water and potential clathrate forming guest molecules could not be performed at this time. However, these simulation problems are computational in nature, and do not reflect an inadequacy of the MD modeling approach.

11. CONCLUSIONS

Molecular simulation methods have been used to model the configurational properties of water clathrates. In so doing we have developed a more complete picture of the nature of the interaction between the encaged guests and the host water lattice. In particular:

1) An accurate and reliable multi-dimensional integration algorithm for the computation of the configurational partition function has been implemented. Results indicate the importance of accurately accounting for the structural characteristics and asymmetries of the rigid host lattice and the entrapped guest molecule.

2) The results of configurational partition function calculations indicate the inadequacy of the current state of intermolecular potential functions, particularly those indicative of the hydrophobic type interactions associated with the modeling of the guest-host intermolecular interaction potential.

3) The contribution that subsequent water shells have on the total guest potential energy has been investigated. Lattice summations indicate that it is essential that these additional interactions be included in the characterization of the guest-host configurational partition function.

4) Based on lattice summation calculations, the effect of the inclusion of guest-guest interactions on the total guest potential energy has been determined to be insignificant, particularly, when considering the errors associated with the guest-host potential energy representation.

5) Configurational partition function and subsequent phase equilbria predictions based on widely the widely used transferable intermolecular potential functions (TIPS) as proposed by Jorgenson (1983) were inadequate for the ethane and cyclopropane systems.

6) Based on the failure of the TIPS potential function parameters to accurately predict the hydrate configurational partition functions, site-to-site Lennard-Jones (6-12) potential constants were determined by fitting them to experimental dissociation pressure data for the ethane and cyclopropane systems.

Functional Group	ε/k (K)	σ (Å)
Ethane CH_3 - O (H_2O)	125.28	3.677
Cyclopropane CH_2 - O (H_2O)	110.19	3.618

7) The trajectories resulting from the molecular dynamics simulations of the structure I cyclopropane-water clathrate system indicate that cyclopropane molecule is indeed rotationally hindered within the tetrakaidecahedral cavity, thus stressing the importance of the accurate modeling of the structural characteristics and asymmetries of the host lattice and guest molecules.

8) Based on the results of our molecular dynamics simulations, we have quantitatively determined that the lattice distortions associated with the larger more asymmetric guests, such as cyclopropane, are no more appreciable than those associated with the smaller, more symmetric guests such as methane.

Although far from being conclusive, these results appear to be consistent with the rigid lattice assumption used by van der Waals and Platteeuw in the development of their model. To be more specific, the assumption which enabled them to separate the system free energy into two terms, specifically a term associated with the host lattice and a term associated with the encaged guests.

9) In order to investigate the hydrophobic relaxation time associated with the guest (solute) - host (solvent) molecular interaction, liquid phase molecular dynamics simulations were performed. In principle, these simulations illustrate the clustering and molecular ordering within the liquid system as a precursor to solid clathrate nucleation. After repeated attempts, we were unsuccessful in obtaining useful liquid phase results. Without exception the liquid system simulation always tended to approach a well-ordered ice structure.

10) Further investigation of the causes of the simulation "freezing" phenomena is recommended. In particular, emphasis should be placed on the choice of the various intermolecular interactions as well as the system size effect.

12. REFERENCES

Alagona, G., and Tani, A., "Structure of a dilute aqueous of argon. A Monte Carlo simulation," *J. Chem. Phys.*, **72**, 580 (1980).

Alper, H. E., and Levy, R. M., "Computer Simulations of the Dielectric Properties of Water: Studies of the Simple Point Charge and Transferrable Intermolecular Potential Models," *J. Chem. Phys.*, **91**, 1242 (1989).

Allen, M. P., and Tildesley, D. J., "Computer Simulation of Liquids," **Clarendon Press, Oxford** (1987).

Anderson, F. E., and Prausnitz, J. M., "Inhibition of Gas Hydrates by Methanol," *AIChE J.*, **32**, 1321 (1986).

Anderson, H. C., "Rattle: a 'Velocity' Version of the Shake Algorithm for Molecular Dynamics Calculations," *J. Chem. Phys.*, **52**, 24 (1983).

Anderson, J., Ullo, J., and Yip, S., "Molecular Dynamics Simulation of the Concentration-Dependent Dielectric Constants of Aqueous NaCl Solutions," *Chem. Phys. Lett.*, **152**, 447 (1988).

Barduhn, A. J., Towlson, H. E., and Ho, Y. C., "The Properties of Some New Gas Hydrates and Their Use in Demineralizing Sea Water," *AIChE J.*, **8**, 176 (1962).

Barraclough, B. L., "Methane Hydrate Resource Assessment Program," *Los Alamos Scientific Laboratory Report LA-8568-PR* (Oct. 1980).

Barraclough, B. L., "Methane Hydrate as an Energy Resource? A Review with Recommended Future Research," *Los Alamos Scientific Laboratory Report LA-8368-MS* (June 1980).

Barraclough, B. L., McGuire, P. L., and Koczan, S. P., "Methane Hydrate Resource Assessment Program," *Los Alamos Scientific Laboratory Report LA-8933-PR* (Sept. 1981).

Basu, P. K, and Mountain, R. D., "Molecular Dynamics Evaluation of Cell Models for Type I Gas Hydrate Crystal Dynamics," *J. Phys. Chem. Solids*, **49**, 587 (1988).

Belosludov, V. R., Dyadin, Y. A., Chekhova, G. N., and Fadeev S. I., "The Description of P, T, X-Phase Diagrams in Systems with Clathrate Formation where the Guest-Guest Interaction is taken into Account. Hydroquinone-Noble Gas Systems," *J. Inclusion Phenomena*, **1**, 251 (1984).

Belosludov, V. R., Dyadin, Y. A., Chekhova, G. N., Kolesov, B. A., and Fadeev S. I., "Hydroquinone Clathrates and the Theory of Clathrate Formation," *J. Inclusion Phenomena*, **3**, 243 (1985).

Berendsen, H. J. C., Postma, J. P. M., Van Gunsteren, W. F., and Hermans, J., "Interaction Models for Water in Relation to Protein Hydration," *Intermolecular Forces* (edited by B. Pullman), **Reidel, Dordrecht** (1981).

Berens, H., and Wilson, K. R., "A computer simulation method for the calculation of equilibrium constants for the formation of physical clusters of molecules: Application to small water clusters," *J. Chem Phys.*, **76**, 637 (1982).

Bernal, J. D., and Fowler, R. H., "Theory of Water and Ionic Solution, with Particular Reference to Hydrogen and Hydroxyl Ions," *J. Chem Phys.*, **1**, 515 (1933).

Bickes, R. W. Jr., Duquette, G., van den Meijdenberg, C. J. N., Rulis, A. M., Scoles, G., Smith, K. M., "Molecular Beam Scattering Experiments with Polar Molecules: Measurements of Differential Collision Cross Sections for H_2O+H_2, He, Ne, Ar, H_2O and NH_3+H_2, He, NH_3," *J. Phys. B: Atom. Molec. Phys.*, **8**, 3034 (1975).

Bolis, G., and Clementi, E., "Methane in Aqueous Solution at 300 K," *Chem. Phys. Letters*, **82**, 147 (1981).

Bolis, G., and Clementi, E. Wertz, D. H., Scheraga, H. A., and Tosi, C. "Interaction of Methane and Methanol with Water," *J. Am. Chem. Soc.*, **105**, 355 (1983).

Bolis, G., Corongiu, G., and Clementi, E., "Methanol in Water Solution at 300 K," *Chem. Phys. Letters*, **86**, 299 (1982).

Bowen, H. J., Donohue, J., Jenkin, D. G., Kennard, O., Wheatley, P. J., Whiffen, D. H., "Tables of Interatomic Distances and Configuration in Molecules and Ions". **Special Publication No. 11, The Chemical Society, London** (1958).

Carnahan, B., Luther, H. A., Wilkes, J. O., "Applied Numerical Methods," **Wiley, New York** (1969)

Carozzo, L., Corongiu, G., Petrongolo, C., and Clementi, E., "Analytical potentials from *ab initio* computations for the interaction between biomolecules. IV. Water with glycine and serine zwitterions," *J. Chem. Phys.*, **68**, 787 (1978).

Chiari, G., and Ferraris, G., "The Water Molecule in Crystalline Hydrates Studied by Neutron Diffration," *Acta Cryst.*, **B38**, 2331 (1982).

Claussen, W. F., "Suggested Structures of Water in Inert Gas Hydrates," *J. Chem. Phys.*, **19**, 259 (1951).

Claussen, W. F., "Erratum: Suggested Structures of Water in Inert Gas Hydrates," J. *Chem. Phys.*, **19**, 662 (1951).

Claussen, W. F., "A Second Water Structure for Inert Gas Hydrate," *J. Chem. Phys.*, **19**, 1425 (1951).

Clementi, E., and Popkie, H., "Study of the Structure of Molecular Complexes. I. Energy Surface of a Water Molecule in the Field of a Lithium Positive Ion," *J. Chem. Phys.*, **57**, 1077 (1972).

Clementi, E., Corongiu, G., Jönsson, B., and Romano, S., "Monte Carlo simulations of water clusters around Zn^{++} and linear $Zn^{++}.CO_2$ complex," *J. Chem. Phys.*, **72**, 260 (1980).

Clementi, E., and Habitz, P., "A New Two-Body Water-Water Potential," *J. Phys. Chem.*, **87**, 2815 (1983).

Corongiu, G., and Clementi, E., "Study of the structure of molecular complexes. XVI. Doubly charged cations interacting with water," *J. Chem. Phys.*, **69**, 4885 (1978).

Dang, L. X., Pettitt, B. M., "Simple Intramolecular Model Potentials for Water," *J. Phys. Chem.*, **91**, 3349 (1987).

Dashevsky, V. G., and Sarkisov, G. N., "The solvation and hydrophobic interaction of non-polar molecules in water in approximation of interatomic potentials: The Monte Carlo method," *Mol. Phys.*, **27**, 1271 (1974).

Davidson, D. W., "The Motion of Guest Molecules in Clathrate Hydrates," *Can. J. Chem.*, **49**, 1224 (1971).

Davidson, D. W., Garg, S. K., Gough, S. R., Handa, Y. P., Ratcliffe, C. I., and Ripmeester, J. A., "Some Structural and Thermodynamic Studies of Clathrate Hydrates," *J. Inclusion Phenomena*, **2**, 231 (1984).

Davidson, D. W., Garg, S. K., Gough, S. R., Hawkins, R. E., and Ripmeester, J. A., "Characterization of Natural Gas Hydrates by Nuclear Magnetic Resonance and Dielectric Relaxation," *Can. J. Chem.*, **55**, 3641 (1977).

Davidson, D. W., Handa, Y. P., Ratcliffe, C. I., Tse, J. S., and Powell, B. M., "The Ability of Small Molecules to Form Clathrate Hydrates of Structure II," *Nature*, **311**, 143 (1984).

Davidson, D. W., Ratcliffe, C. I., and Ripmeester, J. A., "2H and 13C NMR Study of Guest Molecule Orientation in Clathrate Hydrates," *J. Inclusion Phenomena*, **2**, 239 (1984).

Deaton, W. H., and Frost, E. M., *U. S. Bur. Mines Monogr.*, No. 8 (1946).

Dharmawardana, M. W. C., "Thermal Conductivity of the Ice Polymorphs and the Ice Clathrates," *J. Phys, Chem.*, **87**, 4185 (1983).

Dharmawardhana, P. B., Parrish, W. R., and Sloan, E. D., "Experimental Thermodynamic Parameters for the Prediction of Natural Gas Hydrate Dissociation Conditions," *Ind. Eng. Chem. Fundam.*, **19**, 410 (1980).

Dharmawardhana, P. B., Parrish, W. R., and Sloan, E. D., "Experimental Thermodynamic Parameters for the Prediction of Natural Gas Hydrate Dissociation Conditions," *Ind. Eng. Chem. Fundam.*, **20**, 306 (1981).

Egelstaff, P. A.,, and Root, J. H., "The Temperature Dependence of the Structure of Water," *Chem. Phys.*, **76**, 405 (1983).

Edberg, R., Evans, D. J., and Moriss, G. P., "Constrained Molecular Dynamics: Simulations of Liquid Alkanes with a New Algorithm," *J. Chem. Phys.*, **84**, 6933 (1986).

Evans, D. J., Hoover, W. G., Failor, B. H., Moran, B., and Ladd, A. J. C., "Nonequilibrium Molecular Dynamics via Gauss's Principle of Least Constraint," *Phys. Review A*, **28**, 1016 (1983).

Evans, M. W., Lie, G. C., and Clementi, E., "Molecular Dynamics Simulation of Water from 10 to 1273 K," *J. Chem. Phys.*, **88**, 5157 (1988).

Falabella, B. J., and Vanpee, M., "Experimental Determination of Gas Hydrate Equilibrium Below the Ice Point," *Ind. Eng. Chem. Fundam.*, **13**, 228 (1974).

Frost, E. M., and Deaton, W. M., "Gas Hydrate Composition and Equilibrium Data," *Oil and Gas J.*, **15**, 170 (1946).

Gear, C., W., "Numerical Initial Value Problems in Ordinary Differential Equations," **Prentice Hall, Englewood Cliffs, New Jersey** (1971).

Glew, D. N., and Rath, N. S., "Variable Composition of the Chlorine and Ethylene Oxide Clathrate Hydrates," *J. Chem. Phys.*, **44**, 1710 (1966).

Goldberg, P., "Free Radicals and Reactive Molecules in Clathrate Cavities," *Science*, **142**, 378 (1963).

Goldstein, H., "Classical Mechanics," 2nd Edition, **Addison-Wesley, Reading, Massachusetts** (1980).

Goodfellow, J. M., Finney, J. L., and Barnes, P., "Monte Carlo computer simulation of water-amino acid interactions," *Proc. Roy. Soc. Lond. B.*, **214**, 213 (1982).

Gunsteren, W. F. van, and Berendsen, H. J. C., "Algorithms for Macromolecular Dynamics and Constraint Dynamics," *Mol. Phys.*, **34**, 1311 (1977).

Hafemann, D. R., and Miller, S. L., "The Clathrate Hydrates of Cyclopropane," *J. Phys. Chem.*, **73**, 1392 (1969).

Hammerschmidt, G., "Formation of Gas Hydrates in Natural Gas Transmission Lines," *Ind. Eng. Chem.*, **26**, 851 (1934).

Hahn, T., Editor, "International Tables for Crystallography," *D. Reidel*, Dordrecht (1988).

Handa, P. Y., and Tse, J. S., "Thermodynamic Properties of Empty Lattices of Structure I and Structure II Clathrate Hydrates," *J. Phys. Chem.*, **90**, 5917 (1986).

Hill, T. L., "Statistical Mechanics Principles and Selected Applications," **Dover Publications, New York** (1957).

Hirschfelder, J. O., Curtiss, C. F., and Bird, R. B., "Molecular Theory of Gases and Liquids," **Wiley, New York** (1954).

Holder, G. D., Corbin, G., and Papadopoulos, K. D., "Thermodynamic and Molecular Properties of Gas Hydrates from Mixtures Containing Methane, Argon, and Krypton," *Ind. Eng. Chem. Fundam.*, **19**, 282 (1980).

Holder, G. D., and Hand, J. H., "Multiple-Phase Equilibria in Hydrates from Methane, Ethane, Propane, and Water Mixtures," *AIChE J.*, **28**, 440 (1982).

Holder, G. D., and Hwang, M. J., "Adsorption Theory in Clathrate Hydrates," Fundamentals of Adsorption, Liapis, A. I., Editor, *Engineering Foundation* (edited by A. I. Liapis), **New York** (1987).

Holder, G. D., John, V. T., and Yen, S., "Geological Implications of Gas Production from *In-situ* Gas Hydrates," *Presented at SPE/DOE Symposium on Unconventional Gas Recovery*, **SPE/DOE 8929** (1980).

Holder, G. D., Malekar, S. T., and Sloan, E. D., "Determination of Hydrate Thermodynamic Reference Properties from Experimental Hydrate Composition Data," *Ind. Eng. Chem. Fundam.*, **23**, 123 (1984).

Hollander, F., and Jeffrey, G. A., "Neutron Diffration Study of the Crystal Structure of Ethylene Oxide Deuterohydrate at 80 K," *J. Chem Phys.*, **66**, 4699 (1977).

Jeffrey, G. A., "Water Structure in Organic Hydrates," *Accounts of Chemical Research*, 2, 43 (1967).

Jeffrey, G. A., "Pentagonal Dodecahedral Water Structure in Crystalline Hydrates," *Material Research Bulletin*, **7**, 1259 (1972).

Jeffrey, G. A., "Hydrate Inclusion Compounds," *J. Inclusion Phenomena*, **1**, 211 (1984).

Jeffrey, G. A., and McMullan, R. K., "The Clathrate Hydrates," *Prog. Inorg. Chem.*, **8**, 43 (1967).

John, V. T., and Holder, G. D., "Choice of Cell Size in the Cell Theory of Hydrate Phase Gas-Water Interactions," *J. Phys. Chem.*, **85**, 1811 (1981).

John, V. T., and Holder, G. D., "Contribution of Second and Subsequent Water Shells to the Potential Energy of Guest-Host Interactions in Clathrate Hydrates," *J. Phys. Chem.*, **86**, 455 (1982).

John, V. T., and Holder, G. D., "Langmuir Constants for Spherical and Linear Molecules in Clathrate Hydrates. Validity of the Cell Theory," *J. Phys. Chem.*, **89**, 3279 (1985).

John, V. T., Padadopoulos, K. D., and Holder, G. D., "A Generalized Model for Predicting Equilibrium Conditions for Gas Hydrates," *AIChE J.*, **31**, 252 (1985).

Jorgensen, W. L., "Transferable Intermolecular Potential Functions for Water, Alcohols, and Ethers. Application to Liquid Water". *J. Am. Chem. Soc.*, **103**, 335 (1981).

Jorgensen, W. L., "Transferable Intermolecular Potential Functions. Application to Liquid Methanol Including Internal Rotation," *J. Am. Chem. Soc.*, **103**, 341 (1981).

Jorgensen, W. L., " Simulation of Liquid Ethanol Including Internal Rotation," *J. Am. Chem. Soc.*, **345** (1981).

Jorgensen, W. L., "Monte Carlo simulation of n-butane in water. Conformational evidence for the hydrophobic effect," *J. Chem. Phys.*, **77**, 5757 (1982).

Jorgensen, W. L., Chandrasekhar, J., Madura, J. D., Impey, R. W., and Klein, M. L., "Comparson of simple potential functions for simulating liquid water ," *J. Chem. Phys.*, **79**, 926 (1983).

Keller, E., "Some Computer Drawings of Molecular and Solid-State Structures," *J. Appl. Cryst.*, **22**, 19 (1989).

Kihara, T., "Virial Coefficients and Models of Molecules in Gases," *Reviews of Mod. Phys.*, **25**, 831 (1953).

Kistenmacher, H., Popkie, J., and Clementi, E., "Study of the structure of molecular complexes. II. Energy surfaces for a water molecule in the field of a sodium or potassium cation," *J. Chem. Phys.*, **58**, 1689 (1973).

Kistenmacher, H., Popkie, H., and Clementi, E., "Study of the structure of molecular complexes. III. Energy surface of water molecule in the field of a fluorine or chlorine anion," *J. Chem. Phys.*, **58**, 5627 (1973).

Kistenmacher, H., Lie, G. C., Popkie, H., and Clementi, E., "Study of the structure of molecular complexes. VI. Dimers and small clusters of water molecules in the Hartree-Fock approximation," *J. Chem. Phys.*, **61**, 546 (1974).

Kistenmacher, H., Popkie, H., Clementi, E., and Watts, R. O., " Study of the structure of molecular complexes. VII. Effect of correlation energy corrections to the Hartree-Fock water-water potential on Monte Carlo simulations of liquid water," *J. Chem. Phys.*, **60**, 4455 (1974).

Lennard-Jones, J. E., "On the Determination of Molecular Fields. III. - From Crystal Measurements and Kinetic Thery Data," *Roy. Soc. Proc.*, **A106**, 709 (1924).

Lennard-Jones, J. E., and Ingham, A. E., "On the Calculation of Certain Crystal Potential Constants, and on the Cubic Crystal of Least Potential Energy," *Roy. Soc. Proc.*, **A107**, 636 (1925).

Lie, G. C., and Clementi, E., "Study of the structure of molecular complexes. XII Stucture of liquid water obtained by Monte Carlo simulation with the Hartree-Fock potential corrected by inclusion of dispersion forces"., *J. Chem. Phys.*, **62**, 2195 (1975).

Linse, P., and Jönsson, B., " A Monte Carlo study of the electrostatic interaction between highly charged aggregates. A test of the cell model applied to micellar systems". *J. Chem. Phys.*, **78**, 3167 (1983).

Losonczy, M., and Moskowitz, J. W., and Stillinger, F. H., "Hydrogen Bonding Between Neon and Water," *J. Chem. Phys.*, **59**, 3264 (1973).

Maitland, G. C., Rigby, R., Smith, B. E., and Wakeham, W. A., "Intermolecular forces," **Clarendon Press, Oxford** (1981).

Mak, T. C. W., and and McMullan, R. K., "Polyhedral Clathrate Hydrates. X. Structure of the Double Hydrate of Tetrahydrofuran and Hydrogen Sulfide," *J. Chem. Phys.*, **42**, 2732 (1965).

Marchi, M., and Mountain, R. D., "Thermal Expansion of a Structure II Hydrate Using Constant Pressure Molecular Dynamics," *J. Chem. Phys.*, **86**, 6454 (1987).

Marchi, M., Tse, J. S., and Klein, M. L., "Lattice Vibrations and Infrafed Absorbtion of Ice Ih," *J. Chem. Phys.*, **85**, 2414 (1986).

Matsuo, T., and Suga, H., "Molecular Motion and Phase Transition in Hydroquinone Clathrate Compounds," *J. Inclusion Phenomena*, **2**, 49 (1984).

Matsuoka, O., Clementi, E., and Yoshimine, M., " CI study of the water dimer potential surface," *J. Chem. Phys.*, **64**, 1351 (1976).

Mazo, R. M., "Note on the theory of dissociation pressures of gas hydrates," *Mol. Phys.*, **8**, 515 (1964).

McIntyre, J. A., and Petersen, D. R., "Thermal and Composition Expansion of Clathrates in Ethylene Oxide-Water System," *J. Chem. Phys.*, **47**, 3850 (1967).

McKoy, V., and Sinanoglu, O., "Theory of Dissociation Pressures of Some Gas Hydrates," *J. Chem. Phys.*, **38**, 2946 (1963).

McMullan, R. K., and Jeffrey, G. A., "Polyhedral Clathrate Hydrates. IX. Structure of Ethylene Oxide Hydrate," *J. Chem. Phys.*, **42**, 2725 (1965).

McQuarrie, D. A., "Statistical Mechanics," *Harper & Row, New York* (1976).

Mehrotra, P. K., Mezei, M., and Beveridge, D. L., "Convergence acceleration in Monte Carlo computer simulation on water and aqueous solutions," *J. Chem. Phys.*, **78**, 3156 (1983).

Metropolis, N., Rosenbluth, A. W., Rosenbluth, M. N., Teller, A. H., and Teller, E., "Equation of State Calculations by Fast Computing Machines," *J. Chem. Phys.*, **21**, 1087 (1953).

Mezei, M., Mehrotra, P. K., and Beveridge, D. L., " Monte Carlo Computer Simulation of Aqueous Hydration of the Glycine Zwitterion at 25°C," *J. Biomolecular Structure and Dynamics*, **2**, 1 (1984).

Miller, B., and Strong, E. R., "Possibilities of Storing Natural Gas in the Form of a Solid Hydrate," *Proc. Am. Gas. Assoc.*, **27**, 80 (1945).

Mills, W. C., and Wrighton, M. S., "Monte Carlo Computer Simulation of Hydrophobic Bonding," *J. Am. Chem. Soc.*, **191**, 5832 (1979).

Mountain, R. D., "Molecular Dynamics Investigation of Expanded Water at Elevated Temperatures," *J. Chem. Phys.*, **90**, 1866 (1989).

Morse, M. D., and Rice, S. A., "Tests of effective pair potentials for water: Predicted ice structures," *J. Chem. Phys.*, **76**, 650 (1982).

Nagata, I, and Kobayashi, R., "Calculation of Dissociation Pressures of Gas Hydrates Using the Kihara Model," *Ind. Eng. Chem. Fundam.*, **5**, 344 (1966).

Nagata, I, and Kobayashi, R., "Prediction of Dissociation Pressures of Mixed Gas Hydrates Using from Data for Hydrates of Pure Gases with Water," *Ind. Eng. Chem. Fundam.*, **5**, 466 (1966).

Owicki, J. C., and Scheraga, H. A., "Monte Carlo Calculations in the Isothermal-Isobaric Ensemble. 2. Dilute Aqueous Solution of Methane," *J. Am. Chem. Soc.*, **99**, 7413 (1977).

Parrish, W. R., and Prausnitz, J. M., "Dissociation Pressures of Gas Hydrates Formed by Gas Mixtures," *Ind. Eng. Chem. Proc. Des. Develop.*, **11**, 26 (1972).

Pauling, L, and Marsh, R. E., "The Structure of Chlorine Hydrate," *Proc. Nat.* Acad. *Sci.*, **38**, 112 (1952).

Pearson, C. F., Halleck, P. M., McGuire, P. L., Hermes, R., and Mathews, M., "Natural Gas Hydrate Deposits: A Review of *in Situ* Properties," *J. Phys. Chem.*, **87**, 4180 (1983).

Peng, D., and Robinson, D. B., "A New Two-Constant Equation of State," *Ind. Eng. Chem. Fundam.*, **15**, 59 (1976).

Plummer, P. L. M., and Chen, T. S., "A Molecular Dynamics Study of Water Clathrates," *J. Phys. Chem.*, **87**, 4190 (1983).

Plummer, P. L. M., and Chen, T. S., "Investigation of structure and stability of small clusters: Molecular dynamics studies of water pentamers," *J. Chem. Phys.*, **86**, 7149 (1987).

Powell, H. M., "The Structure of Molecular Compounds. Part IV. Clathrate Compounds," *J. Chem. Soc.* (*London*), **61** (1948).

Press, W. H., Flannery, B. P., Teukolsky, S. A., Vetterling, W. T., " Numerical Recipes: The Art of Scientific Computing," **Cambridge University Press, Cambridge** (1988).

Ragazzi, M., Ferro, D. R., and Clementi, E., "Analytical potentials from ab initio computations for the interaction between biomolecules. V. Formyl-triglycyl amide and water," *J. Chem. Phys.*, **70**, 1040 (1979).

Rahman, A., and Stillinger, F. H., "Proton Distribution in Ice and the Kirkwood Correlation Factor," *J. Chem. Phys.*, **57**, 4009 (1972).

Reamer, H. H., Selleck, F. T., and Sage, B. H., "Some Properties of Mixed Paraffinic and Olefinic Hydrates," *Petroleum Trans.*, **195**, 197 (1952).

Reid, R. C., Prausnitz, J. M., and Poling, B. E., "The Properties of Gases and Liquids," **McGraw-Hill, New York** (1987).

Ripmeester, J. A., Tse, J. S., Ratcliffe, C. I., and Powell, B. M., "A New Clathrate Hydrate Structure," *Nature*, **325**, 135 (1987).

Rodger, P. M., "Cavity Potential in Type I Gas Hydrates," *J. Phys. Chem.*, **93**, 6850 (1989).

Rodger, P. M., "Stability of Gas Hydrates," *J. Phys. Chem.*, **94**, 6080 (1990).

Roberts, O. L., Brownscombe, E. R., Howe, L. S., and Ramser, H., "Phase Diagrams of Methane and Ethane Hydrates," *Petroleum Engineer*, **12**, 56 (1941).

Ryckaert, J. P., Ciccotti, G., and Berendsen, J. C., "Numerical Integration of the Cartesian Equations of Motion of a System with Constraints: Molecular Dynamics of n-Alkanes," *J. of Comp. Phys.*, **23**, 327 (1977).

Stackelberg, M. von, and Muller, H. R., "On the Structure of Gas Hydrates," *J. Chem. Phys.*, **19**, 1319 (1951).

Stackelberg, M. von, and Muller, H. R., "Feste Gashydrate II, Struktur und Raumchemie," *Zeitschrift fur Elektrochemie*, **58**, 25 (1954).

Stillinger, F. H., and Rahman, A., "Revised central force potentials for water," *J. Chem. Phys.*, **68**, 666 (1978).

Stillinger, F. H., and Weber, T. A., "Inherent Structure in Water," *J. Phys. Chem.*, **87**, 2833 (1983).

Stroud, H. J. F., and Parsonage, N. G., "Low-Temperature Calorimetric Study of Methane in Linde 5A Sieve," *Adv. Chem. Ser. No. 102*, **2**, 138 (1971).

Stroud, H. J. F., Richards, E., Limcharoen, P., and Parsonage, N. G., "Thermodynamic Study of the Linde Sieve 5A + Methane System," *J. Chem. Soc. Faraday Trans. I*, **72**, 942 (1976).

Swaminathan, S., Harrison, S. W., and Beveridge, D. L., "Monte Carlo Studies on the Structure of a Dilute Aqueous Solution of Methane," *J. Amer. Chem. Soc.*, **100**, 5705 (1978).

Tanaka, H., Nakanishi, K., and Watanabe, N., "Constant temperature molecular dynamics calculation on Lennard-Jones fluid and its application to water," *J. Chem. Phys.*, **78**, 2626 (1983).

Tee, L. S., Gotoh, S., and Stewart, W. E., "Molecular Parameters for Normal Fluids," *Ind. Eng. Chem. Fundam.*, **5**, 363 (1966).

Tester, J. W., Bivins, R. L., and Herrick, C. C., "Use of Monte Carlo in Calculating the Thermodynamic Properties of Water Clathrates," *AIChE J.*, **18**, 1220 (1972).

Tobiàs, D. J., and Brooks, C. L., "Molecular Dynamics with Internal Coordinate Constraints," *J. Chem. Phys.*, **89**, 5115 (1988).

Tse, J. S., and Davidson, D. W., "Intermolecular potentials in gas hydrates," Proc. 4th *Can. Permafrost Conf.*, 329 (1982).

Tse, J. S., Handa, Y. P., Ratcliffe, C. I., and Powell, B. M., "Structure of Oxygen Clathrate Hydrate by Neutron Powder Diffraction," *J. Inclusion Phenomena*, **4**, 235 (1986).

Tse, J. S., and Klein, L., "Dynamical Properties of the Structure II Clathrate Hydrate of Krypton," *J. Phys. Chem.*, **91**, 5790 (1987).

Tse, J. S., and Klein, L., "Molecular Dynamics Studies of Ice Ic and the Structure I Clathrate Hydrate of Methane," *J. Phys. Chem.*, **87**, 4198 (1983).

Tse, J. S., and Klein, M. L., McDonald, I. R., "Dynamical properties of the structure I clathrate hydrate of xenon," *J, Chem. Phys.*, **78**, 2096 (1983).

Tse, J. S., Klein, M. L., and McDonald, I. R., "Lattice vibrations of ices Ih, VIII, and IX," *J. Chem. Phys.*, **81**, 6124 (1984).

Tse, J. S., Klein, M. L., and McDonald, I. R., "Computer simulation studies of the structure I clathrate hydrates of methane, tetrafluoromethane, cyclopropane, and ethylene oxide," *J. Chem. Phys.*, **81**, 6146 (1984).

Tse, J. S., McKinnon, W. R., and Marchi, M., "Expansion of Structure I Ethylene Oxide Hydrate," *J. Phys. Chem.*, **91**, 4188 (1987).

van der Waals, J. H., "The Statistical Mechanics of Clathrate Compounds," Trans. Faraday *Soc.* (*London*), **52**, 184 (1956).

van der Waals, J. H., and Platteeuw, J. C., "Clathrate Solutions," *Adv. Chem.* Phys., **2**, 1 (1959).